AFAPL-TR-71-37

NOISE DETECTABILITY PREDICTION METHOD FOR LOW TIP SPEED PROPELLERS

FRANK W. BARRY
BERNARD MAGLIOZZI
HAMILTON STANDARD

TECHNICAL REPORT AFAPL-TR-71-37

JUNE 1971

AIR FORCE AERO PROPULSION LABORATORY
AIR FORCE SYSTEMS COMMAND
WRIGHT-PATTERSON AIR FORCE BASE, OHIO

DOCUMENT CONTROL DATA - R&D

(Security classification of title, body of abstract and indexing annotation must be entered when the overall report is classified)

1 ORIGINATING ACTIVITY (Corporate author) Hamilton Standard Division United Aircraft Corporation Windsor Locks, Connecticut	2a REPORT SECURITY CLASSIFICATION Unclassified 2b GROUP

3 REPORT TITLE

NOISE DETECTABILITY PREDICTION METHOD FOR LOW TIP SPEED PROPELLERS

4 DESCRIPTIVE NOTES (Type of report and inclusive dates)

Final Report, 1 May 1970 to 1 May 1971

5 AUTHOR(S) (Last name, first name, initial)

Barry, Frank W.
Magliozzi, Bernard

6 REPORT DATE	7a TOTAL NO. OF PAGES	7b NO. OF REFS
1 May, 1971	192	39

8a CONTRACT OR GRANT NO	9a ORIGINATOR'S REPORT NUMBER(S)
F33615-70-C-1583 b PROJECT NO 3066 c d	HSER 5834 9b OTHER REPORT NO(S) (Any other numbers that may be assigned this report) AFAPL-TR-71-37

10 AVAILABILITY/LIMITATION NOTICES

11 SUPPLEMENTARY NOTES	12 SPONSORING MILITARY ACTIVITY
	Air Force Aero Propulsion Laboratory Air Force Systems Command Wright-Patterson AFB, Ohio

13 ABSTRACT

Experience in the field of quiet aircraft for reconnaissance/surveillance applications indicated a need for a reliable quiet propeller design procedure. This report describes the development of a computer program intended to fulfill this need.

The propeller noise detectability computer program predicts propeller harmonic rotational noise using non-steady blade loads and broad-band noise using a new integration method and compares these predictions with an appropriate aural detectability criterion to estimate the minimum undetectable flight altitude. Supporting tasks include development of aural detectability criteria, a theoretical study of the effect of airfoil section shape on vortex noise, static noise tests of several propeller configurations, correlation of unsteady blade loads corresponding to measured harmonic noise levels, design and testing of a new quiet propeller, and a propeller noise detectability trend study.

The major conclusions are (1) static propeller noise levels can be calculated with acceptable accuracy by the computer program only when empirically-derived unsteady blade loads are included, (2) low tip-speed propellers have an unexplained noise source giving rise to narrow-band random noise, and (3) the prediction of the noise from a propeller in flight using this computer program requires further investigation.

The effect of forward flight on propeller noise and the sources of propeller noise observed in this study should be investigated further. If necessary the computer program should be modified to establish correlation with flight data.

DD FORM 1 JAN 64 1473

14 KEY WORDS	LINK A		LINK B		LINK C	
	ROLE	WT	ROLE	WT	ROLE	WT
Propeller Noise						
Tone Noise						
Vortex Noise						
Harmonic Noise						
Aural Detectability						
Rotational Noise						
Harmonic Loading						
Loading Noise						
Thickness Noise						
Narrow-Band Random Noise						

INSTRUCTIONS

1. ORIGINATING ACTIVITY: Enter the name and address of the contractor, subcontractor, grantee, Department of Defense activity or other organization *(corporate author)* issuing the report.

2*a*. REPORT SECURITY CLASSIFICATION: Enter the overall security classification of the report. Indicate whether "Restricted Data" is included. Marking is to be in accordance with appropriate security regulations.

2*b*. GROUP: Automatic downgrading is specified in DoD Directive 5200.10 and Armed Forces Industrial Manual. Enter the group number. Also, when applicable, show that optional markings have been used for Group 3 and Group 4 as authorized.

3. REPORT TITLE: Enter the complete report title in all capital letters. Titles in all cases should be unclassified. If a meaningful title cannot be selected without classification, show title classification in all capitals in parenthesis immediately following the title.

4. DESCRIPTIVE NOTES: If appropriate, enter the type of report, e.g., interim, progress, summary, annual, or final. Give the inclusive dates when a specific reporting period is covered.

5. AUTHOR(S): Enter the name(s) of author(s) as shown on or in the report. Enter last name, first name, middle initial. If military, show rank and branch of service. The name of the principal author is an absolute minimum requirement.

6. REPORT DATE: Enter the date of the report as day, month, year, or month, year. If more than one date appears on the report, use date of publication.

7*a*. TOTAL NUMBER OF PAGES: The total page count should follow normal pagination procedures, i.e., enter the number of pages containing information.

7*b*. NUMBER OF REFERENCES: Enter the total number of references cited in the report.

8*a*. CONTRACT OR GRANT NUMBER: If appropriate, enter the applicable number of the contract or grant under which the report was written.

8*b*, 8*c*, & 8*d*. PROJECT NUMBER: Enter the appropriate military department identification, such as project number, subproject number, system numbers, task number, etc.

9*a*. ORIGINATOR'S REPORT NUMBER(S): Enter the official report number by which the document will be identified and controlled by the originating activity. This number must be unique to this report.

9*b*. OTHER REPORT NUMBER(S): If the report has been assigned any other report numbers *(either by the originator or by the sponsor)*, also enter this number(s).

10. AVAILABILITY/LIMITATION NOTICES: Enter any limitations on further dissemination of the report, other than those imposed by security classification, using standard statements such as:

(1) "Qualified requesters may obtain copies of this report from DDC."

(2) "Foreign announcement and dissemination of this report by DDC is not authorized."

(3) "U. S. Government agencies may obtain copies of this report directly from DDC. Other qualified DDC users shall request through _____."

(4) "U. S. military agencies may obtain copies of this report directly from DDC. Other qualified users shall request through _____."

(5) "All distribution of this report is controlled. Qualified DDC users shall request through _____."

If the report has been furnished to the Office of Technical Services, Department of Commerce, for sale to the public, indicate this fact and enter the price, if known.

11. SUPPLEMENTARY NOTES: Use for additional explanatory notes.

12. SPONSORING MILITARY ACTIVITY: Enter the name of the departmental project office or laboratory sponsoring *(paying for)* the research and development. Include address.

13. ABSTRACT: Enter an abstract giving a brief and factual summary of the document indicative of the report, even though it may also appear elsewhere in the body of the technical report. If additional space is required, a continuation sheet shall be attached.

It is highly desirable that the abstract of classified reports be unclassified. Each paragraph of the abstract shall end with an indication of the military security classification of the information in the paragraph, represented as *(TS)*, *(S)*, *(C)*, or *(U)*.

There is no limitation on the length of the abstract. However, the suggested length is from 150 to 225 words.

14. KEY WORDS: Key words are technically meaningful terms or short phrases that characterize a report and may be used as index entries for cataloging the report. Key words must be selected so that no security classification is required. Identifiers, such as equipment model designation, trade name, military project code name, geographic location, may be used as key words but will be followed by an indication of technical context. The assignment of links, rules, and weights is optional.

AFAPL-TR-71-37

NOISE DETECTABILITY PREDICTION METHOD FOR LOW TIP SPEED PROPELLERS

FRANK W. BARRY
BERNARD MAGLIOZZI
HAMILTON STANDARD

FOREWORD

This report was prepared by the Hamilton Standard Division of United Aircraft Corporation, Windsor Locks, Connecticut, for the Air Force Aero Propulsion Laboratory, Wright-Patterson Air Force Base, Ohio, under Contract F33615-70-C-1585. The contract was initiated under Project 3066, Task 306612. The Hamilton Standard report number is HSER 5834. This report covers work conducted from 1 May 1970 to 1 May 1971.

Capt. Paul A. Shahady, (AFAPL/TBC), was Project Engineer for the Air Force Aero Propulsion Laboratory.

Acknowledgement is due to Mr. Martin R. Fink who conducted the analytical studies of the effects of airfoil section on vortex noise.

This report was submitted by the authors in May 1971.

Publication of this report does not constitute Air Force approval of the report's findings or conclusions. It is published only for the exchange and stimulation of ideas.

Ernest C. Simpson

ERNEST C. SIMPSON
Director
Turbine Engine Division
Air Force Aero Propulsion Laboratory

June 1971

ABSTRACT

Experience in the field of quiet aircraft for reconnaissance/surveillance applications indicated a need for a reliable quiet propeller design procedure. This report describes the development of a computerized design technique intended to fulfill this need.

The propeller noise detectability computer program, developed under this contract, predicts propeller harmonic rotational noise using unsteady blade loads and broad-band noise using a new integration method and compares these predictions with an appropriate aural detectability criterion to estimate the minimum undetectable flight altitude. Supporting tasks include development of aural detectability criteria, a theoretical study of the effect of airfoil section shape on vortex noise, static noise tests of several propeller configurations, correlation of unsteady blade loads corresponding to measured harmonic noise levels, design and testing of a new quiet propeller, and a propeller noise detectability trend study.

The major conclusions are: (1) static propeller noise levels can be calculated with acceptable accuracy by the computer program only when empirically-derived unsteady blade loads are included, (2) low tip-speed propellers have an unexplained noise source giving rise to narrow-band random noise, and (3) the prediction of the noise from a propeller in flight using this computer program requires further investigation.

The effect of forward flight on propeller noise and the sources of propeller noise observed in this study should be investigated further. If necessary, the computer program should be modified to establish correlation with flight data.

TABLE OF CONTENTS

LIST OF FIGURES

LIST OF TABLES

SYMBOLS

AF	propeller activity factor
a	speed of sound in ambient air
B	number of propeller blades
b	blade chord
$b_{.7}$	blade chord at 0.7 propeller radius
C	coefficient
C_F	force coefficient in vortex noise theory
C_f	frequency coefficient in vortex noise theory
C_L	lift coefficient
C_P	power coefficient
C_T	thrust coefficient
D	diameter of propeller or cylinder
d	differential operator
d	distance between observer and propeller center
dB	decibels, for sound pressure level reference is 0.0002 microbars
e	base of natural logarithms, 2.718...
F	force
f	cyclic frequency, $\omega/2\pi$, Hz
HP	propeller shaft horsepower
Hz	abbreviation for Hertz, cps
h	blade thickness
$h_{.7}$	blade thickness at 0.7 propeller radius
i	$\sqrt{-1}$
J_n	Bessel function of first kind of order n and argument $n\,\Omega\,Yr/(aS_0)$
K	thickness noise doublet strength proportionality factor
k	$mB\Omega/a$
ℓ	length of cylinder

ln	natural logarithm to base 2.718...
log	common logarithm to base 10
M	flight Mach number
M. A. F.	minimum audible field
M. A. P.	minimum audible pressure
m	order of rotational sound, ratio of harmonic frequency to blade-passing frequency Bn/60
n	propeller rpm
p	sound pressure
Q	propeller torque
R	Reynolds number
r	radius from propeller axis
S	$\sqrt{X^2+(1-M^2)(Y^2-2Yr\cos\phi+r^2)}$
S_b	propeller blade area, $B\int_{hub}^{tip} bdr$
SPL	sound pressure level, dB re 0.0002 microbar
S_t	Strouhal number
S_0	$\sqrt{X^2+(1-M^2)\,Y^2}$
T	propeller thrust
t	time
V	velocity
V_t	tip velocity
$V_{.7}$	rotation velocity at 0.7 propeller radius
W	sound power
X	distance to observer from propeller plane at time sound heard, positive if observer ahead of propeller
X_p	distance to observer from propeller plane at time sound produced
Y	distance to observer from propeller axis
α	blade angle of attack at 0.7 radius

β	blade angle
θ	blade angle relative to propeller plane
$\theta_{.75}$	blade angle at 0.75 propeller radius
λ	order of harmonic loading forces
π	pi, 3.14159...
ρ	mass density of air
σ	$(MX+S)/(1-M^2)$
σ_0	$(MX+S_0)/(1-M^2)$
ϕ	circumferential angle about propeller axis, 0 in plane of observer
ψ	azimuth angle between vector from propeller center to field point and propeller axis, 0 in forward axis, 90^o in propeller plane
Ω	propeller angular velocity, $n\pi/30$, radians/sec.
ω	circular frequency, radians/sec.

SECTION I

INTRODUCTION

Considerable interest has developed recently in quiet propellers for reconnaissance and surveillance aircraft. These propellers are operated at low tip speeds in order to avoid aural detection at relatively low flight altitudes. Recent USAF experience in the field of quiet aircraft has indicated the need for a computerized propeller design technique to calculate propeller performance and noise and to compare the noise to aural detectability criteria. The objective of the study summarized in this report was the development of such a technique. This propeller design technique is in two parts: a proprietary propeller performance computer program previously made available by Hamilton Standard for AF Aero Propulsion Laboratory use and a new propeller noise detectability program written under this contract.

Over the past several years, Hamilton Standard has developed a propeller noise computer program which has been supplied to the AFAPL. However, this program is directed primarily towards commercial applications that require predictions of propeller noise annoyance rather than aural detectability. Several parts of this computer program served as bases for the development of the new propeller noise detectability program. The new program predicts propeller rotational noise and broad-band noise for a specified operating condition and compares these predictions with the appropriate aural detectability criterion to determine the minimum undetectable flight altitude. The rotational noise prediction method is derived from an existing Hamilton Standard method with the calculation of noise due to non-steady blade loads added. A second major objective was to develop a new broad-band noise prediction method in order to be able to evaluate the effects of blade geometry changes on the broad-band noise produced.

In support of the computer program development the following tasks were completed:

a. Development of aural detectability criteria for tone and broad-band noise for two jungle background noise environments.

b. A theoretical investigation of the effects of airfoil section shape on vortex noise.

c. Measurement and analysis of harmonic and broad-band noise data from tests on an outdoor static test rig of four low-tip-speed, 11.25-ft diameter, propeller configurations.

d. Correlation of measured and predicted harmonic noise levels. The lack of correlation obtained led to the selection of non-steady blade loads for use in the computer program which significantly improved correlation.

e. Correlation of measured broad-band noise levels with predicted broad-band noise levels by empirical adjustment of the coefficients in the theory.

f. Design and test of a propeller with new blades which was predicted, and measured, to produce over 3 dB less broad-band noise.

g. Performance of a detectability trend study using the developed computer program.

The major results of this program were 1) the development of a computer program that links detectability and propeller design parameters and 2) the development of a detailed understanding of the noise signature of low-tip-speed propellers at static conditions. Analysis of data acquired on four different propeller configurations in this program revealed the presence of a source producing narrow-band random noise with peaks at frequencies coinciding with the harmonics of blade passage frequency. This type of noise, which is not predicted by existing propeller noise theories, will be the controlling factor in aural detection if it persists in forward flight.

SECTION II

AURAL DETECTABILITY

1. INTRODUCTION

The aural detection of an aircraft by an observer depends upon several factors including: a) the amplitude and frequency characteristics of the noise generated by the aircraft, b) the effects of the atmosphere on the noise propagation, c) the distance from the aircraft to the observer, d) the influence on the noise of the terrain in the vicinity of the observer, e) the ambient background noise characteristics in the vicinity of the observer, and f) the physiological and psychological characteristics of the observer.

Items a) through d) deal with the definition of the noise source and the propagation of the noise to the observer. These will be discussed in subsequent sections of this report. In this section, consideration will be given to items e) and f) above with simplifying assumptions to remain within the scope of the program. Thus, factors such as the variable attention span and fatigue of the observer, the increased difficulty in detecting a fluctuating signal in a non-steady noise environment as opposed to a steady signal of known character in the presence of noise of constant level, and the influence in the observer's decision of the consequences he would face in the case of a false alarm or failure to report a detection were not considered. Rather, the detection criteria developed are based on laboratory test data on the threshold of hearing and the critical bandwidth concept to determine the masking effects of a steady ambient noise. This method is considered somewhat conservative since it represents the detection of a signal under ideal conditions.

2. REVIEW OF BASIC APPROACHES

The reports on the detection of acoustic signals, with and without the presence of noise, presented in the Bibliography were reviewed.

Essentially, three procedures for determining the aural detection of a signal were found in the literature. The three procedures were identical at low frequencies, where it was agreed that signal detection is uniquely dependent on the auditory threshold. However, at the mid and high frequencies, where it is assumed that the ambient noise exceeds the hearing threshold, the criterion for detection depends on the ear's ability to identify the signal in a masking noise. The three procedures for determining the detection of an acoustic signal in noise are a) the differential level change method, b) the signal-to-noise ratio criterion and c) the masking noise level concept based on the critical bandwidth of the ear. The first procedure predicts

detection when a differential level change of 0.5 dB occurs; i.e., when the signal-plus-noise exceeds the noise alone by 0.5 dB or more. The second procedure determines detection at some probability level depending on the signal-to-noise ratio. The third approach predicts detection when the signal exceeds a certain level which is a function of the level of the noise and the critical bandwidth of the ear.

The third approach is considered the most consistent with the scope of this program. It was, therefore, selected as the procedure to be used for this study. Thus, the aural detection criteria presented herein are essentially those described by Smith and Paxson[1], but with notable exceptions which will be brought out in the discussion which follows.

3. AUDITORY THRESHOLDS

The aural detection of a low-frequency signal depends primarily on the hearing threshold. In the laboratory, the auditory threshold in a free-field environment (i.e., the minimum audible field (M.A.F.)) is determined from the minimum level that can be heard, usually an average of the responses from a group of subjects. At very low frequencies, where it is not feasable to generate high-intensity uniform fields in a chamber, other means are employed such as close coupled ear phones, in which case the minimum audible pressure (M.A.P.) is determined. The results from the two methods are not necessarily the same. Figure 1 shows the results from experiments conducted by Robinson and Dadson[2]. It is seen that the M.A.P. threshold over the range 80 to 600 Hz is about 9 dB higher than the M.A.F. Up to 3.6 dB of this difference might be due to monaural versus binaural listening[3]. However, there remains approximately 6 dB of unexplained difference.

Figure 2 shows the pure tone threshold of hearing for an average young subject at age 18 to 25 years as presented in ISO Recommendation R226[4]. Also shown are the M.A.P. from 1.5 to 100 Hz as measured by Yeowart, et. al[5] and from 5 to 200 Hz according to Corso[6]. In the range 25 to 100 Hz there is good agreement between Yeowart, et. al. and Corso with both being approximately 15 dB above the M.A.F. Between 100 and 200 Hz, the difference between the M.A.P. and the M.A.F. is about 8 dB which is in agreement with that reported in Reference 2. Corso's[6] threshold at 5 Hz does not appear consistent with those measured by other investigators. In Figure 2 of his paper, he compares his results with those of others and he appears to be more than 20 dB lower than Bekesy at 5 Hz. Adding 20 dB to his results at 5 Hz would then make him consistent with Yeowart and Bekesy.

Inasmuch as it was desired to extend the aural detection criteria to 1.5 Hz, the curves of Figure 2 were reconciled as shown by the dashed line and the M.A.F curve. This was done by lowering Yeowart's curve by 10 dB and then smoothly joining it to the M.A.F. curve in the region of overlap.

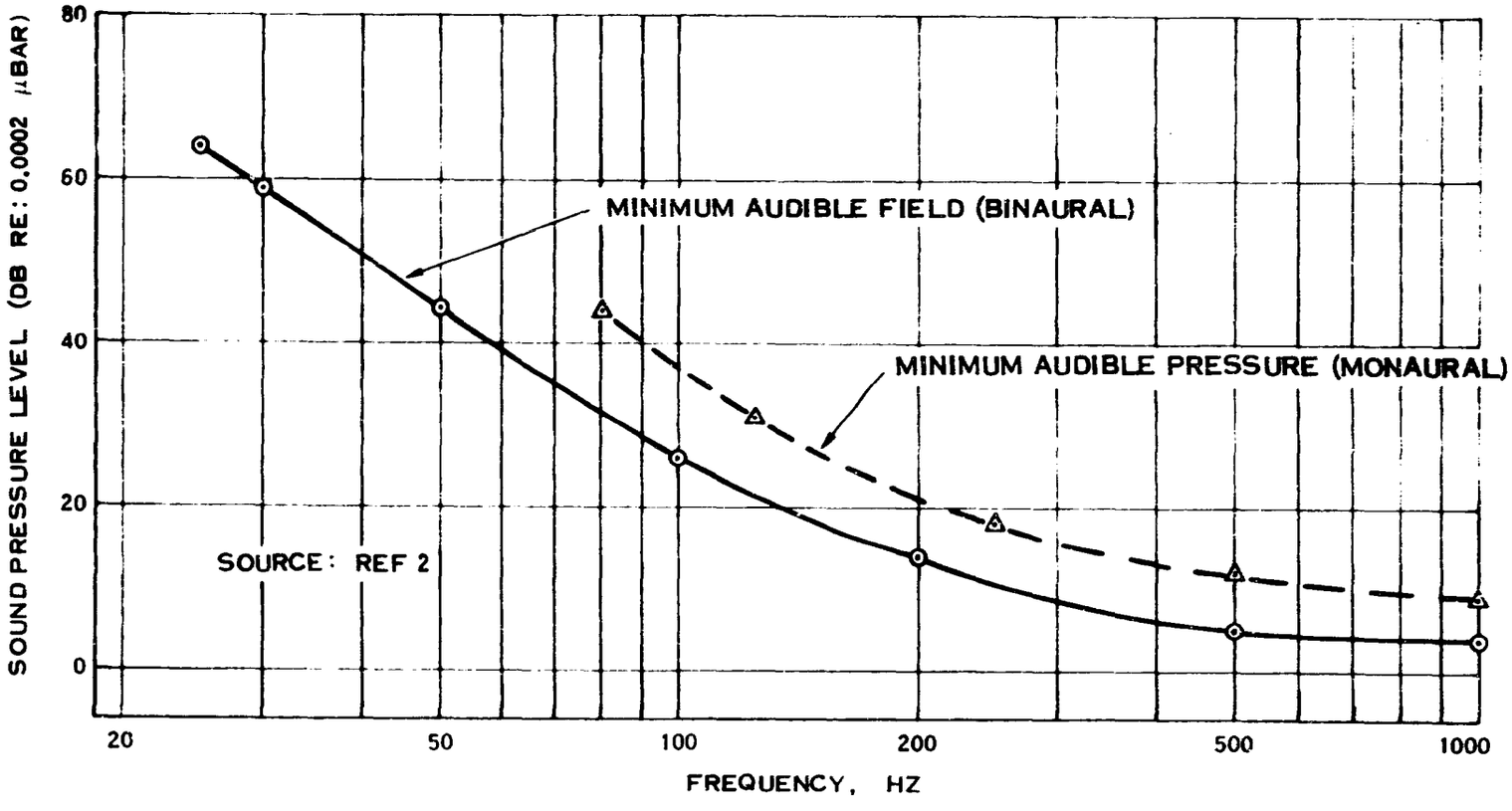

Figure 1. Comparison of Minimum Audible Field and Minimum Audible Pressure

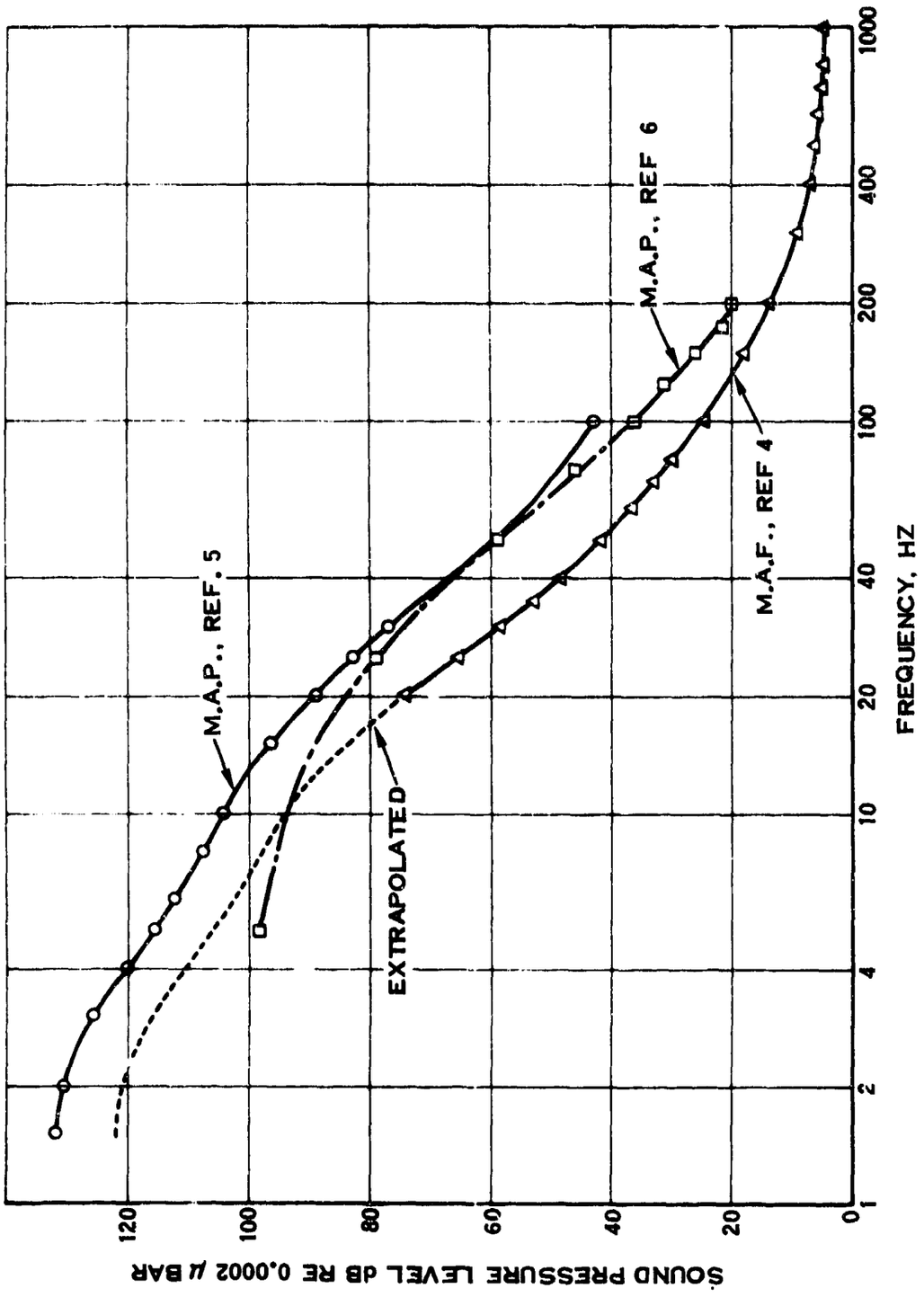

Figure 2. Comparison of Low-Frequency M.A.P. and M.A.F.

It has been observed that the hearing threshold for octave bands of noise is slightly lower at low frequencies and slightly higher at the mid- and high-frequencies[7,8]. Actually, over the range 4 to 125 Hz, the average difference between the threshold for tones and bands of noise is approximately 2.5 dB with a maximum difference of 5.5 dB at 16 Hz[7]. Since the difference between the threshold for tones and bands of noise is small at low frequencies where the hearing threshold is used, and it is expected that the low-frequency detection of propeller noise would be due to rotational components, it was decided to ignore the differences between the thresholds for tones and bands of noise and the criterion adopted is the one shown in Figure 2 as described in the preceding paragraph.

4. DETECTION OF AN AUDITORY SIGNAL IN A MASKING NOISE

It has been shown that the part of the noise that is effective in masking a tone (or narrow band of noise) is the part of the spectrum lying near the tone and containing the same amount of power as the tone, and that the parts of the spectrum that are far from the tone contribute no masking[9]. Table I presents a) the ratio between the monaural masked threshold of a pure tone and the level per Hertz of the masking noise, measured at the frequency of the pure tone at the one-third octave band center frequencies of 100 to 10,000 Hz, as obtained from Reference 9, and b) the width of the band of frequencies that actually contributes to the masking of a tone located at the center of the band as defined by the levels in the center column. It is easy to see that for a typical noise environment, the masking level (i.e., the level of a tone or narrow band of noise below which it will not be detected in the noise) is given by:

$$M.L. = SPL - 10 \log BW + 10 \log \Delta f \qquad (1)$$

where

M.L. = Masking Level, dB

SPL = Sound Pressure Level of the Noise, dB

BW = Bandwidth of the Noise, Hz

Δf = Critical bandwidth, Hz

Thus, if the level of a tone or the spectrum level of a band of noise exceeds the masking level, it will be detected.

5. BACKGROUND NOISE SOURCES

The masking noise considered in this study is that which exists in a quiet jungle environment. Figure 3 presents average one-third octave band sound pressure levels (1/3-octave band SPL) from 100 to 1000 Hz measured in a daytime and nighttime Thailand jungle[10]. Figures 4 and 5 show these levels converted to masking levels

TABLE I

WIDTH OF CRITICAL BANDS

Frequency	Ratio Between the Monaural Masked Threshold of a Pure Tone and the Level per Hertz of the Masking Noise	Equivalent Band-Width of the Masking Noise
100 Hz	19.0 dB	80 Hz
125	17.9	62
160	17.2	53
200	17.0	50
250	16.8	48
315	16.8	48
400	17.0	50
500	17.1	51
625	17.6	57
800	17.9	62
1000	18.5	70
1250	19.0	79
1600	19.5	90
2000	20.6	115
2500	21.6	145
3150	22.6	180
4000	23.8	240
5000	24.9	310
6250	26.3	430
8000	27.8	600
10000	29.1	810

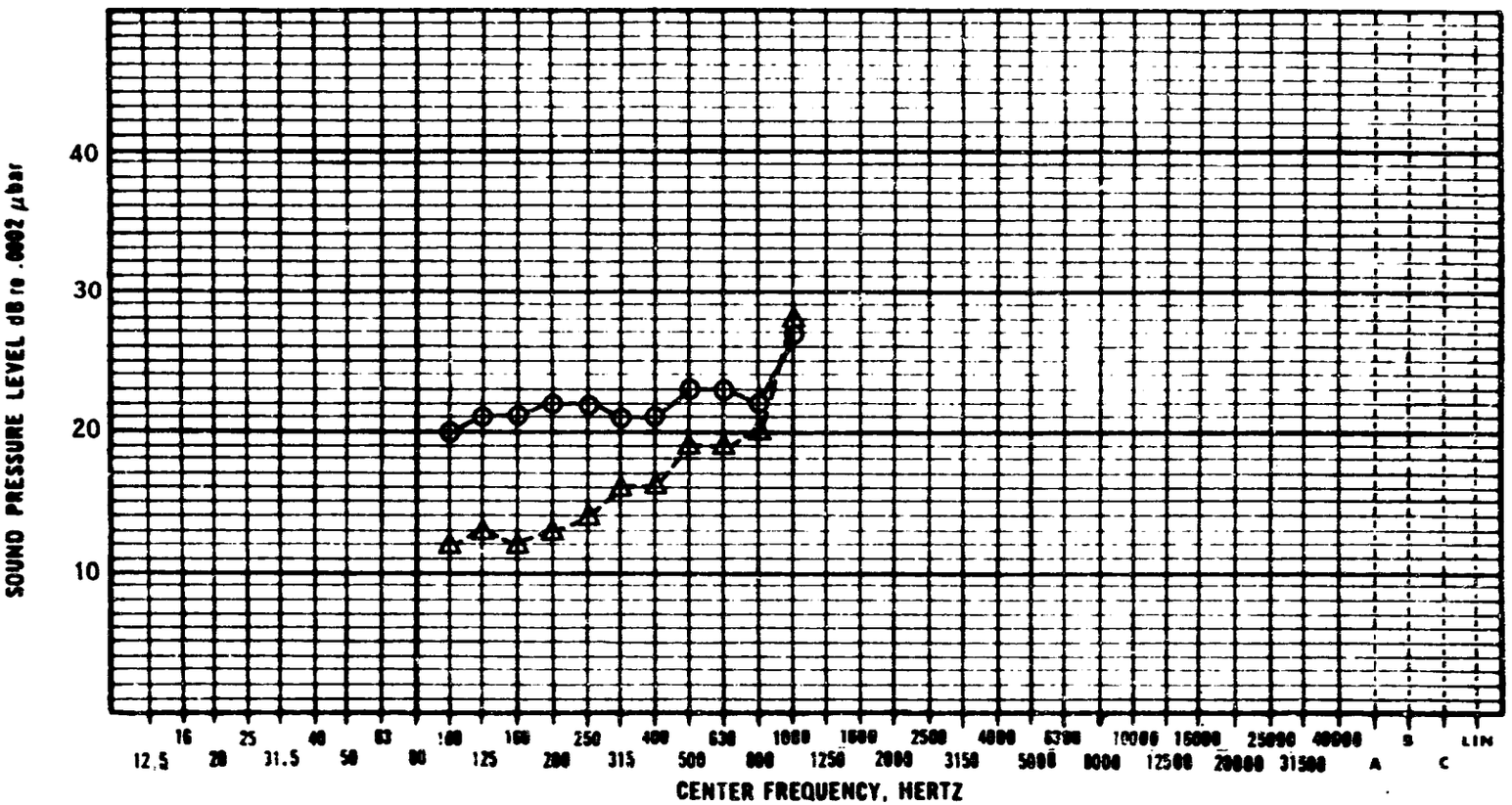

SOURCE: REF. 10

Figure 3. Average Noise Level in Thailand Jungle

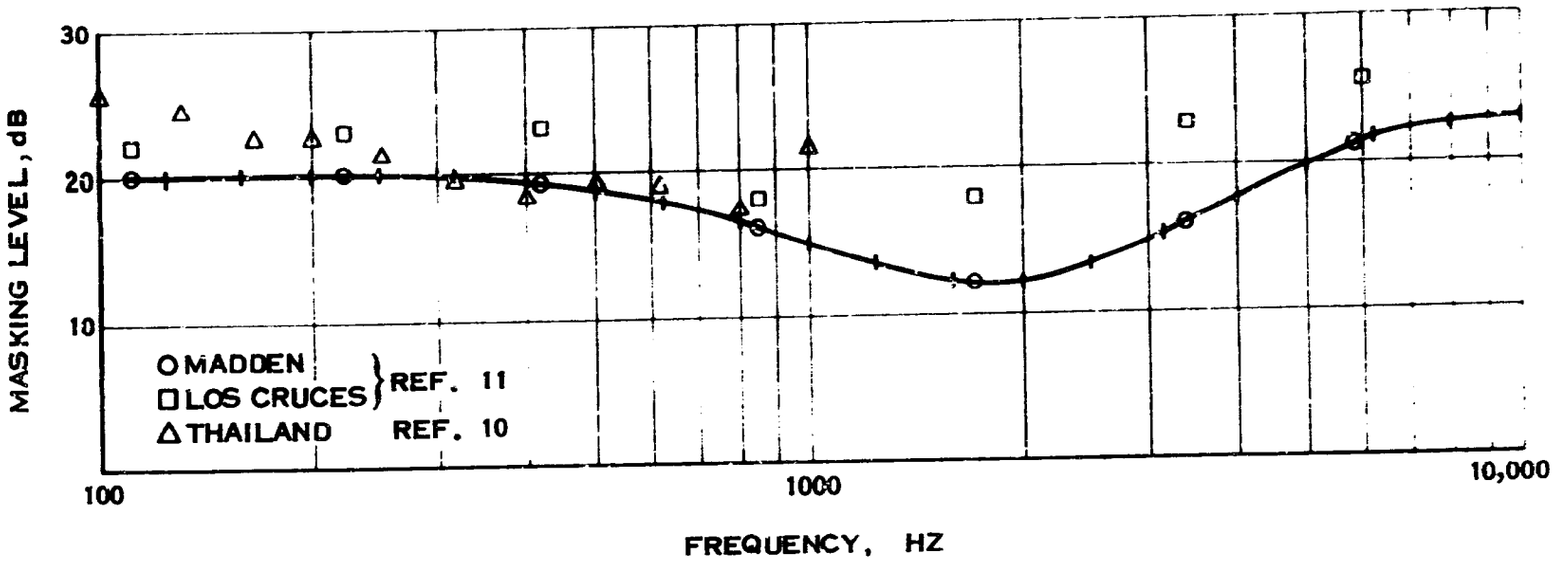

Figure 4. Daytime Jungle Noise Masking Levels

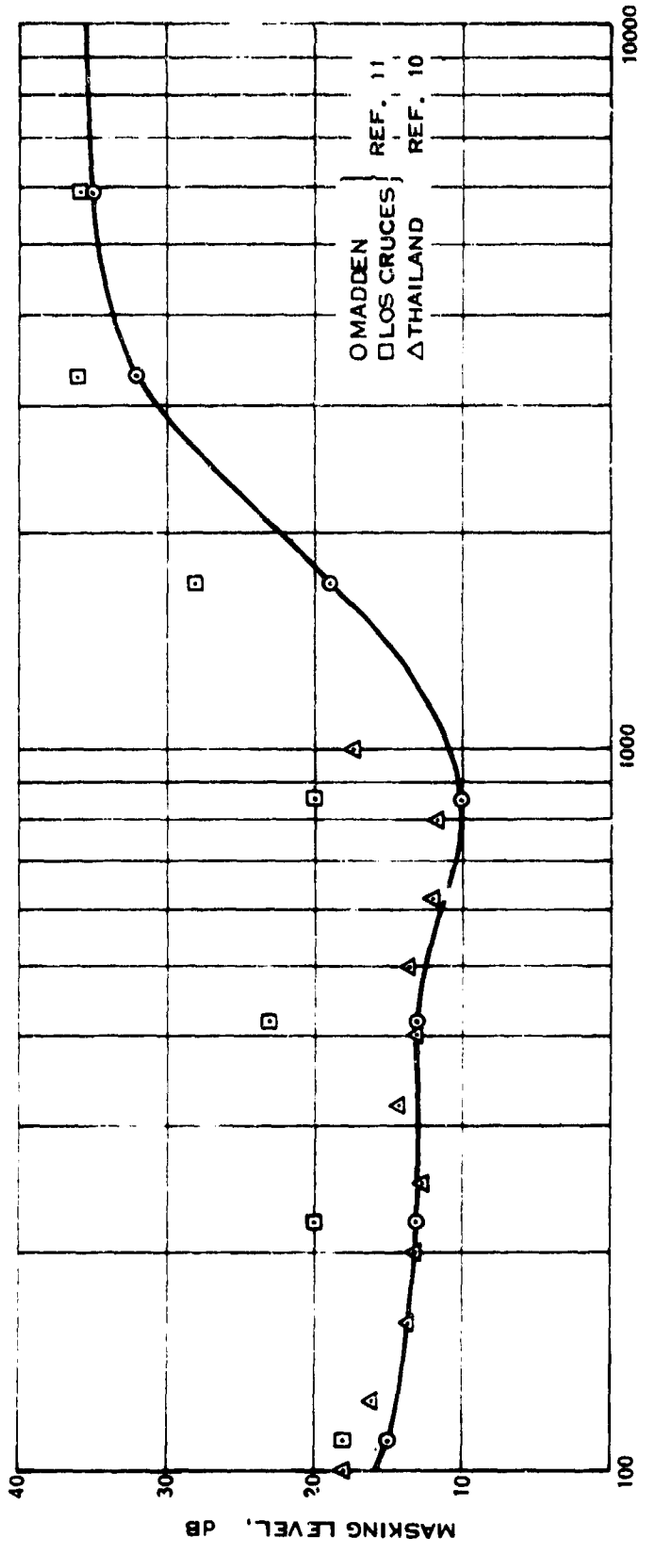

Figure 5. Nighttime Jungle Noise Masking Levels

compared to those from two Panama jungles[11]. It is seen that there is good agreement between the Thailand and Madden Jungle ambient noise levels. It was, thus, decided to use the Madden Jungle noise levels throughout the frequency spectrum for consistency. Also, the masking levels were extrapolated to 10,000 Hz.

6. AURAL DETECTION CRITERIA

The elements developed in the previous sections were combined into aural detection criteria for tones and bands of noise for a daytime and a nighttime jungle. Figure 6 shows the detection criteria for pure tones. It is seen that at low frequencies, the curve is the threshold of hearing while at the other frequencies it is determined by the jungle noise. A smooth transition was drawn at the junction of the two curves.

In the computer program, the levels of the tones which are calculated are compared to the detection criteria. To facilitate this comparison, the curves of Figure 6 were approximated by several polynomial equations from least - squares curve fits. The resulting series of equations, summarized in Table II, are then used to establish detection of pure tone components by entering the frequency of the pure tone into the appropriate equation and comparing the thus-computed detection level to the predicted level of the tone.

As an example, say a pure tone component has a frequency of 73 Hz. Then, from Table II, the detection criterion for a daytime jungle for a pure tone at 73 Hz is given by:

$$SPL_D = 585.3 - 286.929 \ln(73) + 48.6023 \left[\ln(73)\right]^2 - 2.75325 \left[\ln(73)\right]^3$$

$$= 31.5 \text{ dB}$$

If the level of the tone equals or exceeds 31.5 dB it will be detected.

The criteria presented in Figure 6 and Table II could be used for broad-band noise signals as well, since no distinction is made between the response of the ear to bands of noise or tones. However, inasmuch as the noise estimating method calculates broad-band noise in 1/3-octave band SPL's, it is economical to convert Figure 6 into equivalent 1/3-octave band SPL's. That is to say, the levels of the 1/3-octave bands (of constant energy within bandwidths) which have spectrum levels equal to the detection level at each band-center frequency were computed and are shown in Table III.

To illustrate the derivation of the levels shown in Table III, consider a 1/3-octave band SPL of band-center frequency of 800 Hz. The width of this band is 183 Hz. Thus, for it to have a spectrum level of 10 dB (the nighttime jungle detection criterion at 800 Hz from Figure 6), it must have a sound pressure level of:

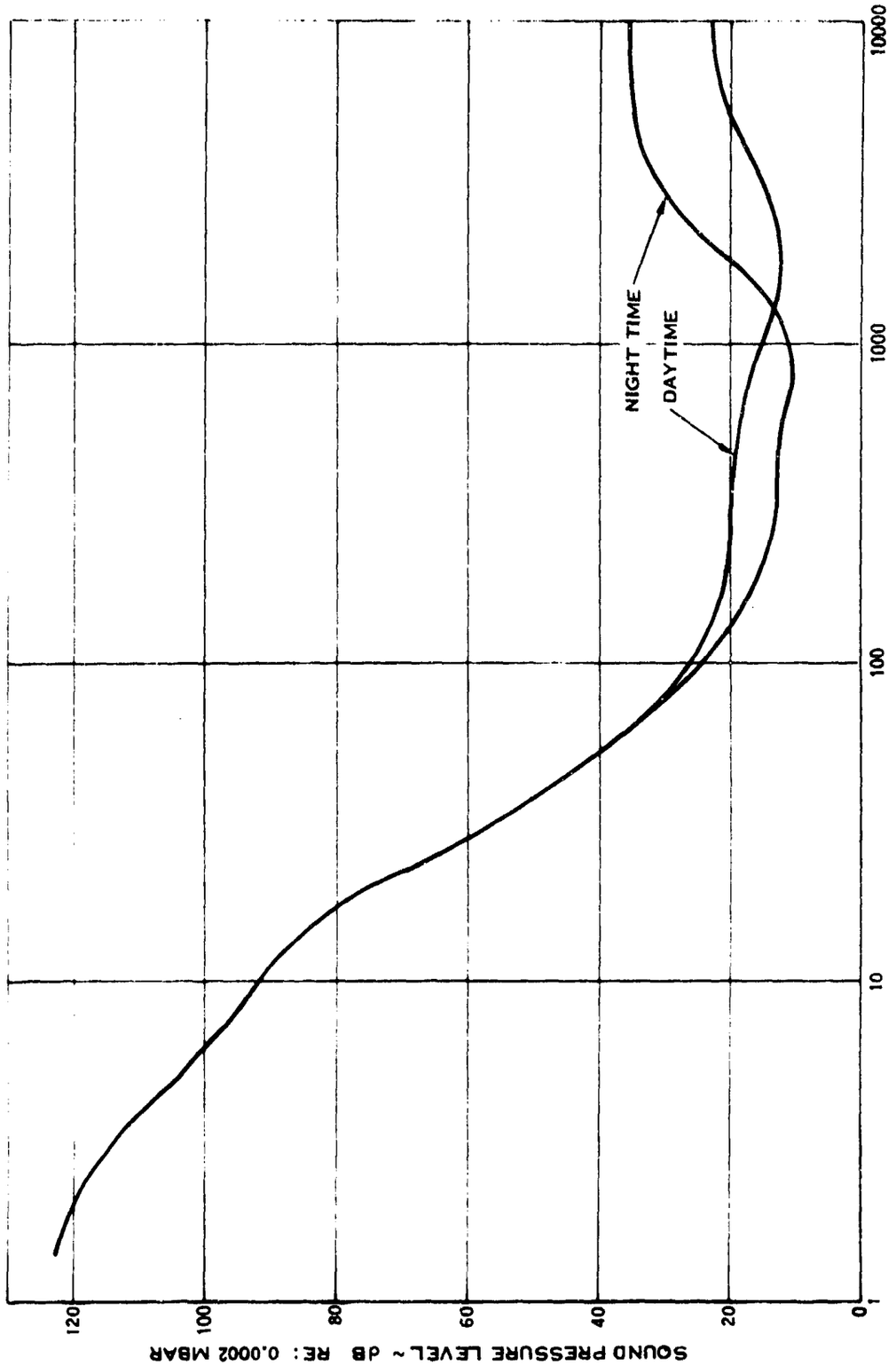

Figure 6. Aural Detection Criteria for Pure Tones

TABLE II

EQUATIONS FOR PURE TONE AURAL DETECTABILITY CRITERIA

The detection level, SPL_D, at a given frequency, f, is given by:

$$SPL_D = C_0 + C_1 \ln f + C_2 (\ln f)^2 + \ldots + C_N (\ln f)^N$$

where the coefficients C_0, C_1, ... , C_N are defined as follows:

1. Daytime jungle environment

Coefficient	Frequency Range		
	1.5 to 67 Hz	67 to 900 Hz	900 to 10,000 Hz
C_0	125.2	585.3	169.2
C_1	0.698014	-286.929	-2.38024
C_2	-15.1156	48.6023	-1.10338
C_3	6.16882	-2.75325	-1.47127
C_4	-1.34790	0	0.137120
C_5	0.299928	0	0.016260
C_6	-0.109861	0	-0.001549
C_7	0.014986	0	0

2. Nighttime jungle environment

Coefficient	Frequency Range			
	1.5 to 67 Hz	67 to 735 Hz	735 to 6,000 Hz	6,000 to 10,000 Hz
C_0	125.2	261.4	480.2	36.4
C_1	0.698014	-56.2722	-94.0359	0
C_2	-15.1156	-2.34364	-4.44855	0
C_3	6.16882	-0.591769	0.181656	0
C_4	-1.34790	0.438657	0.312787	0
C_5	0.299928	-0.027795	-0.024082	0
C_6	-0.109861	-0.00114	0	0
C_7	0.014986	0	0	0

TABLE III

AURAL DETECTABILITY CRITERIA FOR 1/3-OCTAVE BANDS OF NOISE

Band Center Frequency	Daytime Jungle	Nighttime Jungle
1.6 Hz	121.5 dB	121.5 dB
2	120	120
2.5	117	117
3.2	113.5	113.5
4	109	109
5	104	104
6.3	99.5	99.5
8	95	95
10	91.5	91.5
12.5	87.5	87.5
16	82	82
20	74.5	74.5
25	65	65
31.5	56	56
40	48	48
50	41.5	41.5
62.5	37	35.5
80	34	32
100	33.5	30
125	34.5	29
160	35.5	29.5
200	36.5	29.5
250	37.5	30.5
315	38.5	31.5
400	39	32.5
500	39.5	33
625	39.5	32.5
800	39	32.5
1000	38.5	33.5
1250	38	37
1600	38	42
2000	39	47.5
2500	41	53.5
3150	44	59
4000	47	63
5000	50.5	65
6250	53.5	66.5
8000	55	68
10000	56.5	69

SPL = 10 + 10 log (183) = 32.5 dB

The other bands were treated in a similar fashion.

7. ALTERNATE METHOD USED BY AIR FORCE

The Air Force developed an alternate method for calculating aural detection range of broad-band propeller noise after the draft of this report was submitted. A description of this alternate method was prepared by the Air Force and is included as Appendix II of this report at their request. Use of this alternate method may increase the minimum undetectable altitude of broad-band noise by about a factor of three relative to the method discussed above.

8. SUMMARY

In summary, aural detection criteria were derived for pure tones of frequency range 1.5 to 10,000 Hz and 1/3-octave bands of noise of center frequencies from 1.6 to 10,000 Hz based on laboratory test data for the auditory thresholds and the masking effects of a quiet daytime and nighttime jungle noise.

The detection criteria for pure tones were converted to equation form expressing the detection level as a function of frequency. Also, the detection criteria for broad-band noise was converted to equivalent 1/3-octave band SPL's. In each case, detection is said to occur if any component of the noise signal equals or exceeds the detection criteria.

SECTION III

PROPELLER NOISE THEORY

1. INTRODUCTION

Theoretical methods of predicting propeller rotational noise have been under continuous development since 1936 when the work of Gutin[12] was published describing the basic disc theory of noise due to blade loading. Rotational noise is a tone noise which occurs at harmonics of the blade passing frequency Bn/60 Hz. For moderate-to-high tip speeds used in nearly all applications of propellers, calculations based on the theory show generally good agreement with test data.

The first theory of vortex noise was developed in 1944 by Yudin[13] and was based on a dimensional analysis of flow parameters around rotating rods. The term "vortex noise" has been given to the broad-band noise produced by a propeller or rotor, because it was believed to be caused by an oscillating force associated with a Karman vortex street, such as is observed behind a rod normal to a moving stream. Subsequent work has produced several empirical procedures for predicting vortex noise.

Experimental data for medium- and high-tip speed propellers and published data for helicopters show noise frequency spectra which usually have the following general characteristics: a) there are a series of tone noises, the first at the blade-passing frequency of Bn/60 Hz and the rest at multiples of this frequency; b) the SPL of these rotational tone noises decreases with increasing harmonic number until the tones become lost in broad-band noise; and c) there is a broad-band noise which has a maximum sound level at a frequency of a few hundred Hertz. The harmonic noise levels are a maximum just behind the propeller plane, near $\psi = 105^{o}$, and decrease near the propeller axis. The broad-band noise levels, on the other hand, are a maximum on the axis and a minimum near the propeller plane. The theory for propeller rotational noise and the empirical procedures for vortex noise result in the same frequency spectrum shape as that described above based on measurements.

The theories for propeller noise contain several assumptions which may not always be stated explicitly. Therefore, it is appropriate to discuss these common assumptions in the following section. The theories of propeller rotational and vortex noise are discussed in Section III.3. Some general considerations of geometrical acoustics which apply to propeller noise are presented in Section III.4. Lastly the effects of reflection of the noise from the ground on the noise at the observer are described.

2. ASSUMPTIONS

The usual noise theories are based on the following assumptions:

a. The sound waves are weak and propagate at the speed of sound, which is proportional to the square root of the absolute temperature of the ambient air.

b. The sound waves propagate through air which is at rest (no wind or turbulence) and has a constant speed of sound. Therefore, air velocities induced by the propeller and aircraft are not considered.

c. The basic wave equations may be linearized, so that independent solutions for each sound source may be added. Therefore nonlinear effects[14] are ignored.

d. Absorption of sound[15], which is proportional to distance and depends on temperature, humidity and sound frequency, is not considered. However, the propeller noise detectability computer program discussed in Section VIII does include a correction for sound absorption.

e. The propeller is either operating statically or is moving along the propeller axis at constant speed.

f. The noise from separate propellers has a random phase relation. Therefore, the addition of sound from more than one propeller adds 10 log (number of propellers) to the sound pressure level of one propeller. Thus, two propellers are 3 dB noisier than one and would be detected nearly 1.4 times as far away.

g. The propeller blades are identically loaded, geometrically identical, equally spaced, and located in a disc normal to the propeller axis and flight path. The effects of non-equal spacing in fans has been investigated and it has been shown that sound energy can be redistributed among the harmonics. However, further development is required if these effects are to be included in propeller noise theory.

h. The propeller and observer are in a free field; i.e., there is no sound reflecting surface nearby. The consequences of this assumption are discussed in Section III.5.

3. NOISE SOURCES

Historically, propeller noise has been divided into three sources: loading noise, thickness noise and vortex noise. The first two sources, collectively called rotational noise, result in a series of harmonic tones at frequencies which are multiples of the blade passing frequency, Bn/60 Hz. The third source, vortex noise, is often associated with a periodic force on the blades due to a periodic wake, similar to the Karman vortex street from a cylinder normal to the flow.

First consider rotational noise. To an observer rotating in a reference frame fixed to the rotating propeller, the B blades produce a steady disturbance pressure field which has a circumferential period of $360^{o}/B$. The disturbance pressures are due to the loads (conventionally resolved into thrust and torque components) on the blades and due to the volume (thickness) of the blades. But to an observer who is stationary (not rotating), the disturbance pressure field is rotating with the propeller at n rpm and, therefore, the pressure at the observer not on the axis oscillates with a fundamental frequency of Bn/60 Hz. This oscillating pressure is the harmonic rotational noise and may be Fourier analyzed to determine the pressure amplitude of each harmonic of the blade passing frequency. On the propeller axis the pressure is constant and, therefore, there is no rotational noise. Theoretically, the thickness noise is a maximum in the propeller plane and zero on the propeller axis. Loading noise is a maximum just behind the propeller plane. However, if a circumferential variation in blade loading exists, there is loading noise present on the axis and the variation in loading noise with direction decreases. The variation in blade loading may be due to operation of the aircraft at an angle of attack and to interference from the airframe.

The theory of broad-band propeller noise is much less developed and understood than the theory for harmonic noise. The published theories all rely on at least one empirical factor, unlike the harmonic noise theories. Several possible sources of broad-band noise have been suggested, including a) an alternating vortex shedding at the trailing edge of the blade, b) fluctuating pressures in the turbulent boundary layer flowing over the blade, and c) turbulence in the incoming airflow.

4. GEOMETRIC ACOUSTICS

Several factors which affect the noise characteristics heard by an observer, but which do not depend on the noise source, are discussed in this section.

Near the propeller, the sound pressure level varies with distance from the propeller in a complicated way because of the way that noise from different parts of the propeller combines. However, in the far-field, typically over 3 to 5 diameters away, the variation with distance becomes quite simple: a 6 dB decrease in noise SPL for each doubling of distance.

If the sound is propagated vertically the simple relation of 6 dB/doubling of distance should be modified because of the vertical gradients in atmospheric density and speed of sound. If the sound intensity at the observer is not altered by these gradients, the square of the amplitude of the sound pressure is proportional to the product of density and speed of sound at the observer. Because both these parameters decrease with altitude (below 36089 feet for the standard atmosphere[16]) the SPL at an observer below the propeller is larger than at an observer at the same altitude as

the propeller. This effect increases the SPL by 0.142 dB/1000 ft altitude difference for the standard temperature lapse rate of 6.5°K/Km. This increment in SPL is included in the calculation of the minimum undetectable altitude by the computer program.

As the distance between the propeller and the observer becomes large, especially for high frequencies, the sound pressure level is further reduced by the effects of molecular absorption in the atmosphere. Published reports on absorption coefficients[15] show that the SPL is reduced by an amount which is proportional to the sound propagation distance. The proportionality factor, or coefficient of atmospheric absorption, is a function of the atmospheric temperature and relative humidity and of the sound frequency. The coefficient is small at low frequencies but increases rapidly with frequency above 1000 Hz. The computer program uses the equations for the coefficients of atmospheric absorption from Ref. (15).

Motion of the aircraft through the air has several effects on the propeller noise. Motion changes the sound power level produced and the directivity pattern of the noise produced. The theory for harmonic loading noise with the observer stationary relative to the aircraft (both moving or only air moving) is presented in Ref. (17). For a fixed observer, as assumed in the computer program, the sound pressure level is unaltered relative to the case of a moving observer but the sound frequency is altered by the familiar Doppler effect. For an airplane flying at a Mach number M along a straight path which is Y feet from the observer, the frequency is multiplied by a factor $1 / (1 - Xp\, M/\sqrt{Xp^2 + Y^2})$ where Xp is the distance to the observer forward of the propeller plane when the sound was produced. The result is to increase the frequency while the plane is approaching ($Xp > 0$) and to decrease the frequency as the plane leaves ($Xp < 0$).

Because the speed of sound is small relative to the speed of light, the airplane is not seen at the location at which the sound being heard was produced. If the observer is at distance X forward of the propeller plane when a sound is heard, the observer was at a distance Xp forward when the sound was produced, where

$$Xp = \frac{X + M\sqrt{X^2 + (1 - M^2)\, Y^2}}{1 - M^2} \qquad (2)$$

This distance is required because the atmospheric absorption is proportional to $\sqrt{Xp^2 + Y^2}$, the distance the sound propagated. The relation between these various distances is illustrated in the following sketch.

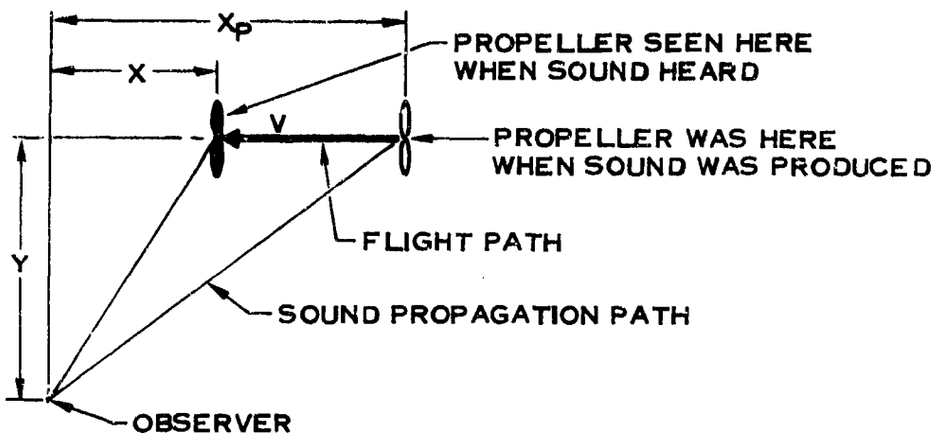

5. GROUND REFLECTION

When an acoustic wave impinges on a rigid surface, it is generally reflected. Thus, in an aircraft flyover the noise emanating from the aircraft will propagate to the ground and be reflected. This reflected wave will then interact with the direct wave and give rise to interference patterns in the acoustic field. At some location and frequency, there may be constructive interference (when the incoming and reflected waves are in phase) in which case the acoustic pressure is greater than for free-field conditions (no obstructions in the acoustic field). Conversely, destructive interference will occur elsewhere or at some other frequency in which case the acoustic pressure will be less than for a free-field.

The exact magnitude of this effect, relative to free-field conditions, is difficult to estimate. However, theory indicates that the correction to free-field estimates would vary from a reduction of infinity dB for complete destructive interference to an increase of 6 dB when the reflected and direct waves are of equal amplitude and in phase. The actual effect at some field point depends on several factors, including a) the amplitude and frequency characteristics of the source, b) the altitudes of the source and field point above the ground, c) the distance from the source to the field point, d) the angle of incidence of this wave onto the ground surface, and e) the complex impedance of the ground.

To our knowledge, a comprehensive ground reflection effect calculation procedure is not available at the present time, although several investigations are presently under way. In was thus decided not to include this effect in the computer program developed

for this contract. However, it could be included at some later time when results of current work become available.

However, due consideration is given to the phenomenon of ground reflection in correcting the test data acquired in the course of this program to equivalent free-field conditions. Thus, in Section VI, a description is given of the empirically-derived effects of ground reflections on the noise measured for the propeller configurations tested.

SECTION IV

HARMONIC ROTATIONAL NOISE THEORY

1. INTRODUCTION

Development of theoretical methods of predicting propeller rotational noise was started in 1936 when Gutin[12] published a paper describing the basic disc theory of noise due to the thrust and torque loads on propeller blades. Gutin's theory is limited to a stationary (i.e., not flying, as on a ground test rig) propeller in still air, and approximations are made which limit the theory to the fundamental and first overtones at a distance exceeding several propeller diameters.

Several workers have removed these limitations to produce the currently-accepted theories for propeller loading noise[17 to 22] Experience has shown that these theories provide generally good agreement with test data at moderate to high tip speeds.

Development of theoretical methods of predicting propeller thickness noise had a similar history, resulting in Arnoldi's theory[23] Calculations have shown that thickness noise may exceed loading noise in the higher harmonics if the blade is large; i.e., if the chord width and thickness are large.

The theoretical equations for harmonic loading and thickness noise developed from the above works which are used in the propeller noise detectability program are presented in this section. Two significant comments regarding the equations embodied in this program are worth making. First, the effective-radius approximation which concentrates the propeller load and volume noise sources at one radius, usually 80% of the tip radius, is not used. Therefore changes in the radial distribution of propeller blade loads and geometry are accounted for. Second, in order to account for effects of large blade chords, the blade loads are assumed to be distributed uniformly over the blade chord rather than concentrated on a radial line. The effect of blade angle reducing the projection of the chord onto the propeller plane is allowed for. Experience with another program by Hamilton Standard has shown that using a distributed load has little effect on the level of the fundamental, but does reduce the level of the higher harmonics compared to calculations with a concentrated load. It is believed that the program, which does not use either the effective radius or the concentrated load assumptions, is more accurate and will show the effects of changes in blade geometry.

2. HARMONIC LOADING NOISE THEORY

Because the development of the harmonic loading noise theory is readily available in the literature, (e.g., in Refs. 17 and 18) it will not be presented here. The theory is based on an array of non-steady point forces in the propeller disc representing the blade thrust and torque forces. Each of these point forces is zero except when a propeller blade is located in the same part of the disc. Thus, each force acts as a series of pulses with a fundamental frequency equal to the blade-passing frequency and a pulse width proportional to the blade chord. These point forces move along the flight path with the propeller, but do not rotate with the blades. The assumption is made of a constant chordwise blade loading over the projection of the chord onto the propeller plane rather than the common zero-chord assumption. The assumption is made that the blade loads do not vary circumferentially; i.e., the blade loads are constant. The equation for the disturbance pressure at a field point with coordinates (X, Y) relative to the propeller centerline is:

$$p_m = e^{-imB\Omega t} \frac{\rho \Omega^2 D^4}{4\pi^4 mB} \int_{hub}^{tip} \frac{r}{b \cos\theta} \sin\left(\frac{mBb \cos\theta}{2r}\right) \int_0^{\pi} \frac{\cos(mB\phi)}{S} \left[-\frac{dC_T}{dr} \left\{ \left(\frac{X}{S^2} + \frac{ik(M + X/S)}{1 - M^2} \right) \cos(k\sigma) + \left(\frac{k(M + X/S)}{1 - M^2} - \frac{iX}{S^2} \right) \sin(k\sigma) \right\} + \frac{mB\Omega}{2\pi r^2} \frac{dC_p}{dr} \left\{ \sin(k\sigma) + i\cos(k\sigma) \right\} \right] d\phi\, dr \qquad (3)$$

The derivation of the equation is outlined in Appendix I.

This equation is valid in the near field at distances greater than a chord from the tip provided that the wavelength of the sound exceeds the chord. The propeller noise detectability computer program performs the circumferential (ϕ) integration by Simpson's 1/3 rule using at least 100 intervals and the radial (r) integration using a 10-point Gauss integration. The term $r \sin(mBb \cos\theta/2r)/b \cos\theta$ depends on the solidity or activity factor and is a result of assuming a constant chordwise loading. The formulation of the equation for loading noise presented in Ref. (18) is that used by the computer program.

The disturbance pressure is the sum of harmonics, which are multiples of the blade-passing frequency Bn/60 Hz. The amplitude of each harmonic is given by Eq. (3) without the $e^{-imB\Omega t}$ term and the corresponding sound pressure level is 124.572 + 20 log (amplitude), where the amplitude is expressed in psf. This equation

follows from the definition of sound pressure level, 20 log (p/p_0) dB, where p is the rms sound pressure (= pressure amplitude $/\sqrt{2}$) and p_0 is the reference pressure (0.0002 microbar = 4.177×10^{-7} psf). The constant 124.572 equals -20 log $(\sqrt{2}\ (4.177 \times 10^{-7}))$.

For static operation, torque loading noise is a maximum in the propeller plane, symmetrical about the propeller plane, and zero on the axis. Thrust loading noise, on the other hand, has two lobes at about $\psi = 45^{\circ}$ and 135° and is zero on the axis and in the propeller plane. Addition of these two loading noises results in a maximum noise about 15° behind the propeller plane. In flight these directivity patterns are somewhat distorted. These characteristics of the directivity pattern are not readily apparent from an examination of Eq. (3). However, they may be demonstrated by calculation using the propeller noise detectability program. Alternatively, if the far-field approximation is used the equation for harmonic loading noise may be changed to a form which readily shows the directivity pattern discussed. This equation is presented as Eq. (5) in a following section.

A significant result of the assumption of constant blade loading is that the propeller noise field is symmetrical about the propeller axis and, therefore, the location of field point, or observer, may be specified in terms of only two variables (e.g., X and Y).

3. HARMONIC THICKNESS NOISE THEORY

The development of the harmonic thickness noise theory used by the propeller noise detectability program is presented in Ref. (23) and will not be repeated here. It assumes that a doublet, or dipole, moving along a helical path is the noise source. The disturbance pressure is proportional to the strength of this doublet which, in turn, is proportional to the product of blade chord and thickness. The proportionality factor is called the thickness noise doublet strength proportionality factor by Arnoldi, who presents a method for computing this factor from a chordwise pressure distribution over the blade airfoil. However, it is usually satisfactory to use an approximate area formula for thin airfoils which states that this factor equals the ratio of the blade section cross-sectional area to the product of blade chord and thickness. Typical values of the factor are near 0.7.

Arnoldi's[23] equation for thickness noise, after modifications described in Appendix I, is

$$p_m = e^{-imB\Omega t} \frac{\rho m^2 \Omega^2 B^3}{2\pi^2 (1 - M^2)} \int_{hub}^{tip} Khb \int_0^{\pi} \frac{\cos (mB\phi)}{S}$$

$$\left[\left\{ \left(\frac{\sigma}{S}\right)^2 + \left(\frac{M}{kS}\right)^2 \left(1 - 3\left(\frac{X}{S}\right)^2\right) \right\} (1 - M)^2 (\cos (k\sigma) - i \sin (k\sigma)) \right.$$

$$\left. + \frac{M}{kS} \left\{ M \left(1 - 3\left(\frac{X}{S}\right)^2\right) - 2\frac{X}{S} \right\} (\sin (k\sigma) + i \cos (k\sigma)) \right] d\phi\, dr \qquad (4)$$

The propeller noise detectability computer program uses the same method to integrate this equation as it uses for the loading noise Eq. (3).

It can be seen from Eq. (4) that thickness noise increases as the blade cross sectional area is increased, by increasing chord for example. Calculations by Hamilton Standard show that thickness harmonic noise is likely to predominate over loading harmonic noise if the propeller is lightly loaded or if the blade is large. For static operation, thickness noise is a maximum in the propeller plane, is symmetrical about the propeller plane, and is zero on the axis. In flight this directivity pattern is somewhat distorted. The phase of the pressure changes induced by the two harmonic noise sources is such that they tend to add behind the propeller plane and to subtract in front of the propeller plane. These characteristics are not readily apparent from an examination of Eq. (4) but have been demonstrated by calculations performed by the propeller noise aural detectability program.

4. FAR-FIELD APPROXIMATION

If the field point is far from the propeller, the equations for loading and thickness harmonic noise may be simplified. The dividing line between the near-field, in which only equations (3) and (4) are valid and the far field, in which equations (5) and (6) are also valid, is generally set at 3 to 5 diameters. The computer program uses 5 diameters as a criterion. In the far-field, terms with higher orders of the reciprocal of the distance became insignificant and therefore it is possible to perform the circumferential integration analytically, resulting in Bessel functions of the first kind appearing in the equation. Often the radial integration is replaced by an effective-radius approximation, but this approximation has not been used in the propeller noise detectability program.

Because of the saving in machine time, and because the near-field calculations may encounter numerical problems with circumferential integration at low noise levels, it is recommended that the far-field approximation be used whenever possible. Sample computer runs have shown agreement in SPL levels computed by the near-field and far-field methods. However, the oscillatory pressure components of the ground

pressures do not agree. This disagreement is acceptable because a phase term which is left out of both the following far-field noise equations does not change the relative phase between the loading and thickness noise pressures.

The equation for far-field loading noise is:

$$p_m = e^{-imB\Omega t} \frac{\rho\Omega^2 D^4}{4\pi^3 S_0} \int_{hub}^{tip} \frac{r}{b\cos\theta} \sin\left(\frac{mBb\cos\theta}{2r}\right) \left[-\frac{(M + X/S_0)\Omega}{a(1 - M^2)^4} \frac{dC_T}{dr} + \frac{D}{2\pi r^2} \frac{dC_p}{dr} \right] \left[J_{mB} - \frac{(1 - M^2)Yr}{2S_0^2} (J_{mB-1} - J_{mB+1}) \right] dr \qquad (5)$$

Appendix I includes the derivation of Eq. (5). The argument of the Bessel functions is $mB\Omega Yr/aS_0$. The characteristics of the Bessel functions in this equation are such that they are zero if the argument is zero. Therefore Eq. (5) shows that for field points on the propeller axis, where Y = 0, there is no loading noise, as was discussed earlier in connection with the near-field Eq. (3). The torque loading noise is a maximum for field points in the propeller plane where the argument of the Bessel function, and therefore the function itself, is a maximum. The thrust loading noise, on the other hand, for static operation (i.e., M = 0) is shown by Eq. (5) to be zero in the propeller plane where X = 0. In addition, behind the propeller plane (X < 0) the thrust and power terms add and ahead of the propeller plane (X > 0) they partially cancel. Calculations have shown that the combined effect is that the harmonic loading noise is a maximum about 15° behind the propeller plane for static conditions.

The equation for far-field thickness noise derived in Appendix I is:

$$p_m = e^{-imB\Omega t} \frac{\rho m^2\Omega^2 B^3}{2\pi(1 - M^2)^2} \frac{(S_0 + MX)^2}{S_0^3} \int_{hub}^{tip} Khb \left[J_{mB} - \frac{(1 - M^2)Yr}{2S_0^2} (J_{mB-1} - J_{mB+1}) \right] dr \qquad (6)$$

As discussed above, the Bessel functions in Eq. (6) cause the calculated thickness noise to be a maximum in the propeller plane for static operation and zero on the propeller axis, thus substantiating the statements made about the directivity pattern of thickness noise in the preceding section.

The two Bessel functions J_{mB-1} and J_{mB+1} appear because a more-exact far-field approximation than is usually presented in the literature is employed. This approximation as used here is:

$$\int_0^{2\pi} \frac{e^{-imB\phi - ik\sigma}}{S} d\phi \approx 2\pi i^{mB} \frac{e^{-ik\sigma_0}}{S_0} \left[J_{mB} - i \frac{(1 - M^2)Yr}{2S_0^2} (J_{mB-1} - J_{mB+1}) \right] \tag{7}$$

This equation differs from that originally published by Arnoldi because a typographical error has been corrected.

5. EFFECT OF HARMONIC LOADS ON LOADING NOISE

The theory for harmonic loading noise which resulted in Eq. (3) contains the assumption that the blade loading does not vary as the blade rotates. This assumption permits some analytical simplification and is expected to be valid if the propeller axis is not inclined to the flight direction and there is no interference from non-symmetrical objects. For a helicopter in forward flight, for example, this assumption cannot be expected to be valid and therefore far-field equations for rotor harmonic loading noise with unsteady harmonic loads were developed (e.g., Refs. (19) to (22)). The Fourier components of the thrust and torque loads are used. The zero-order loads are the average steady-state loads. The equation for the mth harmonic or loading noise pressure in the far-field derived in Appendix I is:

$$p_m = \sum_{\lambda=0}^{\infty} \frac{i^{-(mB-\lambda)}}{4\pi d} \left[\frac{mB\Omega X}{ad} \left\{ ia_{\lambda T} \left(J_{mB-\lambda} + (-1)^{\lambda} J_{mB+\lambda} \right) \right.\right.$$

$$\left. -b_{\lambda T} \left(J_{mB-\lambda} - (-1)^{\lambda} J_{mB+\lambda} \right) \right\} - \frac{1}{r^2} \left\{ ia_{\lambda Q} \left((mB-\lambda) J_{mB-\lambda} \right.\right.$$

$$\left. + (-1)^{\lambda} (mB+\lambda) J_{mB+\lambda} \right) - b_{\lambda Q} \left((mB-\lambda) J_{mB-\lambda} - (-1)^{\lambda} \right. \quad (8)$$

$$\left.\left. \left. (mB+\lambda) J_{mB+\lambda} \right) \right\} \right]$$

where $a_{\lambda T}$ and $b_{\lambda T}$ are the real and imaginary components of the thrust harmonic T_λ, and $a_{\lambda Q}$ and $b_{\lambda Q}$ are the real and imaginary components of the torque harmonic Q_λ. Note that the $b_{0T} = b_{0Q} = 0$. Furthermore, with the assumption that the blade loads are concentrated at an effective radius of 0.4D, one has $a_{0T} = T$ and $a_{0Q} = Q = 5252.1$ HP/n. Except for an unusual combination of harmonic load components, the presence of the harmonic loads will increase the harmonic loading noise sound pressure level. This increase is largest near the propeller axis and in the higher harmonic orders.

In general, it is possible to predict the lower-order harmonic loads required in Eq. (8) due to angle of attack of the propeller axis or interference from the wings and fuselage. Hamilton Standard has a computer program that can predict up to four loading harmonics due to interference. A separate program which can use many more load harmonics predicts the resulting loading noise. Unfortunately, the present limit of four loading harmonics means that not even the first noise harmonic can be predicted accurately. It appears from the test data measured during the experimental phase of this contract that harmonic loads are present even with an apparently "clean" installation. In this case neither the phase nor the radial distribution of the harmonic loads may be known. Therefore the discussion of the effect of harmonic loads on propeller loading noise will be restricted to the far-field effective-radius static case with a random phasing of the harmonic loads assumed.

Lowson and Ollerhead[20] to [22] have shown that only loading harmonics or orders in the range $mB(1 \pm V_t/a)$ contribute significantly to the harmonic noise of order m. Therefore a noise pressure with an amplitude squared of

$$p_m^2 = \sum_{\lambda = mB(1-V_t/a)}^{mB(1+V_t/a)} \left[\frac{mB\Omega}{4\pi S_0 a} J_{mB-\lambda} \right]^2 \left[\left(\frac{X_p T_\lambda}{S_0} \right)^2 + (mB-\lambda)^2 \left(\frac{aQ_\lambda}{mB\Omega r^2} \right)^2 \right] \quad (9)$$

must be added to that computed from Eq. (5). Equation (9) is derived in Appendix I.

Depending on the magnitude of the harmonic loads, they will add significantly to the levels of harmonic loading noise for uniform loads computed from Eq. (5). The harmonic loads are most likely to increase the higher harmonics. Also, with harmonic thrust loads present loading noise is predicted to occur on the axis whereas for uniform loading the previous discussion has shown that there is no harmonic noise on the axis.

Levels for the loading harmonics of helicopter rotors were presented by Ollerhead and Lowson[21]. They suggest that the level of a load harmonic equals the steady-state load divided by the load order to the 2.5 power. For a compressor the exponent appears to be 1.0 rather than the 2.5 for helicopters. Estimates of the loading harmonics were derived from the harmonic noise data measured in the experimental program and are discussed in a later Section VII.2b, where an exponent of 1.43 is recommended.

SECTION V

BROAD-BAND NOISE THEORY

1. INTRODUCTION

The first theory of vortex noise was developed by Yudin[13] in 1944 and was based on a dimensional analysis of flow parameters around rotating rods. The theory is based on the observation that a Karman vortex street is observed behind the rod over a significant range of Reynolds numbers and produces an oscillating force on the rod. Because of difficulties with a rigorous mathematical analysis, later studies have concentrated on determining empirical coefficients which apply to propellers or helicopter rotors. These will be discussed in the next section.

Most empirical broad-band noise prediction methods are incomplete because they do not predict directivity effects, noise levels and spectrum shape. All three are required for a detectability study. Also, they involve gross parameters such as total thrust and blade area without including the radial distribution of these parameters. Two methods, developed previously by Hamilton Standard, are complete and are incorporated into the propeller noise detectability program as options. A third method was developed in the present program and is incorporated into the propeller noise detectability program. This new method predicts the broad-band noise level in each 1/3-octave band and, unlike most other methods, uses a detailed description of the propeller blade geometry. Thus, it is the most complete method for predicting propeller broad-band noise available. The selection of the 3 empirical coefficients required by the method is based on noise data measured during the test phase of this program and is discussed in a later section. Development of this new broad-band noise method is one of the major tasks of this contract and is presented in Section V.3.

A study of the effect of airfoil shape (or chordwise thickness distribution) on vortex noise follows in Section V.4. Although this study showed only small improvements due to airfoil shape the possibility of noticeable improvement was considered sufficient to incorporate NACA series 66A section in the blades of a new low-noise propeller designed, fabricated and tested in this contractual program.

2. PREDICTION METHODS IN THE LITERATURE

From a dimensional analysis of a cylinder in a stream, Yudin[13] showed that the vortex sound power is proportional to $\rho V^6 D \ell S_t^2 / a^3$ where D is the diameter and ℓ the length of the cylinder, and the Strouhal number S_t is about 0.2. The frequency of the sound is $S_t V/D$. Unfortunately this theory cannot predict the absolute level of the vortex noise because the proportionality factor is not known theoretically.

Several investigators have developed equations for sound pressure levels of propellers or rotors based on Yudin's formulation. Usually the product $D\ell$ is replaced by an area S_b, and suitable reference values for S_t, ρ and a are introduced. As a result, the overall sound pressure level becomes proportional to 10 log $(S_b V^6/d^2)$. A directivity pattern of a force dipole aligned with the axis is often assumed. Therefore 10 log $(\cos\psi)$ should be added to the SPL and the vortex noise is a maximum on the propeller axis and zero in the propeller plane. Some investigators have included a frequency spectrum with a sound level relative to the overall SPL and the frequency referenced to a peak frequency (e.g., see Figure 7).

Experimental data of Stowell and Deming and others led to Hubbard's[24] expression for the sound pressure level of propellers at a distance of 300 feet:

$$SPL = 10 \log \frac{3.8\, S_b\, V_{.7}^{6}}{10^{11}} \text{ dB} \tag{10}$$

The formulation is inadequate for detectability studies, however, because no directivity effect or frequency information is provided.

Davidson and Hargest[25] fitted experimental helicopter noise data at 500 feet distance by an equation of the form:

$$SPL = 10 \text{ Log } (V_t^6 C_L^2 S_b) + 10 \log (\cos\psi) - 84 \text{ dB} \tag{11}$$

Eq. (11) differs from (10) by the inclusion of a C_L term and by introducing an extreme directivity correction (no vortex noise in rotor plane). However, no data on frequency distribution is presented.

Schlegel, King and Mull[19] present an equation of the following form for sea level 70°F conditions:

$$SPL = 10 \log (V_{.7}^2 T^2/S_b d^2) + 13.8 \text{ dB} \tag{12}$$

The vortex noise in any octave band is computed by using a spectrum shape presented graphically and a peak frequency determined by the equation:

$$f = \frac{0.28\, V_{.7}}{h_{.7} \cos\alpha + b_{.7} \sin\alpha} \text{ Hz} \tag{13}$$

This correlation of rotor vortex noise includes a frequency spectrum but is limited to a direction of 17° behind the rotor. No directivity effect is presented.

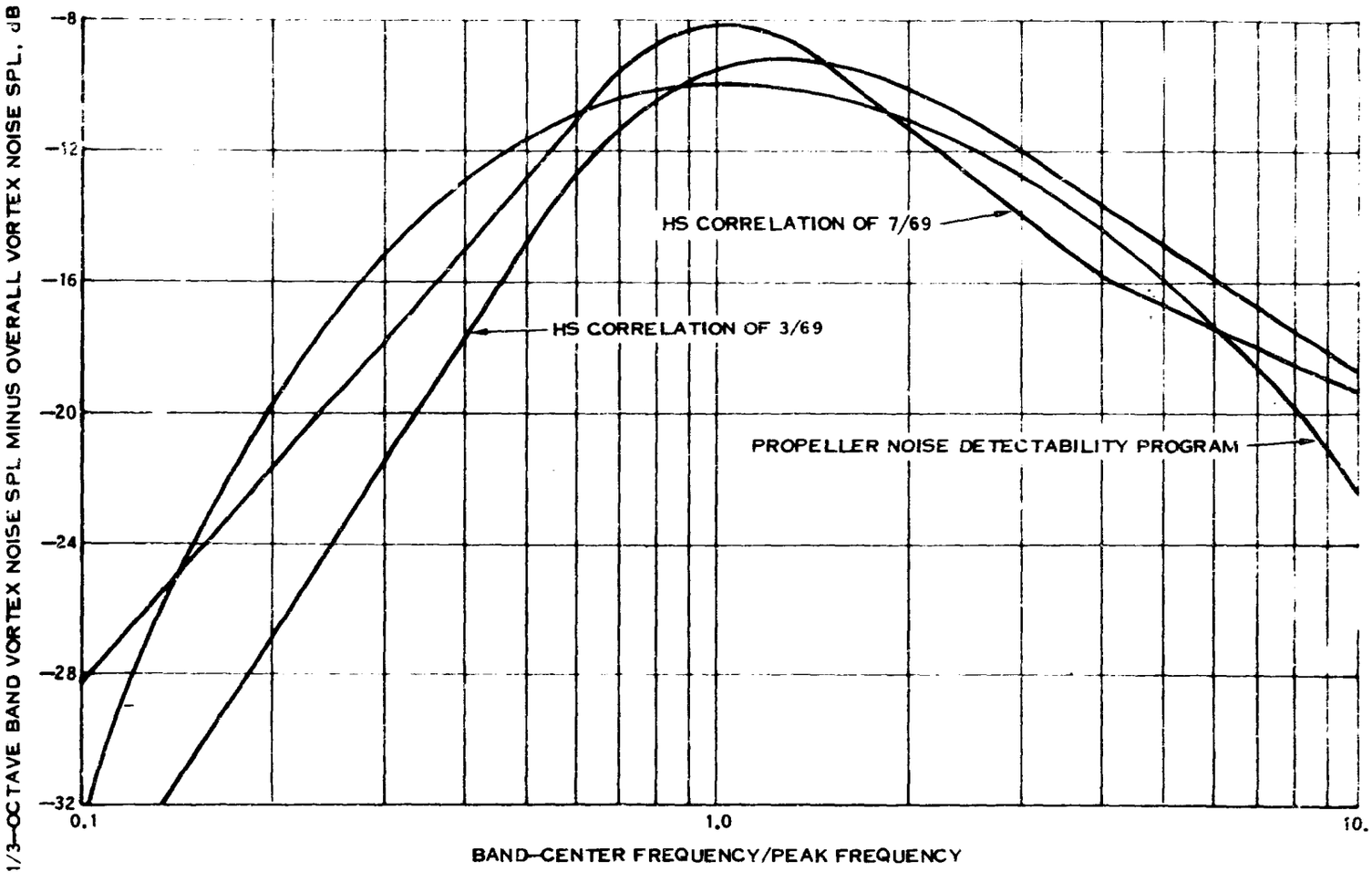

Figure 7. Broad-Band Noise Spectra

Stuckey and Goddard[26] obtained the following formula from tests of a particular rotor:

$$SPL = 10 \log (V_t^{2.68} T^{1.66}/d^2) + 20 \log (\cos \psi) + 2.8 \text{ dB} \tag{14}$$

and introduce another frequency spectrum.

Ollerhead and Lowson[21] discuss previous work on vortex noise and state that what has been considered to be a broad-band vortex noise may really be high-order harmonics of rotational noise which usual data-reduction procedures do not show as occurring at discrete frequencies. With very-narrow-band filters some data presented do show the presence of what appears to be high-order harmonic rotational noise. An equation for directivity is suggested which, unlike other equations, has a total variation of only 10.5 dB in overall noise from on the axis of rotation to in the plane of the rotor. This equation is

$$\Delta SPL = 10 \log \left(\frac{\cos^2 \psi + 0.1}{\cos^2 70^o + 0.1} \right) \text{ dB} \tag{15}$$

Widnall[27] correlates measured rotor vortex noise data in the form

$$SPL = 10 \log (V_t^6 S_b/d^2) + f (T/S_b V_t^2) \text{ dB} \tag{16}$$

where the function f is plotted as a band encompassing plotted data. For low values of the parameter $(T/S_b V_t^2)$, which are typical of a quiet propeller, the function f is constant. This correlation is based on a quasi-two-dimensional model of vortex noise derived from that Yudin[13]. However, frequency and directionality data are not presented.

Sharland[28] investigated possible mechanisms of broad-band noise generation in axial flow fans. One mechanism is alternating "vortex shedding" at the trailing edge of the blade which produces lift fluctuations. By making some estimates of the frequency and a correlation area he obtained the following formula for sound power:

$$W = \frac{\rho}{120 \pi a^3} \int b V^6 R^{-.4} dr \tag{17}$$

If, further, an ideal dipole directivity distribution is assumed, the maximum rms acoustic pressure is:

$$p = \frac{\rho}{4 \sqrt{10 \pi} ad} \sqrt{\int b V^6 R^{-.4} dr} \tag{18}$$

For a direction which is not normal to the airfoil the rms pressure should be multiplied by the cosine of the angle to the normal. Another mechanism investigated by Sharland[28] is the turbulent boundary layer pressure fluctuations on the surface. Using a value of the rms surface pressure fluctuation of $0.012\ \rho V^2$, which experimental data supports, Sharland derives an equation for the sound power

$$W = \frac{10^{-7}\rho}{a^3} \int bV^6 dr \tag{19}$$

Again assuming a dipole directivity distribution, the maximum rms acoustic pressure is:

$$p = \sqrt{\frac{3}{4\pi 10^7}}\ \frac{\rho}{ad} \sqrt{\int bV^6 dr} \tag{20}$$

For a Reynolds number of one million the ratio of the sound pressure level due to vortex shedding (Eq. (18)) to the sound pressure level due to turbulent boundary layer fluctuations (Eq. (20)) is 20 dB. Therefore, noise due to turbulent boundary layer fluctuations is not significant relative to noise due to vortex shedding. A third mechanism considered by Sharland is turbulence in the airflow inducing fluctuations in lift. His equation for the sound power due to this mechanism is:

$$W = \frac{\rho}{48\,\pi a^3} \int \phi^2\, bV^4\, \overline{(w)^2}\, dr \tag{21}$$

where ϕ is the average lift curve slope and $\overline{(w)^2}$ is the mean turbulent velocity fluctuation. Sharland concludes that "broad-band noise in fans arises from vortex shedding at the blade trailing edges under normal conditions, but that any large scale turbulence can increase the noise significantly".

Hamilton Standard developed two complete empirical vortex noise procedures in 1969. The first used Schlegel, King and Mull's[19] formula for noise level and peak frequency and the directivity formula of Ollerhead and Lowson[21]. The formulae used are:

$$SPL = 10 \log \left(\frac{V_t^2 C_L^2 S_b\, (\cos^2 \psi + 0.1)\ .217}{d^2} \right) - 44.645 \text{ dB} \tag{22}$$

$$\text{peak frequency} = \frac{0.28\ V_{.7}}{h_{.7} \cos\alpha + b_{.7} \left|\sin\alpha\right|} \text{ Hz} \tag{23}$$

The frequency spectrum is labelled "HS Correlation of 3/69" in Figure 7.

The second empirical procedure uses the formulation of Widnall[27] and is based on static noise data obtained by Hamilton Standard from a 4-bladed propeller designed for a quiet STOL aircraft. This propeller blade is similar to blade design 47X-394 tested in the first test period of the present program.

$$SPL = -71.02 + 57000\left(\frac{T}{S_b V_t^2}\right) + 10 \log\left(\frac{V_t^6 S_b}{d^2}\right) - 3.3 \sin^2(\psi + 10^o)\,dB \quad (24)$$

$$\text{peak frequency} = \frac{0.06\, V_{.7}}{h_{.7}\,(1-.265\, X_{stall})}\,Hz \quad (25)$$

X_{stall} is the radius ratio where the section angle of attack is 11^o. The frequency spectrum is labelled "HS Correlation of 7/69" in Figure 7. These two procedures are included as options 2 and 3 in the propeller noise detectability computer program because they are complete, unlike most other prediction methods described in this section, and because they are well understood.

The correlations of broad-band noise described above were derived for propellers and helicopter rotors. Another source of broad-band noise is a gliding aircraft. Two published reports, which present and correlate broad-band data obtained with several aircraft, are discussed in this paragraph. Smith et al[29] correlates overall noise level from three sailplanes by the formula

$$SPL = 10 \log (V^6 S_b/d^2) - 42.7\,dB \quad (26)$$

where S_b is the wing area with turbulent flow. Inspection of the data indicated a better fit would be obtained by the formula

$$SPL = 10 \log (V^{3.1} S_b/d^2) + 19.1\,dB \quad (27)$$

which shows a smaller variation with velocity. Lockheed[30] measured data from 5 gliding aircraft with engines off and propellers feathered and correlated the data by a formula which may be converted to the form

$$SPL = 10 \log \left(\frac{V^6 S_b}{d^2} \quad \frac{\text{chord}}{\text{span}}\right) - 15.2\,dB \quad (28)$$

A 1/3-octave band spectrum is presented with the peak frequency defined by the relationship

$$f = 1.1\, V/h\ Hz \quad (29)$$

This spectrum is labelled as "propeller noise detectability program" in Figure 7.

To summarize, it can be seen that most of these vortex noise prediction methods show that the SPL varies as 10 log ($V^6 S_b/d^2$). This selection of variables is probably influenced by Yudin's[13] analysis. However, a smaller variation with velocity is suggested by Smith's sailplane data (Eq. (27)) and by Sharland's analysis of "vortex shedding" noise (Eq. (17)).

3. NEW HAMILTON STANDARD VORTEX NOISE THEORY

A major task of this study program was the development of an integration technique to predict propeller broad-band noise and to incorporate this technique into the propeller noise detectability computer program. The source of the broad-band noise is assumed to be an oscillating force normal to the blade chord. The amplitude and frequency of this force are related to the flow conditions and blade geometry in a way which would correspond to Yudin's [13] theory. Therefore, the predicted broad-band noise might be called vortex noise. However, unlike the various correlations of propeller and rotor broad-band noise previously discussed which involve overall parameters such as tip speed, total thrust and blade area, the theory developed during this contract includes the radial distribution of blade geometry and flow conditions as parameters. The broad-band noise at the observer is obtained by numerical integration in the circumferential and radial coordinates.

The theory does not determine the magnitude of the oscillating force or its frequency. However, these parameters are proportional to a force factor C_F and a frequency factor C_f respectively. Values of these two factors were determined by correlating predicted 1/3-octave band noise levels with measured data obtained during the experimental program discussed in Section VI of this report.

The theory is based on Lowson's theory for the sound field of a moving force[31]. Cartesian coordinates, with subscripts 1, 2 and 3, are used and the origin of these coordinates is the propeller center. The "1" axis is the propeller axis with a positive ordinate forward of the propeller. The field point lies in the "1" - "2" plane. The point force is translating along the positive "1" axis at a Mach number of M and rotating about the "1" axis at a radius of r and a speed of Ω rad/sec. The force is oscillating at a circular frequency ω and is normal to the blade chord. It is resolved into three components F_1, F_2 and F_3.

The basic result of Lowson's paper is the following equation for the far-field sound pressure radiation from a point force in arbitrary motion

$$p = \left[\frac{x_j - y_j}{4\pi (1-M_r)^2 \, ad^2} \left\{ \frac{\partial F_j}{\partial t} + \frac{F_j}{1-M_r} \frac{\partial M_r}{\partial t} \right\} \right] \qquad (30)$$

where x_j and y_j are the coordinates of the observer and source, respectively, and M_r is the component of the convection Mach number in the direction of the observer.

The axial component of the force F_1 is proportional to the magnitude of the force F and the cosine of the blade angle θ, therefore

$$F_1 = F \cos\theta \, e^{-i\omega t} \tag{31}$$

The other two components vary with circumferential angle ϕ:

$$F_2 = F \sin\theta \sin\phi \, e^{-i\omega t} \tag{32}$$

$$F_3 = -F \sin\theta \cos\phi \, e^{-i\omega t} \tag{33}$$

The three components of the convection Mach number are:

$$M_1 = M \tag{34}$$

$$M_2 = -\frac{r\Omega}{a} \sin\phi \tag{35}$$

$$M_3 = \frac{r\Omega}{a} \cos\phi \tag{36}$$

The coordinates of the observer are:

$$\begin{aligned} x_1 &= X_p \\ x_2 &= Y \\ x_3 &= 0. \end{aligned} \tag{37}$$

and of the point force are:

$$\begin{aligned} y_1 &= 0. \\ y_2 &= r\cos\phi \\ y_3 &= -r\sin\phi \end{aligned} \tag{38}$$

Therefore

$$d^2 = X_p^2 + (Y - r\cos\phi)^2 + r^2 \sin^2\phi \tag{39}$$

The component of the convection Mach number in the direction of the observer is:

$$M_r = \frac{(x_j - y_j)\, M_j}{d} \tag{40}$$

which becomes, upon substituting Eqs. (33) to (39),

$$M_r = \frac{MX_p}{d} - \frac{\Omega r}{ad} \sin\phi\,(Y - 2r\cos\phi) \tag{41}$$

Upon substituting into Eq. (30), the equations for the pressure field due to the three components of the force become:

$$p_1 = -\frac{iX_p\,\omega F\cos\theta}{4\pi\, a(1-M_r^2)\, d^2}\, e^{-i\omega t}$$

$$p_2 = \frac{(Y - r\cos\phi)\, F \sin^{9}}{4\pi\, a(1-M_r^2)\, d^{2}} \cdot \left[-i\omega\sin\phi + \Omega\cos\phi\right] e^{-i\omega t} \tag{42}$$

$$p_3 = \frac{r\, F\sin\theta\sin\phi}{4\pi\, a(1-M_r^2)\, d^2} \left[i\omega\cos\phi + \Omega\sin\phi\right] e^{-i\omega t}$$

These three terms are summed to derive the desired equation for the sound pressure:

$$p = \frac{F}{4\pi\, a(1-M_r^2)\, d^2} \left[-i\,\omega \left\{ X_p\cos\theta + (Y - 2r\cos\phi)\sin\theta\sin\phi \right\} + \right.$$
$$\left. \Omega\sin\theta \left\{ r\sin^2\phi + (Y - r\cos\phi)\cos\phi \right\} \right] e^{-i\omega t} \tag{43}$$

Integration over the angle ϕ and radius r determines the total noise at the field point.

The expressions for the magnitude and frequency of the oscillating force were derived from the form of the expressions for broad-band noise presented in the preceding section. The form of these expressions for overall noise is SPL $\approx$ 10 log $(V^6 S_b)$ and for peak frequency is $f = S_t V/h$ Hz. Therefore, the frequency is evaluated from the equation

$$f = \omega/2\pi = C_f\, V/h \text{ Hz} \tag{44}$$

where C_f is an empirical frequency coefficient and V is the sectional velocity determined by the propeller performance program. Experimental data[32] on vortex shedding frequency from an NACA0006 airfoil show that C_f is about 0.042. The equation for the force level finally selected is:

$$F = C_F \rho h \sqrt{b \Delta r} \; V^2 \left(\frac{R}{10^6} \right)^{exp} \tag{45}$$

The force coefficient C_F, like the frequency coefficient C_f, is an empirical factor to be derived from test data. The Reynolds number factor was introduced to obtain a better fit of the trend of broad-band noise level with rpm to experimental data from this program which show a variation like 10 log V^4 rather than 10 log V^6. Some correlations of vortex noise include a thrust term, suggesting that angle of attack or lift coefficients should be introduced into Eq. (45). Some unpublished data available to Hamilton Standard shows that angle of attack changes do alter the noise from an airfoil in a jet. However, since there is insufficient data to establish a trend at this time, this factor is not included. It is believed to be small for the small range of lift coefficients associated with a quiet propeller.

Because of the expected random phase of the force from one blade to another, the sound power of one blade is multiplied by the number of blades. Therefore, doubling the number of blades increases the broad-band SPL by 3 dB.

The phase of the oscillating force is expected to be correlated only over a small radial distance called the "correlation distance". For a two-dimensional airfoil in a uniform stream it is well known that theory predicts that a reduction of the correlation length from a value equal to the span reduces the radiated sound power. At the beginning of this contract it was planned to introduce a correlation length explicitly into the broad-band calculation program. However, this plan was changed for several reasons. First, no data were available in time to provide a good value for the correlation length of a non-rotating airfoil. Second, with the assumption that the correlation length equals the chord (corresponding to the diameter of a rod, a representative value), only about 5 correlated areas were required for the moderate chords of the first blades tested. With the wider blades tested at the end of the program even fewer correlated areas would be used. It is believed that more than 5 areas are required to provide a valid calculation of vortex noise. Third, the combination of radial changes in airfoil thickness and sectional velocity result in changes in frequency computed from Eq. (44) of over 2 orders of magnitude. This large radial gradient in frequency should reduce the correlation length significantly. No data on correlation lengths for rotating blades was available for use in this program. Lastly, programming is simplified if the ten radial stations used by the Hamilton Standard propeller performance program are used, thereby avoiding interpolation. Therefore, it was decided to sum the squares of the sound pressures calculated for each of the ten radial stations provided by the propeller performance program. These same radial stations are used to compute harmonic rotational noise.

Theory[33, 34] shows that a harmonically-oscillating force moving in a circular path produces a series of tones centered about the force frequency. The theory[33] also shows that a source of white noise moving in a circular path produces a white noise at the observer. However, it is known from flight data[29, 30] and from tests of airfoils in jets that the noise frequency spectrum is neither a discrete tone nor a white noise but a peaked broad-band spectrum like those shown in Figure 7. The theory for this type of noise spectrum has not been developed and at the time this program was started the development of the theory was believed to be beyond the scope of the program. An extension of the theory by Tanna and Morfey[34] was not available when the new vortex noise theory was developed. The possibility of further refinement of the theory using their approach warrants further study. For this reason, and because of the other approximations discussed above which are used, it was decided to use the following procedure to integrate Eq. (43):

a. Integrate radially the squares of the sound pressures in each 1/3-octave band using the 10 radial stations of the propeller performance program.

b. For each radius, sum the squares of the sound pressures calculated for 36 values of circumferential angle ϕ at 10^{o} increments.

c. For each radius r and angle ϕ, compute the pressure amplitude and frequency (with a Doppler correction) from Eqs. (39), (41), (43), (44) and (45).

d. For each radius and angle this pressure amplitude is converted to an overall vortex noise SPL and the noise frequency is considered to be a peak frequency. The noise SPL in each 1/3-octave band is computed from the overall vortex noise SPL and peak frequency using the broad-band noise spectra in Figure 7.

A numerical procedure based on the theory described in this section is coded in the propeller noise detectability program as vortex noise option 1.

4. EFFECT OF AIRFOIL SHAPE ON VORTEX NOISE

The design of low-noise propellers involves a compromise between rotational noise and broad-band vortex noise. It would be useful to find geometric parameters that have little or no effect on rotational noise but which could be adjusted to reduce the vortex noise. One such parameter is the blade airfoil shape, or thickness distribution. A presently-accepted theory for propeller vortex noise[28] contains no direct effect of airfoil shape on vortex noise. However, the mechanism by which vortex noise is generated depends strongly on the airfoil boundary layer. This, in turn, can be strongly influenced by changes of airfoil shape. For moderate subsonic flight speeds, the choice of propeller airfoil shape traditionally had been determined by a need for large values of drag-divergence Mach number. It seemed possible that

some other airfoil sections might provide reductions in vortex noise at the lower Mach numbers encountered with advanced low-noise propellers. Therefore, a study of the effect of airfoil shape on vortex noise was conducted.

To establish analytically the effect of airfoil shape on broad-band vortex noise, one must start with a clear definition of the mechanism by which such noise is generated. Simplified analyses have tried to relate the broad-band noise of a slender streamlined airfoil to that of a bluff body having the same maximum thickness. The bluff body sheds an unsteady wake and a vortex street; fluctuations of wake flow direction are accompanied by fluctuations of normal force on the body. Thus, the separated flow downstream of the body generates an acoustic dipole oriented normal to the airflow. A large fluctuating wake does not occur downstream of conventional airfoils, so the direct analogy between airfoil and bluff-body flows is not correct. In Ref. 28 a different approach was used. The attached turbulent boundary layer was assumed to fluctuate about its root-mean-square position. This fluctuation was assumed to cause a fluctuation of instantaneous angle of attack, whose magnitude in radians was given by the ratio of trailing-edge boundary layer thickness to airfoil chord. The instantaneous normal force was assumed equal to the product of the normal force coefficient slope and the fluctuation of angle of attack. Thus, the acoustic dipole would be caused by shedding of vortices caused by fluctuations in bound vorticity as the outer potential flow adjustments to the unsteady viscous inner flow.

This description would be reasonable if boundary layers on airfoils grew linearly with chordwise distance. However, different airfoil shapes with different chordwise pressure distributions could have vastly different variations of boundary layer growth along their chords but the same boundary layer thickness at the trailing edge. For the study described in this section, it was assumed that turbulent fluctuations in the boundary layer displacement thickness along the airfoil upper and lower surfaces were not correlated. The chordwise distribution of the difference between these two displacement thicknesses could then be regarded as an instantaneous camber line whose shape and incidence undergoes fluctuation. The normal force coefficient at any instant of time was assumed proportional to that which would be computed from steady-state theory[35] for a thin airfoil with that combination of camber and incidence. (Within that theory, the effects of geometric camber, viscous-induced camber caused by the time-average difference between the upper-surface and lower-surface displacement thickness, and fluctuations in that viscous-induced camber can be linearly added.) The fluctuating normal force coefficient then becomes a sum of three contributions. One comes from a fluctuation of mean-line angle of attack as in Ref. 28. The other two are the design lift coefficient of the instantaneous camber line and the fluctuating difference between the instantaneous angle of attack and the camber-line ideal angle of attack. That is, one must consider both the incidence of a hypothetical straight line joining the effective leading and trailing edge points and the combined camber and incidence of the mean camber line between those points.

To use this approach, a camber line must be defined from the calculated chordwise variation of displacement thickness. At first glance, ordinates of this line might be assumed proportional to the local displacement thickness on one surface. That assumption would not be correct because it would fail to reproduce the relatively large effects expected in a region where a strong local adverse pressure gradient occurs, but the boundary layer is relatively thin. Instead, the camber line was calculated as the difference between upper-surface and lower-surface displacement thicknesses, calculated for an uncambered airfoil at zero incidence, but with a different turbulence level at each surface. The assumed turbulence levels, 0.1 and 1.0 percent, were not large enough to cause significant chordwise movement of the transition region. Their primary effect was on the displacement-thickness growth rate in the transition region and in regions of adverse pressure gradient.

Boundary layer growth was calculated with a computer program originally developed for prediction of heat transfer to turbine blades and vanes. Airfoil pressure and temperature distributions, free-stream flow properties, surface roughness, and turbulence level were supplied as input. The computer program then determined the growth of the laminar boundary layer, transition region, and turbulent boundary layer. All airfoils were assumed to have 10-inch chord, 100-microinch surface roughness, and adiabatic wall temperature. Free-stream static conditions were standard sea level atmospheric, and the velocities were chosen to provide Reynolds numbers of 2×10^6 and 3×10^6 based on airfoil chord. The calculated differences in displacement thickness were smoothed and used as input to an existing digital computer program that calculates the camber-induced loading distribution and lift coefficient, and the angle of attack at which that loading would occur.

The airfoil sections were taken as uncambered, 9%-thickness-ratio NACA airfoils. Use of the NACA 0009, 65-009, 66-009, and 67-009 airfoils provided minimum-pressure locations of approximately 10, 50, 60, and 70% chord. Further comparison with the NACA 16-009 airfoil, which has its minimum pressure near 65% chord, added a brief look at the effect of the variation of adverse pressure gradient with chordwise distance. Thickness distributions and incompressible-flow pressure distributions for the NACA 0009, 66A009, and 16-009 airfoils are shown in Figure 8. The 66A009 airfoil section, which has a practical trailing-edge shape, is shown in preference to the 66-009 which has a cusped trailing edge.

At these conditions, the transition Reynolds numbers as determined by the computer program were in the range of 0.4 to 0.5×10^6 for the lower nominal turbulence level. Thus, the boundary layer always was turbulent upstream of the minimum-pressure location for all but the NACA 4-digit series airfoil. Increasing the nominal turbulence level moved the transition location forward, reducing the transition Reynolds number to about 0.25×10^6. Thus, the slope of the boundary layer displacement thickness was increased over a forward portion of the airfoil, giving a change in camber similar to that for deflection of a leading-edge flap. This change was larger for the 4-digit airfoil, for which it occurred in a region of adverse pressure gradient, than for the other airfoils. Downstream of this transitional region, the boundary

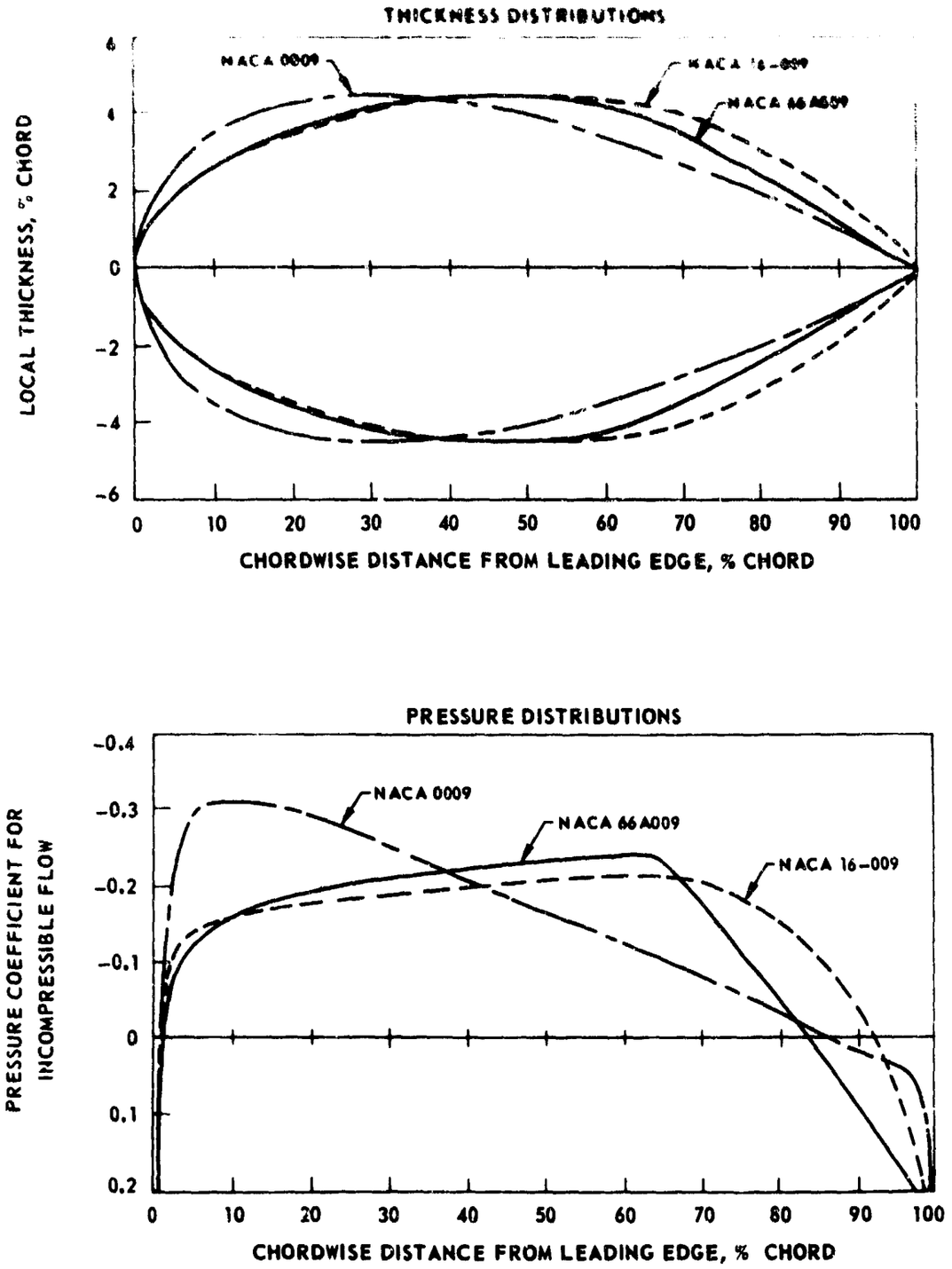

Figure 8. Typical Airfoil Thickness and Pressure Distributions

layer thickened more rapidly and was more responsive to turbulence level in an adverse pressure gradient than in a mild favorable pressure gradient. Thus, the NACA 4-digit airfoil had a rapid growth of effective camber-line ordinate on the forward portion, moderate growth along much of the chord, and more rapid growth near the trailing edge. As the airfoil section was changed to move the minimum-pressure location aft the change in ordinate was decreased on the forward portion, reduced to essentially zero along the mid-chord region, and increased near the trailing edge. Thus, the airfoil with a forward location of minimum pressure had an effective camber line that qualitatively resembled a large leading-edge flap deflected downward and a large leading-edge flap deflected upward through a small angle. Aft movement of the minimum-pressure location reduced both the effective size and effective deflection angle of the leading-edge flap and reduced the extent but increased the angle of the trailing-edge flap. Details of the calculated solutions on the aft part of the airfoil were sensitive to the velocity distribution assumed very near the trailing edge. In all cases the tabulated velocity gradient between 90 and 95% chord was arbitrarily continued to the trailing edge in place of the tabulated trailing-edge stagnation point or cusp flow.

Resulting calculated fluctuating lift coefficients are listed in Table IV. The absolute numerical values are unimportant because they are based on a steady-state lift-curve slope and a perfectly correlated flow. These effects cause the numerical values to be roughly 50 times the corresponding estimates from Ref. 28. Two sets of numbers are given for each case. The upper set are for an angle of attack (in radians) equal to the change in trailing-edge displacement thickness divided by the airfoil chord. The lower numbers are the combined effects of camber and incidence, were small at a Reynolds number of 3×10^6 but were 1/4 to 1/2 as large as those due to incidence at a Reynolds number of 2×10^6. That lower Reynolds number is representative of the tip region of practical quieted propellers. At that condition, aft movement of the minimum-pressure location had small beneficial effects until, for the 67 series airfoil, the boundary layer was dominated by the strong adverse pressure gradient on the aft region. The NACA 66 series, which has nearly the same minimum-pressure location as the NACA 16 series, has a relatively constant adverse pressure gradient. In contrast, the adverse pressure gradient for the 16 series becomes stronger as the trailing edge is approached. It was expected that a constant gradient, or even one that is initially large and becomes weaker with increasing distance, would cause less overall disturbance than an increasing gradient.

For a Reynolds number of 2×10^6, moving the minimum pressure point downstream (that is, changing from the four-digit airfoil to the 65 series and then the 66 series) caused a small increase and then decrease of calculated lift fluctuation caused by combined camber and incidence. The magnitude of this decrease corresponds to less than a 1.4 dB reduction of sound pressure level. The 16 series airfoil, with its increasing adverse pressure gradient on the aft portion, would be about 0.8 dB louder than the 66-series airfoil. Both of these airfoil series have about the same location of minimum pressure and their shapes are nearly identical over the forward half of the chord. The 66-series airfoil is slimmer than the familiar 16-series propeller

TABLE IV

FLUCTUATING LIFT COEFFICIENTS INDUCED BY BOUNDARY LAYER DISPLACEMENT

	Airfoil				
	0009	65-009	66-009	16-009	67-009
Reynolds number = 2 x 10^6					
Incidence only	0.0348	0.0285	0.0315	0.0325	0.0440
Incidence plus camber	0.0436	0.0448	0.0382	0.0419	0.0648
SPL above that for 16-009, dB	0.36	0.59	-0.80	0	3.81
Reynolds number = 3 x 10^6					
Incidence only	0.0231	0.0194	-	0.0173	-
Incidence plus camber	0.0177	0.0205	-	0.0187	-
SPL above that for 16-009, dB	-0.48	0.81	-	0	-

[illegible] over the aft part of the chord (Figure 5). A further aft movement of the minimum pressure location, obtained by use of the 67-series airfoil, caused very large thickening of the boundary layer on the aft quarter of the chord. This airfoil, which would also be expected to have poor aerodynamic performance, is predicted to be 4.6 dB noisier than the 66-series airfoil.

Although calculations were not made for the 66-series airfoil at a Reynolds number of 3×10^6, it is expected that this airfoil would also be best at that condition. The calculated effects of viscous-induced camber were much smaller at this Reynolds number than at the lower Reynolds number. Apparently this difference was caused by the smaller chordwise extent of laminar flow, which reduced the amount of forward effective camber. The indicated reduction of lift fluctuation with an increase of Reynolds number, at constant airfoil shape, is much larger than would be predicted from Ref. 28. Apparently this large numerical effect was caused by use of the same nondimensional turbulence perturbation at both Reynolds numbers. It is not obvious how this quantity should have been scaled or the extent to which this apparent trend should be believed.

In conclusion, the calculated effect of airfoil shape on broad-band vortex noise at a Reynolds number of 2×10^6 is relatively small when attention is confined to airfoils known to have good aerodynamic performance. The calculated noise was increased by use of an airfoil with poor aerodynamic performance. The NACA 66A-series of airfoils is recommended as it is about one decibel quieter than the more conventional airfoil shapes. Since the 66A sections have not been defined by NACA the following procedure is used. Up to and including, 45% chord use NACA 66-series section thicknesses. For chordwise distances $>45\%$ use NACA 65A-series section thicknesses at $(5 + 55X)/60\%$ chord where X is the % chord for the 65A-series thickness.

Hamilton Standard has two sets of noise data from tests of two 8.5-foot diameter 0V-10 propellers which show an effect of airfoil section on propeller noise. One propeller had blades made with NACA series 16 and 64 series sections and the other had blades made with NACA series 65 sections. Aside from the difference in sections, the propellers are identical. That is, the same camber, planform, thickness and twist are incorporated into both blade designs. Therefore, any difference in noise, for the same power and rpm, should be due only to the difference in blade section. Noise data were obtained at tip Mach numbers from .6 to .9, which are above that appropriate for a quiet aircraft. Analysis of harmonic noise levels determined from the far-field data shows that, for the higher harmonics, the NACA 65 sections are several dB quieter than the 16/64 sections. The data have not been analyzed for broad-band noise. These data indicate that harmonic noise can be reduced by optimizing blade airfoil section, but any effect on broad-band noise has not been determined yet.

SECTION VI

EXPERIMENTAL PROGRAM

1. INTRODUCTION

During the course of the contract, five acoustic noise test programs were conducted to provide a data bank on the noise characteristics of very-low-tip-speed propellers for the verification and development of the propeller noise detectability program. Four-bladed and two-bladed 11.25-foot diameter propellers tested as tractors were included in these test programs. In addition, a test of a four-bladed pusher propeller was included to investigate the effect of the test rig on noise. All tests were conducted on an outdoor propeller test rig located at the Hilltop Facility of Hamilton Standard. The tests were conducted during the night, generally between the hours of midnight and six a.m., when the most favorable wind and ambient noise conditions exist.

The noise was measured on a 50-foot radius with two data recording systems. One used a microphone located at ground level to measure the low frequency rotational (tone) noise and the other used a microphone located at approximately 4.5 feet from the ground to measure the mid- and high-frequency vortex noise. The effects of the ground plane on the measured noise were evaluated experimentally and appropriate corrections applied to the measured noise.

The low-frequency noise was analyzed using a narrow, constant-bandwidth frequency filter to determine the levels of the harmonics of rotational noise. The mid- and high-frequency components were analyzed by 1/3-octave bands.

2. PROPELLER TEST FACILITY

The propellers tested in this program were run on the propeller test rig shown in Figures 9 and 10. The centerline of the horizontal drive shaft is 17 feet above the ground so that the propeller ground clearance is approximately 12 feet. The shaft is direct-driven by a 100-horsepower, variable-speed electric motor whose output power with shaft rotational speed is shown in Figure 11.

The propeller shaft speed was measured with a magnetic pickup excited by a 30-tooth wheel on the speed-control tachometer drive (rotating at twice shaft speed) and read directly on a frequency counter. The short-term stability and accuracy of measurement was ± 1 rpm from near zero to 1200 rpm.

Figure 9. Propeller Test Rig - Front View

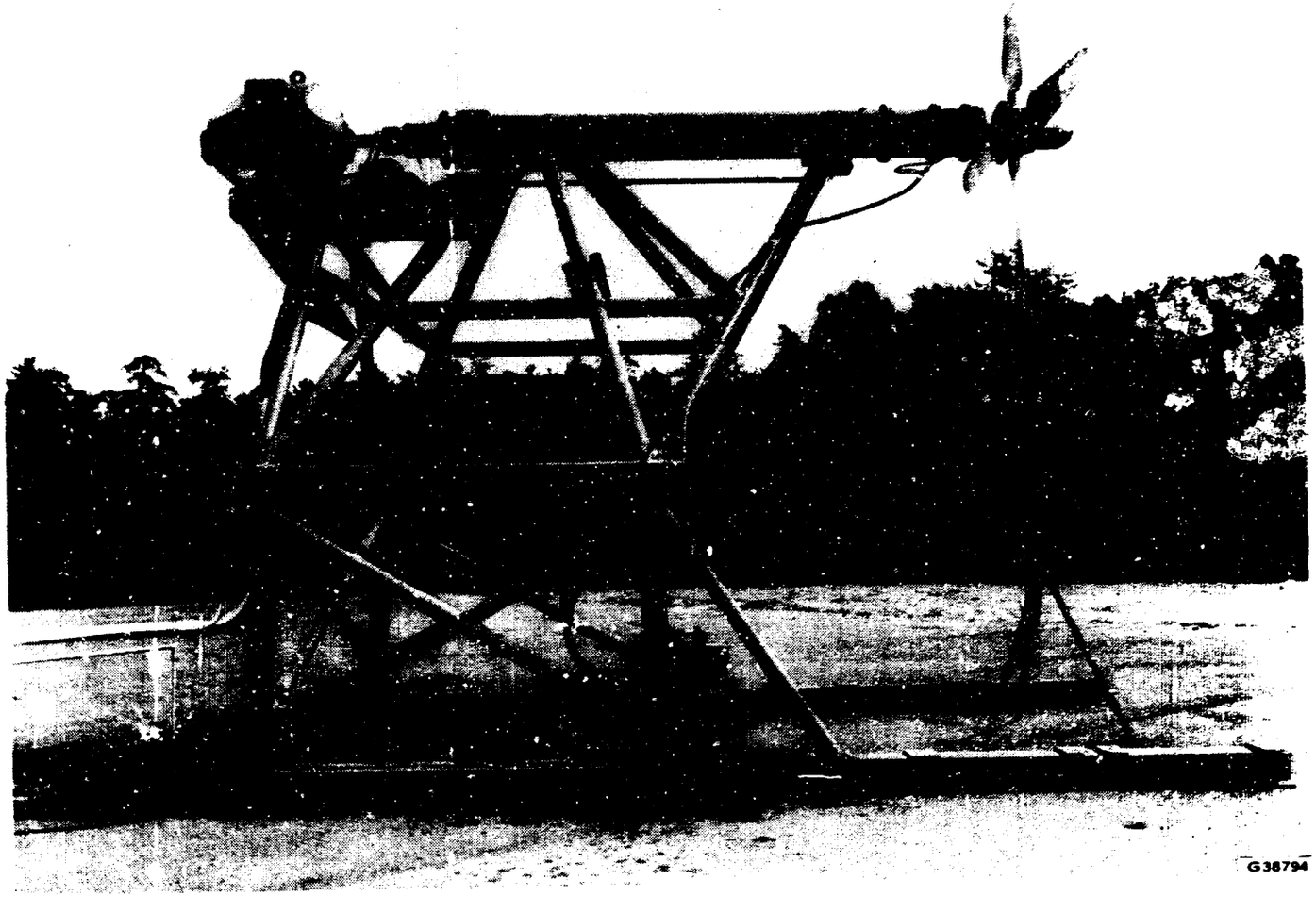

Figure 10. Propeller Test Rig - Side View

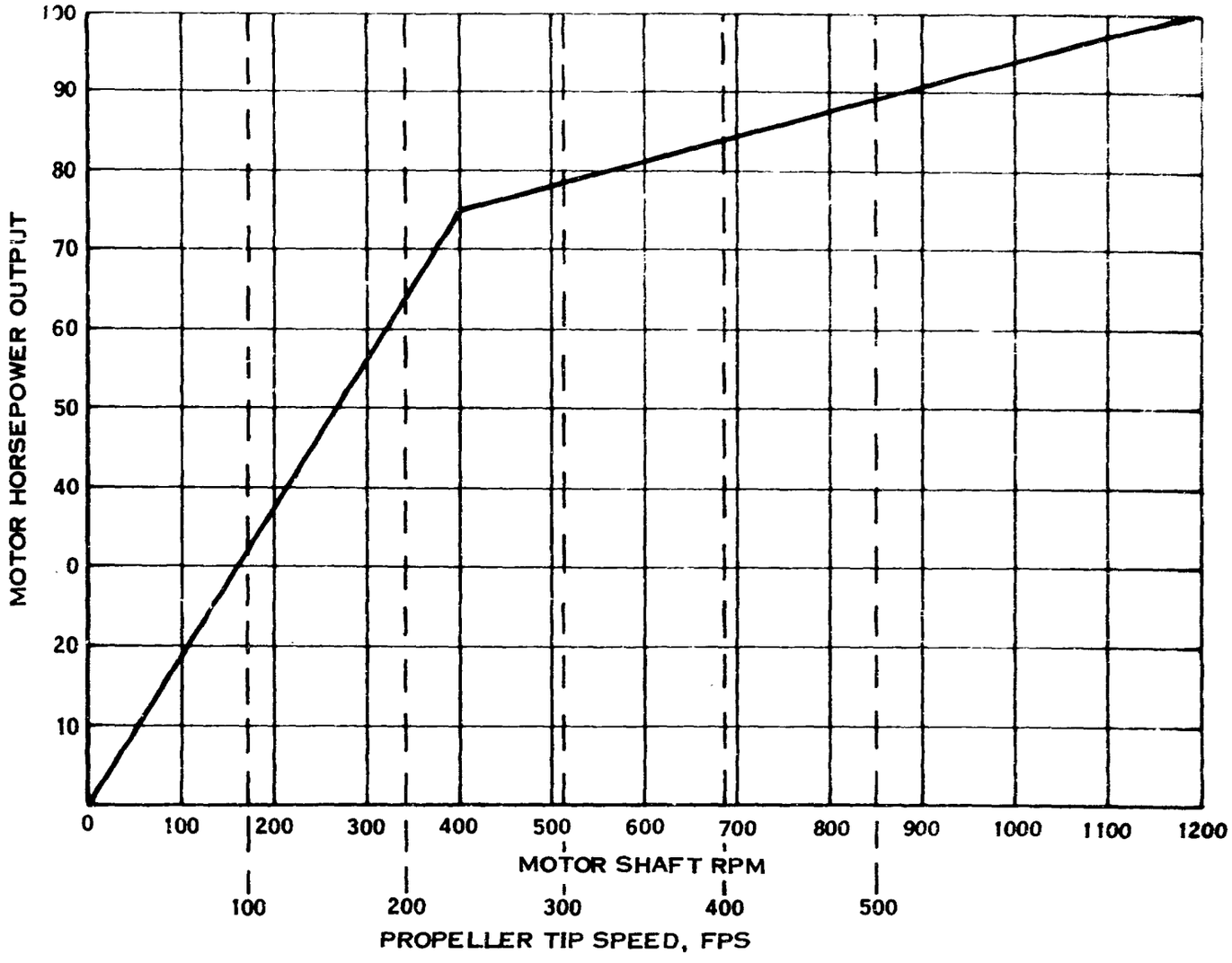

Figure 11. Relation Between Rig Drive Motor Output Power And Shaft Speed

[illegible] was measured using a [illegible]-pound full scale axial thrust ring mounted [illegible] of the thrust bearing cartridge. The meter is a four-arm strain-gage bridge, the output of which was fed through an amplifier and read out in pounds on a digital display. The thrust meter was calibrated as a system using a Bytex JP2000 precision load cell of nominal accuracy of 2 pounds. The readout accuracy, including non-linearity and temperature effects, is about ±4% of full scale, or ±80 pounds.

Propeller torque was measured using a BLH strain gage torque meter having a full scale of 10,000 ft-lb. This meter was calibrated as a system using dead weights and a known moment arm to a full scale of 1000 ft-lb. The accuracy of the torque system is approximately ±5% of full scale, or ±50 ft-lb.

A back-up system was used to monitor motor input power. The armature current and voltage were measured and the propeller input power derived from these measurements and the motor efficiency curve shown in Figure 12. This efficiency curve was derived from motor input power measurements made at several motor speeds at no load (i.e., without a propeller).

It is recognized that the measurements of thrust and torque made with the load cells described above are of limited use due to their large full-scale capacity. These load cells existed in the test rig which was used in the past for testing significantly higher thrust propellers. It is believed, however, that the data from these load cells are useful in interpreting the test data.

3. PROPELLER NOISE MEASUREMENT LOCATIONS

Propeller noise was measured at the locations shown schematically in Figure 13. Rotational tone noise was measured using a microphone located at ground level on a 50-foot radius from the center of the propeller at true azimuths of 45°, 67.5°, 90°, 112.5°, and 135° (0 is on the propeller axis in the forward direction) for the first three tests. During the last two tests (with 47X-464 blades) two microphone locations were added in order to permit estimating the tone noise levels on the axis by extrapolation in azimuth angle. One was at 50 feet and 20° azimuth; the other was at 80 feet and 12° off the axis.

The broad-band noise was measured using a microphone mounted on a tripod at approximately 4.7 feet above the ground. Propeller noise measurements were made on a 50-foot radius from the center of the propeller. For the first three tests, measurements were made at 22.5°, 45°, 67.5°, 90°, 112.5°, and 135° true azimuth. Also, one microphone was located at 12 feet above the ground plane to measure the noise at 6° azimuth. For the last two tests, the last microphone location described above was changed to 4.7 feet above the ground, resulting in an azimuth of 14°.

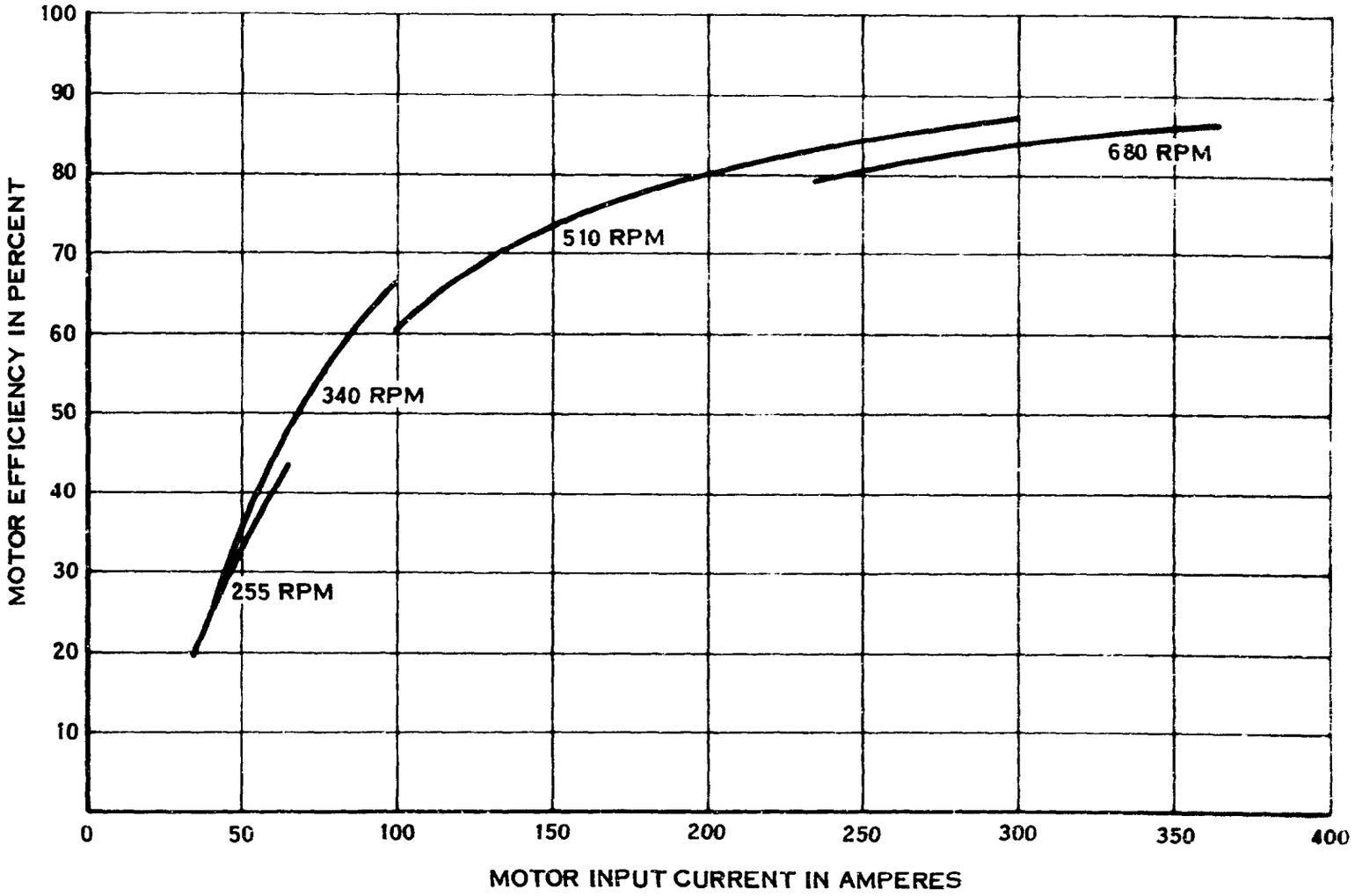

Figure 12. Rig Drive Motor Efficiency

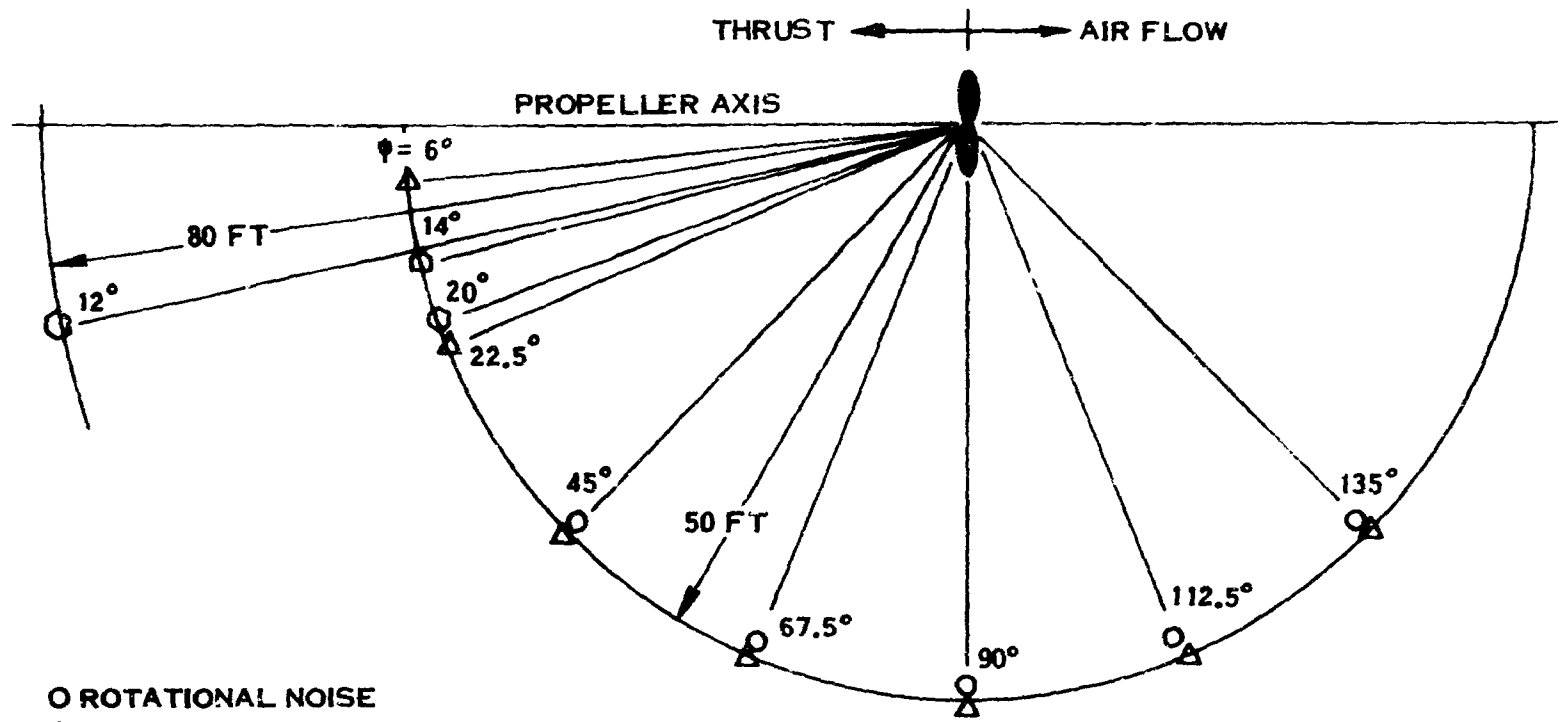

Figure 13. Schematic Representation of Microphone Locations

The 50-foot radius was selected because it represented a good compromise between near and far acoustic fields, ambient background noise, evenness of the ground, and the location of major obstructions in the acoustic field.

4. ACOUSTIC FIELD CALIBRATION AND AMBIENT NOISE MEASUREMENT

The effects of the ground plane on the noise were investigated and appropriate correction factors derived for adjusting the data to free-field conditions. For the low-frequency harmonic noise, measured by a microphone on the ground, it was anticipated that a pressure doubling effect would occur, resulting in a 6-dB increase over the same measurement made in a free-field environment. This was verified as follows. A speaker was mounted on the propeller test rig at the location on the propeller center. A sine-wave oscillator was used to generate tones through the speaker. A microphone, placed on the ground at 50 feet from the speaker, was used to measure the level of the tone. The microphone was then slowly raised above the ground until a minimum level was indicated. This reading was noted. The microphone was then raised further until a maximum reading was again obtained. This was done for the frequency range 60 to 250 Hz. It was not practical to go lower than 60 Hz because: a) the output from the speaker was decreasing, b) the background noise was higher at low frequencies, c) it was not possible to raise the microphone to a sufficient height to obtain a minimum, and d) even had the microphone been raised to the null point, the difference in path length between the direct wave and the reflected wave would result in errors.

The minimum reading occurs when the reflected wave and the direct wave arrive exactly out of phase and thus cancel. If the intensity of the two are the same, then they cancel completely and no sound is heard. On the other hand, at the maximum the two waves reinforce and the level measured is their sum. We thus have two equations in two unknowns as follows:

$$P_{max} = P_D + P_R$$

$$P_{min} = P_D - P_R$$

from which:

$$\Delta dB \quad 20 \log (P_{max}/P_D) = 20 \log \frac{2P_{max}}{(P_{max} + P_{min})}$$

where P_{max} is the acoustic pressure measured during reinforcement, P_{min} is the acoustic pressure measured during cancellation, P_D is the acoustic pressure of the direct wave, P_R is the acoustic pressure of the reflected wave, and ΔdB is the increase in measured sound pressure level due to one reflection. Figure 14 presents

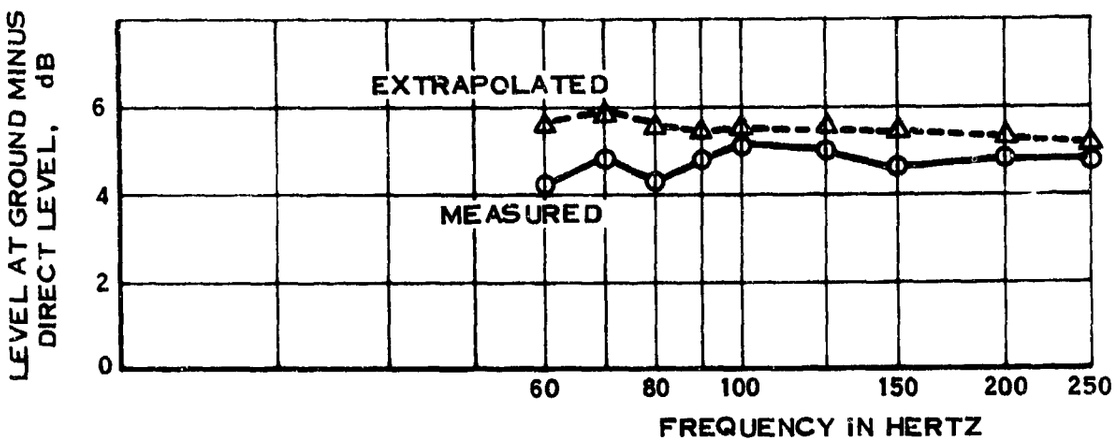

Figure 14. Ground Reflection Corrections for Tone Noise

the results obtained by applying the above equation to the measurements. Also shown are the estimated actual increments derived from interpolations to the actual P_{min}, since it was not possible to obtain this value directly due to background noise. The resulting curve approaches 6 dB, i.e., the ground appears to be a near-perfect reflector at low frequencies. It was thus concluded that a 6 dB correction should be applied to all the data from the ground-plane microphone to adjust the measurements to equivalent free-field conditions.

The acoustic field corrections for the microphones mounted on the tripods were determined using random noise output from the speaker located at the center of the propeller. The signal was analyzed by 1/3-octave bands. The microphone was then moved toward the speaker, from 50 feet to 12.5 feet, along a line passing from the microphone to the center of the speaker. Assuming spherical spreading of sound, any reflected wave would be at least 10 dB below the direct wave at the 12.5 foot location (the distance to the ground being 17 feet, the ratio of the path length of one reflection from the ground to the distance from the speaker to the microphone is 3). The 1/3-octave band levels from the microphone at 12.5 feet were decreased by 12 dB for spherical spreading from 12.5 to 50 feet and compared to those measured at 50 feet. The difference was attributed to ground reflections. The corrections thus derived are shown in Table V. These levels are to be added to the measured levels for correction to equivalent free-field conditions.

Note that it is not simpler to use a microphone located at ground level to measure the broad-band noise as well as the low frequency tone noise because at high frequency: a) the ground is not a perfect reflector, b) the reflections would be diffuse and, thus, the correction to be applied would be dependent on the local ground composition, c) the dimensions of the microphone (one-inch diameter) approach the wavelength of the sound, d) the acoustic field would have to be calibrated anyway.

The ambient background noise and noise of the propeller rig were measured at each of the noise measurement locations. The rotational speed of the rig had a negligible effect on the rig noise. Table VI summarizes the average background and rig noise which was found to be typical for a windless night. The azimuths given are those of the broad-band noise measurement locations.

5. ACOUSTIC DATA ACQUISITION AND DATA REDUCTION SYSTEMS

The acoustic data from the first two tests were acquired using a system consisting of:

a. A Bruel & Kjaer (B&K) one-inch condenser microphone type 4131.

b. A B&K type 2203 sound level meter.

c. A Kudelski Nagra III single-track magnetic tape recorder operated at 7.5 inches per sec with CCIR equalization.

TABLE V

GROUND REFLECTION CORRECTIONS FOR BROAD-BAND PROPELLER NOISE

1/3-Octave Band Center Frequency	Acoustic Field Corrections for the 4.7-ft Mic.	Acoustic Field Corrections for the 12-ft Mic.*
25 Hz	-6 dB	-6 dB
31.5	-6	-6
40	-5.5	-5
50	-5	-4
62.5	-3.5	-1
80	-1.5	2
100	-2	-2
125	-2.5	-2
160	9	-4
200	5	-2
250	-1	0
315	-5	-3
400	-4.5	-1
500	-1.5	-4
625	-2.5	-2
800	-4	-3
1000	-2	-2
1250	-2.5	-2.5
1600	-2	-2
2000	-3	-3
2500	-2	-2
3150	-2	-2
4000	-3	-3
5000	-2.5	-2.5
6250	-1.5	-1.5
8000	-1	-1
10000	-1	-1

*Used during the first two test periods only.

TABLE VI

GENERAL BACKGROUND AND PROPELLER TEST RIG NOISE

1/3-Octave Band Center Frequency	Azimuth Angle						
	6-14.5°	22.5°	45°	67.5°	90°	112.5°	135°
25 Hz	51 dB	58 dB	50 dB	53 dB	51 dB	50 dB	50 dB
31.5	54	55	53	54	58	55	54
40	46	50	46	48	46	46	47
50	49	52	50	49	49	50	51
62.5	48	50	51	48	48	48	50
80	47	48	50	48	48	51	52
100	44	47	48	48	49	50	53
125	46	50	50	52	51	51	51
160	43	48	51	52	53	53	53
200	39	46	47	47	46	46	47
250	40	45	44	45	46	47	48
315	42	44	42	45	47	47	50
400	42	41	43	45	46	48	50
500	43	40	40	41	42	45	47
625	41	36	38	41	41	43	45
800	40	35	36	37	39	42	42
1000	36	33	35	35	36	38	41
1250	36	32	34	35	35	37	38
1600	45	37	39	42	40	45	41
2000	33	29	29	30	31	33	34
2500	29	26	27	28	29	30	32
3150	27	28	29	29	33	31	32
4000	26	25	23	29	27	25	28
5000	23	24	23	26	24	23	24
6250	22	24	23	23	23	22	25
8000	21	21	21	23	22	21	22
10000	20	24	20	21	20	20	21

d. A B&K type 4230 microphone calibrator producing a 94 dB acoustic signal at 1000 Hz.

e. A B&K one-inch condenser microphone affixed to a B&K type AO-0033 10-foot extension cable (for the microphone located 12 feet above the ground).

The data from the last three tests were acquired using the above equipment except that the recording station was remote from the microphone. Thus, a B&K type 2801 power supply was used in conjunction with a 200-foot extension cable to power a B&K type 2613 one-inch cathode follower.

The tape recordings were played back on an Ampex AG500 tape player. The equalization of this machine was adjusted such that the frequency response of the total data acquisition/playback system was within ± 1 dB from 20 to 14,000 Hz with a gradual roll-off to -3 dB at 10 Hz.

The data from the ground-plane microphone were analyzed by means of a Spectral Dynamics SD101B Frequency Analyzer. A 5-Hz bandwidth filter was used for all the data except that from 90^{o} azimuth microphone where a 1.5 Hz filter was required to extract the levels of the tones from the other noise components. The analysis range was 10 to 210 Hz for the 150 and 200 ft/sec tip speed conditions, and 10 to 410 Hz for the higher tip speed conditions, except for the data from the final test. Since this test was run with a two-bladed propeller rather than a four-bladed propeller, the analysis frequency ranges were halved. These ranges covered approximately 10 harmonics of the blade passage frequency. A -6dB correction for ground reflection was added to all the tone data.

The data from the vortex noise microphone positions were analyzed using a General Radio 1921 Real Time 1/3-Octave Band Analyzer with band center frequencies from 25 to 10,000 Hz. Each band level was corrected for background noise as follows:

$$\text{Corrected level} \quad 10 \log \left[\text{antilog}\,(\text{SPL}/10) - \text{antilog}\,(\text{BKG}/10)\right]$$

where SPL is the measured 1/3-octave band level and BKG is the background noise level in that band at that measurement location (from Table VI). Since the measured levels were rounded to the nearest decibel, the background correction was applied only when the measured level exceeded the background noise by 1 dB or more. If this was not the case, then no further correction was applied to the data and it was considered to be background noise rather than signal and, thus, not to be used. The data were then adjusted for ground reflections by applying the corrections from Table V.

In some cases, particularly in the low-frequency bands and for the higher tip-speed operating condition, it was observed that some bands were distinctly higher in level than the bands immediately on either side, indicating the presence of a tone. Thus, a similar analysis to that described for the rotational noise was done on this on this data. Where a tone was noted, its level (or in the case of a band covering the frequency range of several tones the logarithmic sum of the tone levels), was compared to the level of the 1/3-octave band of that frequency range. If the levels agreed within 3 dB, it was assumed that the 1/3-octave band level was due to tones and not to broad-band noise and, thus, not used for comparison with estimated vortex noise.

The width of a 5 Hz filter did not allow the determination of the signal level between tones. Therefore, the data from the fourth test were more extensively analyzed using a narrower filter. For this analysis the vortex noise data were analyzed over the range 10 to 600 Hz using a 1.5 Hz bandwidth filter. The tones were eliminated and the rest integrated between 1/3-octave band frequency limits and the corresponding 1/3 octave band sound pressure levels calculated. These were then corrected for background noise and ground plane effects and used for correlation with vortex noise calculations.

6. DISCUSSION OF TEST RESULTS

a. Propeller Test Configurations

Four propeller configurations were tested in this program. All were 11.25 feet in diameter. The first three propellers were four-bladed. The last configuration tested was the third propeller with two blades removed. Figure 15 and the following table present the blade characteristics of the propellers tested while Figure 16 shows a comparison of their planforms. All propellers were tested in the tractor mode; i.e., the propeller wake passed through the rig supporting structure.

Blade designation	47X-394 and 47X-451	47X-464
Activity factor	112.9	213.8
Maximum chord	11.4 in.	19.1 in.
Integrated design C_L	0.60	0.5384
Airfoil section	NACA 64A	NACA 66A

The first blade configuration (47X-394) was an existing configuration designed for a STOL aircraft. The second blade configuration (47X-451) was derived from the first blade configuration by increasing the blade twist near the tip. The purpose of this change was to reduce blade loading and angle of attack near the tip in order to simulate typical conditions in flight rather than static operation. The third blade

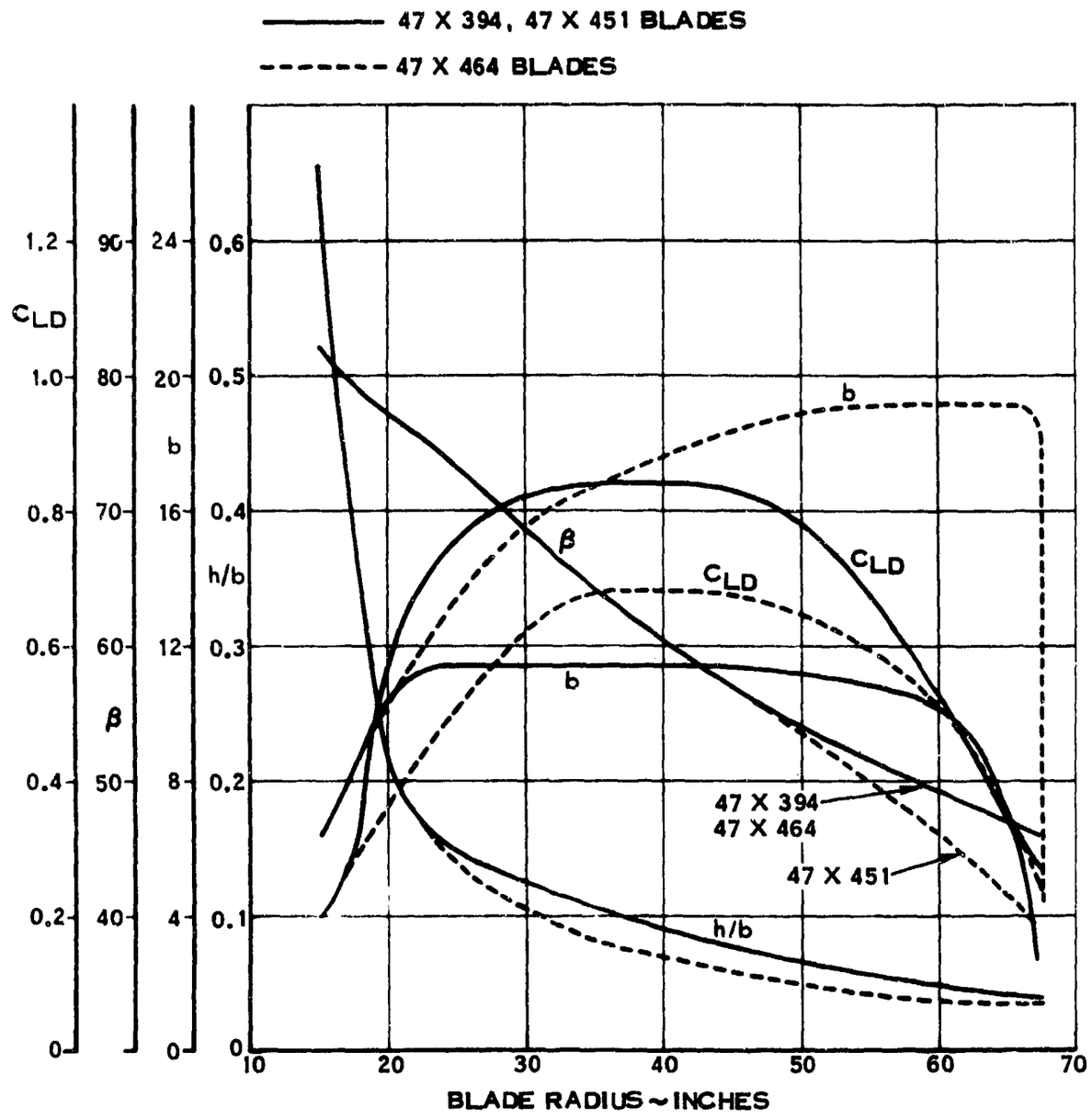

Figure 15. Blade Characteristics

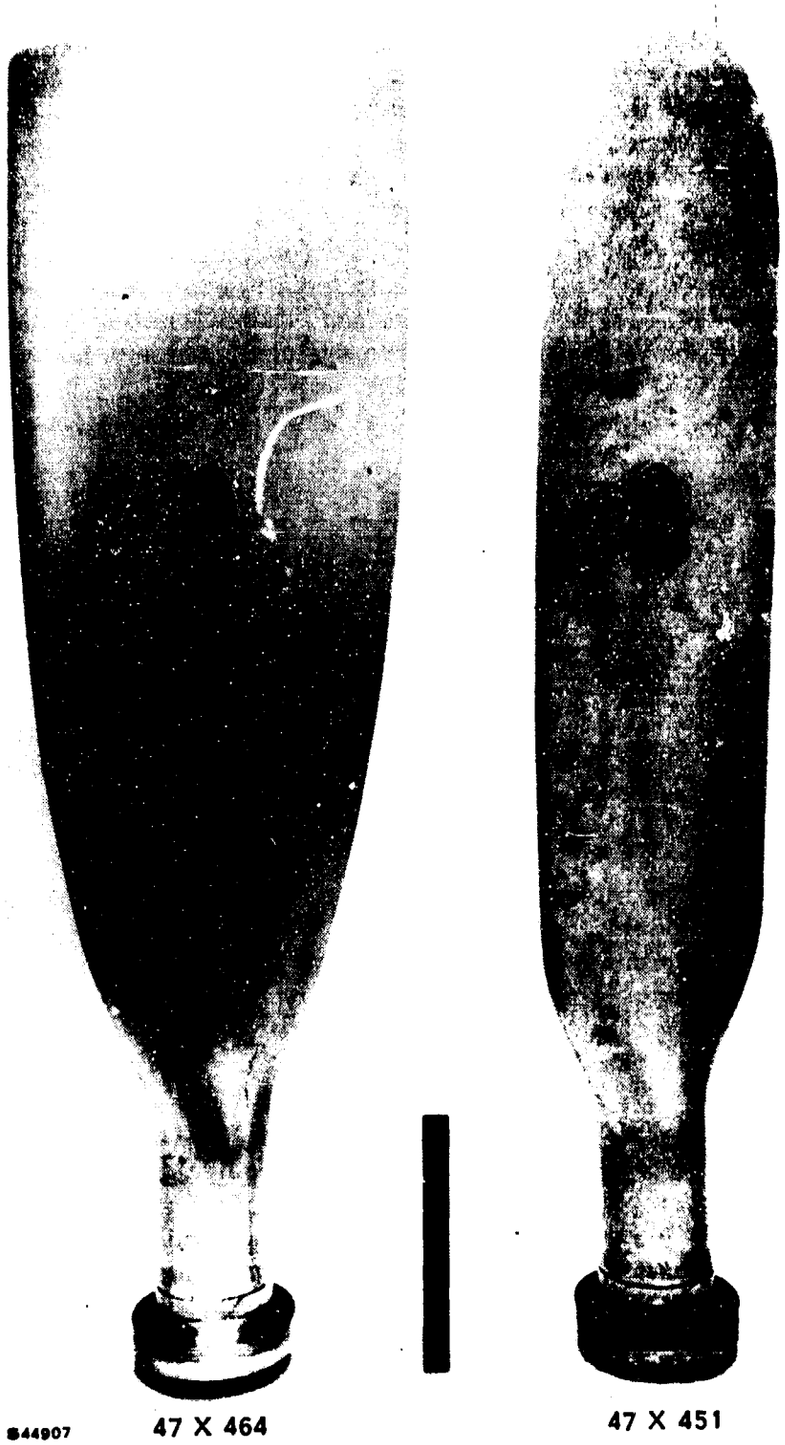

Figure 16. Blade Planforms

configuration was designed to minimize both harmonic loading noise and broad-band noise within the capabilities of an available propeller hub and blade forging. Theory indicates that increasing blade chord reduces harmonic loading noise for a given rpm and thrust. A design study of vortex noise trends was made using a preliminary version of the new vortex noise method with the coefficients based on broad-band noise data from the first two propellers tested. The study indicated that increasing blade chord also would reduce propeller vortex noise. The use of an existing blade forging resulted in a chord of about 19 inches and the activity factor to 213.8 compared to a chord of 11.4 inches and an activity factor of 112.9 for the first two blade configurations tested. Based on the study of airfoil sections reported in Section V.4, NACA 66A sections were used in order to reduce vortex noise further. The method of determining the thickness distribution for this new section is described at the end of Section V.4. In order to facilitate a comparison with the first two propeller configurations, the diameter of 11.25 feet was retained. The hub permitted tests of both 4-bladed and 2-bladed configurations of the new wide 47X-464 blades.

A brief investigative program was conducted after the second test period in order to determine rig blockage effects on the propeller noise. For this third test program, the second propeller test configuration was reversed and run as a pusher propeller.

b. Propeller Test Conditions

The test conditions for the five test periods are summarized in Table VII. The thrust and power are averages of the rotational noise and broad-band noise data runs for the tip speed and blade angle shown. The powers shown are based on the rpm and measured torque.

Although the wind speed is given as a range, most of the data samples were taken during calm periods since it was possible to see the anemometer and thus record data between gusts. In many cases the anemometer was still; i.e., the wind was less than 1 mph.

c. Rotational Harmonic Noise

The measured harmonic noise levels are presented in Tables VIII through XII. All the levels shown have been adjusted to equivalent free-field conditions.

Figure 17 presents the rotational noise harmonics for the middle blade angle and 200 ft/sec tip speed at three azimuths. It can be seen that the levels of the harmonics do not decrease rapidly as is commonly predicted by theory for low tip speed propellers. One possible explanation for this phenomenon appeared to be interference from the rig. As a consequence, the third test program was conducted

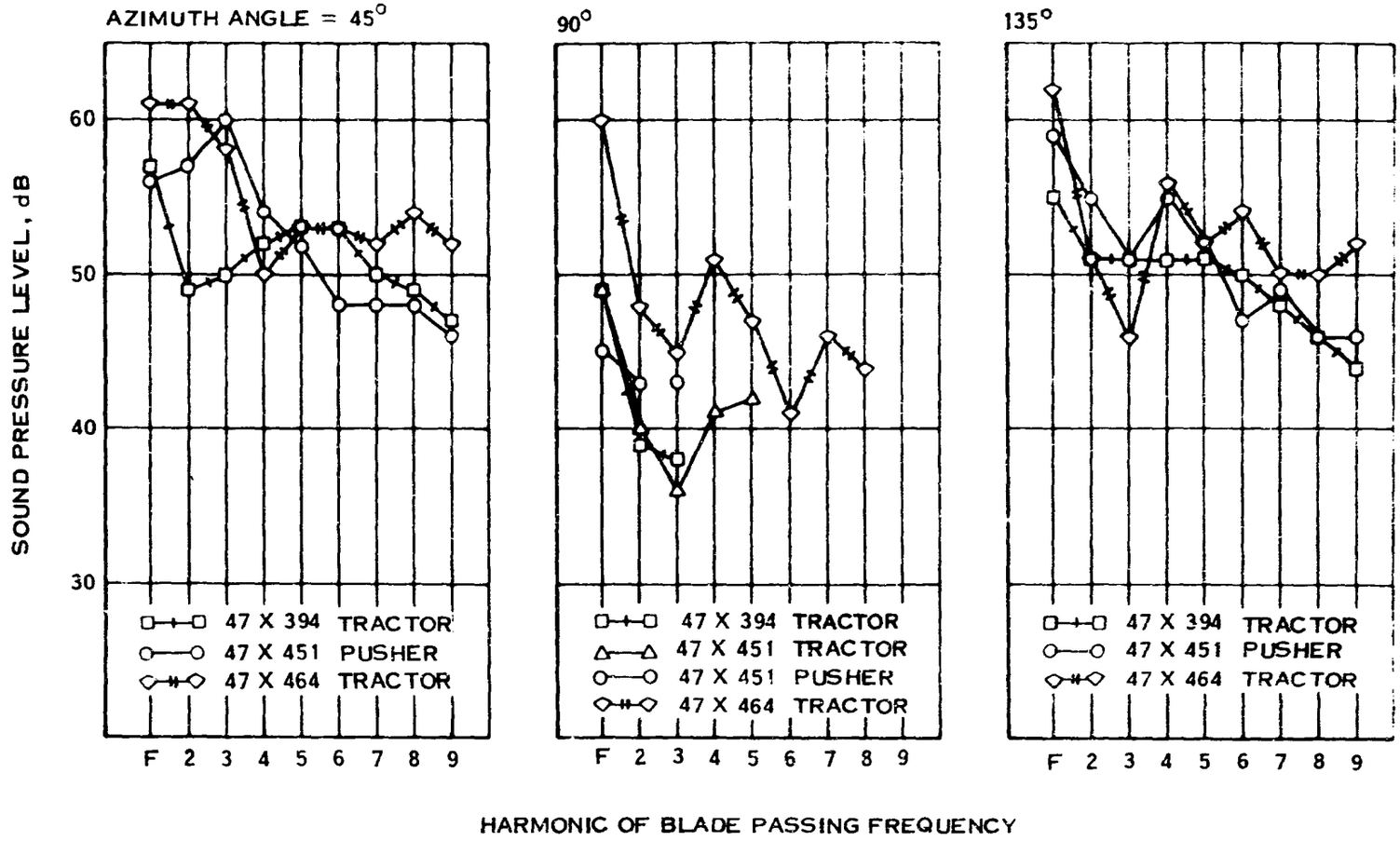

Figure 17. Rotational Noise Summary

TABLE VII

PROPELLER TEST CONDITIONS

Test Period No. 1. 47 x 394 blades. August 22, 1970

RPM	Tip Speed	Blade Angle at 0.75 Radius	Thrust	Horsepower
255	150 ft/sec	19.7°	134 lbs	6.7
339	200	19.7°	250	17.4
547	322	19.7°	729	72.7
254	150	13.7°	95	3.9
340	200	13.7°	201	8.0
510	300	13.7°	490	34.1
650	383	13.7°	805	72.9
255	150	8.7°	65	2.1
341	200	8.7°	156	6.1
511	300	8.7°	370	19.8
750	442	8.7°	751	72.7

Temperature range: 45 to 54°F
Barometric pressure: 29.95 to 30.02 in. Hg
Wind speed: 0 to 2 mph

Test Period No. 2. 47 x 451 blades. October 17, 1970

RPM	Tip Speed	Blade Angle at 0.75 Radius	Thrust	Horsepower
250	147 ft/sec	16.4°	186 lbs	5.0
340	200	16.4°	315	10.5
600	353	16.4°	800	69.6
250	147	12.4°	130	3.8
340	200	12.4°	215	7.5
510	300	12.4°	484	32.8
670	395	12.4°	832	78.6
340	200	8.4°	167	6.0
520	306	8.4°	359	18.4
750	442	8.4°	743	70.0

Temperature range: 34 to 37°F
Barometric pressure: 30.07 in. Hg
Wind speed: 0 to 2 mph

TABLE VII (Cont.)

Test Period No. 3. 47 x 451 Blades, Pusher Configuration. January 30, 1971

RPM	Tip Speed	Blade Angle at 0.75 Radius	Thrust	Horsepower
255	150 ft/sec	12.5°	130 lbs	3.8
340	200	12.5°	215	7.5
510	300	12.5°	484	32.8
650	383	12.5°	790	75.0

Meteorological data not taken.

Test Period No. 4. 47 x 464 Blades, 4 Blades. February 17, 1971

RPM	Tip Speed	Blade Angle at 0.75 Radius	Thrust	Horsepower
255	150 ft/sec	15.0°	321 lbs	8.7
340	200	15.0°	475	19.2
510	300	15.0°	896	59.7
255	150	11.4°	199	6.7
340	200	11.4°	301	13.8
510	300	11.4°	640	44.4
600	353	11.4°	881	73.2
255	150	8.1°	187	6.7
340	200	8.1°	292	13.6
510	300	8.1°	551	35.7
680	400	8.1°	916	77.1

Temperature range: 9 to 18°F
Barometric pressure: 30.13 in. Hg
Wind speed: 0 to 3 mph

TABLE VII (Concluded)

Test Period No. 5. 47 x 464 Blades, 2 Blades. March 2, 1971

RPM	Tip Speed	Blade Angle at 0.75 Radius	Thrust	Horsepower
255	150 ft/sec	10.9°	40 lbs	4.4
340	200	10.9°	125	8.6
510	300	10.9°	345	25.0
600	353	10.9°	485	38.0
680	400	10.9°	631	53.0
765	451	10.9°	819	75.0

Temperature range: 28 to 30°F
Barometric pressure: 30.00 in. Hg
Wind speed: 0 to 3 mph

TABLE VIII

SUMMARY OF THE TONE LEVELS FOR THE 47 X 394 BLADES

19.7^{O} Blade Angle

Tip Speed	Harmonic	Azimuth Angle				
		45^{O}	67.5^{O}	90^{O}	112.5^{O}	135^{O}
150 ft/sec	1	61 dB	53 dB	52.5 dB	53.5 dB	60.5 dB
	2	50.5	49.5	39	47	52
	3	54.5	47.5	47	47	53
	4	52	47.5	41	46	51
	5	48.5	44.5	43	41	48
	6	47	41			47
200	1	64.5	60	51.5	61	58
	2	63	53.5	44	58	61
	3	60	52	40.5	56	57.5
	4	58	50.5	42.5	54	57
	5	55	51		53.5	58
	6	55.5	49.5		52	57
	7	53	49.5		50.5	56
	8	51	50.5		49.5	53
	9	49.5	47		47	52
	10	49.5	46		49	55
	11	51	47.5		50.5	52
	12	50.5	47		50	51.5
	13	48.5	47		49.5	52.5
322	1	68.5	67.5	64	66	70.5
	2	64	65	54.5	68	73
	3	64.5				73
	4	60.5				69
	5	60				69
	6	61				70.5
	7	61.5				70
	8	63				70.5
	9	62				68
	10	60				67

TABLE VIII (Cont.)

13.7° Blade Angle

Tip Speed	Harmonic	Azimuth Angle				
		45°	67.5°	90°	112.5°	135°
150 ft/sec	1	50 dB	49 dB	51.5 dB	50 dB	46.5 dB
	2	40	36.5	34.5	37.5	44
	3	39	42	43.5	45	47
	4	40	38	31.5	36	39.5
	5	42	37	32	38.5	44.5
200	1	57	52	49	53.5	55
	2	49	46	39	46	51
	3	49.5	42	37.5	43	51
	4	52	41	36	42	50.5
	5	52.5	45	38.5	40	50.5
	6	53				50
	7	50				48
	8	49				46
	9	46.5				44
	10	43.5				46
	11	46				48
	12	46.5				49.5
	13	47				47
	14	47				45
300	1	62	65	63	58.5	64.5
	2	62	59	48	55	58.5
	3	58.5	54	49	53.5	60.5
	4	59	56.5	44.5	49.5	57.5
	5	59.5	57	42	50.5	55.5
	6	57	52			57
	7	57	52			61
	8	59	53			62
	9	58	53			56
	10	57	52.5			55
	11	56	52			55.5

TABLE VIII (Cont.)

13.7° Blade Angle (Concluded)

Tip Speed	Harmonic	Azimuth Angle				
		45°	67.5°	90°	112.5°	135°
383 ft/sec	1	62.5 dB	70 dB	74 dB	72.5 dB	70 dB
	2	63.5	61	52.5	63.5	66
	3	63	60	51.5	61	63
	4	62	62	50	59.5	64.5
	5	62	59		60	64.5
	6	66	61		60.5	65
	7	66	61.5		62	67
	8	66	60.5		60	64.5
	9	63	59.5		58.5	66.5

8.7° Blade Angle

Tip Speed	Harmonic	Azimuth Angle				
		45°	67.5°	90°	112.5°	135°
150 ft/sec	1	57 dB	52 dB	54 dB	50 dB	51.5 dB
	2	41.5	40.5	36.5	40.5	42.5
	3	39.5	43	47	47	51
	4	37.5	38	33	38	43.5
	5	40.5	39	38.5	40.5	44
200	1	54.5	47.5	46.5	45.5	55
	2	53	42	40.5	45.5	47
	3	45	42.5	37.5	43.5	50.5
	4	49	42.5	40.5	41.5	48.5
	5	44.5	40.5	41.5	42.5	45.5

TABLE VIII (Concluded)

8.7° Blade Angle (Concluded)

Tip Speed	Harmonic	Azimuth Angle				
		45°	67.5°	90°	112.5°	135°
300 ft/sec	1	61 dB	55.5 dB	61 dB	56 dB	56 dB
	2	59	52	47	54	58
	3	57	52	47.5	54	56
	4	54.5	49	42	47	55
	5	53	50.5	40	48.5	53
	6	49	43		46.5	52
	7	52	45.5		50	51
	8	52	47.5		50	53
	9	54	47.5		48	53
	10	52	48		48.5	53
	11	51	47		46.5	49
442	1	68	64	65	70	69
	2	69	62	53.5	61	64
	3	62	64.5	54	62	65
	4	62	61	52.5	59	61
	5	61	59.5		59.5	62
	6	62.5	58		63	61.5
	7	61	58.5		61.5	63
	8	61.5	55		62	62

TABLE IX

SUMMARY OF THE TONE LEVELS FOR THE 47X451 BLADES

All data for 90° azimuth angle

Blade Angle at 0.75 Radius	Maximum	Tip Speed, ft/sec					
		147	200	300	353	395	442
16.4°	1	45 dB	48 dB		63 dB		
	2	40	45		57		
	3	40	45		60		
	4	35	45		53		
	5	42	47		56		
	6		43		54		
	7				54		
	8				51		
12.4°	1	46	49	56 dB		72 dB	
	2	36	40	53		73	
	3	40	36	55		74	
	4	31	41	47		71	
	5	40	42	50		78	
	6	35		41		75	
	7	39		47		78	
	8	28				71	
	9					71	
8.4°	1		44	57			70 dB
	2		36	45			56
	3		40	44			51
	4		41	47			48
	5		41	47			52
	6			39			49
	7			44			46
	8			38			49

TABLE X

SUMMARY OF THE TONE LEVELS FOR THE 47X451 BLADES WITH THE PROPELLER IN A PUSHER CONFIGURATION

All data at 12.5° blade angle

Tip Speed	Harmonic	Azimuth				
		45°	67.5°	90°	112.5°	135°
150 ft/sec	1	48 dB	54 dB	39 dB	42 dB	50 dB
	2	48	48	45	48	48
	3	48	44		45	49
	4	48	42		44	46
	5	46	44		43	41
	6	44	42		42	40
	7	44	40		39	41
	8	43	41		39	40
	9	41	38		38	40
	10	41	39		39	39
200	1	56	55	45	58	59
	2	57	54	43	54	55
	3	60	56	43	52	51
	4	54	52		52	55
	5	52	53		47	52
	6	48	47		45	47
	7	48	46		44	49
	8	48	43		43	46
	9	46	40			46
300	1	65	66	57	64	65
	2	62	60	51	63	65
	3	65	59	46	63	65
	4	60	55	44	59	63
	5	56	54	41	58	60
	6	56	49	40	54	58
	7	56	48	42	52	56
	8	55	47	40	50	55
	9	53	46		48	52
383	1	72	69	74	72	78
	2	76	68	56	66	67

TABLE X (Concluded)

All data at 12.5° blade angle

Tip Speed	Harmonic	Azimuth				
		45°	67.5°	90°	112.5°	135°
383 ft/sec	3	73 dB	64 dB	62 dB	64 dB	68 dB
	4	74	58	56	60	64
	5	69	58	54	58	60
	6	68	58	52	56	60
	7	66	53	52	51	58
	8	63	48	52	52	58

TABLE XI

SUMMARY OF THE TONE LEVELS FOR THE 47X464 BLADES

15.0° blade angle

Tip Speed	Harmonic	Azimuth Angle						
		12°(80 ft)	20°	45°	67.5°	90°	112.5°	135°
150 ft/sec	1	59 dB	54 dB	57 dB	52 dB	45 dB	63 dB	57 dB
	2	54	55	54	49	39	60	54
	3	56	55	48	48	37	58	54
	4	52	52	50	49	40	58	58
	5	54	53	51	51	41	59	55
	6	54	54	54	49	40	56	59
	7	54	50	49	47	42	58	52
	8	51	52	50	47	37	56	52
	9	52	50	51	47	36	56	51
	10	50	52	50	47	37	58	53
200	1	57	61	64	56	53	68	68
	2	54	56	60	53	52	66	62
	3	49	61	60	48	49	64	62
	4	50	61	61	47	48	67	62
	5	50	59	58	51	47	64	64
	6	48	63	62	48	47	62	62
	7	49	60	59	47	53	64	59
	8	49	57	48	47	47	63	62
	9	50	59	50	46	42	62	60
300	1	74	74	66	69	62	66	66
	2	66	66	71	66	54	60	64
	3	71	69	67	58	56	63	70
	4	68	68	66	56	52	62	70
	5	72	70	69	57	52	61	65
	6	68	71	68	60	51	62	66
	7	70	72	66	60	52	62	68
	8	67	68	64	56	51	57	66
	9	66	66	64	56	49	60	66
	10	62	68	62	56	48	58	60

TABLE XI (Cont.)

11.4° blade angle

Tip Speed	Harmonic	Azimuth Angle						
		12°(80 ft)	20°	45°	67.5°	90°	112.5°	135°
150 ft/sec	1	61 dB	54 dB	56 dB	52 dB	52 dB	53 dB	52 dB
	2	55	49	50	48	43	45	47
	3	49	45	45	42	42	40	44
	4	46	44	42	43	40	40	45
	5	50	47	45	46	44	44	44
	6	50	50	44	45	42	40	47
	7	49	44	44	47	50	42	48
	8	49	45	43	43	41	43	46
	9	48	46	42	43	43	40	46
	10	45	45	42	44	43	43	45
200	1	66	58	61	56	60	54	62
	2	66	56	61	47	48	48	51
	3	56	48	58	44	45	45	46
	4	58	52	50	46	51	48	56
	5	60	52	53	46	47	46	52
	6	59	55	53	46	41	49	54
	7	56	54	52	46	46	49	50
	8	57	50	54	46	44	48	50
	9	57	54	52	46	40	46	52
300	1	68	71	68	66	48	64	71
	2	59	66	65	60	39	58	69
	3	64	68	60	60	40	58	64
	4	63	69	64	59	43	60	58
	5	65	72	66	57	42	58	62
	6	64	71	67	59	33	61	61
	7	64	70	61	60	40	57	66
	8	62	65	62	56	43	56	63
	9	60	67	64	57	35	56	60
	10	60	66	62	59	34	56	58
353	1	69	66	74	68	66	77	70
	2	70	61	69	62	45	66	69
	3	67	70	67	69	44	61	71
	4	67	72	64	64	37	64	67

TABLE XI (Cont.)

11.4° blade angle (Concluded)

Tip Speed	Harmonic	Azimuth Angle						
		12°(80 ft)	20°	45°	67.5°	90°	112.5°	135°
353 ft/sec	5	67 dB	74 dB	68 dB	68 dB	33 dB	66 dB	66 dB
	6	69	72	67	68	33	61	70
	7	66	70	67	67	41	61	68
	8	66	69	66	68	36	64	67
	9	64	66	64	64	39	60	66
	10	60	65	63	62	36	58	64

TABLE XI (Cont.)

8.1° blade angle

Tip Speed	Harmonic	Azimuth Angle						
		12°(80 ft)	20°	45°	67.5°	90°	112.5°	135°
150 ft/sec	1	46 dB	53 dB	56 dB	49 dB	44 dB	50 dB	56 dB
	2	47	45	52	50	42	44	48
	3	48	42	49	42	31	44	45
	4	44	40	48	44	31	45	46
	5	45	43	50	44	35	44	50
	6	49	46	52	40	33	42	48
	7	45	44	51	42	37	44	50
	8	46	45	51	38	33	44	48
	9	46	46	49	40	34	42	48
	10	44	45	50	40	33	44	46
200	1	63	61	56	56	52	57	56
	2	57	55	48	47	41	49	53
	3	51	56	47	54	38	52	50
	4	53	54	49	52	41	50	52
	5	54	53	50	47	40	51	48
	6	50	54	50	50	38	48	50
	7	51	56	47	50	38	49	52
	8	54	54	48	52	38	49	51
	9	50	50	47	49	36	48	50
300	1	63	67	60	66	68	61	62
	2	58	63	66	54	48	64	62
	3	56	64	56	55	49	60	61
	4	56	64	56	58	48	63	60
	5	58	60	60	53	46	59	60
	6	57	63	55	54	46	61	61
	7	54	63	58	53	45	56	63
	8	54	61	56	52	50	57	63
	9	52	60	57	50	47	57	61
	10	55	59	54	53	40	55	58
400	1	70	74	69	76	74	76	74
	2	69	71	71	62	56	64	72
	3	66	69	67	65	56	66	71
	4	62	66	70	62	54	64	75

TABLE XI (Concluded)

8.1° blade angle (Concluded)

Tip Speed	Harmonic	Azimuth Angle						
		12°(80 ft)	20°	45°	67.5°	90°	112.5°	135°
400 ft/sec	5	65 dB	71 dB	68 dB	62 dB	48 dB	60 dB	68 dB
	6	62	67	67	63	51	61	68
	7	60	66	69	60	53	62	65
	8	62	66	67	60	52	63	64
	9	54	64	70	58	52	62	63

TABLE XII

SUMMARY OF TONE LEVELS FOR THE 47X464 BLADES IN A TWO-BLADED PROPELLER CONFIGURATION

10.9° blade angle

Tip Speed	Harmonic	Azimuth Angle						
		12° (80 ft)	20°	45°	67.5°	90°	112.5°	135°
150 ft/sec	1	33 dB	38 dB	42 dB	39 dB	38 dB	37 dB	41 dB
	2	46	51	50	49	42	41	48
	3	44	48	49	44	36	38	42
	4	42	50	45	40	37	38	43
	5	41	47	46	40	32	37	39
	6	46	49	47	42	39	31	42
	7		44	43		33		41
	8		43	41		35		
	9		45	45				
	10		44	45				
200	1	49	61	62	53	53	50	51
	2	51	71	63	48	46	49	52
	3	54	69	63	47	50	47	52
	4	52	67	62	46	39	46	49
	5	50	65	60	43	40	45	50
	6	49	62	56	43		41	50
	7	46	59	57	42		44	47
	8	48	57	58			42	47
	9						42	
300	1	67	74	72	72	72	72	68
	2	64	80	76	60	57	63	63
	3	65	79	76	61	50	58	62
	4	64	75	71	62	52	58	62
	5	63	74	70	62		60	61
	6	59	76	68	58		56	62
	7	61	71	66	56		59	61
	8	59	71	68	58		56	61
	9	58	69	68	57		58	60
	10	57	68	67	58		56	60

TABLE XII (Concluded)

10.9° blade angle

Tip Speed	Harmonic	Azimuth Angle						
		12°(80 ft)	20°	45°	67.5°	90°	112.5°	135°
353 ft/sec	1	68 dB	77 dB	76 dB	74 dB	78 dB	78 dB	72 dB
	2	72	81	70	61	63	67	66
	3	72	82	68	60	59	64	63
	4	72	77	68	59	59	63	65
	5	70	77	71	60	56	62	64
	6	67	74	70	62	56	61	66
	7	67	74	72	62		62	64
	8	70	70	66	61		61	65
	9	68	72	67	60		60	65
	10	68	71	64	60		63	64
451	1	73	82	84	84	88	88	85
	2	82	86	82	71	76	78	79
	3	82	86	82	74	69	72	81
	4	83	83	78	74	68	71	82
	5	80	83	79	75	69	69	81
	6	78	82	78	72	70	70	78
	7	75	83	76	70	70	69	80
	8	72	78	72	67		68	80

in which the 47X451 propeller was run in a pusher configuration; i.e., the propeller wake was moving away from the rig rather than through it. The results, shown in Table X, do not appear to be significantly different from those of the other propeller configurations. A more detailed analysis of the data is discussed in Section VII. 2. a.

Another area of significance is in the directivity pattern of the harmonic rotational noise. Figure 18 shows the directivity of the first, second, and tenth harmonics of blade passing frequency for the 47X464, 4-bladed propeller at 300 ft/sec tip speed. Whereas from theory one would expect the maximum to occur slightly behind the plane of rotation with little or no tone noise ahead and behind the propeller, the pattern shown in Figure 18 appears to be rotated 90°, with the maximum occurring along the propeller axis and very little noise in the plane of rotation.

d. Broad-Band Vortex Noise

The 1/3-octave band vortex noise levels are presented in Tables XIII through XV. The levels shown have been corrected for background noise and are adjusted to equivalent free-field conditions.

The data from the fourth test, on the 47X464 blades in a four-bladed configuration, were derived from narrow-band analyses as described previously. Figure 19 shows a typical plot generated for this analysis. Of significance is the width of the peaks. These are seen to be narrow and approximately equal to the filter-response curve at the low-frequencies but are broader at the higher frequencies indicating the presence of narrow-band random noise. Further discussion of this figure is presented in Section VII. 2. c.

A comparison of the broad-band noise spectrum from the three blade configurations tested is presented in Figure 20 for one particular microphone location and operating condition. The 47X-464 blades were designed to reduce both the theoretical loading noise and the broad-band noise predicted by the new method. The predicted decrease in broad-band noise in the 250-1000 Hz frequency range is 3. 3 dB relative to the 47X-451 blades and the average measured decrease is 3. 4 dB for comparable test conditions and microphone locations. This agreement between prediction and measurement provides confidence in the validity of the new propeller vortex noise method developed in Section V. 3 in predicting broad-band noise of static propellers.

Figure 21 illustrates the effects of blade angle on the measured broad-band noise for one operating condition at one microphone position. The effects are seen to be small.

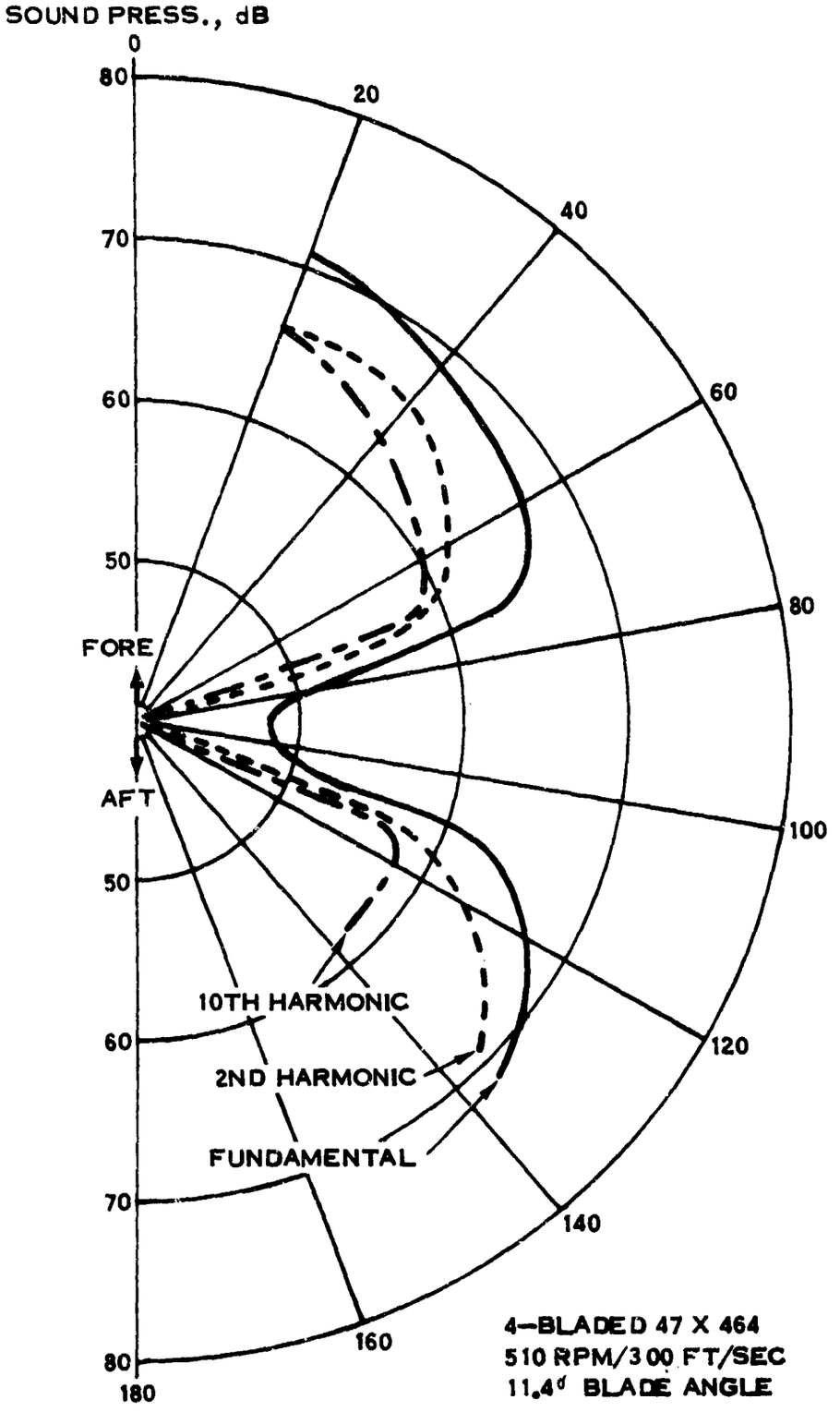

Figure 18. Typical Directivity Pattern of Rotational Noise

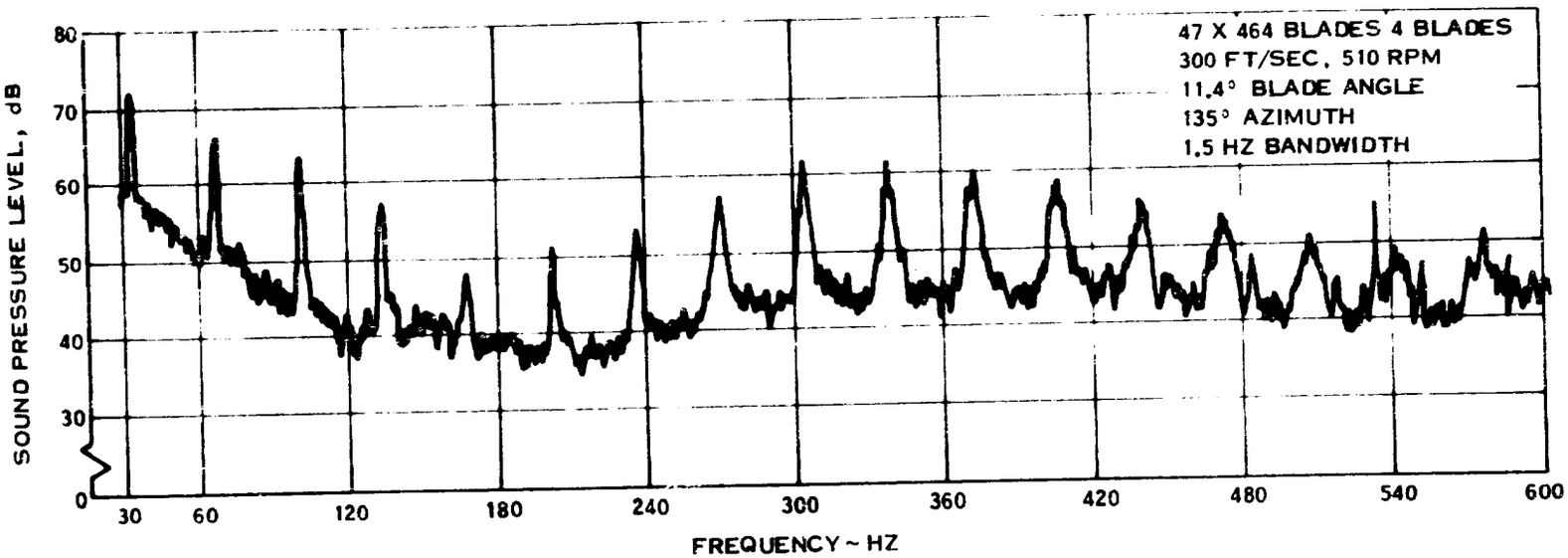

Figure 19. Typical Frequency Spectrum

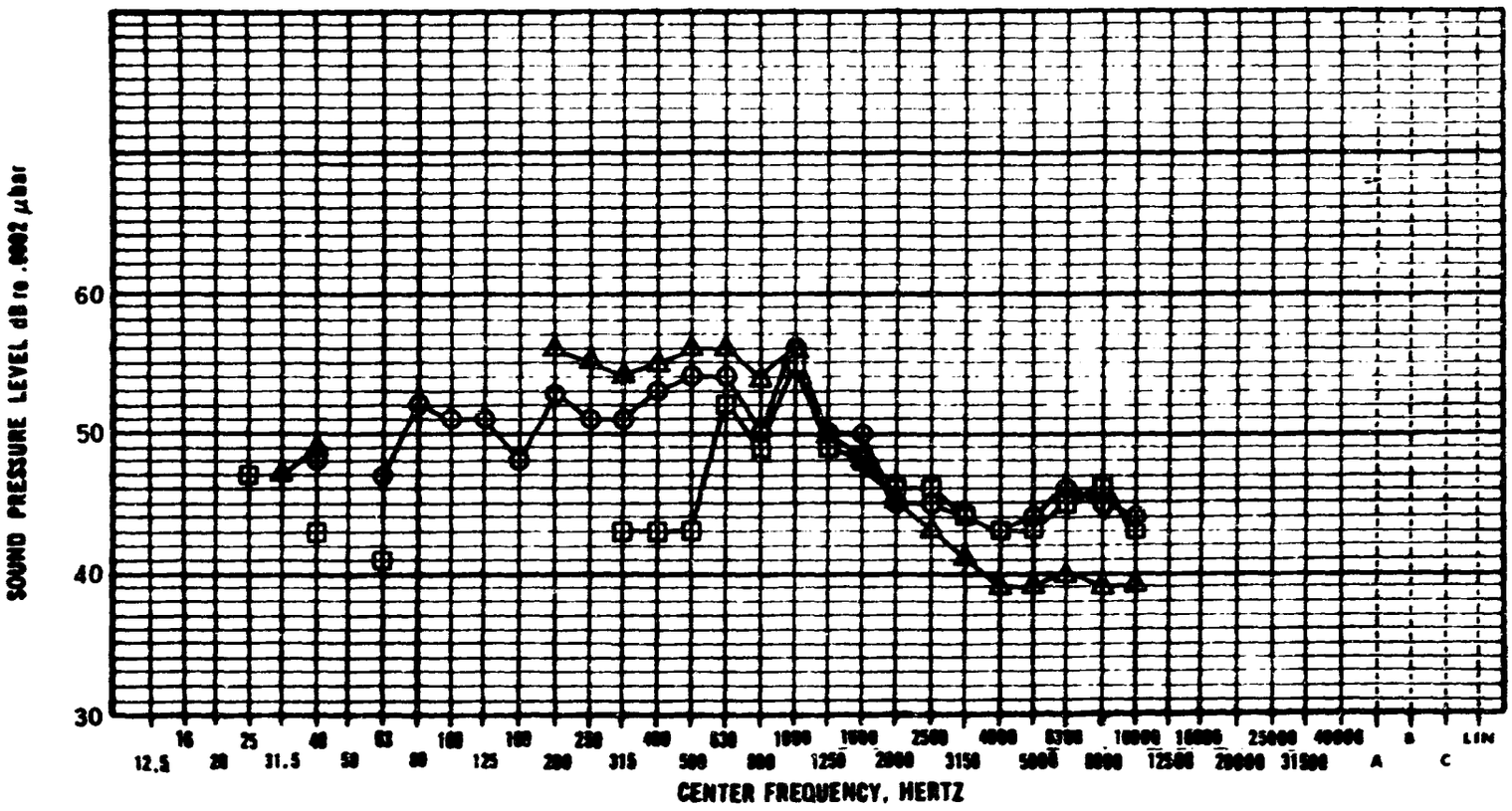

BLADE	$\theta_{.75}$
○ 47 X 394	13.7
△ 47 X 451	12.4
□ 47 X 464	11.4

MIC LOCATION $\psi = 112.5°$, $d = 50$ FT, 340 RPM

Figure 20. Effect of Propeller Configuration on Broad-Band Noise Spectrum

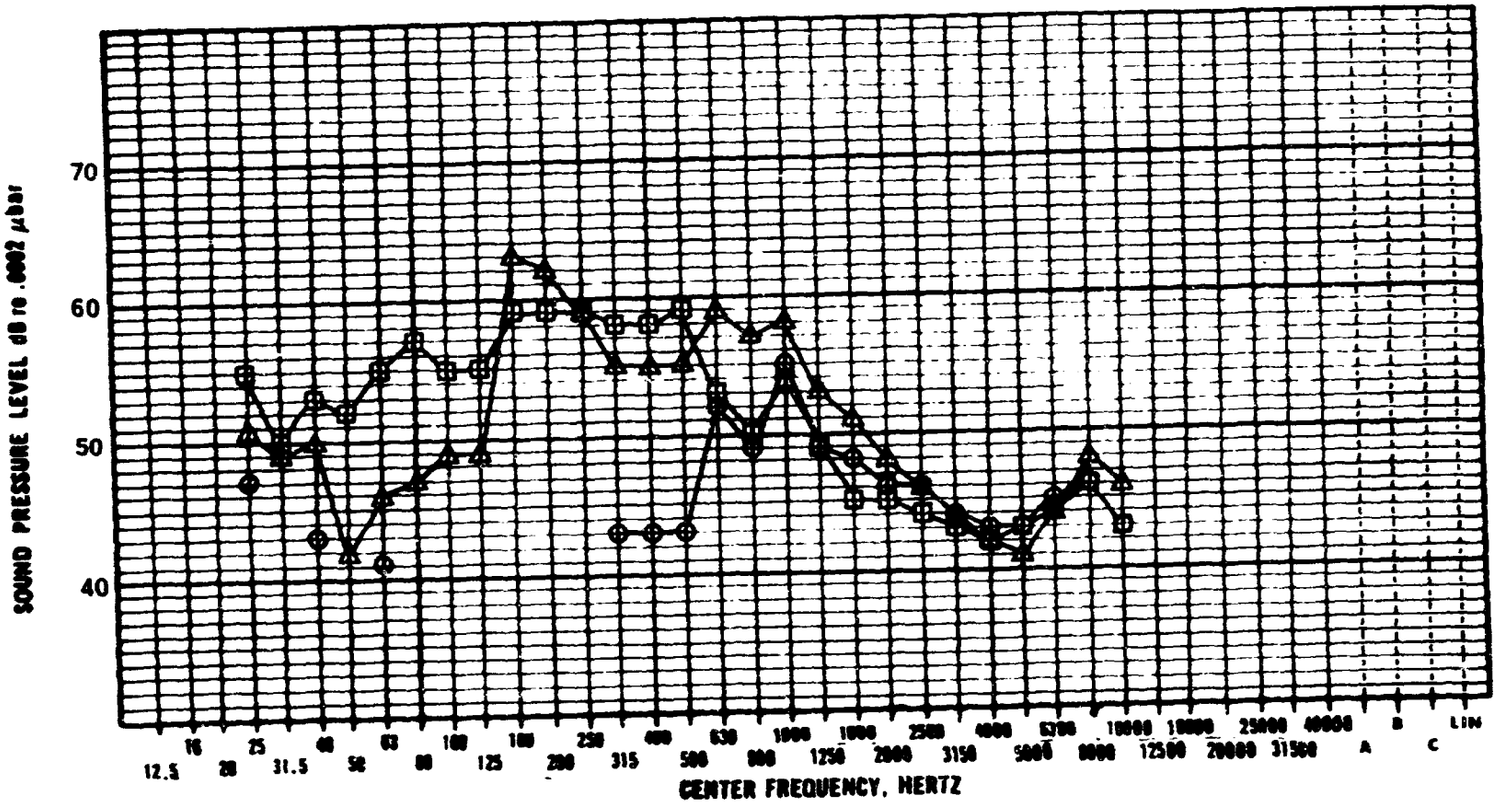

θ.75
△ 15.0°
○ 11.4°
□ 8.1°

MIC LOCATION $\psi = 112.5°$, d = 50 FT 47 X —464 , 340 RPM

Figure 21. Effect of Blade Angle on Propeller Broad-Band Spectrum

TABLE XIII
1/3 - OCTAVE BAND LEVELS FOR THE 47x394 BLADES

19.7° Blade Angle

1/3 Octave Band Center Frequency	150 ft/sec tip speed Azimuth Angle							200 ft/sec tip speed Azimuth Angle						
	6°	22.5°	45°	67.5°	90°	112.5°	135°	6°	22.5°	45°	67.5°	90°	112.5°	135°
25 Hz	B	B	51	B	B	B	B	49	[T]	[T]	[T]	[T]	[T]	[T]
32	B	[T]	[T]	B	B	44	[T]	48	49	52	52	50	52	52
40	B	39	46	B	B	B	42	47	51	51	50	50	80	54
50	B	48	[T]	B	B	B	[T]	49	[T]	[T]	[T]	[T]	[T]	[T]
63	B	47	[T]	B	B	47	[T]	49	[T]	[T]	[T]	[T]	[T]	[T]
80	B	53	[T]	B	B	48	[T]	B	57	52	49	52	53	58
100	B	51	46	B	42	49	[T]	48	[T]	[T]	[T]	[T]	[T]	[T]
125	48	48	45	42	48	49	50	56	[T]	[T]	[T]	48	[T]	[T]
160	51	59	59	B	B	58	B	56	64	60	B	B	59	66
200	59	55	50	47	B	57	50	58	59	57	56	53	56	61
250	54	55	52	51	56	54	55	58	58	56	54	50	52	59
315	50	54	51	49	47	49	51	56	57	57	52	52	55	59
400	53	55	51	49	44	50	53	59	59	57	54	54	61	61
500	50	55	54	49	50	53	55	55	60	57	55	53	62	64
625	50	53	53	50	47	54	54	55	59	57	53	51	58	60
800	47	50	49	47	44	48	47	52	54	53	52	51	54	56
1000	48	50	49	48	46	51	50	54	57	55	53	53	58	58
1250	45	48	47	43	44	47	48	53	55	53	51	51	54	55
1600	47	47	45	44	43	46	42	52	54	52	51	51	52	54
2000	43	44	43	39	40	43	43	49	51	50	48	48	51	51
2500	43	43	42	39	39	43	42	50	51	50	49	48	51	51
3150	41	41	40	38	36	39	40	49	50	49	48	48	49	50
4000	38	39	39	37	35	39	39	47	48	48	47	48	49	49
5000	38	39	39	37	37	39	39	47	49	48	49	48	48	49
6250	39	39	39	38	39	40	39	48	49	49	50	48	48	48
8000	38	39	39	38	39	39	39	46	48	49	49	48	47	47
10000	38	38	38	37	38	39	39	46	48	48	48	46	45	45

B indicates no data due to background noise
T indicates tones

TABLE XIII (Cont)

19.7° Blade Angle (Concluded)

1/3 Octave Band Center Frequency	322 ft/sec tip speed Azimuth Angle						
	6°	22.5°	45°	67.5°	90°	112.5°	135°
25 Hz	57	61	62	63	63	65	64
32	60	59	65	65	66	67	68
40	T	T	T	T	T	T	T
50	60	63	65	65	66	66	67
63	62	63	64	64	65	64	65
80	T	T	T	T	T	T	T
100	T	T	T	T	T	T	T
125	66	66	65	60	59	60	65
160	70	T	T	T	T	T	T
200	74	T	T	T	T	T	T
250	74	67	70	65	60	60	67
315	70	69	69	65	60	61	68
400	72	71	70	65	62	64	73
500	68	72	71	66	64	67	75
625	69	70	70	66	63	66	71
800	65	65	66	63	62	64	65
1000	66	67	67	65	64	65	67
1250	65	65	66	64	61	64	65
1600	66	65	65	64	64	64	65
2000	64	64	63	63	67	61	62
2500	63	64	63	63	63	62	62
3150	64	63	63	63	62	61	61
4000	62	63	63	63	62	61	61
5000	63	64	64	65	63	61	61
6250	64	66	66	67	65	62	62
8000	64	65	66	67	64	62	61
10000	63	65	65	66	63	61	60

T indicates tones

TABLE XIII (Cont)

13.1° Blade Angle

1/3 Octave Band Center Frequency	150 ft/sec tip speed Azimuth Angle							200 ft/sec tip speed Azimuth Angle						
	6°	22.5°	45°	67.5°	90°	112.5°	135°	6°	22.5°	45°	67.5°	90°	112.5°	135°
25 Hz	B	B	B	B	B	B	B	[T]	[T]	[T]	[T]	[T]	[T]	[T]
32	[T]	[T]	[T]	[T]	[T]	B	B	44	B	B	44	48	B	44
40	39	45	39	B	B	B	39	45	48	B	46	46	48	56
50	45	[T]	B	B	B	B	[T]	49	[T]	50	50	B	[T]	[T]
63	B	[T]	B	B	B	B	B	B	[T]	54	50	B	47	[T]
80	B	55	45	49	B	45	51	B	54	52	53	51	52	63
100	50	54	46	50	[illegible]	42	50	51	57	53	57	50	51	[T]
125	55	54	45	42	45	42	51	59	52	55	55	48	51	65
160	56	61	59	63	61	58	63	59	[T]	[T]	[T]	[T]	48	[T]
200	55	57	52	53	B	B	56	58	59	61	58	48	53	63
250	56	55	50	55	57	53	54	60	56	58	56	49	51	59
315	52	53	49	46	46	46	49	57	56	57	53	48	51	60
400	55	52	48	46	44	45	48	59	59	57	55	50	53	60
500	51	56	52	50	49	50	51	55	61	59	57	52	55	63
625	51	52	49	48	47	52	52	55	56	57	52	50	55	59
800	46	46	46	46	45	43	46	51	51	52	52	50	50	54
1000	45	47	46	44	46	48	46	50	52	53	51	51	56	54
1250	43	44	43	40	41	42	43	48	49	49	48	47	50	52
1600	44	43	42	37	35	37	46	50	49	48	46	46	50	50
2000	39	39	38	35	33	36	37	47	47	46	45	42	45	48
2500	40	40	37	36	33	35	38	47	47	46	44	43	45	47
3150	39	39	36	35	30	35	37	46	46	44	43	41	44	46
4000	39	38	37	36	32	35	37	45	45	44	42	41	43	45
5000	37	37	36	35	33	36	37	45	46	44	44	41	44	46
6250	37	37	36	36	33	37	39	46	47	45	45	44	46	47
8000	37	37	36	36	33	37	38	45	46	45	44	42	45	46
10000	35	36	35	34	34	37	38	43	44	43	43	41	44	45

B indicates no data due to background noise
T indicates tones

TABLE XIII (Cont)

13.7° Blade Angle (Concluded)

1/3 Octave Band Center Frequency	300 ft/sec tip speed Azimuth Angle							383 ft/sec tip speed Azimuth Angle						
	6°	22.5°	45°	67.5°	90°	112.5°	135°	6°	22.5°	45°	67.5°	90°	112.5°	135°
25 Hz	53	54	58	60	61	61	59	57	59	62	62	65	64	64
32	[T]	[T]	[T]	[T]	63	[T]	[T]	56	61	63	65	67	67	66
40	60	62	63	60	62	62	64	[T]	[T]	[T]	[T]	[T]	[T]	[T]
50	53	56	56	57	59	60	[T]	65	69	71	71	70	70	67
63	[T]	[T]	[T]	63	59	61	[T]	61	63	64	65	67	67	[T]
80	57	64	64	59	59	59	70	70	74	76	73	66	66	70
100	65	[T]	[T]	64	58	59	[T]	63	69	70	67	63	64	65
125	67	69	66	58	54	55	72	77	72	71	63	59	62	65
160	69	[T]	[T]	[T]	63	62	[T]	75	79	75	73	[T]	[T]	[T]
200	70	73	68	67	59	57	73	77	75	73	70	63	64	70
250	72	67	67	61	56	57	70	78	71	70	67	60	62	66
315	68	68	68	63	54	58	70	73	72	73	68	59	62	69
400	71	71	71	65	56	61	72	77	75	75	70	61	67	71
500	67	74	72	67	61	61	75	73	79	76	71	63	71	74
625	68	69	66	63	58	61	70	74	73	72	68	61	68	71
800	65	64	65	61	56	59	65	71	69	71	66	61	63	67
1000	69	66	65	62	57	62	67	70	72	70	67	61	65	70
1250	62	63	63	61	58	59	65	68	68	69	66	61	63	67
1600	62	61	61	59	56	57	64	68	67	67	65	60	63	67
2000	59	58	58	57	52	54	60	65	65	64	61	57	59	64
2500	59	58	57	56	54	55	60	64	65	63	62	58	60	63
3150	58	57	56	55	53	54	57	64	63	62	60	58	60	62
4000	56	56	55	53	53	54	57	62	63	62	60	58	60	62
5000	57	57	55	54	53	54	57	63	63	62	61	60	61	63
6250	58	58	56	55	54	55	58	64	64	63	62	62	62	64
8000	57	57	55	55	54	55	57	63	63	62	61	60	62	63
10000	55	55	54	54	53	54	56	62	62	61	61	59	60	62

T indicates tones

TABLE XIII (Cont)

8.7° Blade Angle

1/3 Octave Band Center Frequency	150 ft/sec tip speed Azimuth Angle							200 ft/sec tip speed Azimuth Angle						
	0°	22.5°	45°	67.5°	90°	112.5°	135°	0°	22.5°	45°	67.5°	90°	112.5°	135°
25 Hz	42	B	B	B	B	B	B	[T]	[T]	[T]	[T]	[T]	[T]	[T]
32	B	44	48	B	B	B	B	B	50	55	44	48	B	48
40	47	48	46	45	42	42	42	45	54	55	49	46	45	48
50	49	48	B	B	B	B	B	49	[T]	[T]	[T]	B	[T]	[T]
63	52	57	53	54	47	50	44	54	54	57	51	47	[T]	[T]
80	57	60	59	59	52	51	48	54	55	[T]	52	[T]	[T]	58
100	46	54	51	53	B	46	46	46	55	59	54	48	53	59
125	48	51	48	49	45	49	48	53	51	55	51	45	51	55
160	48	61	59	55	B	B	B	55	59	65	55	B	B	59
200	48	54	50	47	48	49	50	58	55	61	55	48	49	58
250	48	54	50	47	48	49	50	58	55	61	55	48	49	58
315	50	50	48	46	44	42	48	54	54	57	52	47	50	56
400	52	50	48	47	44	45	48	58	56	57	55	49	54	56
500	48	52	52	51	49	50	51	55	60	60	55	52	54	58
625	49	51	49	48	46	52	54	56	57	58	52	50	54	58
800	46	46	46	47	48	45	44	53	53	54	51	51	50	53
1000	45	47	46	44	45	50	46	52	54	54	51	51	55	54
1250	42	43	43	42	42	44	43	48	51	53	48	47	49	51
1600	40	40	40	39	39	51	B	49	49	50	45	43	46	48
2000	38	38	38	35	33	36	33	46	45	47	43	41	43	44
2500	37	37	36	34	31	35	36	44	44	45	43	39	42	43
3150	36	36	34	32	B	31	32	43	43	43	40	35	40	40
4000	32	33	32	30	27	31	29	39	41	41	37	35	39	37
5000	38	31	29	27	27	30	29	38	39	38	35	35	37	36
6250	21	27	21	24	21	25	26	36	38	37	34	34	36	36
8000	B	20	B	B	B	B	B	32	35	35	29	28	35	32
10000	B	16	B	B	B	B	B	24	29	29	25	18	29	27

B Indicates no data due to background noise
T Indicates tones

TABLE XIII (Concluded)

8.7° Blade Angle (Concluded)

1/3 Octave Band Center Frequency	300 ft/sec tip speed Azimuth Angle							442 ft/sec tip speed Azimuth Angle						
	6°	22.5°	45°	67.5°	90°	112.5°	135°	6°	22.5°	45°	67.5°	90°	112.5°	135°
25 Hz	50	53	54	57	58	57	54	57	59	62	63	63	66	63
32	T	T	T	T	T	T	T	57	61	64	64	66	67	66
40	58	63	65	60	57	59	57	61	64	68	67	69	69	68
50	51	57	53	56	55	60	55	T	T	T	T	T	T	T
63	T	T	T	T	T	T	T	64	65	69	67	68	68	69
80	63	69	65	64	60	63	61	66	68	68	66	68	70	71
100	65	T	T	T	59	T	T	T	T	T	T	66	T	T
125	70	67	63	61	54	60	60	70	66	65	61	60	66	69
160	70	73	70	68	63	69	71	T	T	T	T	T	T	T
200	70	68	68	67	59	61	66	75	75	76	70	70	69	78
250	69	67	67	67	56	59	62	78	71	73	66	63	67	72
315	69	67	67	67	53	60	66	75	72	73	68	62	69	75
400	70	68	67	64	55	61	68	79	74	76	69	64	70	77
500	66	69	69	65	62	63	71	74	76	77	71	66	72	84
625	68	67	66	64	57	61	67	74	74	75	69	63	70	80
800	64	64	64	61	55	59	61	72	70	71	67	63	67	72
1000	63	64	65	62	56	61	63	71	73	73	68	64	69	75
1250	61	62	63	60	56	58	61	69	70	72	68	63	67	72
1600	60	60	61	59	53	56	59	69	69	71	67	62	67	72
2000	57	56	56	55	50	53	55	67	66	67	65	60	63	69
2500	55	55	55	54	49	52	54	66	67	66	64	60	63	67
3150	54	53	52	51	46	49	51	65	64	64	61	58	61	65
4000	50	51	50	19	45	48	49	60	62	61	58	55	59	62
5000	49	49	49	48	49	47	48	58	60	59	58	54	57	60
6250	47	48	48	47	44	47	47	57	58	58	56	54	58	58
8000	43	44	44	44	40	44	45	53	54	54	51	51	52	54
10000	37	38	38	39	36	39	43	46	48	47	45	45	47	47

T indicates tones

TABLE XIV

1/3 OCTAVE BAND LEVELS FOR THE 47 X 451 BLADES

16.4° Blade Angle

1/3 Octave Band Center Frequency	147 Ft Sec Tip Speed							200 Ft Sec Tip Speed							353 Ft Sec Tip Speed						
	Azimuth Angle							Azimuth Angle							Azimuth Angle						
	6°	22.5°	45°	67.5°	90°	112.5°	135°	6°	22.5°	45°	67.5°	90°	112.5°	135°	6°	22.5°	45°	67.5°	90°	112.5°	135°
25Hz	57	50	44	45	45	55	59	T	T	T	T	T	T	T	T	61	64	64	65	63	65
32	T	T	T	T	B	T	59	42	52	52	54	B	55	T	62	64	64	66	67	64	66
40	T	T	T	T	42	T	56	52	55	53	52	50	T	T	T	T	T	T	T	T	T
50	56	T	T	T	44	T	T	T	T	T	T	50	T	T	61	66	65	67	67	65	66
63	54	T	54	52	T	T	T	57	60	58	53	51	T	60	62	66	67	67	67	65	67
80	58	T	58	56	T	T	T	61	T	T	57	56	T	62	T	T	T	T	68	T	T
100	57	59	56	53	50	53	57	57	T	T	57	53	54	61	61	68	67	65	64	64	66
125	59	56	52	47	46	50	55	63	T	56	54	52	52	58	T	T	T	T	62	T	T
160	59	63	60	59	56	60	65	63	T	63	63	56	60	67	T	T	T	T	68	72	79
200	59	57	59	59	54	56	62	65	69	63	59	54	58	64	T	T	T	T	69	70	74
250	60	55	56	57	50	57	60	67	66	62	58	52	56	62	T	T	T	T	63	T	T
315	58	55	56	54	49	54	58	62	65	62	56	49	55	60	T	T	T	T	61	T	T
400	60	57	56	52	49	54	57	66	65	62	56	53	57	63	T	T	T	T	62	T	T
500	55	58	57	57	51	55	59	61	67	63	59	53	57	63	71	T	T	71	64	70	75
630	54	55	55	54	51	53	56	62	64	62	56	52	56	61	63	73	72	69	64	68	71
800	51	51	51	52	50	52	52	58	59	58	55	53	54	57	69	66	69	66	62	66	67
1000	50	51	51	51	49	52	53	57	60	58	54	54	57	57	68	69	69	65	62	67	69
1250	48	48	47	50	47	47	50	55	57	55	52	51	52	55	67	66	67	65	60	64	67
1600	46	46	47	47	44	45	50	54	54	53	50	47	49	53	67	65	64	63	58	63	65
2000	43	42	42	45	41	43	45	51	51	50	47	44	46	48	62	61	62	59	56	60	62
2500	42	42	41	43	40	42	43	51	51	49	46	43	45	48	63	61	60	58	56	59	61
3150	42	40	40	41	38	41	42	49	49	47	44	41	43	46	61	60	58	56	55	58	59
4000	39	38	39	40	37	40	40	47	48	45	43	40	42	44	59	58	57	55	54	56	58
5000	39	37	39	39	36	40	40	47	47	46	43	40	43	44	59	58	57	54	54	57	57
6300	40	38	39	41	37	40	39	48	48	47	44	42	44	46	59	59	57	56	55	58	58
8000	39	38	38	40	37	39	38	47	47	46	43	41	44	45	58	58	57	54	54	57	58
10000	37	36	36	38	36	38	38	45	46	45	43	40	43	44	57	57	56	54	53	56	57

T indicates Tones
B indicates Background Noise

TABLE XIV (Cont'd)

12.4° Blade Angle

1/3 Octave Band Center Frequency	147 Ft/Sec Tip Speed							200 Ft/Sec Tip Speed							300 Ft/Sec Tip Speed							395 Ft/Sec Tip Speed						
	Azimuth Angle							Azimuth Angle							Azimuth Angle							Azimuth Angle						
	6°	22.5°	45°	67.5°	90°	112.5°	135°	6°	22.5°	45°	67.5°	90°	112.5°	135°	6°	22.5°	45°	67.5°	90°	112.5°	135°	6°	22.5°	45°	67.5°	90°	112.5°	135°
25Hz	43	B	T	T	T	T	T	T	T	58	T	T	T	T	61	54	61	60	65	61	62	58	62	63	64	66	66	66
32	T	T	T	T	B	T	51	48	54	50	54	52	47	48	T	T	T	T	T	T	T	59	63	65	66	68	68	67
40	T	T	T	46	41	47	T	52	54	50	52	50	49	50	60	64	64	69	64	68	70	T	T	T	69	71	T	70
50	T	T	T	T	42	T	T	T	T	T	T	50	T	T	56	58	58	59	60	60	60	T	T	T	68	71	T	70
63	B	50	T	48	46	45	53	T	T	T	T	51	T	T	T	T	T	T	64	T	T	62	67	68	66	67	68	66
80	T	T	T	T	50	T	T	T	T	T	T	56	T	T	65	64	64	74	64	71	76	T	T	T	T	70	69	T
100	T	T	T	48	49	48	T	T	T	T	T	52	T	T	T	T	T	T	T	T	T	T	T	T	T	67	66	T
125	T	T	48	44	46	43	T	T	T	T	T	49	T	55	T	T	T	T	T	T	T	T	T	T	68	T	T	T
160	T	59	58	59	56	56	T	T	T	60	61	B	60	62	T	T	70	T	T	T	T	T	T	T	74	73	68	T
200	T	56	55	54	49	51	57	T	61	61	61	51	56	62	T	T	T	71	62	69	T	T	T	T	72	72	66	T
250	56	54	54	53	48	51	54	63	59	59	58	51	55	59	T	T	T	T	60	T	T	T	T	T	T	68	T	T
315	54	53	53	50	47	52	54	60	59	58	55	51	54	57	T	T	T	T	T	T	T	T	T	T	T	66	T	T
400	56	54	52	49	48	50	53	62	60	60	54	53	55	59	T	T	T	T	T	T	T	T	T	T	T	69	T	T
500	52	57	54	53	49	52	55	58	61	59	59	52	56	60	68	70	68	71	63	73	77	73	82	80	75	68	71	75
630	52	54	53	51	51	53	54	58	59	58	56	52	56	58	70	68	68	66	62	68	70	74	77	74	71	66	69	73
800	49	50	50	49	49	51	51	55	55	55	54	52	54	55	66	66	65	64	59	64	65	71	72	71	69	65	66	70
1000	47	49	49	47	48	51	50	53	56	54	53	52	56	55	65	66	65	64	59	65	66	70	75	72	70	66	68	71
1250	44	45	45	44	44	44	48	52	52	53	52	50	50	54	63	64	64	63	57	64	64	69	72	71	69	64	66	69
1600	41	44	44	42	41	37	46	50	49	50	49	45	48	51	62	61	62	61	55	62	63	68	70	69	67	63	64	68
2000	41	41	41	39	38	39	42	46	47	46	45	43	45	47	59	58	57	58	52	58	58	65	68	65	64	61	60	64
2500	41	41	40	38	36	38	40	45	46	45	44	41	43	45	58	57	56	55	52	56	58	64	66	64	62	60	60	63
3150	38	38	38	36	33	35	36	44	44	43	40	38	41	43	55	55	54	53	50	54	55	62	64	61	60	58	58	60
4000	35	35	35	32	31	33	34	41	42	41	38	37	39	40	53	53	52	51	48	53	53	59	62	60	58	56	56	58
5000	33	34	33	33	33	34	36	41	42	40	37	37	39	41	52	51	51	52	47	51	52	58	61	59	57	55	55	57
6300	32	33	33	34	34	36	36	40	41	40	37	39	40	42	51	51	51	51	47	52	52	57	62	59	56	56	56	57
8000	32	32	33	34	34	36	36	38	38	38	37	37	39	41	51	50	48	49	46	51	51	56	59	57	55	54	54	55
10000	31	32	33	35	35	39	39	36	37	37	36	36	39	40	48	47	46	48	45	51	50	54	58	55	53	53	53	54

B indicates Background Noise
T indicates Tones

TABLE XIV (Concluded)

8.4° Blade Angle

1/3 Octave Band Center Frequency	200 Ft/Sec Tip Speed							300 Ft Sec Tip Speed							442 Ft Sec Tip Speed						
	Azimuth Angle							Azimuth Angle							Azimuth Angle						
	6°	22.5°	45°	67.5°	90°	112.5°	135°	6°	22.5°	45°	67.5°	90°	112.5°	135°	6°	22.5°	45°	67.5°	90°	112.5°	135°
25Hz	[T]	[T]	[T]	[T]	[T]	[T]	[T]	50	46	55	56	56	58	55	61	62	63	65	65	67	65
32	46	43	47	46	50	47	51	[T]	[T]	[T]	[T]	[T]	[T]	[T]	61	62	65	66	67	67	66
40	47	48	48	43	49	45	49	55	57	55	55	56	58	57	63	65	66	67	69	69	68
50	[T]	[T]	[T]	[T]	47	[T]	[T]	52	56	55	54	55	56	55	[T]	[T]	[T]	[T]	[T]	[T]	[T]
63	50	51	T	T	49	T	T	54	[T]	57	[T]	55	56	56	66	67	67	68	67	68	67
80	55	[T]	T	T	54	[T]	T	54	58	56	56	56	57	57	65	69	68	68	67	69	69
100	52	T	[T]	T	50	53	T	[T]	[T]	58	57	56	57	56	[T]	[T]	[T]	[T]	64	66	[T]
125	[T]	T	49	T	46	50	55	[T]	55	52	51	50	50	52	72	63	62	60	60	60	61
160	[T]	T	58	[T]	B	56	62	56	63	62	59	60	60	62	[T]	[T]	73	[T]	68	[T]	[T]
200	58	56	54	54	49	54	59	57	61	57	55	54	57	59	T	73	70	65	63	66	68
250	58	56	54	51	48	52	58	59	58	55	54	52	56	56	T	66	66	63	62	65	66
315	55	55	53	51	48	53	54	57	58	55	52	49	56	53	T	[T]	[T]	[T]	[T]	[T]	[T]
400	59	57	54	51	50	53	60	61	60	58	53	53	55	55	[T]	[T]	[T]	[T]	[T]	[T]	[T]
500	55	59	58	57	52	55	58	58	63	61	61	59	58	61	72	73	71	64	61	67	71
630	57	58	56	53	53	56	58	60	62	60	58	59	62	62	74	68	67	63	62	65	67
800	54	54	54	53	52	54	54	59	59	59	57	55	58	58	72	65	66	63	62	63	65
1000	54	56	54	53	53	57	56	60	62	61	58	56	60	60	73	68	67	64	62	66	67
1250	52	53	53	51	50	52	54	59	61	61	58	56	58	61	71	68	69	65	62	64	68
1600	50	51	51	49	45	48	52	59	60	59	57	54	57	59	71	68	68	65	61	64	68
2000	47	47	47	46	42	46	48	57	57	56	54	50	54	56	69	66	66	63	60	62	65
2500	48	48	47	45	42	46	47	55	56	55	53	49	53	55	68	67	66	64	60	63	65
3150	50	49	49	47	43	48	48	54	53	52	51	47	51	51	66	66	64	62	58	61	63
4000	50	50	50	49	43	51	49	51	52	51	49	47	50	50	63	63	62	60	57	60	61
5000	46	46	47	47	41	50	46	53	54	53	51	48	52	53	62	62	61	60	57	60	61
6300	44	45	45	44	41	47	45	56	58	55	54	52	56	56	62	63	61	60	59	61	62
8000	42	42	42	42	40	44	43	53	55	54	54	51	57	56	60	61	59	58	58	60	61
10000	38	38	39	39	39	42	41	49	51	51	51	49	55	53	59	60	58	58	58	60	60

T indicates Tones
B indicates Background Noise

TABLE XV

1/3 - OCTAVE BAND LEVELS FOR THE 47 x 464 BLADES

15^{o} Blade Angle

1/3 Octave Band Center Frequency	150 Ft Sec Tip Speed							200 Ft Sec Tip Speed							300 Ft/Sec Tip Speed						
	Azimuth Angle							Azimuth Angle							Azimuth Angle						
	14.5^{o}	22.5^{o}	45^{o}	67.5^{o}	90^{o}	112.5^{o}	135^{o}	14.5^{o}	22.5^{o}	45^{o}	67.5^{o}	90^{o}	112.5^{o}	135^{o}	14.5^{o}	22.5^{o}	45^{o}	67.5^{o}	90^{o}	112.5^{o}	135^{o}
25Hz	52	B	B	B	B	B	B	53	B	50	47	52	51	51	57	58	59	63	63	63	61
32	45	B	B	B	B	B	B	48	B	47	42	B	49	49	58	60	60	63	63	64	62
40	44	B	34	B	34	37	35	50	44	47	47	52	50	49	58	61	60	62	62	64	62
50	B	B	B	B	B	B	B	51	41	47	45	47	42	49	58	61	61	62	62	62	62
63	44	B	B	41	B	41	B	54	48	48	47	50	46	53	60	62	61	61	62	51	61
80	51	43	B	43	43	46	B	56	51	50	46	53	47	53	61	64	62	61	61	62	60
100	53	46	B	43	B	45	B	58	52	52	46	50	49	52	62	65	61	60	58	60	57
125	52	B	B	B	B	B	B	58	48	48	B	B	49	53	60	62	58	56	54	57	53
160	62	B	B	B	B	B	B	68	61	53	B	B	63	63	71	71	67	62	62	66	62
200	58	B	45	53	B	51	52	65	59	60	B	52	62	59	68	68	68	62	59	64	64
250	57	39	52	55	45	50	54	65	59	60	49	50	59	57	66	66	67	58	58	62	63
315	55	41	51	52	43	49	54	63	61	60	50	52	55	59	65	67	66	59	57	62	63
400	54	46	49	47	42	49	54	61	61	59	50	52	55	58	67	67	67	59	58	62	63
500	55	50	51	52	45	49	52	64	59	59	53	53	55	60	69	67	69	62	60	63	64
630	55	50	54	53	51	51	53	64	61	61	55	54	59	61	72	70	73	62	64	66	69
800	50	47	51	50	48	49	49	58	58	58	53	53	57	56	68	67	68	60	62	64	65
1000	51	48	49	47	48	51	50	60	59	58	52	55	58	57	70	69	68	60	62	65	67
1250	47	45	46	45	44	46	46	57	56	55	50	52	53	55	67	66	66	60	61	63	64
1600	41	42	43	40	42	37	43	55	54	54	49	50	51	53	66	66	66	61	62	63	64
2000	41	39	40	39	39	39	40	51	51	51	47	48	48	49	64	64	64	61	61	61	62
2500	40	37	39	37	37	36	38	50	50	49	47	46	46	49	63	64	64	61	61	61	62
3150	38	36	38	35	35	33	35	47	47	48	46	44	44	46	61	62	62	60	59	59	60
4000	38	36	38	35	35	32	34	44	44	45	44	42	42	43	58	59	60	57	56	56	57
5000	40	39	40	38	37	36	38	44	44	45	43	41	41	42	56	56	57	55	54	54	55
6300	40	39	42	40	38	38	39	48	48	48	46	44	44	45	54	55	56	55	53	53	54
8000	35	33	37	36	36	36	39	50	50	50	48	46	48	48	56	57	57	55	52	52	54
10000	34	31	35	34	34	36	38	43	42	46	44	45	46	43	59	60	60	57	54	54	55

B = No Data Due to Background Noise

TABLE XV (Cont'd)

11.4° Blade Angle

1/3 Octave Band Center Frequency	150 Ft/Sec Tip Speed							200 Ft/Sec Tip Speed							300 Ft/Sec Tip Speed							353 Ft/Sec Tip Speed						
	Azimuth Angle							Azimuth Angle							Azimuth Angle							Azimuth Angle						
	14.5°	22.5°	45°	67.5°	90°	112.5°	135°	14.5°	22.5°	45°	67.5°	90°	112.5°	135°	14.5°	22.5°	45°	67.5°	90°	112.5°	135°	14.5°	22.5°	45°	67.5°	90°	112.5°	135°
25 Hz	39	B	B	B	B	B	B	46	B	49	45	46	47	47	52	55	58	59	61	61	60	58	63	64	65	67	62	65
32	B	B	B	B	B	B	B	B	B	44	B	B	B	43	53	57	59	60	59	60	60	60	63	64	64	67	63	66
40	41	B	B	B	B	B	B	47	38	47	42	42	43	47	54	59	58	59	58	59	58	62	62	64	64	65	64	64
50	44	B	B	B	B	B	B	48	B	45	38	B	B	40	55	58	58	58	57	59	57	62	63	64	63	65	62	63
63	47	B	B	B	B	B	B	52	B	45	44	38	41	43	58	59	56	57	55	58	57	63	62	62	62	63	63	63
80	49	B	B	40	B	B	B	55	40	48	43	46	B	51	57	60	57	58	56	59	54	65	64	63	63	64	63	64
100	52	42	B	B	B	B	B	58	45	52	B	B	B	B	60	61	56	57	53	59	51	65	62	63	61	62	55	62
125	51	B	B	B	B	B	B	57	B	52	B	B	B	B	58	59	53	52	49	53	48	63	61	60	56	58	54	56
160	58	51	B	B	B	B	B	67	51	63	B	B	B	B	67	71	63	66	B	60	B	76	70	72	67	68	60	68
200	57	52	B	B	B	48	B	64	51	59	B	B	B	53	70	68	60	60	49	62	56	73	68	68	62	63	61	66
250	56	51	43	46	B	46	B	63	50	57	49	43	B	52	65	67	60	60	49	61	59	72	69	69	60	60	61	65
315	56	50	44	45	B	48	42	63	52	56	50	43	43	52	66	64	62	58	50	60	59	73	67	68	62	59	60	63
400	54	50	44	46	38	45	47	62	54	57	48	46	43	54	68	67	62	58	54	59	61	72	73	68	62	61	59	65
500	54	52	46	50	42	46	49	64	56	59	52	48	43	57	72	69	62	63	56	62	63	73	72	71	64	63	63	67
630	51	50	48	49	48	50	51	59	54	54	55	52	52	58	69	67	65	65	62	65	63	72	72	74	67	65	69	69
800	47	46	47	48	48	48	47	55	52	54	53	50	49	54	65	63	63	63	59	61	62	67	69	71	66	63	67	66
1000	48	46	45	45	45	51	48	57	53	53	51	51	55	55	66	65	63	62	58	62	61	71	70	71	65	63	67	68
1250	45	45	44	43	41	45	45	54	51	52	49	48	49	53	63	61	61	60	59	60	61	68	67	69	63	63	65	66
1600	36	43	42	37	36	39	43	53	51	51	48	47	48	52	63	62	60	59	58	60	61	67	67	68	62	63	65	65
2000	41	41	40	38	37	40	41	51	49	49	46	45	46	49	61	59	59	57	57	57	58	65	64	66	61	62	62	63
2500	40	41	40	37	36	39	40	50	48	48	46	44	46	48	60	59	59	57	57	57	58	64	64	65	61	62	63	64
3150	38	38	39	37	34	37	37	48	47	47	45	43	44	47	58	58	58	56	55	56	57	64	62	64	61	62	62	62
4000	37	38	38	36	34	36	36	45	45	46	44	42	43	45	56	56	56	55	54	54	55	62	61	62	59	60	59	60
5000	39	38	38	38	35	38	39	45	44	45	44	42	43	45	54	54	55	54	53	53	55	61	60	60	59	59	58	59
6300	39	37	39	37	39	39	40	47	45	46	45	44	45	45	54	54	54	54	52	53	55	59	59	60	59	59	58	59
8000	30	29	33	34	35	37	38	48	45	46	45	45	46	47	54	54	55	54	52	53	55	59	58	59	57	56	57	58
10000	29	26	30	31	33	36	38	41	38	41	41	41	43	43	55	54	55	55	51	53	55	58	57	57	56	55	56	57

B = No Data Due to Background Noise

TABLE XV (Concluded)

8.1° Blade Angle

1/3 Octave Band Center Frequency	150 Ft/Sec Tip Speed							200 Ft/Sec Tip Speed							300 Ft/Sec Tip Speed							400 Ft/Sec Tip Speed						
	Azimuth Angle							Azimuth Angle							Azimuth Angle							Azimuth Angle						
	14.5°	22.5°	45°	67.5°	90°	112.5°	135°	14.5°	22.5°	45°	67.5°	90°	112.5°	135°	14.5°	22.5°	45°	67.5°	90°	112.5°	135°	14.5°	22.5°	45°	67.5°	90°	112.5°	135°
25 Hz	B	B	B	B	B	B	B	B	B	B	B	42	55	B	52	B	52	55	55	55	54	59	62	63	64	66	63	65
32	B	B	B	B	B	B	B	B	B	B	B	B	50	B	52	50	51	55	53	55	53	60	62	63	64	66	64	65
40	B	B	B	B	B	40	B	41	B	40	B	40	53	36	54	52	54	56	54	55	54	60	61	63	64	65	63	64
50	B	B	B	B	B	B	B	41	B	B	B	B	52	B	55	54	52	55	51	55	50	62	61	64	64	64	63	63
63	B	B	B	B	B	38	B	47	B	B	38	42	55	B	54	54	50	55	51	56	49	63	64	64	63	63	62	63
80	B	B	B	40	B	B	B	50	43	B	40	47	57	B	56	56	52	56	49	56	52	65	64	65	62	64	61	64
100	42	B	B	B	B	B	B	52	42	40	40	41	55	B	55	56	53	56	47	56	B	64	62	63	59	61	55	63
125	B	B	B	B	B	B	B	49	B	B	B	B	55	B	52	53	44	51	B	54	42	62	60	61	57	57	53	58
160	52	B	B	B	B	B	B	52	B	B	B	B	59	B	55	55	52	53	48	56	B	65	61	63	57	57	56	58
200	46	B	46	B	B	53	B	53	B	46	B	47	59	B	58	57	55	56	45	57	52	67	63	63	59	64	58	63
250	42	B	50	40	B	51	41	55	46	50	41	45	59	47	56	57	53	56	46	58	53	66	59	62	59	62	58	64
315	44	39	48	41	B	48	B	54	50	50	43	42	58	46	55	57	53	56	49	57	53	65	60	62	57	60	59	61
400	44	44	48	40	B	44	B	53	52	51	43	43	58	45	56	59	55	57	49	57	52	63	62	65	57	60	58	63
500	45	49	52	45	37	51	39	53	52	53	49	47	59	46	58	62	57	58	52	59	55	66	64	66	61	63	59	65
630	46	46	51	46	48	58	46	54	52	54	51	49	53	52	60	54	61	60	58	60	61	70	66	70	65	61	64	66
800	43	44	49	47	47	52	42	51	50	52	52	49	50	48	56	59	59	58	56	58	57	65	65	66	63	61	62	63
1000	45	45	46	43	43	49	43	52	51	51	50	49	54	50	59	62	60	58	54	59	59	67	67	68	63	61	64	65
1250	43	43	45	41	41	46	41	50	48	50	47	46	49	48	57	59	60	57	53	57	57	66	65	66	62	59	62	63
1600	B	41	42	37	36	37	32	48	47	48	46	41	45	44	57	60	59	57	53	56	56	67	66	66	63	59	62	63
2000	39	39	40	38	35	40	35	47	45	46	44	41	45	43	55	57	56	54	51	54	53	65	64	64	61	59	60	61
2500	39	39	40	37	34	38	35	46	45	46	44	41	44	42	54	56	55	53	51	54	51	64	64	64	60	59	60	60
3150	39	38	39	38	32	38	34	45	44	45	44	40	43	41	54	55	55	53	50	52	51	63	63	63	60	58	59	59
4000	38	38	38	36	31	36	34	44	43	44	43	39	42	40	52	53	53	53	49	51	49	61	60	62	59	57	57	57
5000	36	35	37	36	32	35	34	45	44	44	44	40	43	41	52	53	52	52	49	51	50	61	60	61	59	57	57	57
6250	33	32	35	35	33	36	34	45	43	45	44	41	44	42	54	54	54	53	50	51	51	61	61	62	59	58	58	58
8000	33	32	36	39	39	42	39	44	40	45	45	43	46	44	56	55	55	54	51	54	53	61	61	61	60	59	59	59
10000	32	29	33	34	36	37	37	39	38	40	42	42	43	42	53	53	54	55	51	54	53	60	60	60	60	58	59	58

B - No Data Due to Background Noise

SECTION VII

CORRELATION OF TEST DATA WITH THEORY

1. INTRODUCTION

The test program described in the previous section had three major objectives: a) to provide harmonic rotational noise data to validate the propeller noise detectability computer program calculation procedure for rotational noise, b) to provide the 1/3-octave-band noise data bank needed to determine values of the 3 empirical coefficients in the new vortex noise prediction procedure developed under this contract, and c) to demonstrate the reduction in noise obtained from a propeller with new blades designed for reduced detectability.

Earlier evaluations by Hamilton Standard of the rotational noise calculation procedure for moderate- and high-tip-speed propellers had shown fair agreement between predicted and measured harmonic noise levels. The evaluations were done for field points both near and far from the propeller and for both static and flight operation. However, the predicted rotational noise differed greatly from the low-tip-speed data obtained during the test programs described above. Not only were the measured higher harmonics much larger than predicted, but even the fundamental (first) harmonic was significantly larger than predicted. An extensive investigation of possible causes of the lack of agreement and of ways to improve agreement was undertaken and is reported in the following section.

The 1/3-octave band data bank obtained from the test program was used to select the force coefficient C_F, the frequency coefficient C_f, and the Reynolds number exponent which provide best agreement between the vortex noise predicted by the method developed under this contract and data. This method is discussed in Section V.3. The values of the three parameters selected are 8.0, 0.06, and -1.0, respectively.

The theories for harmonic and vortex noise were used to design new blades for reduced detectability. The theory for harmonic loading noise indicates that increasing blade chord reduces rotational noise. Therefore, the propeller with the new wider 47X-464 blades should produce less rotational loading noise than the first two propellers tested at the beginning of the program. However, the increased chord increases thickness noise sufficiently that it is predicted to exceed loading noise. The measured data show no significant change in the harmonic noise levels. The new vortex noise method predicts a reduction of 3.3 dB in vortex noise with the wider blades. A comparison of the measured noise in the bands from 250 to 1000 Hz shows a decrease of 3.4 dB.

2. HARMONIC ROTATIONAL NOISE

At the start of the contract it was planned to use the harmonic noise data to verify the accuracy of the rotational noise levels predicted by the computer program and to permit small changes to improve correlation. However the first test period showed significant differences between the test data and predictions. These differences also were present in the data from the other four test periods.

The predicted harmonic noise levels had the following general characteristics: a) the SPL of the fundamental (at blade passing frequency) harmonic noise increases by about 37 dB per doubling of rpm, b) the harmonic fall-off is rapid, the first overtone is about 60 dB lower than the fundamental, and c) the noise is loudest slightly behind the propeller plane and drops to zero on the axis. In contrast, the test data show: a) the SPL of the fundamental increases about 19 dB per doubling of rpm, b) the harmonic SPL's, up to the 10th harmonic, are within 30 dB of the fundamental, and c) the harmonic noise data shows a sharp dip near the propeller plane and does not decrease near the axis.

A thorough study of possible noise sources which would explain the lack of correlation with theory was undertaken. The results are presented in the next two sections.

a. Correlation of Test Data with Theory

The significant differences between the harmonic noise test data and the predictions are outlined in the preceding paragraphs. Some specific examples are presented here. Also, several possible sources of the harmonic noise which were investigated are discussed.

The variation of the fundamental measured harmonic noise level with rpm (and tip speed) is shown in Figure 22 for a representative case at 12.5° behind the propeller plane. At the two highest tip speeds the theory for harmonic rotational noise with uniform loading (see Sections IV.2 to 4) agrees fairly well with the measured data. But at the two lower speeds the agreement becomes poor. Unfortunately, the propeller noise detectability program is expected to be applied to low-tip-speed propellers where Figure 22 shows the harmonic noise prediction with uniform loads is inaccurate. The curve for the predicted variation with loading harmonics included in order to improve the accuracy of the prediction is discussed in the following Section VII.2.b.

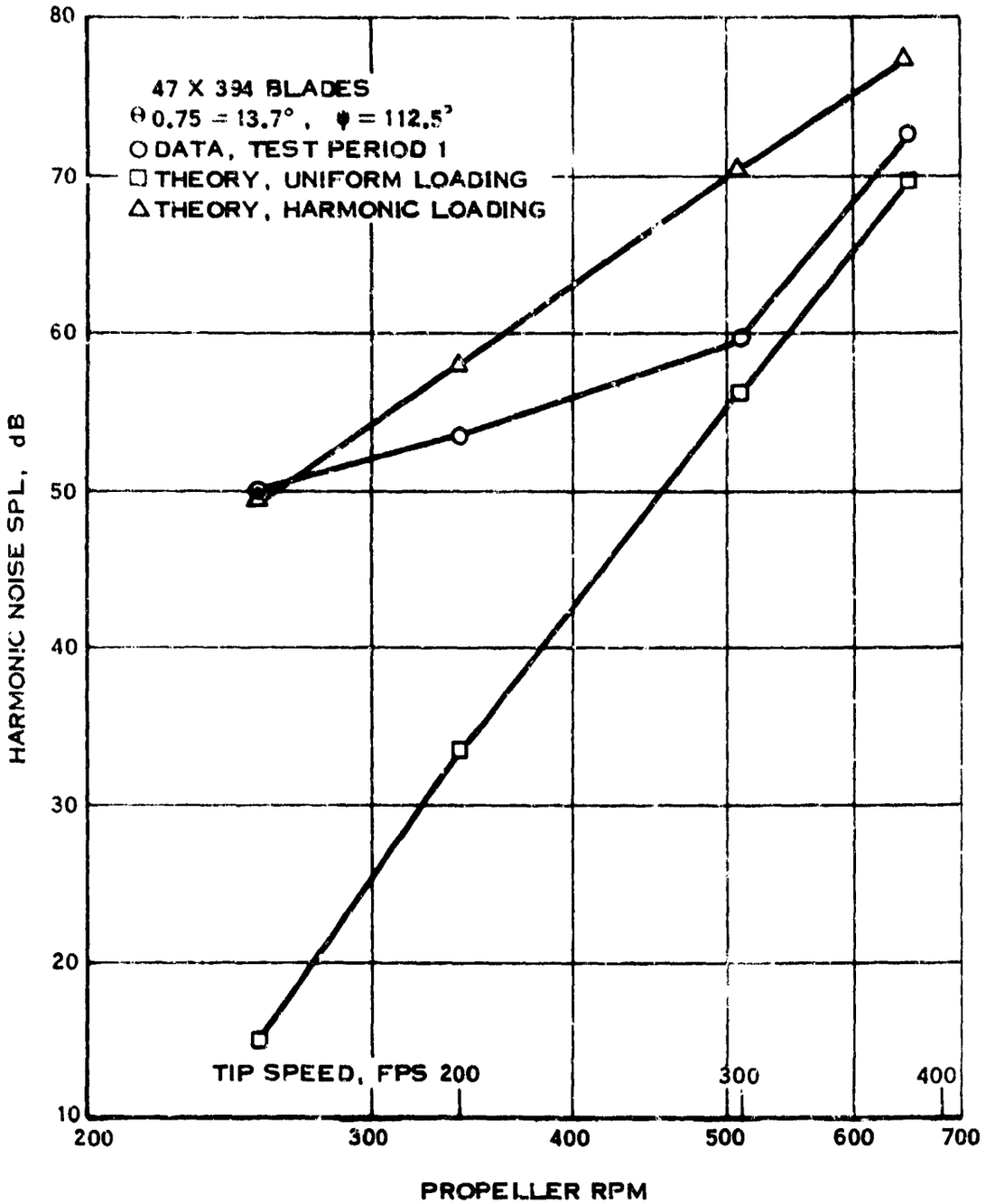

Figure 22. Variation of Fundamental Harmonic SPL with RPM

Figure 17 presents the measured rotational noise harmonics of four 4-bladed propeller configurations at three azimuth angles. It can be seen that the harmonic levels do not decrease rapidly with harmonic number (and frequency). Although there are individual differences shown in the limited sample represented by Figure 17, a study of all the harmonic noise data in Tables VIII to XII does not indicate any significant difference between the various configurations tested. Figure 23 presents the harmonic noise data for one configuration in Figure 17. The predicted noise levels for the theory with uniform loading are also presented by square symbols. The fundamental harmonic is much less than the measured value, as discussed above in connection with Figure 22. Even more significant in terms of detectability is the fact that all predicted overtones are very much quieter than measured, by about 60 dB for the second harmonic, for example, and even more for higher harmonics.

Figure 24 shows the measured directivity pattern of the fundamental and fifth harmonics of blade passing frequency. The directivity pattern of the fundamental harmonic predicted by the standard theory with uniform loading is shown by square symbols and is dominated by thickness noise rather than by loading noise because the chord of the 47X464 blades is large. Therefore, the directivity pattern predicted for the fundamental harmonic has a maximum in the propeller plane, $\psi = 90^{\circ}$, rather than the measured minimum shown.

The lack of correlation between test data and prediction in level, harmonic content and directivity pattern described above shows that the standard calculation of propeller harmonic noise is inadequate for predictions of harmonic noise for the test conditions. This does not mean that the theory is inadequate for all conditions. Indeed, it has proved to be generally adequate at higher tip speeds, both in flight and statically. Because of the observed lack of correlation, other sources of harmonic noise on the rig at low propeller speeds were investigated. The results are summarized in Table XVI. The first two sources are expressed by the standard calculation, as in Equations (3) and (4), and, as the preceding discussion shows, do not predict the measured data. With the exception of the last 3 items in the table the sources of harmonic loads described were dismissed from further consideration during the investigation for the reasons given in the table. The velocity field at the strut due to the trailing tip vortex (item 13) was calculated by a Hamilton Standard computer program. At 4 feet from the propeller axis the predicted velocity normal to the strut varies from 10 fps to 132 fps as the propeller turns. High velocities near 132 fps occur only over a small fraction of the distance between blades and therefore the force on the strut would be rich in harmonics. The first 3 harmonics of the noise due to the resulting oscillating force on the struts were calculated and compared favorably with the data. Therefore, test program 3 was conducted to verify that the rig support struts were the source of the harmonic noise. The 47X-451 propeller blades were rotated 180° in the hub and the direction of propeller rotation was reversed. Thereby the propeller was operated as a pusher with the trailing vortex moving away from the rig rather than towards it. As Figure 17 shows, the harmonic noise did not decrease significantly. Also, an observer could recognize that the noise source was the propeller rather than the rig even in the normal tractor mode. Therefore, this noise source was discarded as a cause of the observed harmonic noise.

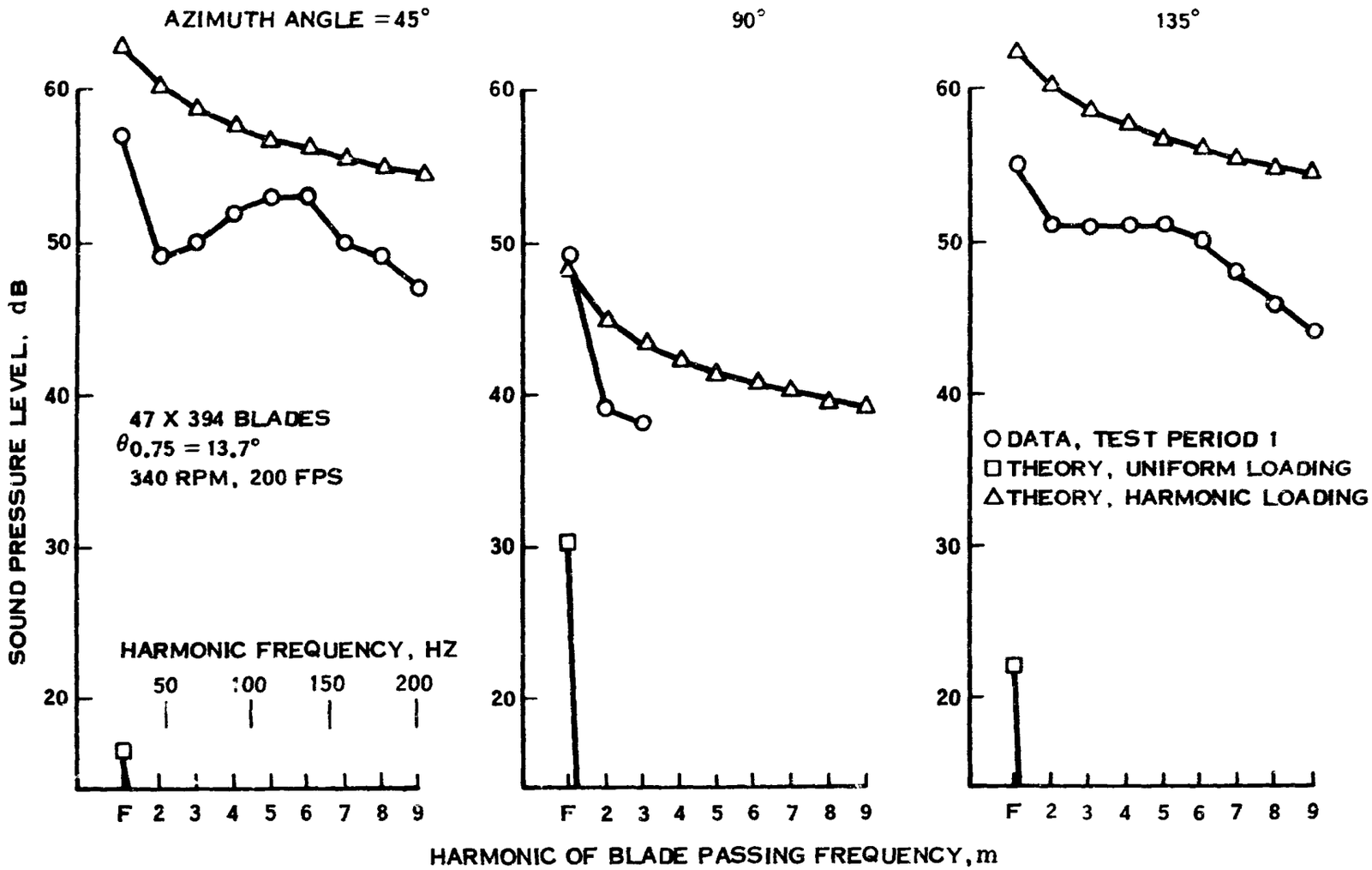

Figure 23. Comparison of Measured and Predicted Harmonics of Rotational Noise

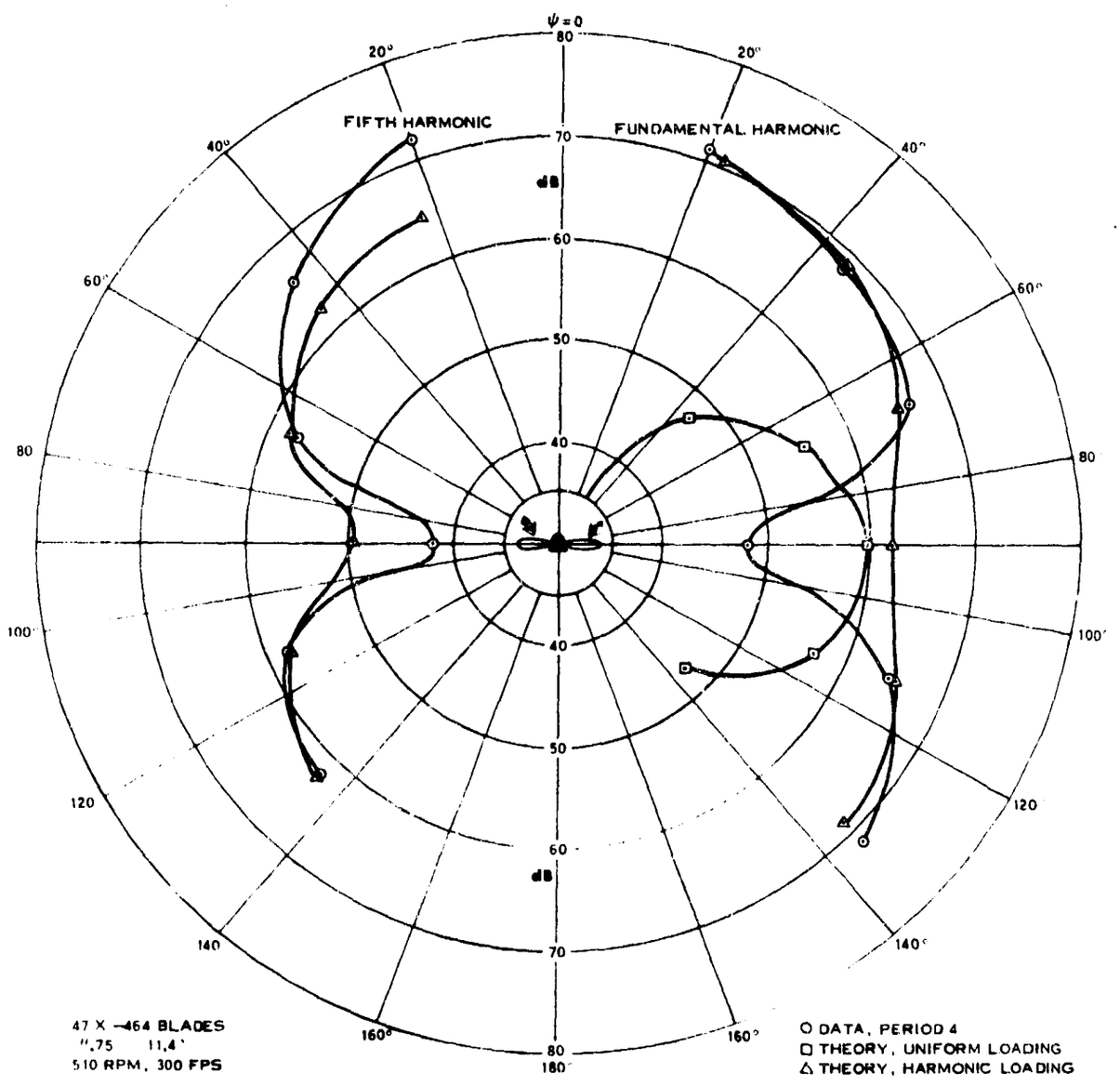

Figure 24. Comparison of Measured and Predicted Directivity Patterns of Rotational Noise

TABLE XVI

SUMMARY OF HARMONIC NOISE SOURCE STUDY

Harmonic Noise Source	Comments
1. Axially-symmetric thrust and torque loadings	Theory (Eq. (3)) predicts a large variation with rpm, rapid harmonic fall-off, and noise maximum near $\psi = 105^{o}$. As discussed in text, these 3 trends differ from those observed.
2. Blade thickness	Theory (Eq. (4)) generally predicts lower harmonic noise than does theory of loading noise (Eq. (3)) and noise maximum in propeller plane.
3. Radial blade loads	The theory[22] predicts maximum noise in propeller plane. Should be small because of small blade deflections, unlike a helicopter rotor.
4. Blade vibration	Not source because vibration frequencies are not always multiples of blade passing frequency.
5. Quadrupole sources studied by Ffowcs Williams and Hawkings[33]	Studies at United Aircraft Corporation Research Laboratories show these sources would produce less noise than that from uniform loading (Item 1).
6. Second-order sources studied by Morfey[14]	Believed insignificant because of low axial Mach numbers and large spacing between the propeller and stand support struts, see Figure 10.
7. Atmospheric turbulence causing varying blade loading	Turbulence believed to be small. Data obtained during a wind gust, with presumably more turbulence, shows only moderate increases in noise level.
8. Asymmetric blade loading due to ground blockage inducing asymmetric flow through the propeller	Believed insignificant because the propeller axis is over 3 propeller radii above the ground.

TABLE XVI (Concluded)

Harmonic Noise Source	Comments
9. Wind producing asymmetric blade loading	Most of data obtained with winds less than 1 knot (see Sect. VI 6b). Data obtained during a gust show low-order harmonics may increase by 10 dB and the higher-order harmonics by less than 2 dB.
10. Asymmetric blade loading due to non-uniform flow induced by blockage of stand support struts	Velocity through propeller disc is reduced .14% ahead of each strut. The resulting asymmetric loading is insufficient to produce the measured fundamental harmonic noise level.
11. Boundary layer velocity wake from blades causing an oscillating force on struts	Calculated noise level is 15 dB below measured data.
12. Bound vortex on blades causing an oscillating force on struts	Calculated velocity change at struts of .1 fps is too small to cause significant noise.
13. Trailing tip vortex from blades causing an oscillating force on struts	Calculated velocity change produces harmonic noise similar to data but observer hears noise coming from propeller, not rig.
14. Asymmetric blade loading	Source unknown, see Sect. VII 2b.
15. Narrow-band random	See Sect. VII 2c.

The last 2 noise sources are discussed in the following 2 sections, respectively. Harmonic loading (item 14) has been correlated and does provide improved agreement with the test data. The last source, item 15, is shown to be present by the 1.5 Hz bandwidth spectra obtained from test period 4 and illustrated in Figure 19. None of the existing propeller noise theories predict the observed narrow-band random noise. This noise is discussed further in Section VII.2.c.

b. Derived Harmonic Loads

The effects of harmonic loads on harmonic loading noise are discussed in Section IV.5, where Equation (9) for the loading noise due to harmonic loads is presented. The problem considered here is the inverse one, that of deriving the harmonic loads which correspond to the measured harmonic sound pressure levels. In order to make this problem tractable it is necessary to use the far-field approximation, to assume that the loads are concentrated at 80% of the tip radius (effective-radius approximation), and to assume random phasing between each loading harmonic. Also operation at zero forward speed, (static) is assumed because the noise data obtained in the program is from a static test stand.

With these assumptions, the equation for the sound pressure level of order m is:

$$dB_m = 124.572 + 10 \log \left[\frac{1}{16\pi^2} \sum_{\lambda=0}^{\infty} \left\{ \left(\frac{mBnX}{ad^2} T_\lambda \right)^2 + \left(\frac{(mB-\lambda)}{.2dD^2} Q_\lambda \right)^2 \right\} J_{mB-\lambda}{}^2 + \left(\frac{mB}{.8\pi dD^2} Q_0 J_{mB-\lambda} \right)^2 \right] \quad (46)$$

This equation involves Bessel functions with an argument of (πDBnY/75da)m and order mB- λ . On the propeller axis the argument is zero, because Y = 0, and the only non-zero Bessel frunction is J_0 (0) = 1.0. Therefore, only harmonic thrust loads of order λ = mB contribute to the harmonic loading noise on the axis. Equation (46) can be solved for these harmonic thrust loads in terms of the measured harmonic noise levels dB_m:

$$T_{mB} = T_\lambda = \frac{120\ ad}{mBn} e^{(dB_m - 124.572)/8.68589} \quad (47)$$

In the propeller plane ($\psi = 90^{o}$) only harmonic torque loads Q contribute in Equation (46), which can be put in the form

$$(mBQ_0 J_{mB})^2 + \sum_{\lambda=1}^{\infty} \left\{(mB-\lambda)Q_\lambda J_{mB-\lambda} \ (\pi DmBn/75a)\right\}^2 \left(.8\pi dD^2 e \ (dB_m - 124.572)/8.68589\right)^2 \tag{48}$$

Experience with helicopters [21] suggests that the torque harmonics vary inversely with the harmonic order to some exponent. Therefore, the following trend is assumed, with the factor C to be determined

$$Q_\lambda = C/\lambda^{2.5} \tag{49}$$

Substituting Equation (49) into Equation (48) results in the equation

$$(mB)^5 \left[\sum_{j=1}^{mB-1} j^2 \left\{\left(\frac{1}{mB-j}\right)^5 + \left(\frac{1}{mB+j}\right)^5\right\} J_j \left(\frac{\pi DmBn}{75a}\right)^2\right] Q_{mB}^2 + (mBQ_0 J_{mB})^2 \left[0.8\pi d D^2 e \left(dB_m - 124.572 \ /8.68589\right)\right]^2 \tag{50}$$

Harmonic torque loads were derived from Equation (50) using harmonic sound pressure levels measured in the propeller plane ($\psi = 90^{o}$). These harmonic torque loads, expressed as a percentage of the steady (zero-order) torque are shown in Figure 25. A least-squares fit to the data of $17\%/\lambda^{1.34}$ is shown by the solid line. The discrepancy between this slope of -1.34 and the local slope of -2.5 assumed in Equation (49) is not believed to make a significant change in the results shown. With the exception of the derived torque harmonics at the higher harmonics from tests of the pusher propeller (diamond symbols) the rest of the solid symbols fall together. It is noticeable that use of a pusher, rather than a tractor, test configuration reduced the higher torque harmonics but did not change the lowest three torque harmonics. For the same test conditions the correlation is $6.8\%/\lambda^{.86}$ for tractor operation and $38\%/\lambda^{1.95}$ for pusher operation. Loading harmonics over the 5th are lower for a pusher rather than a tractor operation with these correlations.

Calculation of harmonic thrust loads from Equation (47) requires that harmonic noise data be measured on the propeller axis. Obtaining meaningful harmonic noise data on the axis is difficult because some of the noise recorded does not come directly from the propeller as assumed but is reflected from the ground in front of the test stand. For the test stand, shown in Figures 9 and 10, with the axis 17 feet off the

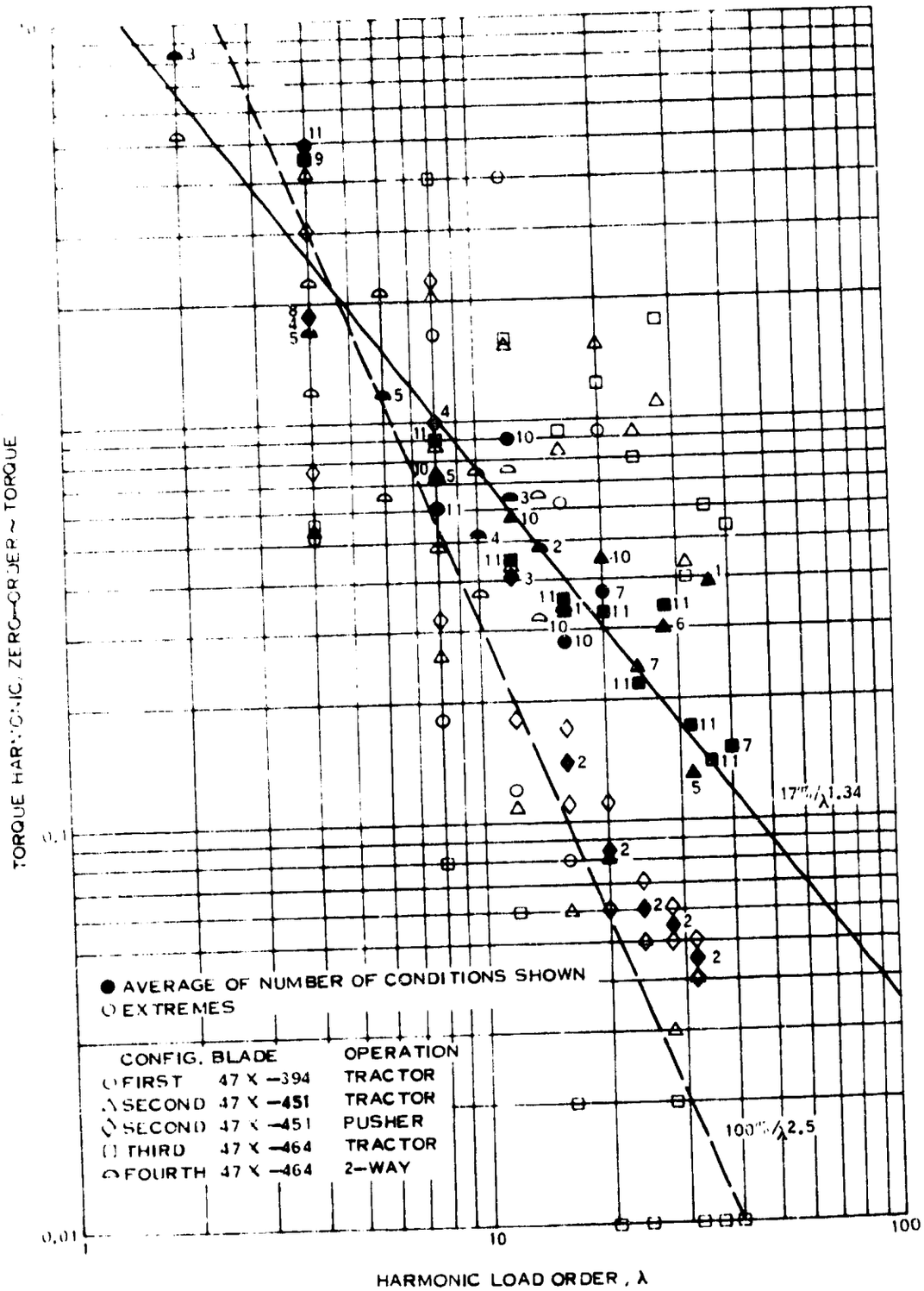

Figure 25. Derived Harmonic Torque Loads

ground a microphone 50 feet ahead on the axis picks up reflected sound that is emitted at 34^{o} from the axis and, therefore, includes significant noise due to the torque forces. The increased path length of the reflected noise reduces it by only 1.6 dB so that it is significant. The first three test periods had been completed before the need to derive harmonic thrust loads became apparent. Because the range of azimuth angles for measured harmonic noise in these tests was only 45^{o} to 135^{o}, it was not possible to extrapolate to 0^{o} (on the axis) with any confidence. Therefore, no derived harmonic thrust loads were calculated from the data from the first three periods. Several approaches to the problem of obtaining valid on-axis noise data during tests of the third blade configuration (47X-464) were investigated. It was decided to use the approach of adding two microphones, at 50 feet and 20^{o} and at 80 feet and 12^{o}, and to use these two additional locations to extrapolate to $\psi = 0$. For conditions where this extrapolation of the harmonic noise data to $\psi = 0$ appeared reasonable the results are presented in Figure 26. The harmonic thrust loads derived from Eq. (47) are expressed as a percentage of the measured thrust and plotted against harmonic load order λ mB. A least-squares fit to the data of $8.4\%/\lambda^{1.38}$ is shown by the solid line.

The derived harmonic torque and thrust loads are combined in Figure 27. The slope of -1.36 corresponds to a reduction in harmonic noise level of 2.2 dB per doubling of noise order, or frequency. The combined curve is weighted towards the torque curve because of the larger number of data points represented by the torque curve. If only data points for which both torque and thrust harmonics are available are included, the two curves are closer together and are fitted by the equation $12.4\%/\lambda^{1.46}$. This line is between the thrust and torque lines in Figure 27.

A comparison of harmonic loads derived from the 2-bladed configuration noise data with loads derived from the 4-bladed configuration with nearly the same blade angle shows that the harmonic loads for the 2-bladed configuration are over two times larger. Most of this difference can be explained by assuming that the harmonic load on each blade does not depend on the number of blades. Therefore, the percentage harmonic loads of a 2-bladed propeller should be double the percentage loads of a 4-bladed propeller.*

Analysis of the harmonic loads derived from noise data obtained with the 47X-464 blades shows a considerable variation of the percentage harmonic loads with rpm. The purpose of this study of derived harmonic loads is to develop a correlation of harmonic loads which might be used to predict the harmonic loading noise of the propeller of a quiet aircraft. These propellers are expected to operate at low tip speeds of 300 fps or less. Therefore, only data from a 4-bladed tractor configurations with tip speeds less than or equal to 300 fps were included in the data bank used to establish the trend equation $21.4\%\ \lambda^{1.43}$, shown in Figure 28. Using the effect of number of blades discussed in the preceding paragraph, the correlation of the harmonic loads derived from the harmonic noise measured during tests conducted during this program

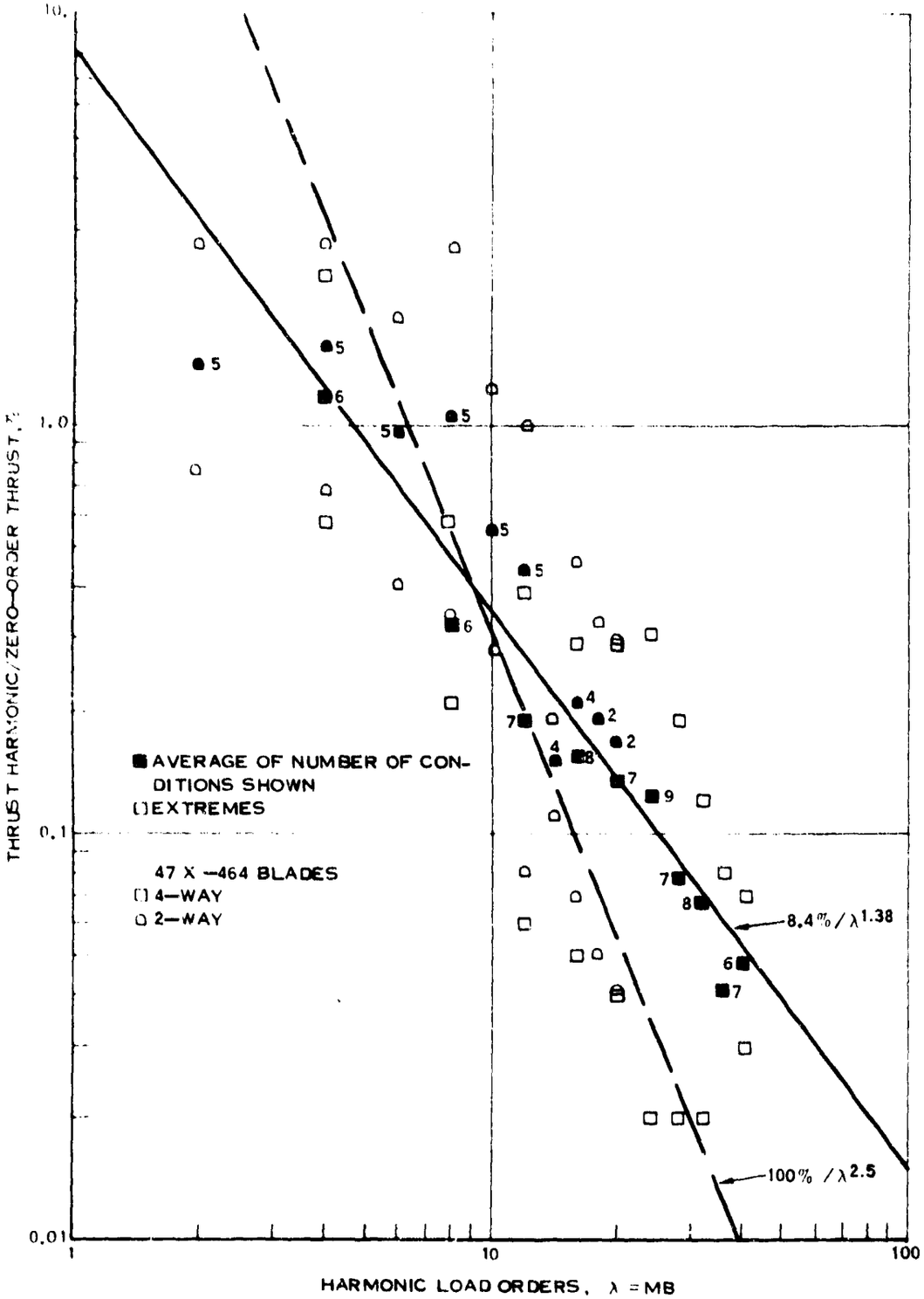

Figure 26. Derived Harmonic Thrust Loads

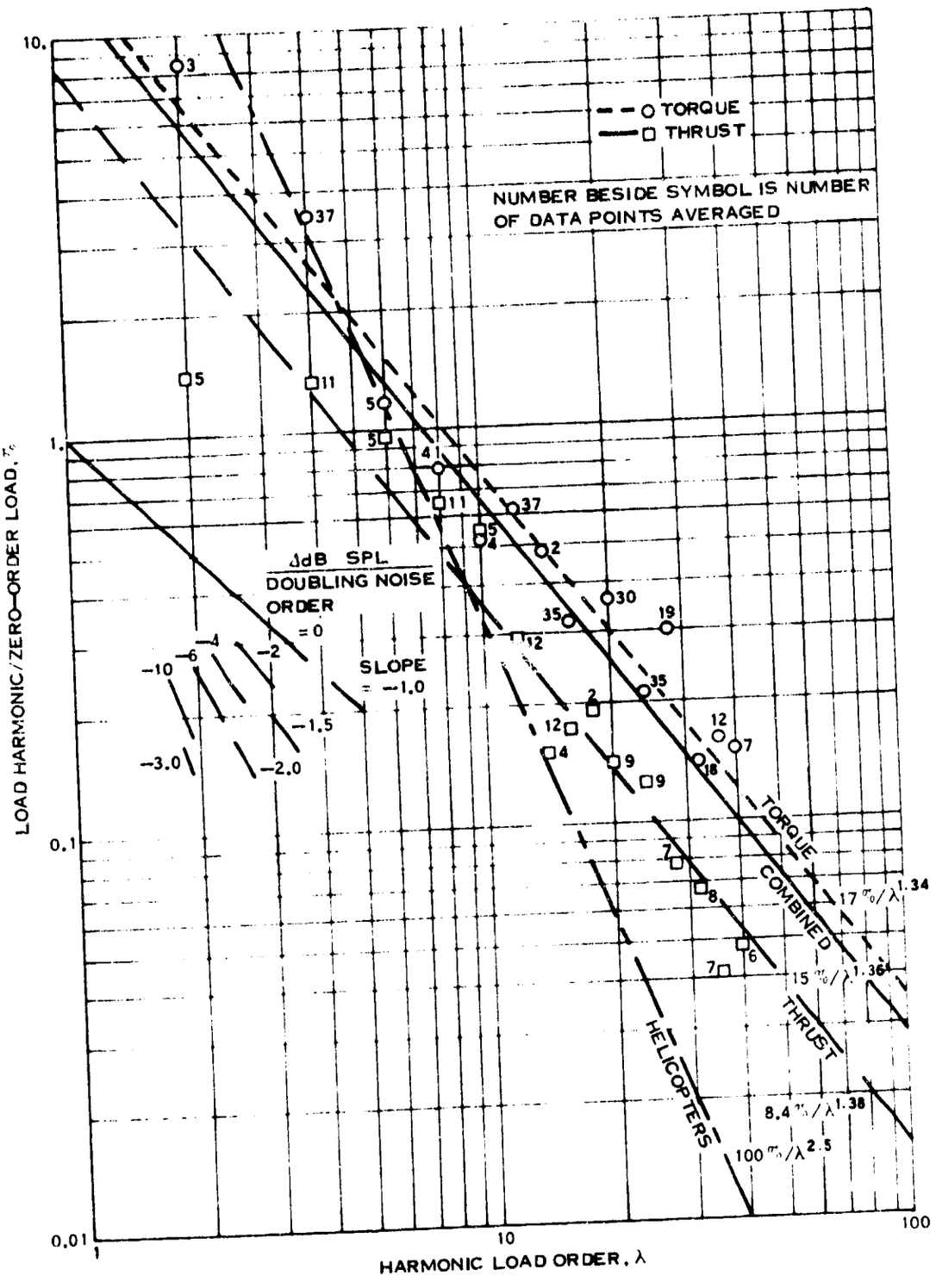

Figure 27. Derived Harmonic Loads

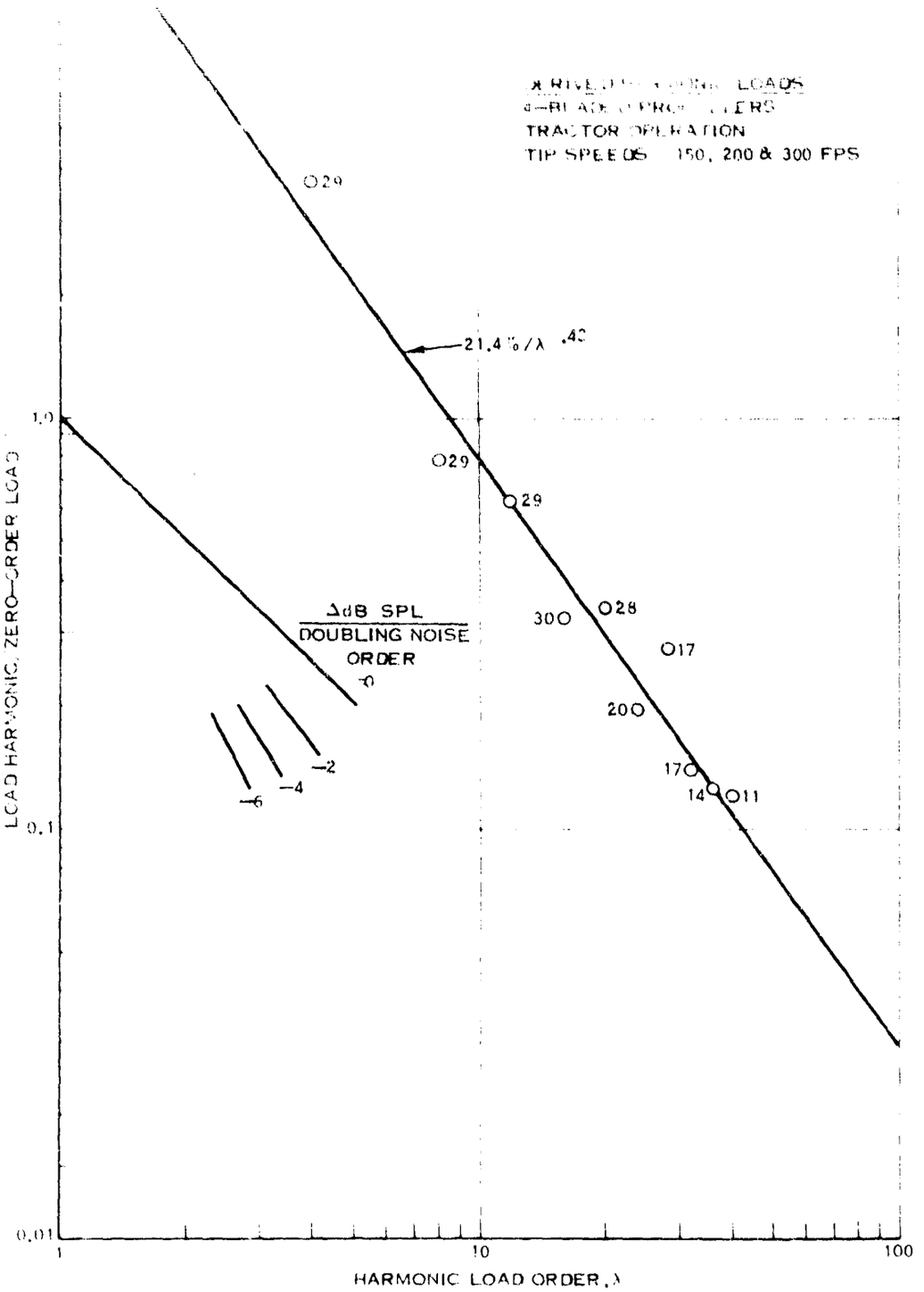

Figure 28. Derived Harmonic Loads for Low Tip Speeds

[illegible] on Audibility of Harmonic Noise [illegible]

This correlation of harmonic levels was used to calculate the harmonic rotational noise levels shown by triangles in Figures 22 to 24. In Figure 22 the correlation with data at the two lower speeds is markedly improved. The improvement for the overtones shown in Figure 22 is even more significant, since the higher overtones rather than the fundamental would be detected first. The improved correlation of directivity pattern is demonstrated in Figure 24. As discussed previously, for the fundamental harmonic (shown on right of figure) in the propeller plane the thickness noise predominates and is not changed by adding harmonic loading.

The discussion of Figure 19 in the next section points out that the higher-order harmonic noise is not a true tone noise but appears to be a narrow-band random noise. However, no distinction was made between these sources of harmonic noise in deriving the harmonic load correlations presented in this section. If, in fact, these higher-order noise harmonics are not caused by harmonic loading, the derived harmonic loads for orders of about 20 and above are not valid. The high-order harmonic loads would be less than those derived and, therefore, the correlations shown in Figures 25 to 28 would be steeper, perhaps with a slope of -2. rather than near -1.4. Because the propeller noise theories which are represented in the computer program do not predict this narrow-band random harmonic noise, and because the aural detectability criteria approach selected does not differentiate between tones and narrow-band random harmonic noise, use of the harmonic load correlation presented in Figure 28 is believed to be proper for detectability studies.

c. Discussion of Harmonic Noise Sources

An intensive investigation of the observed harmonic noise characteristics was undertaken in an effort to explain, and thereby be able to predict, the harmonic noise of a propeller operating at low tip speeds. Three approaches were pursued: a) listening to the propeller on the test stand, b) a very narrow band analysis of some of the data, and c) a literature search for theories which predict noise characteristics like those measured.

It was observed at the beginning of the test program that the propeller is heard to be much quieter close to the propeller plane and about equally loud elsewhere. If one stands under the shaft, but slightly ahead or behind the propeller, one hears a series of bursts of hissing noise. The noise appears to come from about the 70% radius station of the blade approaching the observer. By moving to one side the source appears to move around the axis so as to always approach the observer. The frequency of repetition of the bursts of noise is the blade passing frequency. Thus, to the observer, it appears that the harmonic noise is due to a high-frequency sound source

on each blade which has a particular directivity pattern relative to the blade. It requires that little noise is produced directly forward or in the rear half circle. Theoretically, a dipole oscillating in a direction normal to its motion produces a similar noise pattern. However, theoretically the tip Mach number is too low to produce the distortion required.

Recent high-speed movies of a tip vortex from a helicopter rotor on a test stand have shown that both the blade and the vortex oscillate axially with a period of one revolution. The relative motion between the flapping blade and the tip vortex also has a period of one revolution and induces large changes in angle of attack at about 80% radius. These angle of attack changes result in a harmonic load change and, therefore, in harmonic noise. It is not known if the same angle of attack changes would occur if the blades were stiff, as in a propeller, so that they did not flap as in a rotor. That is, it is not known whether blade flapping or vortex oscillation initiates the observed effects. However, numerical studies by UAC have shown that the trailing tip vortex is unstable, so that its position has a random variation. Consequently, it is expected that oscillation of the tip vortex will occur even with stiff blades. In forward flight, or with fewer blades, the effects of the oscillation of the tip vortex are expected to be reduced.

A frequency spectrum obtained with a 1.5-Hz bandwidth filter is shown in Figure 19. It illustrates several significant points. First, the width of the first four spikes is very narrow and is known to correspond to the filter-response curve. Therefore, these spikes represent a tone noise. Second, the level of these tones decreases with increasing frequency. Third, the widths of the spikes at higher frequencies are considerably broader than the filter response curve. Therefore, these spikes are not due to harmonic tones, but suggest, instead, a narrow-band random noise. Fourth, the higher-frequency spikes have an envelope which is a maximum at about the 9th harmonic. Lastly, the level of the broad-band noise between the spikes follows the envelope of the spikes closely.

Hamilton Standard obtained some noise data from a DHC-5 aircraft with one propeller replaced by a propeller designed for a quiet STOL aircraft. Data were obtained during both static (on the ground) and 80-knot flyover operation with a tip speed of 630 fps. The noise spectrum shown in Figure 29 for static operation exhibits many harmonics of rotational noise. The spectrum from flight operation exhibits fewer harmonics of rotational noise. For static operation, the fundamental and the 4th through the 7th harmonics would be detected whereas for flyover operation only the 2nd harmonic would be detected. Although these data were not obtained at the very low tip speeds typical of a quiet aircraft, they are cited because they demonstrate an effect of flight speed on the harmonic noise content which may invalidate use of harmonic loadings derived from static data for flight noise predictions.

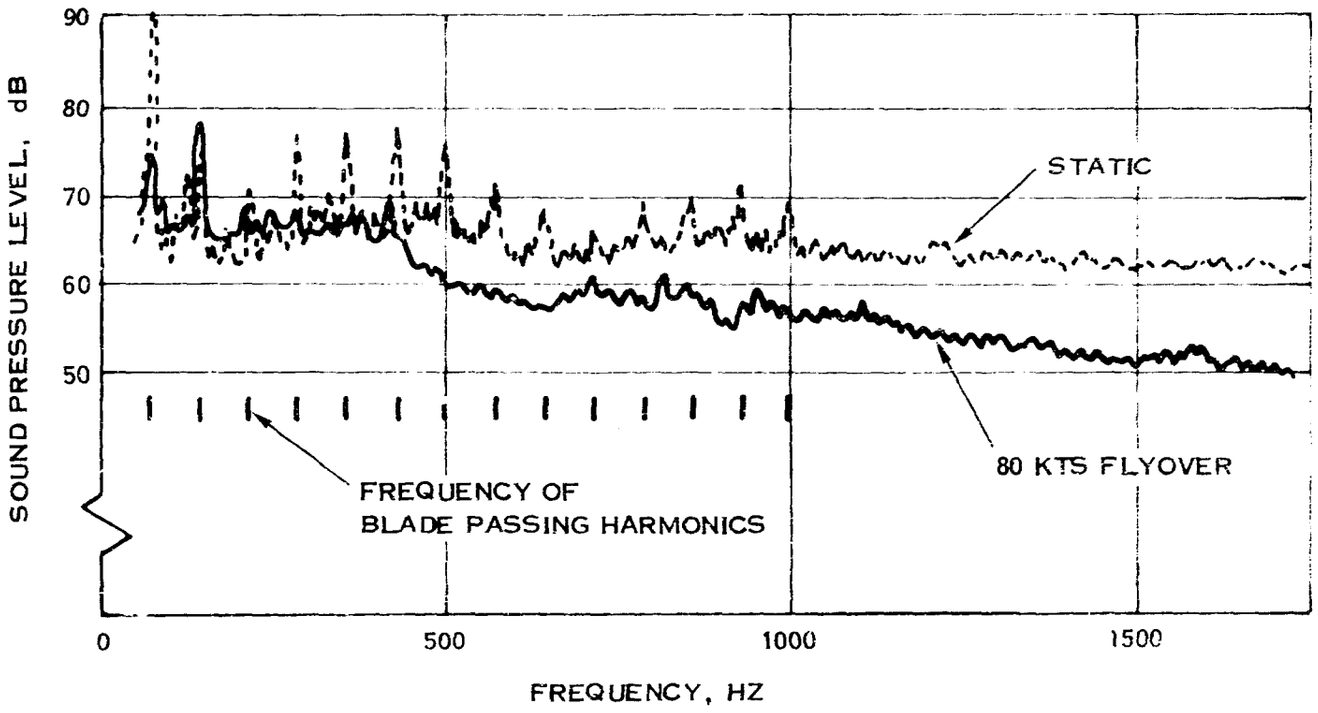

Figure 29. Comparison of a Static Propeller Noise Spectrum with that from a Propeller in Flight, Both Operating at 630 Ft/Sec Tip Speed and 1050 SHP

An investigation of the propeller noise data from the 47X-464 blades using various low- and high-pass filters and an oscilloscope revealed that the noise level is not steady, but has an apparently random variation, suggesting that turbulence might be the source. Mr. Ramani Mani, of the Department of Mechanical and Aerospace Engineering of the University of Massachusetts, has studied the problem of sound generation due to free-stream turbulence incident on a rotor. He presents, in an unpublished paper, predicted noise spectra which resemble those shown in Figure 19 at the higher frequencies, that is, that have broad rounded spikes which peak at harmonics of the blade passing frequency. The ratio of the length scale of turbulence to the spacing between the blades is a significant parameter in his analysis. As this ratio increases above roughly unity, the shape of the spectrum is changed little but the level decreases. As this ratio decreases below roughly unity the spectrum becomes smooth and the peaks at harmonics of the blade passing frequency disappear. Extensive data on atmospheric turbulence, in the form of power spectral density plots, show that turbulence power varies as the 5/3 or large power of wavelength in the range of wavelengths of significance here. Also, the wavelength for maximum energy decreases as the ground is approached. Therefore, turbulence may be present with the length scale required to produce the peak in the spectrum predicted by Mr. Mani. Reducing the number of blades in order to increase the ratio of turbulence scale length to distance between blades may not reduce the noise levels as much as predicted because the turbulent energy at large scale lengths is greater. This was, in part, confirmed during the last test at Hamilton Standard which showed that the shape of the noise spectrum from a propeller with two blades removed is not significantly different from that of the basic four-bladed configuration even though the spacing between blades is more than doubled.

Griffiths [36] studied the spectrum of compressor noise due to small random fluctuations in the amplitude and phase of the acoustic disturbances. The noise, which he calls "narrow-band random noise" has a frequency spectrum similar to that between 200 Hz and 500 Hz shown in Figure 19.

Studies of propulsion noise in the last decade have concentrated on compressor and jet noise. The test data obtained in this program show that the conventional sources of propeller noise do not explain the observed sound patterns. The theoretical concepts which have been developed recently for compressors appear to be able to explain the observed characteristics of propeller noise. Therefore, these theories should be applied to propellers and developed into a useable form. It is anticipated that a unified theory can be developed to predict both the harmonic noise and the broad-band noise.

3. BROAD-BAND NOISE

The 1/3-octave band noise data were obtained in this program primarily to determine empirically the best values of the coefficients in the new method for predicting broad-band vortex noise developed in this program. The three coefficients are a

force coefficient C_F, a frequency coefficient C_f and a Reynolds number exponent. Recommended values of these three coefficients are 8.0, 0.06 and -1.0, respectively.

Figure 30 is a plot of vortex noise SPL versus rpm, or up speed. The first attempt at a correlation between theory and data did not include any Reynolds number term in the theory. Predicted levels for a zero exponent, thereby excluding any Reynolds number factor, are shown by square symbols. The relative levels of these symbols is not significant because the other 2 coefficients used were selected to correlate with the data using an exponent of -1.0. However, it is apparent that the predicted variation in noise with rpm shown by the squares does not match the data. The measured variation is more like V^4 than V^6 predicted by Yudin [13] or $V^{5.6}$ predicted by Sharland [28] for vortex noise. Therefore, a Reynolds number term was included in Eq. (45) for the force and an exponent of -1 selected. Correlation with data shown by the triangles in Figure 30 demonstrates the value of this choice. Data from the 47X-451 blades, which are about half as wide as the 47X-464 blades and, therefore, have half the Reynolds number, confirm this selection of the exponent.

The overall noise level in the seven 1/3-octave bands from 250 Hz to 1000 Hz was selected as the noise parameter in Figure 30 because studies showed that the broad-band noise is most likely to be detected in this range of frequencies. The level of broad-band noise generally decreases outside this range and the aural detectability criteria (see Table III) are generally less critical outside this range.

A change in the frequency coefficient shifts the predicted frequency spectrum along the frequency axis. The recommended coefficient of .06 is near that obtained by Chuan and Magnus [32]. A change in either the force or frequency coefficient changes the sound pressure level, since the sound pressure is proportional to both coefficients.

Figure 31 presents a comparison between measured and theoretical 1/3-octave band spectra at tip speeds of 150 and 353 fps. The effects of increased tip speed are to increase both the measured and predicted noise levels and to displace the predicted spectra towards higher frequencies. The measured noise data shows considerable unevenness in contrast to the smooth curves of the two predictions. The 3rd option prediction is somewhtat more peaky and does not fall off as rapidly at the highest frequencies. The spectra predicted by option 1, the new method, appear to correlate more closely with the data shown at the more significant middle frequencies than the spectra predicted by option 3. The third vortex noise option method is based on data from a propeller with blades like the 47X-394 blades tested in the first test period.

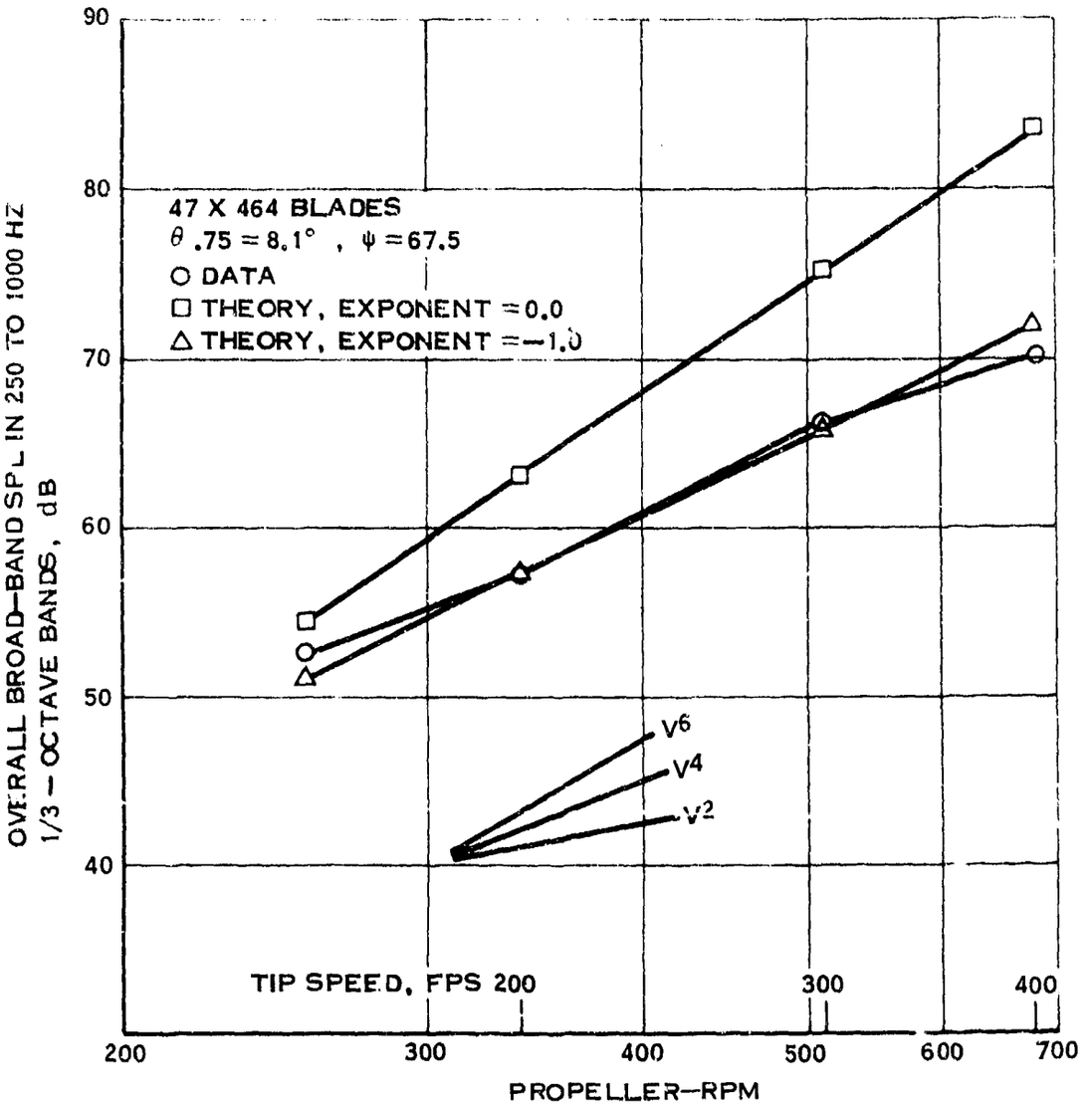

Figure 30. Variation of Propeller Broad-Band Noise with RPM

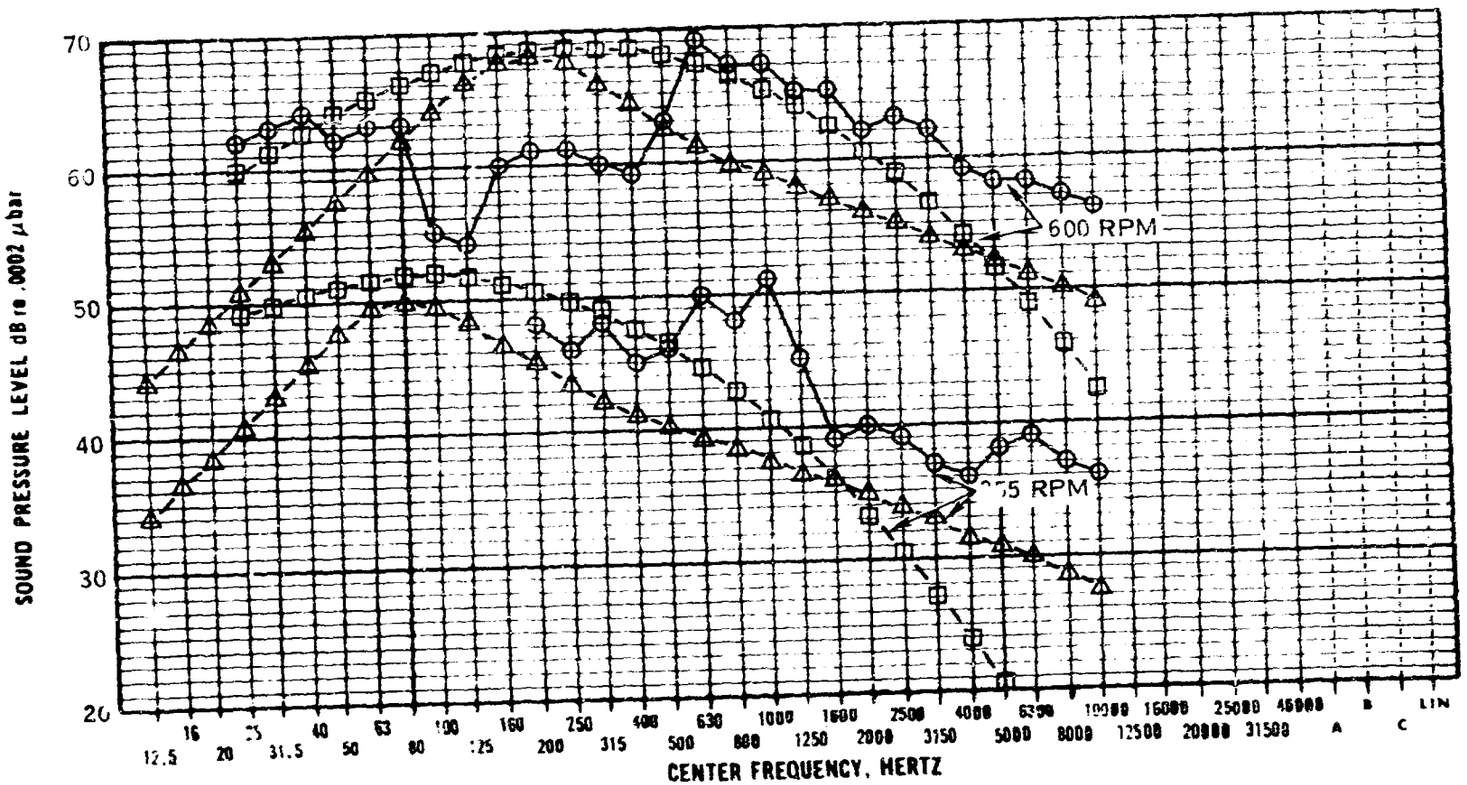

Figure 31. Effect of RPM on Propeller Broad-Band Spectrum

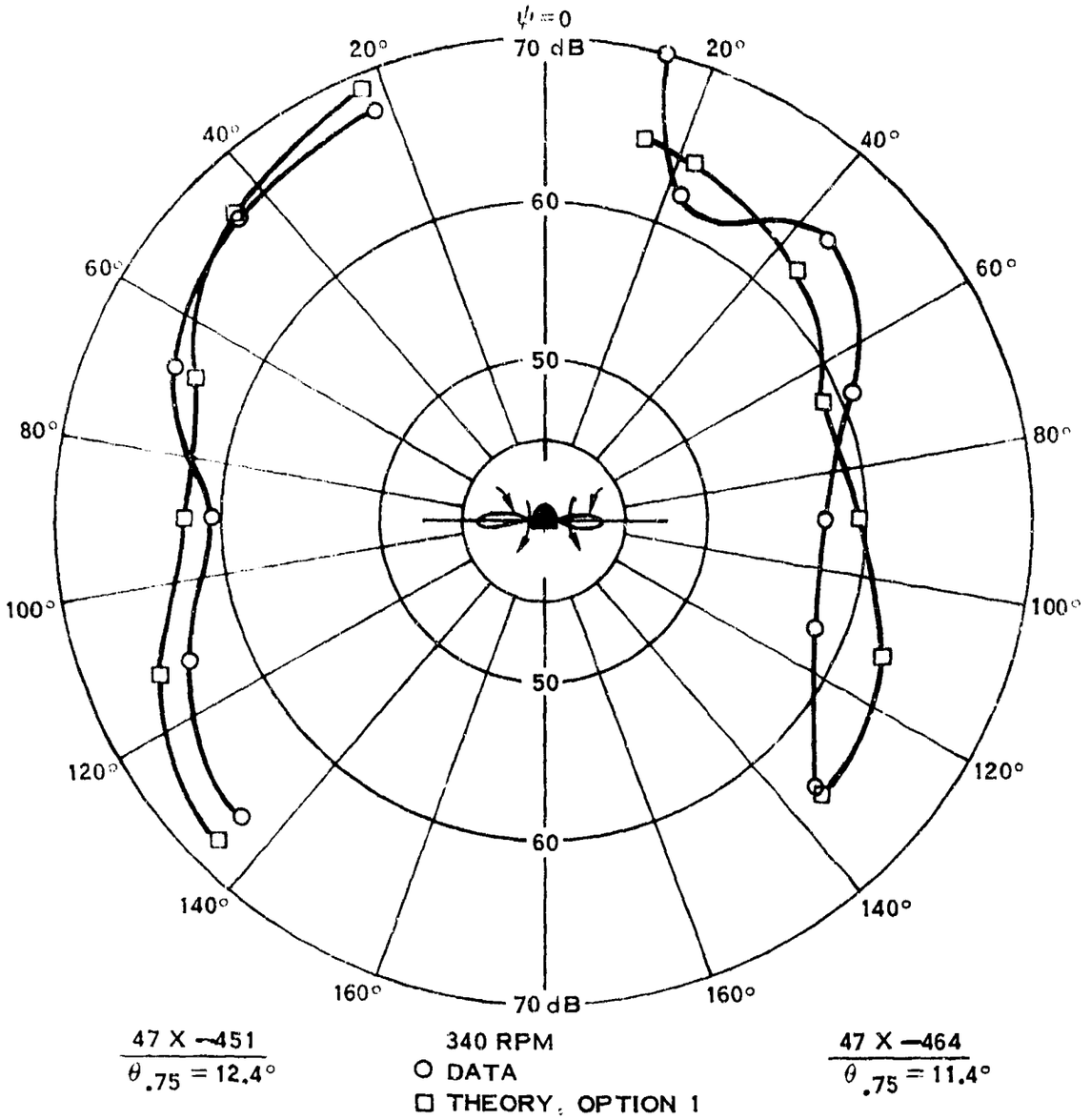

Figure 32. Directivity Pattern of Propeller Broad-Band Noise

Figure 32 presents a comparison between measured and theoretical directivity patterns of broad-band noise for two propeller configurations operating at a tip speed of 200 fps. The noise level shown is the overall SPL in the bands from 250 to 1000 Hz. Although there is some apparent scatter, the agreement between the predicted and measured noise levels is good for both propellers.

Figures 30 to 32 are a small sample illustrating the ability of vortex noise option 1 of the propeller noise detectability program to predict the measured noise data. In order to better evaluate the accuracy of the predicted noise levels, 654 individual 1/3-octave band levels were compared. The probability distribution of the errors in the predicted levels is shown in Figure 33. The average error is nearly zero, demonstrating that the coefficients recommended are satisfactory. The standard deviation of 5.2 dB is largely due to an apparently random unevenness in the measured 1/3-octave band data, as shown in Figure 31. A detailed study of the errors might reveal some trends with blade angle, rpm, microphone location, propeller configuration, and band-center frequency which would permit a reduction in the errors.

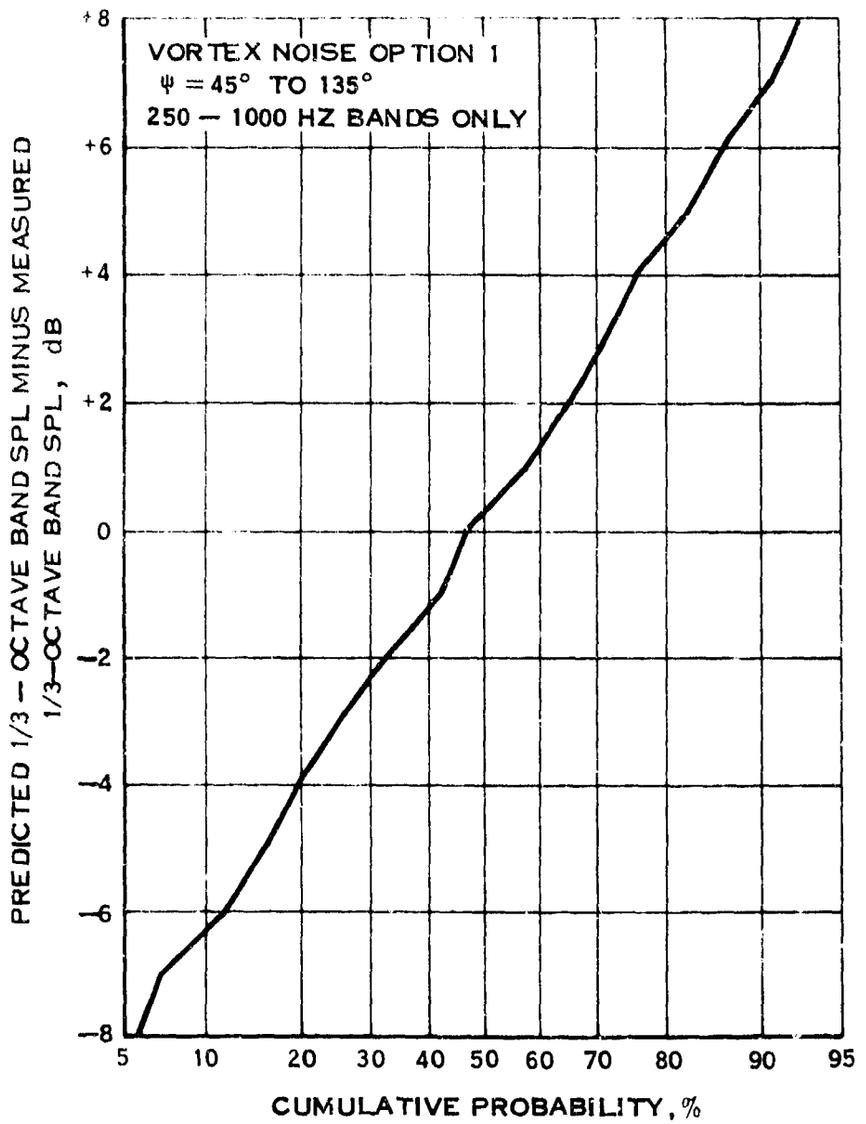

Figure 33. Probability Distribution of Errors in Predicted 1/3-Octave Band SPL

SECTION VIII

PROPELLER NOISE DETECTABILITY COMPUTER PROGRAM

1. INTRODUCTION

The prime objective of the contract was to develop a computerized propeller design technique which would predict propeller performance as well as predict propeller harmonic and broad-band noise levels and compare these levels with a selected aural detectability criterion to determine minimum undetectable flight altitude. This technique consists of two parts: a propeller performance program and a propeller noise detectability program which is called by the propeller performance program. The propeller performance program was developed by Hamilton Standard and made available to the Air Force Aero Propulsion Laboratory.

The propeller noise detectability program was written as ten subroutines and debugged as part of this contract. A detailed discussion of the program and how to use it are provided in the user's manual [37]. This report includes a general discussion of the major options available to the user and a demonstration of the program capabilities by four sample cases in the following two sections.

2. CALCULATION OPTIONS

In order to enhance the value of propeller noise detectability computer program to the user, a number of input and calculation options have been provided. These options are described in detail in the user's manual [37]. The 6 most important options are also described here. The input to the program is summarized in Figure 34, which presents a capsuled outline of all the options and their significance. This figure should be consulted in connection with the following discussion. Several of the options and input parameters were used for developing the program and their use for production runs is not recommended.

The input format was selected so that options most likely to be desired and recommended values of parameters will be used by punching a "0." in the appropriate field of the input data card or by leaving this field blank. The consequences of this possible simplification in input card punching are demonstrated by the fourth sample case. In Figure 34 a "-" means any nonzero negative number (e.g., "-1.") is punched and a "+" means any nonzero positive number (e.g. "1.") is punched in the columns indicated.

The first major option described here is the calculation type option controlled by columns 25 to 30 of input card 14. This option also controls the significance of the

SAMPLE INPUT CARDS. • ALL NUMBERS TO RIGHT OF COLUMN 6 HAVE DECIMAL POINT
BLANK EQUIVALENT TO 0.

COLS CARD 14 • REQUIRED FOR FIRST CASE AND WHENEVER CHANGED • COLS. 13-72 MAY BE BLANK IF NOISE NOT CALCULATED

2-3 14

13-18 LARGEST HARMONIC NUMBER REQUIRED • 0. OR BLANK EQUIVALENT TO 1. • PROGRAM LIMITS TO MAX OF 50. • PROGRAM WILL CONTINUE UNTIL HARMONIC FREQUENCY EXCEEDS A LIMIT FRL PROVIDED BY TONE AURAL DETECTABILITY SUBROUTINE TODETN OR COMPUTED HARMONIC NUMBER IN COLS. 19-24 OF THIS CARD

19-24 LARGEST HARMONIC NUMBER PERMITTED • NUMBER LESS THAN IN COLS. 13-18 OF THIS CARD EQUIVALENT TO NUMBER IN COLS. 13-18 • PROGRAM LIMITS TO MAXIMUM OF 50.

25-30 CALCULATION TYPE OPTION
= - CALCULATE NOISE AND DETECTABILITY WITH X-Y INPUT
= 0 CALCULATE NOISE AND DETECTABILITY WITH X-Y INPUT • VARY X UNTIL FOUND MINIMUM UNDETECTABLE Y
= + CALCULATE NOISE AND DETECTABILITY WITH ANGLE-DISTANCE INPUT

31-36 PRINTING OPTION
= - MAX•• PRINT CONDITION, HARMONIC NOISE AND PRESSURE COMPONENTS, VORTEX NOISE, MINIMUM UNDETECTABLE VALUES OF Y
= 0 PRINT CONDITION, HARMONIC AND VORTEX NOISE, MINIMUM UNDETECTABLE VALUES
= + MIN•• PRINT CONDITION, MINIMUM UNDETECTABLE VALUE OF Y

37-42 INITIAL VALUE OF X (DISTANCE FORWARD FROM PROPELLER PLANE, FT) TO FIELD POINT IF COLS. 25-30 OF THIS CARD = - OR 0. • OTHERWISE
INITIAL ANGLE (FROM FORWARD AXIS, DEG) TO FIELD POINT IF COLS. 25-30 = +

43-48 INCREMENT IN X OR ANGLE • IF COLS. 25-30 OF THIS CARD =0. PROGRAM WILL REPLACE 0, BY SUITABLE VALUE

49-54 NUMBER OF VALUES OF X OR ANGLE TO CALCULATE NOISE FOR • IF COLS. 25-30 OF THIS CARD = 0. PROGRAM REPLACES BY 20. IF UNDER 20. • 0. OR BLANK EQUIVALENT TO 1.

55-60 INITIAL VALUE OF Y (DISTANCE FROM PROPELLER AXIS, FT) TO FIELD POINT IF COLS. 25-30 OF THIS CARD = - OR 0. • OTHERWISE
INITIAL DISTANCE (FT) CENTER OF PROPELLER TO FIELD POINT IF COLS.25-30 = +

61-66 INCREMENT IN Y OR DISTANCE

67-72 NUMBER OF VALUES OF Y OR DISTANCE TO CALCULATE NOISE FOR • BLANK OR 0. EQUIVALENT TO 1.

COLS CARD 15 • REQUIRED FOR FIRST CASE AND WHENEVER CHANGED

2-3 15

13-72 10 VALUES OF THICKNESS NOISE DOUBLET STRENGTH PROPORTIONALITY FACTOR K CORRESPONDING TO 10 GAUSS STATIONS OF CARD 4 • IF = 0. PROGRAM USES AREA FORMULA TO CALCULATE FACTOR FOR AIRFOIL NUMBERS 1.• 2.• 3.• 7.• 8.• AND 14. (CARD 9)

COLS CARD 26 FOLLOWING CARD 24 IF NOISE CALCULATION REQUIRED

2-3 26

13-18 NUMBER OF PROPELLERS • PROGRAM REPLACES 0. OR BLANK BY 1.

19-24 VORTEX NOISE CALCULATION OPTION
= BLANK, 0, OR 1. • USE VORTEX NOISE CALCULATION DEVELOPED UNDER THIS CONTRACT
= 2. USE HSD VORTEX NOISE CALCULATION DATED 3/69
= 3. USE HSD VORTEX NOISE CALCULATION DATED 7/69

25-30 AURAL DETECTABILITY OPTION
= BLANK • 0. OR 1. FOR NIGHTTIME JUNGLE
= 2. FOR DAYTIME JUNGLE

31-36 PROPELLER LOADING OPTION
= BLANK OR 0. • USE MAIN PERFORMANCE PROGRAM VALUES
= + • USE ALPHA,BETA,THETA,CL3,DCP/DX,DCT/DX,CTA AND CPA READ FROM 7 CARDS

Figure 34. Summary of Input Data for Propeller Noise Detectability Program

37-42 NEAR- VS FAR-FIELD CALCULATION OR HARMONIC NOISE OPTION
= - MUST USE FAR-FIELD CALCULATION (AZI PRINTS AS 0.)
= 0 USE FAR-FIELD CALCULATION ONLY IF FIELD POINT OVER 5 DIAMETERS AWAY
= + MUST USE NEAR-FIELD CALCULATION . IF OVER 50. CONTROLS NUMBER OF CIRCUMFERENTIAL STEPS (AZI)
43-48 ATMOSPHERIC SOUND ABSORPTION OPTION
= - READ 39 VALUES OF ABSORPTION ON CARDS 28, 29 AND 30 FOR EACH OPERATING CONDITION
= 0 USE STORED VALUES FOR 70PCT HUMIDITY , 77 DEG F
= + PERCENT RELATIVE HUMIDITY , USE WITH COLS. 49-54 OF THIS CARD TO COMPUTE ABSORPTION FROM EQUATIONS IN PROPOSED REVISION TO ARP 866
49-54 USED IF COLS. 43-48 OF THIS CARD = + , TEMPERATURE
= 0 USE TEMPERATURE FROM COLS. 31-36 OF CONDITION CARD BETWEEN CARDS 23 AND 24
NOT = 0 , AVERAGE TEMPERATURE (DEG F) FOR CALCULATION OF ABSORPTION
55-60 USED IF COLS. 19-24 OF THIS CARD = 0. OR 1. OR BLANK
= FORCE FACTOR FOR VORTEX NOISE , 0. OR BLANK REPLACED BY 8.
61-66 USED IF COLS. 19-24 OF THIS CARD = 0. OR 1. OR BLANK
= FREQUENCY FACTOR FOR VORTEX NOISE , 0. OR BLANK REPLACED BY .06
67-72 USED IF COLS. 19-24 OF THIS CARD = 0. OR 1. OR BLANK
= REYNOLDS NUMBER EXPONENT FOR VORTEX NOISE , 0. REPLACED BY -1.

COLS. CARD 27 FOLLOWING CARD 26
2-3 27
13-18 EMPIRICAL INCREMENT TO ADD TO THEORETICAL HARMONIC SPL , DB
19-24 = 0. , CALCULATE OVERTONES IN SAME WAY AS FUNDAMENTAL TONE SPL
NOT 0. , DO NOT USE THEORY FOR OVERTONES , EQUALS INCREMENT IN SPL BETWEEN SUCCESSIVE TONES , DB
25-30 EMPIRICAL ADJUSTMENT TO VORTEX NOISE IN PROPELLER PLANE , USED IF COLS. 19-24 OF CARD 26 = 0. OR 1. , DB , RECOMMEND 0.
31-36 RATIO OF FIRST-ORDER HARMONIC LOADS TO STEADY (ZERO-ORDER) LOADS , EMPIRICAL FACTOR TO ADJUST HARMONIC NOISE LEVELS , RECOMMEND .86 / NUMBER OF BLADES
37-42 EXPONENT OF LOAD ORDER USED WITH PRECEDING RATIO TO CALCULATE HARMONIC LOADS , PROGRAM SETS TO 1.43 IF 0. LOADED

COLS. CARD 28 , REQUIRE ONE FOR EACH CONDITION CARD ONLY IF COLS. 43-48 OF CARD 26 = - , FIRST CARD 28 FOLLOWS CARD 27
2-3 28
6-70 13 VALUES OF ATMOSPHERIC SOUND ABSORPTION (DB/1000FT) IN 1/3-OCTAVE BANDS STARTING WITH 1.6-HZ BAND AND ENDING WITH 25-HZ BAND , FORMAT F5.2

COLS. CARD 29 , FOLLOWS EACH CARD 28
2-3 29
6-70 13 VALUES OF ATMOSPHERIC SOUND ABSORPTION (DB/1000FT) IN 1/3-OCTAVE BANDS STARTING WITH 31.5-HZ BAND AND ENDING WITH 500-HZ BAND

COLS. CARD 30 , FOLLOWS EACH CARD 29
2-3 30
6-70 13 VALUES OF ATMOSPHERIC SOUND ABSORPTION (DB/1000FT) IN 1/3-OCTAVE BANDS STARTING WITH 630-HZ BAND AND ENDING WITH 10000-HZ BAND

COLS. 7 CARDS REQUIRED FOR EACH CONDITION CARD IF COLS. 31-36 OF CARD 26 = + , FIRST OF THESE 7 CARDS FOLLOWS CARD 27 OR CARD 30 IF PRESENT , FORMAT F6.0
13-72 10 VALUES OF ALPHA , DEG , ON FIRST CARD , CORRESPONDING TO GAUSS STATIONS OF CARD 4
13-72 10 VALUES OF BETA , DEG , ON SECOND CARD
13-72 10 VALUES OF THETA , DEG , ON THIRD CARD
13-72 10 VALUES OF GL3 ON FOURTH CARD

Figure 34. --- Continued

1X,A? 10 VALUES OF DCP/DX ON FIFTH CARD
13-?? 10 VALUES OF DCT/DX ON SIXTH CARD
13-19 CTA ON SEVENTH CARD
19-? CPA ON SEVENTH CARD

CARD 1 OR 25 IS NOW READ

Figure 34. --- Concluded

numbers describing the locations of the field points which are also read from card 14. If this option control is a nonzero negative number the program will interpret these numbers as out-of-plane distances (X) and away-from-axis distances (Y) and calculate propeller noise and aural detectability at a series of field points defined by a rectangular matrix in X-Y coordinates. If, on the other hand, the option control is a nonzero positive number the program will interpret the input ordinates as angles from the axis (ψ) and distances (d) to the field point and calculate noise and detectability at a series of field points defined by a rectangular matrix in ψ-d coordinates. For the third calculation option, selected if the control is a zero, the program will calculate minimum undetectable altitude. The undetectable altitude is calculated for enough values of X at the given Y to be able to interpolate for the largest value, the minimum altitude above the observer at which the propeller noise would not be heard. The three calculation type options are represented in the sample cases of Figure 36 discussed in the next section.

Another major option is the selection of the aural detectability criterion against which the predicted propeller noise levels are compared to determine minimum undetectable altitude. The option is controlled by the number punched in columns 25 to 30 of card 26. The two available criteria are discussed in Section II.

The harmonic loading and thickness rotational noise levels may be calculated by either the near-field procedure, based on Eqs. (3) and (4), or the far-field procedure, based on Eqs. (5) and (6). It is recommended that the control code, punched in columns 37 to 42 of card 26, be zero, thereby letting the computer program select the far-field procedure whenever it is warranted.

The harmonic load noise calculated from Eq. (3) or (5) is less than the rotational noise measured during the test program. The addition of harmonic loads is shown in Section VII.2.b to make a significant improvement in agreement with the data at the higher harmonics, which are most significant in terms of aural detectability. A correlation of harmonic loads is presented in Figure 28. It is recommended that this correlation be used. Therefore, a number equal to (0.86/number of blades) should be punched in columns 31-36 of card 27 to include harmonic loads in the calculation of harmonic noise. Harmonic loads will not be included in the calculation of harmonic loading noise of this field is 0. or blank.

The last option discussed here, the selection of a method of predicting broadband noise, is controlled by the number punched in columns 19-24 of card 26. Options 2 and 3 are the two methods developed by Hamilton Standard in 1969 and described in Section V.2. Option 1. (or 0.) is the new method whose development is presented in Section V.3. The 3 empirical coefficients in it, selected to correlate with the test data obtained under this contract, will be used unless other coefficients are read from columns 55-72 of card 26.

```
 1 SAMPLE CASE 1 • MAXIMUM DATA LOADED • MAXIMUM PRINTING • VARY ANGLE
 2 AND DISTANCE TO OBSERVER • VORTEX NOISE OPTION 1 • NEAR-FIELD + 3DB
 3  SAMPLE PROPELLER CONFIG• A3•     108•9  •5[illegible]  8•     •175
 4          •9892 •9443 •8677 •7662 •6498 •5261 •4087 •3072 •2306 •1857
 5          •0342 •0415 •0491 •0566 •0668 •0886 •1423 •2441 •4379 •6518
 6          •0582 •0643 •0707 •0749 •0763 •0753 •0712 •0620 •0469 •0385
 7          •2303 •3133 •4889 •6534 •7056 •7085 •6941 •6049 •422  •128
 8          -3•95 -3•48 -2•35 -•37  3•06  8•22  14•25 20•22 25•25 28•18
 9          1•    1•    1•    1•    1•    2•    3•    3•    3•    3•
10          •8923 •8667 •8046 •7570 •7269 •6974 •6439 •5554 •4    •248
11          •2866 •3783 •5676 •7253 •7549 •7070 •4563 -•0182-•1006-•1126
12          •2326 •2326 •2326 •2325 •2336 •2248 •1964 •1798 •2212 •2457
13
14          2•    4•    1•    -1•   105•  15•   2•    75•   75•   2•
15          •7    •7    •7    •7    •7    •7    •71   •72   •74   •76
16
17
18
19
20
21
22  1•9999•1•     1•    1•    1•    1•    1•    1•    1•    1•    1•
23  11•    2•     1•    6•
    1600•  2168•  0•    0•    77•                                1•
24
26          1•    1•    2•    1•    1•    -1•         8•    •06   -1•
27          3•
28  •003 •003 •004 •005 •007 •009 •01  •014 •02  •02  •03  •035 •04    A1•6-25
29  •05  •07  •1   •1   •1   •2   •2   •3   •3   •4   •6   •7   •9     A32-500
30  1•1  1•4  1•8  2•2  2•9  3•6  4•6  5•9  8•0  9•3  12•5 17•7 25•4   A630-10K
          1•67  2•67  3•38  4•33  6•25  9•50  13•52 20•89 27•72 30•79 ALPHA
          8•66  8•13  8•55  9•58  11•09 13•06 15•01 13•61 11•81 11•67 BETA
          10•33 10•60 11•93 13•91 17•34 22•50 28•53 34•50 39•53 42•46 THETA
          •569  •748  •929  1•085 1•216 1•352 1•409 1•018 •802  •765  CL3
          •1187 •1431 •1568 •1496 •1222 •0851 •0434 •0128 •0046 •0025 DCP/DX
          •2312 •3074 •3531 •3377 •2719 •1913 •1107 •0396 •0132 •0065 DCT/DX
          •1681 •0744                                               CTA,CPA
 1 SAMPLE CASE 2 • NORMAL DATA LOAD AND PRINT • X-Y LOCATIONS • 2 PROPS
 2 LOAD HARMONICS + ROLLOFF • CALCULATE ABSORPTION • FAR-FIELD • V.N.3
 3 SAMPLE PROPELLER CONFIG• B4•     213•8 •5384 11•25 •176
 4          •9892 •9443 •8679 •7665 •6493 •5266 •4055 •3080 •2316 •1867
 5          •032  •035  •041  •050  •062  •081  •120  •213  •54   1•
 6          •14   •1422 •142  •140  •1341 •1235 •106  •0815 •050  •04
 7          •24   •39   •525  •627  •676  •672  •589  •467  •335  •16
 8          -7•2  -6•4  -4•3  -•7   4•4   10•3  16•3  22•3  27•5  31•0
 9          1•    1•    1•    1•    1•    1•    2•    3•    3•    3•
10          1•    1•    1•    1•    1•    1•    1•    1•    1•    1•
11          0•    0•    0•    0•    0•    0•    0•    0•    0•    0•
12          0•    0•    0•    0•    0•    0•    0•    0•    0•    0•
14          1•    5•    -1•   0•    300•  -300• 3•    1500• 0•    1•
15          0•    0•    0•    0•    0•    0•    0•    0•    0•    0•
23  11•    2•    1•    6•
    162•   340•  1500• 77•   0•
24
26          2•    3•    1•    0•    -1•   80•   90•
27          0•    -6•   0•    •215  1•43
 1 SAMPLE CASE 3 • DETECTABILITY FLYBY • THRUST INPUT
 2
 3 SAMPLE PROPELLER CONFIG• B4•     213•8 •5384 11•25 •176
14          1•    10•   0•    0•    0•    -150• 0•    1500• 0•    1•
```

Figure 35. Listing of Input Data Cards for Four Sample Cases

```
 21  11.     2.      1.      6.
     0225.   340.    1500.   77.     53.65
 24                                          1.
 26              1.      0.      0.      0.      0.      0.              8.      .06     -1.
 27              0.      0.      0.      0.
  1 SAMPLE CASE 4 . SAME AS CASE 3 EXCEPT UNNECESSARY PUNCHING OF INPUT
  2 CARDS OMITTED . LAST CASE . MINIMUM PRINTING
  3 SAMPLE PROPELLER CONFIG. B4.      213.8 .5384 11.25 .176
 14                      10.             1.                              1500.
 23  11.     2.      1.      6.
      225.   340.    1500.   77.
 24                                          1.
 26
 27
 28
```

Figure 35. --- Concluded

A discussion of all the input data required by the propeller noise detectability program is shown in Figure 34 and is presented in detail in the user's manual [37].

3. SAMPLE CASES

In order to illustrate the results which are produced by the propeller noise detectability program, several sample cases were prepared. The input data required for each case and the resulting printed output obtained are discussed in this section. The sample cases were selected to demonstrate the versatility of the program and its use for representative types of calculation.

Figure 35 is a listing of the input cards for the four sample cases whose computer output is presented in Figure 36. The first case demonstrates the use of several options which would not be employed normally. The input is discussed in the following table.

Card	Input
14	Compute at least 2, but no more than 4 harmonics. Field point locations are punched in angle-distance coordinates. Maximum printing option selected. 4 field points at 105^{O} and 120^{O} and distances of 75 and 150 ft.
15	Thickness noise doublet strength proportionality factors are loaded.
23	One performance condition, static.
24	SHP input.
26	One propeller. Vortex noise option 1. Daytime jungle aural detectability option 2. Read propeller loading data after card 30. Use near-field harmonic noise option. Read atmospheric sound absorption coefficients from cards 28, 29 and 30. To calculate broad-band noise use force factor of 8.0, frequency factor of 0.6, and a Reynold's number exponent of -1.
27	Add an empirical correction of 3 dB to the harmonic noise levels.

The second sample case, for which the input cards are listed in Figure 35, is for a different propeller configuration so that new cards 4 to 12 are required. Other features of the input are discussed in the following table:

Card	Input
14	Compute at least 1, but no more than 5 harmonics. Field point locations punched in X-Y coordinates. Three field points located at X = -300, 0 and +300 ft and Y = 1500 ft.
15	Use area formula for thickness noise doublet strength proportionality factors.
26	Two propellers. Vortex noise option 3. Nighttime jungle aural detectability option 1. Use propeller performance program values. Use far-field harmonic noise option. Calculate atmospheric sound absorption coefficients for 80% relative humidity and 90°F.
27	Calculate harmonic rotational noise with no empirical adjustment of the fundamental and a -6 dB rolloff. That is, each harmonic SPL is 6 dB less than the SPL of the next lower harmonic. Include a harmonic loading of $0.215/\lambda^{1.43}$ in calculating the fundamental loading noise.

The third sample case illustrates a representative case in which the minimum altitude at which the aircraft can fly overhead without the propeller noise being detected is computed. Features of the input for this case are:

Card	Input
14	Compute no more than 10 harmonics. Vary X with increments of 150 ft at Y = 1500 ft to find minimum undetectable altitude.
24	Thrust rather than BHP is read from the preceding card.
26	One propeller. Vortex noise option 0, with recommended coefficients. Program selects near-or far-field option. Use stored values of atmospheric sound absorption coefficients for 70% relative humidity and 77°F.
27	Do not use an empirical increment, rolloff or harmonic loadings to compute harmonic rotational noise.

As discussed previously, it is not necessary to punch a "0." since a blank will be interpreted as a zero. Also, for most cases several input fields may be left blank because the noise program will replace the zero read by the proper value. For example, the program will change a 0. read as the number of propellers in columns

13-18 of card 26 to a 1. Therefore, many of the fields punched in cards 14, 26 and 27 of sample case 3 may be left blank without changing the results obtained from the noise program. The fourth sample case is included to demonstrate this simplification in input card punching which is possible if the recommended options and input coefficients are to be used. This sample case performs the same calculations as the third sample case. The only difference is in the printed output which is minimized in the fourth sample case by punching a "1." in columns 31-36 of card 14. A 25 card follows the 27 card because sample case 4 is the last case.

The four sample cases for which the input cards are listed in Figure 35, were run on the UAC UNIVAC 1108 computer and they produced the printed output shown in Figure 36.

The printed output of the propeller noise detectability program follows the output of the propeller performance program and begins with the heading "Computerized Propeller Design Technique Program Written by Hamilton Standard Under Contract No. F33615-70-C-1583 for Aero Prop. Lab". The next three lines list the 10 thickness noise doublet strength proportionality factors used and the 20 (only the first 15 are used) parameters read from cards 26 and 27. For the first sample case, the performance data loaded from the 7 cards following card 30 are printed next. Consequently the initial horsepower of 600 shown on the first page of Figure 36 is replaced by a value of 650.2 printed on the second page. Any alterations made by the program to the numbers loaded have been made before printing. The rotational noise option used is shown by the number in the column headed "AZI": a "0." indicates that the far-field approximation is used, a number "100." or larger indicates that the near-field calculation is used, and a "-1." indicates a specified rolloff loaded from columns 19-24 of card 27 is used. The first sample case includes extra printing which would not normally be required. The vector components of the loading and thickness noise pressures are printed for each noise harmonic. After the last set of these pressure components, but before the harmonic noise summation, ten lines of data relating to vortex noise are printed if vortex noise option 1 is selected. The columns are, in order from the left, an index, radius, blade thickness, blade chord, sectional velocity, force per foot radial increment, frequency, and a parameter proportional to sound power.

The rest of the output for the cases in Figure 36 is self explanatory.

Because of the several options available a very large number of combinations are possible. It is obviously impractical to demonstrate all of these combinations. However, the cases selected are believed to be representative and to demonstrate the major options available. For production runs to determine the minimum undetectable flight altitude of a propeller, it is recommended that the input be in the form of the fourth sample case in Figure 35. Only one change is suggested: harmonic loads should be included by punching 0.86/number of blades in columns 31-36 of card 27.

```
HAMILTON STANDARD COMPUTER PROGRAM DECK NO. 6196 1A


1 SAMPLE CASE 1 , MAXIMUM DATA LOADED , MAXIMUM PRINTING , VARY ANGLE
2 AND DISTANCE TO OBSERVER , VORTEX NOISE OPTION 1 , NEAR-FIELD + 3DB
                              BLADES   AF   CLI  DIA.  S.CO.P.REC.SHROUD
3 SAMPLE PROPELLER CONFIG. A    3.0 108.9  .509  8.50  .175 -.000  -.00

          X=   .9892   .9443   .8677   .7662   .6488   .5261   .4087   .3072   .2306   .1857
        H/B=   .034    .041    .049    .057    .067    .089    .142    .244    .438    .652
        B/D=   .0582   .0643   .0707   .0749   .0763   .0753   .0712   .0620   .0469   .0385
     DES CL=   .230    .313    .489    .653    .706    .708    .694    .605    .422    .128
   DELTA @=  -3.95   -3.48   -2.35   -.37    3.06    8.22   14.25   20.22   25.25   28.18
    AIRFOIL=   1.      1.      1.      1.      1.      2.      3.      3.      3.      3.
      MCRIT=   .892   .857    .805    .757    .727    .697    .644    .555    .400    .248
  (CL A=0)=   .287    .378    .568    .725    .755    .707    .456   -.018   -.101   -.113
       D00=   .233    .233    .233    .232    .234    .225    .196    .180    .221    .246
              -.000   -.000   -.000   -.000   -.000   -.000   -.000   -.000   -.000   -.000
              2.000   4.000   1.000  -1.000  105.000  15.000   2.000  75.000  75.000   2.000
               .700    .700    .700    .700    .700    .700    .710    .720    .740    .760
              -.000   -.000   -.000   -.000   -.000   -.000   -.000   -.000   -.000   -.000
              -.000   -.000   -.000   -.000   -.000   -.000   -.000   -.000   -.000   -.000
              -.000   -.000   -.000   -.000   -.000   -.000   -.000   -.000   -.000   -.000
              -.000   -.000   -.000   -.000   -.000   -.000   -.000   -.000   -.000   -.000
              -.000   -.000   -.000   -.000   -.000   -.000   -.000   -.000   -.000   -.000
              -.000   -.000   -.000   -.000   -.000   -.000   -.000   -.000   -.000   -.000

J LIMIT=99999.0010  1.0000  1.0000  1.0000  1.0000  1.0000  1.0000  1.0000  1.0000  1.0000  1.0000

VON KARMAN EFFECT USED

ALPHA OFF AIRFOIL CHART,SERIES 16 USED AT X= .307

ALPHA OFF AIRFOIL CHART,SERIES 16 USED AT X= .231

ALPHA OFF AIRFOIL CHART,SERIES 16 USED AT X= .186

  BHP     PRPM     ALT.  V-KNOTS TEMP  REQ.CP      J       COMP.CP 03/  AP.EFF.  M.N.  AP.EFF.  EF.EFF. IND.EFF. HI/HO        F/M
  600.00  2168.      0.     .0  537.   .0687     .0000
                                                            .0843  15.31  2788.

ALPHA OFF AIRFOIL CHART,SERIES 16 USED AT X= .307

ALPHA OFF AIRFOIL CHART,SERIES 16 USED AT X= .231

ALPHA OFF AIRFOIL CHART,SERIES 16 USED AT X= .186
                                                            .0722  13.81  2599.

ALPHA OFF AIRFOIL CHART,SERIES 16 USED AT X= .307

ALPHA OFF AIRFOIL CHART,SERIES 16 USED AT X= .231

ALPHA OFF AIRFOIL CHART,SERIES 16 USED AT X= .186
                                                            .0689  13.38  2541.  .8469   2541.   2541.   2552.   .00000  .7557

 J=     .0000  THET34=  13.38 PSI=   .00 OMT=   .00  MS= .8469  S3=-0.  S4= 1.

       X=   .9892   .9443   .8677   .7662   .6488   .5261   .4087   .3072   .2306   .1857
   THETA=  9.43    9.90   11.03   13.01   16.44   21.60   27.63   33.60   38.63   41.56
   ALPHA=  1.33    2.19    2.82    3.67    5.60    8.49   12.12   19.99   26.82   29.88
     PHI=  8.10    7.70    8.20    9.33   10.83   13.11   15.51   13.61   11.81   11.67
```

Figure 36. Output of Propeller Design Technique Program for Four Sample Cases

BETA=	8.10	7.70	6.20	9.33	10.83	13.11	15.51	13.61	11.81	11.67
PHI 0=	.00	.00	.00	.00	.00	.00	.00	.00	.00	.00
CL3=	.522	.696	.868	1.033	1.163	1.369	1.494	1.018	.802	.765
CD/CL=	.0120	.0100	.0092	.0115	.0197	.0341	.0267	.0681	.2223	.3592
DCP/DX=	.1024	.1233	.1386	.1366	.1128	.0861	.0463	.0121	.0043	.0023
DCT/DX=	.2131	.2844	.3310	.3225	.2610	.1936	.1168	.0398	.0132	.0065
SECT.EFF.=	.0000	.0000	.0000	.0000	.0000	.0000	.0000	.0000	.0000	.0000
SECT.LOSS=	.1024	.1233	.1386	.1366	.1128	.0861	.0463	.0121	.0043	.0023
SECT.MN=	.8294	.7925	.7274	.6403	.5397	.4340	.3335	.2529	.1912	.1540
M/MCRIT=	.0000	.0000	.0000	.0000	.0000	.0000	.0000	.0000	.0000	.0000
AIRFOIL=	1.	1.	1.	1.	1.	2.	3.	3.	3.	3.
G=	7.2432	6.6006	5.5731	4.3456	3.1159	2.0488	1.2364	.6986	.3936	.2553

COMPUTERIZED PROPELLER DESIGN TECHNIQUE PROGRAM WRITTEN BY HAMILTON STANDARD UNDER CONTRACT NO.F33615-70-C-1583 FOR AFAL PROP. LAB

K=	.70	.70	.70	.70	.70	.70	.71	.72	.74	.76
QNOISE=	1.00	1.00	2.00	1.00	1.00	-1.00	-.00	8.00	.06	-1.00
	3.00	-.00	-.00	.00	1.43	-.00	-.00	-.00	-.00	-.00

1. PROPELLER(S) , VORTEX NOISE OPTION= 1. , DETECTABILITY OPTION= 2 DAYTIME JUNGLE
NOISE IN DB RE .0002 MICROBAR

VALUES OF ATMOSPHERIC ABSORPTION (DB/1000FT) LOADED ARE

.003	.003	.004	.005	.007	.009	.010	.014	.020	.02	.03	.03	.04	.05	.07	.10	.10	.10	.20		
.20	.30	.30	.40	.60	.70	.90	1.10	1.40	1.80	2.20	2.90	3.60	4.60	5.90	8.00	9.30	12.50	17.70	25.40	

ALPHA=	1.67	2.67	3.38	4.33	6.25	9.50	13.52	20.89	27.72	30.79
BETA=	8.66	8.13	8.55	9.58	11.09	13.00	15.01	13.61	11.81	11.67
THETA=	10.33	10.80	11.93	13.91	17.34	22.50	28.53	34.50	39.53	42.46
CL3=	.569	.748	.929	1.085	1.216	1.352	1.409	1.018	.802	.765
DCP/DX=	.1187	.1431	.1568	.1496	.1222	.0851	.0434	.0128	.0046	.0025
DCT/DX=	.2312	.3074	.3531	.3377	.2719	.1913	.1107	.0396	.0132	.0065

CTA= .1681 CPA= .0744

FLIGHT VELOCITY= 0. KNOTS TAS = 0. KNOTS CAS , MACH NUMBER= .00 , BHP= 650.2 , THRUST= 2632. LB , RPM= 2168.
ROTATIONAL TIP VELOCITY= 964.9 FPS , ROTATIONAL TIP MACH NUMBER= .85 , HELICAL TIP MACH NUMBER= .85

X= -19.4 , Y= 72. , DISTANCE= 75. FT , ANGLE= 105.0 DEG WHEN HEARD , X= -19.4 , DISTANCE= 75. FT WHEN NOISE PRODUCED

HARMONIC NUMBER	AZI	FREQ. HZ	ATMOS. ABSORP	LOADING NOISE	THICKNESS NOISE	HARMONIC NOISE	DETECTABLE TONE NOISE	MINIMUM UNDETECTABLE Y
1	100.	108.	-.0	113.0	96.2	113.1	24.7	264479.

OSCILLATORY PRESSURE COMPONENTS (LBS. PER SQ. FT.)

RADIUS	LOADING (RP)	LOADING (IP)	LOADING	THICKNESS (RP)	THICKNESS (IP)	THICKNESS
4.204	1.95426-01	-4.58485-01	4.98397-01	-3.63928-02	-1.72869-02	4.02899-02
4.013	2.32453-01	-5.47618-01	5.94911-01	-4.85954-02	-2.30574-02	5.37881-02
3.688	2.30698-01	-5.43344-01	5.90292-01	-5.70637-02	-2.70289-02	6.31413-02
3.256	1.83443-01	-4.29158-01	4.66720-01	-5.43328-02	-2.56852-02	6.00981-02
2.757	1.17111-01	-2.70371-01	2.94644-01	-4.31497-02	-2.03611-02	4.77124-02
2.236	6.11237-02	-1.38749-01	1.51616-01	-3.14427-02	-1.48146-02	3.47579-02
1.737	2.29344-02	-5.13176-02	5.62093-02	-2.24011-02	-1.05431-02	2.47582-02
1.306	4.87254-03	-1.07673-02	1.18185-02	-1.29032-02	-6.06884-03	1.42592-02
.980	1.25088-03	-2.71947-03	2.99336-03	-5.84947-03	-2.75038-03	6.46381-03
.789	5.34437-04	-1.15204-03	1.26996-03	-3.16928-03	-1.49016-03	3.50213-03
	2.29066+00	-5.34046+00	2.63633-01	-7.58343-01	-3.58297-01	3.80513-02

2	100.	217.	-.0	109.9	97.5	110.2	19.6	145365.

OSCILLATORY PRESSURE COMPONENTS (LBS. PER SQ. FT.)

RADIUS	LOADING (RP)	LOADING (IP)	LOADING	THICKNESS (RP)	THICKNESS (IP)	THICKNESS
4.204	-4.35838-01	3.59693-01	5.65096-01	5.67204-02	7.34225-02	9.27797-02
4.013	-4.72278-01	3.90964-01	6.13106-01	6.92004-02	8.95361-02	1.13161-01

Figure 36. --- Continued

3.688	-3.89127-01	3.22329-01	5.05288-01	6.80790-02	8.80302-02	.11284-[illegible]
3.256	-2.29165-01	1.89152-01	2.97145-01	4.88003-02	6.30659-02	[illegible].97420-02
2.757	-9.45589-02	7.74154-02	1.22207-01	2.56703-02	3.31608-02	4.19357-02
2.236	-2.74147-02	2.21998-02	3.52761-02	1.07362-02	1.38650-02	1.75358-02
1.737	-4.91162-03	3.94006-03	6.29664-03	3.78930-03	4.89160-03	6.18761-03
1.306	-4.46665-04	3.55874-04	5.71100-04	9.62204-04	1.23982-03	1.56939-03
.980	-4.97206-05	3.95005-05	6.35014-05	1.89604-04	2.42311-04	3.07675-04
.789	-1.12580-05	9.06353-06	1.44531-05	5.54526-05	6.94957-05	8.89081-05
	-3.10654+00	2.56491+00	1.84194-01	5.92728-01	7.66274-01	4.42938-02

1	4.204	.017	.495	943.585	34.840	3346.3	.1056-05
2	4.013	.023	.547	901.986	42.478	2386.0	.1895-05
3	3.688	.030	.601	827.929	48.372	1683.5	.2018-05
4	3.256	.036	.637	728.987	50.534	1213.8	.1691-05
5	2.757	.043	.649	614.329	50.728	850.8	.1195-05
6	2.236	.057	.640	494.617	53.816	523.3	.7095-06
7	1.737	.086	.605	380.895	64.723	265.4	.3574-06
8	1.306	.129	.527	288.090	78.361	134.4	.1846-06
9	.980	.175	.399	217.793	92.431	74.9	.1067-06
10	.789	.213	.327	175.476	100.432	49.4	.4520-07

HARMONIC NOISE SUMMATION - LOADING= 114.7 DB , THICKNESS= 99.9 DB , OVERALL HARMONIC NOISE= 114.9 DB
OVERALL VORTEX NOISE= 108.2 DB WITH MAX SPL AT 8000. HZ , TOTAL OVERALL NOISE= 115.8 DB
1/3-OCTAVE BAND DATA IS

BAND CENTER FREQ. HZ	NUMBER OF HARMONICS	BAND SPL DB	VORTEX BROADBAND SPL - DB	MAXIMUM UNDETECTABLE BROADBAND DB	MINIMUM UNDETECTABLE VERTICAL DISTANCE - FT VORTEX	TOTAL NOISE
1.6	0	5.1	5.1	121.5	0.	0.
2.0	0	11.3	11.3	120.0	0.	0.
2.5	0	17.5	17.5	117.0	0.	0.
3.1	0	23.9	23.9	113.5	0.	0.
4.0	0	30.5	30.5	109.0	0.	0.
5.0	0	36.6	36.6	104.0	0.	0.
6.3	0	43.0	43.0	99.5	0.	0.
8.0	0	48.9	48.9	95.0	0.	0.
10.0	0	52.2	52.2	91.5	1.	1.
12.5	0	56.5	56.5	87.5	2.	2.
16.0	0	59.3	59.3	82.0	5.	5.
20.0	0	62.1	62.1	74.5	17.	17.
25.0	0	64.6	64.6	65.0	69.	69.
31.5	0	66.6	66.5	56.0	244.	244.
40.0	0	68.7	68.6	48.0	774.	774.
50.0	0	70.7	70.4	41.5	2014.	2014.
63.0	0	74.2	71.9	37.0	4081.	4081.
80.0	0	86.5	73.5	34.0	7042.	7042.
100.0	1	113.1	74.9	33.5	8008.	264479.
125.0	0	105.8	76.5	34.5	8516.	8516.
160.0	0	85.6	77.8	35.5	8120.	8120.
200.0	1	110.2	79.4	36.5	8543.	145365.
250.0	0	102.9	81.0	37.5	8359.	8359.
315.0	0	83.7	82.5	38.5	7580.	7580.
400.0	0	84.4	84.3	39.0	7943.	7943.
500.0	0	85.9	85.9	39.5	7627.	7627.
630.0	0	87.7	87.7	39.5	7725.	7725.
800.0	0	89.5	89.5	39.0	7718.	7718.
1000.0	0	91.0	91.0	38.5	7309.	7309.
1250.0	0	92.6	92.6	38.0	7045.	7045.
1600.0	0	94.2	94.2	38.0	6208.	6208.
2000.0	0	95.5	95.5	39.0	5400.	5400.
2500.0	0	96.8	96.8	41.0	4417.	4417.
3150.0	0	97.8	97.8	44.0	3462.	3462.
4000.0	0	98.7	98.7	47.0	2593.	2593.

Figure 36. --- Continued

5000.0	0	99.4	99.4	50.5	2123.	2123.
6300.0	0	99.7	99.7	53.5	1586.	1586.
8000.0	0	99.8	99.8	55.0	1194.	1194.
10000.0	0	99.3	99.3	56.5	880.	880.

MINIMUM UNDETECTABLE Y= 264479. FT AT X= -19.4 FT

X= -37.5 , Y= 65. , DISTANCE= 75. FT , ANGLE= 120.0 DEG WHEN HEARD , X= -37.5 , DISTANCE= 75. FT WHEN NOISE PRODUCED

HARMONIC NUMBER	AZI	FREQ. HZ	ATMOS. ABSORP	LOADING NOISE	THICKNESS NOISE	HARMONIC NOISE	DETECTABLE TONE NOISE	MINIMUM UNDETECTABLE Y
1	100.	108.	-.0	113.8	93.7	113.9	24.7	212434.

OSCILLATORY PRESSURE COMPONENTS (LBS. PER SQ. FT.)

RADIUS	LOADING (RP)	LOADING (IP)	LOADING	THICKNESS (RP)	THICKNESS (IP)	THICKNESS
4.204	2.17262-01	-5.52242-01	5.93443-01	-2.85259-02	-1.30363-02	3.13636-02
4.013	2.57557-01	-6.54901-01	7.03727-01	-3.77685-02	-1.73106-02	4.15648-02
3.688	2.49237-01	-6.30140-01	6.77640-01	-4.38221-02	-2.01522-02	4.82337-02
3.256	1.89154-01	-4.72007-01	5.08498-01	-4.11205-02	-1.89983-02	4.52971-02
2.757	1.13393-01	-2.77157-01	2.99456-01	-3.21946-02	-1.49449-02	3.54943-02
2.236	5.52777-02	-1.31661-01	1.42794-01	-2.31779-02	-1.08040-02	2.55722-02
1.737	1.96265-02	-4.56613-02	4.97007-02	-1.63642-02	-7.65232-03	1.80650-02
1.306	3.98611-03	-9.08091-03	9.91726-03	-9.37039-03	-4.39130-03	1.03483-02
.980	9.69690-04	-2.14932-03	2.35794-03	-4.23381-03	-1.98679-03	4.67680-03
.789	4.02902-04	-8.79453-04	9.67351-04	-2.29039-03	-1.07564-03	2.53039-03
	2.36610+00	-5.89981+00	2.88386-01	-5.71231-01	-2.64366-01	2.85564-02

2	100.	217.	-.0	108.8	92.9	108.9	19.6	117932.

OSCILLATORY PRESSURE COMPONENTS (LBS. PER SQ. FT.)

RADIUS	LOADING (RP)	LOADING (IP)	LOADING	THICKNESS (RP)	THICKNESS (IP)	THICKNESS
4.204	-4.01999-01	3.59703-01	5.39434-01	3.66798-02	4.48120-02	5.79095-02
4.013	-4.29047-01	3.83052-01	5.75160-01	4.38056-02	5.37727-02	6.93573-02
3.688	-3.38561-01	3.00084-01	4.52409-01	4.16878-02	5.15675-02	6.63105-02
3.256	-1.86435-01	1.63178-01	2.47761-01	2.87580-02	3.59051-02	4.60021-02
2.757	-7.07803-02	6.08713-02	9.33550-02	1.45761-02	1.83704-02	2.34507-02
2.236	-1.88141-02	1.58520-02	2.46019-02	5.90892-03	7.50759-03	9.55402-03
1.737	-3.14212-03	2.59988-03	4.07827-03	2.03807-03	2.60466-03	3.30726-03
1.306	-2.70249-04	2.20523-04	3.48805-04	5.10228-04	6.53347-04	8.28972-04
.980	-2.82232-05	2.28932-05	3.63407-05	1.00245-04	1.26883-04	1.61704-04
.789	-6.21981-06	5.17480-06	8.09101-06	2.98972-05	3.65205-05	4.71973-05
	-2.65393+00	2.34393+00	1.61893-01	3.56507-01	4.42930-01	2.59967-02

1	4.204	.017	.495	943.585	34.840	3346.3	.2486-05
2	4.013	.023	.547	901.986	42.478	2386.0	.4478-05
3	3.688	.030	.601	827.929	48.372	1683.5	.4774-05
4	3.256	.036	.637	728.987	50.534	1213.8	.3991-05
5	2.757	.043	.649	614.329	50.728	850.8	.2784-05
6	2.236	.057	.640	494.617	53.816	523.3	.1616-05
7	1.737	.086	605	380.895	64.723	265.4	.7836-06
8	1.306	.129	.527	288.090	78.361	134.4	.3670-06
9	.980	.175	.399	217.793	92.431	74.9	.1784-06
10	.789	.213	.327	175.476	100.432	49.4	.6455-07

HARMONIC NOISE SUMMATION - LOADING= 115.0 DB , THICKNESS= 96.3 DB , OVERALL HARMONIC NOISE= 115.1 DB
OVERALL VORTEX NOISE= 106.7 DB WITH MAX SPL AT 5000. HZ , TOTAL OVERALL NOISE= 115.7 DB
1/3-OCTAVE BAND DATA IS

BAND CENTER FREQ. HZ	NUMBER OF HARMONICS	BAND SPL DB	VORTEX BROADBAND SPL - DB	MAXIMUM UNDETECTABLE BROADBAND DB	MINIMUM UNDETECTABLE VERTICAL DISTANCE - FT VORTEX	TOTAL NOISE
1.6	0	5.8	5.8	121.5	0.	0.
2.0	0	12.0	12.0	120.0	0.	0.
2.5	0	18.2	18.2	117.0	0.	0.

Figure 36. --- Continued

3.1	0	24.6	24.6	113.5	0.	0.
4.0	0	31.2	31.2	109.0	0.	0.
5.0	0	37.4	37.4	104.0	0.	0.
6.3	0	43.6	43.6	99.5	0.	0.
8.0	0	49.8	49.8	95.0	0.	0.
10.0	0	53.2	53.2	91.5	1.	1.
12.5	0	57.5	57.5	87.5	2.	2.
16.0	0	60.3	60.3	82.0	5.	5.
20.0	0	63.1	63.1	74.5	18.	18.
25.0	0	65.6	65.6	65.0	69.	69.
31.5	0	67.6	67.6	56.0	246.	246.
40.0	0	69.7	69.6	48.0	780.	780.
50.0	0	71.8	71.4	41.5	2040.	2040.
63.0	0	75.1	72.9	37.0	4087.	4087.
80.0	0	87.2	74.5	34.0	7010.	7010.
100.0	1	113.9	75.9	33.5	7891.	212434.
125.0	0	106.6	77.3	34.5	8255.	8255.
160.0	0	85.4	78.8	35.5	7888.	7888.
200.0	1	108.9	80.3	36.5	8305.	117982.
250.0	0	101.7	81.8	37.5	7945.	7945.
315.0	0	84.2	83.4	38.5	7249.	7249.
400.0	0	85.2	85.2	39.0	7500.	7500.
500.0	0	86.7	86.7	39.5	7174.	7174.
630.0	0	88.5	88.5	39.5	7223.	7223.
800.0	0	90.0	90.0	39.0	7055.	7055.
1000.0	0	91.5	91.5	38.5	6677.	6677.
1250.0	0	92.8	92.8	38.0	6337.	6337.
1600.0	0	94.2	94.2	38.0	5543.	5543.
2000.0	0	95.2	95.2	39.0	4769.	4769.
2500.0	0	96.1	96.1	41.0	3857.	3857.
3150.0	0	96.8	96.8	44.0	2989.	2989.
4000.0	0	97.2	97.2	47.0	2217.	2217.
5000.0	0	97.5	97.5	50.5	1778.	1778.
6300.0	0	97.5	97.5	53.5	1310.	1310.
8000.0	0	97.0	97.0	55.0	974.	974.
10000.0	0	96.2	96.2	56.5	712.	712.

MINIMUM UNDETECTABLE Y= 212434. FT AT X= -37.5 FT

X= -38.8 , Y= 145. , DISTANCE= 150. FT , ANGLE= 105.0 DEG WHEN HEARD , X= -38.8 , DISTANCE= 150. FT WHEN NOISE PRODUCED

HARMONIC NUMBER	AZI	FREQ. HZ	ATMOS. ABSORP	LOADING NOISE	THICKNESS NOISE	HARMONIC NOISE	DETECTABLE TONE NOISE	MINIMUM UNDETECTABLE Y
1	100.	108.	-.0	106.9	90.1	107.1	24.7	264006.

OSCILLATORY PRESSURE COMPONENTS (LBS. PER SQ. FT.)

RADIUS	LOADING (RP)	LOADING (IP)	LOADING	THICKNESS (RP)	THICKNESS (IP)	THICKNESS
4.234	-1.21218-01	-2.16598-01	2.48211-01	-1.77186-02	9.45111-03	2.00816-02
4.015	-1.44905-01	-2.58468-01	2.96316-01	-2.36529-02	1.26231-02	2.68104-02
3.688	-1.43810-01	-2.56539-01	2.94098-01	-2.77623-02	1.48281-02	3.14741-02
3.256	-1.13501-01	-2.03042-01	2.32612-01	-2.64204-02	1.41243-02	2.99588-02
2.757	7.13691-02	-1.28393-01	1.46896-01	-2.09725-02	1.12214-02	2.37858-02
2.236	-3.65274-02	-6.61937-02	7.56033-02	-1.52765-02	8.17945-03	1.73284-02
1.737	-1.34778-02	-2.45782-02	2.80310-02	-1.08805-02	5.82867-03	1.23434-02
1.306	-2.82177-03	-5.17447-03	5.89386-03	-6.26628-03	3.35781-03	7.10923-03
.980	-7.10579-04	-1.31270-03	1.49268-03	-2.84055-03	1.52223-03	3.22272-03
.789	-3.00526-04	-5.57368-04	6.33226-04	-1.53898-03	8.24690-04	1.74602-03
	-1.38965+00	-2.48961+00	1.31379-01	-3.63020-01	1.94119-01	1.89688-02
2	100.	217.	-.0	103.8	91.4	104.1	19.6	145132.

OSCILLATORY PRESSURE COMPONENTS (LBS. PER SQ. FT.)

RADIUS	LOADING (RP)	LOADING (IP)	LOADING	THICKNESS (RP)	THICKNESS (IP)	THICKNESS

Figure 36. --- Continued

4.204	2.34104-01	1.55992-01	2.81315-01	2.62428-02	-3.80444-02	4.62176-02
4.013	2.54152-01	1.69074-01	3.05252-01	3.20033-02	-4.64068-02	5.63720-02
3.688	2.09528-01	1.39341-01	2.51631-01	3.14666-02	-4.56434-02	5.54388-02
3.256	1.23181-01	8.20716-02	1.48018-01	2.25442-02	-3.27108-02	3.97270-02
2.757	5.06051-02	3.38619-02	6.08892-02	1.18542-02	-1.72039-02	2.08925-02
2.236	1.45834-02	9.81500-03	1.75787-02	4.95657-03	-7.19449-03	8.73661-03
1.737	2.59924-03	1.75792-03	3.13788-03	1.74865-03	-2.53889-03	3.08281-03
1.306	2.35501-04	1.59701-04	2.84544-04	4.42882-04	-6.44202-04	7.81755-04
.980	2.62308-05	1.77120-05	3.16508-05	8.62732-05	-1.26762-04	1.53335-04
.789	6.01715-06	3.92778-06	7.18565-06	2.42441-05	-3.69629-05	4.42044-05
	1.63124+00	1.08668+00	9.17313-02	2.67597-01	-3.88205-01	2.20664-02

1	4.204	.017	.495	943.585	34.840	3346.3	.2511-06
2	4.013	.023	.547	901.986	42.478	2386.0	.4512-06
3	3.688	.030	.601	827.929	48.372	1683.5	.4819-06
4	3.256	.036	.637	728.987	50.534	1213.8	.4057-06
5	2.757	.043	.649	614.329	50.728	850.8	.2884-06
6	2.236	.057	.640	494.617	53.816	523.3	.1723-06
7	1.737	.086	.605	380.895	64.723	265.4	.8733-07
8	1.306	.129	.527	288.090	78.361	134.4	.4535-07
9	.980	.175	.399	217.793	92.431	74.9	.2633-07
10	.789	.213	.327	175.476	100.432	49.4	.1116-07

HARMONIC NOISE SUMMATION - LOADING= 108.7 DB , THICKNESS= 93.8 DB , OVERALL HARMONIC NOISE= 108.8 DB
OVERALL VORTEX NOISE= 101.4 DB WITH MAX SPL AT 6300. HZ , TOTAL OVERALL NOISE= 109.6 DB
1/3-OCTAVE BAND DATA IS

BAND CENTER FREQ. HZ	NUMBER OF HARMONICS	BAND SPL DB	VORTEX BROADBAND SPL - DB	MAXIMUM UNDETECTABLE BROADBAND DB	MINIMUM UNDETECTABLE VERTICAL DISTANCE - FT VORTEX	TOTAL NOISE
1.6	0	-1.0	-1.0	121.5	0.	0.
2.0	0	5.2	5.2	120.0	0.	0.
2.5	0	11.4	11.4	117.0	0.	0.
3.1	0	17.9	17.9	113.5	0.	0.
4.0	0	24.5	24.5	109.0	0.	0.
5.0	0	30.5	30.5	104.0	0.	0.
6.3	0	36.9	36.9	99.5	0.	0.
8.0	0	42.9	42.9	95.0	0.	0.
10.0	0	46.2	46.2	91.5	1.	1.
12.5	0	50.5	50.5	87.5	2.	2.
16.0	0	53.3	53.3	82.0	5.	5.
20.0	0	56.0	56.0	74.5	17.	17.
25.0	0	58.6	58.6	65.0	69.	69.
31.5	0	60.5	60.5	56.0	244.	244.
40.0	0	62.6	62.5	48.0	777.	777.
50.0	0	64.7	64.4	41.5	2013.	2013.
63.0	0	68.1	65.8	37.0	4077.	4077.
80.0	0	80.4	67.5	34.0	7034.	7034.
100.0	1	107.1	68.9	33.5	8007.	264006.
125.0	0	99.8	70.4	34.5	8528.	8528.
160.0	0	79.6	71.8	35.5	8114.	8114.
200.0	1	104.1	73.3	36.5	8538.	145132.
250.0	0	96.8	74.9	37.5	8347.	8347.
315.0	0	77.7	76.4	38.5	7615.	7615.
400.0	0	78.3	78.3	39.0	7911.	7911.
500.0	0	79.8	79.8	39.5	7624.	7624.
630.0	0	81.6	81.6	39.5	7725.	7725.
800.0	0	83.4	83.4	39.0	7720.	7720.
1000.0	0	84.9	84.9	38.5	7313.	7313.
1250.0	0	86.5	86.5	38.0	7050.	7050.
1600.0	0	88.0	88.0	38.0	6212.	6212.
2000.0	0	89.3	89.3	39.0	5404.	5404.
2500.0	0	90.4	90.4	41.0	4407.	4407.

Figure 36. --- Continued

3150.0	0	91.4	91.4	44.0	3457.	3457.
4000.0	0	92.1	92.1	47.0	2600.	2600.
5000.0	0	92.7	92.7	50.5	2129.	2129.
6300.0	0	92.6	92.8	53.5	1589.	1589.
8000.0	0	92.4	92.4	55.0	1196.	1196.
10000.0	0	91.4	91.4	56.5	881.	881.

MINIMUM UNDETECTABLE Y= 264006. FT AT X= -38.8 FT

X= -75.0 , Y= 130. , DISTANCE= 150. FT , ANGLE= 120.0 DEG WHEN HEARD , X= -75.0 , DISTANCE= 150. FT WHEN NOISE PRODUCED

HARMONIC NUMBER	AZI	FREQ. HZ	ATMOS. ABSORP	LOADING NOISE	THICKNESS NOISE	HARMONIC NOISE	DETECTABLE TONE NOISE	MINIMUM UNDETECTABLE Y
1	100.	108.	-.0	107.7	87.6	107.8	24.7	212122.

OSCILLATORY PRESSURE COMPONENTS (LBS. PER SQ. FT.)

RADIUS	LOADING (RP)	LOADING (IP)	LOADING	THICKNESS (RP)	THICKNESS (IP)	THICKNESS
4.204	-1.48075-01	-2.56071-01	2.95802-01	-1.37499-02	7.46548-03	1.56459-02
4.013	-1.75620-01	-3.03662-01	3.50789-01	-1.82260-02	9.88513-03	2.07341-02
3.688	-1.68849-01	-2.92607-01	3.37830-01	-2.11574-02	1.14550-02	2.40594-02
3.256	-1.26233-01	-2.19895-01	2.53552-01	-1.98772-02	1.07392-02	2.25928-02
2.757	-7.38869-02	-1.29788-01	1.49346-01	-1.55817-02	8.40026-03	1.77018-02
2.236	-3.49540-02	-6.20566-02	7.12236-02	-1.12298-02	6.04260-03	1.27523-02
1.737	-1.20752-02	-2.16512-02	2.47908-02	-7.93511-03	4.26349-03	9.00796-03
1.306	-2.39276-03	-4.32935-03	4.94657-03	-4.54629-03	2.44020-03	5.15978-03
.980	-5.63581-04	-1.03213-03	1.17598-03	-2.05488-03	1.10221-03	2.33182-03
.789	-2.29948-04	-4.24077-04	4.82408-04	-1.11191-03	5.96129-04	1.26163-03
	-1.55324+00	-2.70654+00	1.43791-01	-2.71987-01	1.46833-01	1.42425-02

2	100.	217.	-.0	102.7	86.8	102.9	19.6	117829.

OSCILLATORY PRESSURE COMPONENTS (LBS. PER SQ. FT.)

RADIUS	LOADING (RP)	LOADING (IP)	LOADING	THICKNESS (RP)	THICKNESS (IP)	THICKNESS
4.204	2.26731-01	1.44622-01	2.68928-01	1.60649-02	-2.40064-02	2.88857-02
4.013	2.41663-01	1.54333-01	2.86740-01	1.92728-02	-2.87277-02	3.45937-02
3.688	1.89875-01	1.21740-01	2.25551-01	1.84753-02	-2.74278-02	3.30699-02
3.256	1.03780-01	6.69964-02	1.23526-01	1.28578-02	-1.89954-02	2.29380-02
2.757	3.89944-02	2.54144-02	4.65452-02	6.57556-03	-9.66650-03	1.16910-02
2.236	1.02419-02	6.74887-03	1.22656-02	2.68611-03	-3.93218-03	4.76206-03
1.737	1.69235-03	1.12560-03	2.03249-03	9.31124-04	-1.35939-03	1.64771-03
1.306	1.44442-04	9.65543-05	1.73742-04	2.33056-04	-3.40696-04	4.12782-04
.980	1.51274-05	1.00738-05	1.81747-05	4.52574-05	-6.70138-05	8.08646-05
.789	3.35128-06	2.25800-06	4.04100-06	1.32495-05	-1.95029-05	2.35778-05
	1.45102+00	9.32147-01	8.07137-02	1.54996-01	-2.29576-01	1.29637-02

1	4.204	.017	.495	943.585	34.840	3346.3	.5919-06	
2	4.013	.023	.547	901.986	42.478	2386.0	.1067-05	
3	3.688	.030	.601	827.929	48.372	1683.5	.1141-05	
4	3.256	.036	.637	728.987	50.534	1213.8	.9570-06	
5	2.757	.043	.649	614.329	50.728	850.8	.6713-06	
6	2.236	.057	.640	494.617	53.816	523.3	.3920-06	
7	1.737	.086	.605	380.895	64.723	265.4	.1913-06	
8	1.306	.129	.527	288.090	78.361	134.4	.9009-07	
9	.980	.175	.399	217.793	92.431	74.9	.4400-07	
10	.789	.213	.327	175.476	100.432	49.4	.1597-07	

HARMONIC NOISE SUMMATION - LOADING= 108.9 DB , THICKNESS= 90.3 DB , OVERALL HARMONIC NOISE= 109.0 DB
OVERALL VORTEX NOISE= 100.0 DB WITH MAX SPL AT 5000. HZ , TOTAL OVERALL NOISE= 109.5 DB
1/3-OCTAVE BAND DATA IS

BAND CENTER FREQ. HZ	NUMBER OF HARMONICS	BAND SPL DB	VORTEX BROADBAND SPL - DB	MAXIMUM UNDETECTABLE BROADBAND DB	MINIMUM UNDETECTABLE VERTICAL DISTANCE - FT VORTEX	TOTAL NOISE
1.6	0	-.2	-.2	121.5	0.	0.

Figure 36. --- Continued

2.0	0	6.0	6.0	120.0	0.	0.
2.5	0	12.2	12.2	117.0	0.	0.
3.1	0	18.6	18.6	113.5	0.	0.
4.0	0	25.2	25.2	109.0	0.	0.
5.0	0	31.3	31.3	104.0	0.	0.
6.3	0	37.6	37.6	99.5	0.	0.
8.0	0	43.8	43.8	95.0	0.	0.
10.0	0	47.2	47.2	91.5	1.	1.
12.5	0	51.5	51.5	87.5	2.	2.
16.0	0	54.3	54.3	82.0	5.	5.
20.0	0	57.1	57.1	74.5	18.	18.
25.0	0	59.6	59.6	65.0	69.	69.
31.5	0	61.6	61.6	56.0	247.	247.
40.0	0	63.6	63.6	48.0	784.	784.
50.0	0	65.7	65.4	41.5	2039.	2039.
63.0	0	69.0	66.8	37.0	4083.	4083.
80.0	0	81.2	68.5	34.0	7004.	7004.
100.0	1	107.8	69.9	33.5	7895.	212122.
125.0	0	100.5	71.3	34.5	8266.	8266.
160.0	0	79.3	72.7	35.5	7883.	7883.
200.0	1	102.9	74.3	36.5	8300.	117829.
250.0	0	95.6	75.7	37.5	7930.	7930.
315.0	0	78.2	77.4	38.5	7268.	7268.
400.0	0	79.1	79.1	39.0	7481.	7481.
500.0	0	80.7	80.7	39.5	7171.	7171.
630.0	0	82.4	82.4	39.5	7223.	7223.
800.0	0	83.9	83.9	39.0	7056.	7056.
1000.0	0	85.4	85.4	38.5	6680.	6680.
1250.0	0	86.7	86.7	38.0	6339.	6339.
1600.0	0	88.0	88.0	38.0	5545.	5545.
2000.0	0	88.9	88.9	39.0	4771.	4771.
2500.0	0	89.7	89.7	41.0	3848.	3848.
3150.0	0	90.3	90.3	44.0	2984.	2984.
4000.0	0	90.6	90.6	47.0	2215.	2215.
5000.0	0	90.8	90.8	50.5	1783.	1783.
6300.0	0	90.5	90.5	53.5	1313.	1313.
8000.0	0	89.7	89.7	55.0	975.	975.
10000.0	0	88.3	88.3	56.5	712.	712.

MINIMUM UNDETECTABLE Y= 212122. FT AT X= -75.0 FT

Figure 36. --- Continued

```
1 SAMPLE CASE 2 , NORMAL DATA LOAD AND PRINT , X-Y LOCATIONS , 2 PROPS
2 LOAD HARMONICS + ROLLOFF , CALCULATE ABSORPTION , FAR-FIELD , V.N.3
                          BLADES    AF    CLI  DIA,  S.CO.P.REC.SHROUD
3 SAMPLE PROPELLER CONFIG, B   4.0 213.8  .538 11.25  .176 -.000  -.00

              X=   .9892   .9443   .8679   .7665   .6493   .5266   .4095   .3080   .2316   .1867
            H/B=   .032    .035    .041    .050    .062    .081    .120    .213    .540   1.000
            B/D=  .1400   .1422   .1420   .1400   .1341   .1235   .1060   .0815   .0500   .0400
         DES CL=   .240    .390    .525    .627    .676    .672    .589    .467    .335    .160
        DELTA @=  -7.20   -6.40   -4.30    -.70    4.40   10.30   16.30   22.30   27.50   31.00
        AIRFOIL=    1.      1.      1.      1.      1.      1.      2.      3.      3.      3.
          MCRIT=  1.000   1.000   1.000   1.000   1.000   1.000   1.000   1.000   1.000   1.000
       (CL A=0)=   .000    .000    .000    .000    .000    .000    .000    .000    .000    .000
            D00=   .000    .000    .000    .000    .000    .000    .000    .000    .000    .000
                   -.000   -.000   -.000   -.000   -.000   -.000   -.000   -.000   -.000   -.000
                  1.000   5.000  -1.000    .000 300.000-300.000  3.0001500.000    .000   1.000
                   .000    .000    .000    .000    .000    .000    .000    .000    .000    .000
                  -.000   -.000   -.000   -.000   -.000   -.000   -.000   -.000   -.000   -.000
                  -.000   -.000   -.000   -.000   -.000   -.000   -.000   -.000   -.000   -.000
                  -.000   -.000   -.000   -.000   -.000   -.000   -.000   -.000   -.000   -.000
                  -.000   -.000   -.000   -.000   -.000   -.000   -.000   -.000   -.000   -.000
                  -.000   -.000   -.000   -.000   -.000   -.000   -.000   -.000   -.000   -.000
                  -.000   -.000   -.000   -.000   -.000   -.000   -.000   -.000   -.000   -.000

J LIMIT=99999.0010  1.0000  1.0000  1.0000  1.0000  1.0000  1.0000  1.0000  1.0000  1.0000  1.0000

  BHP    PRPM    ALT.  V-KNOTS TEMP  REQ.CP     J      COMP.CP 03/4  AP.EFF.  M.N.  AP.EFF.  EF.EFF. IND.EFF. HI/HO       F/M
 62.00   340.   1500.    77.0  513.   .4574    2.0413
                                                        .2914  40.98   .852
                                                        .3990  42.48   .862
                                                        .4585  43.29   .859  .1170    .859     .859     .893    .00000

                                                                  PROPELLER THRUST=  225.20

J=    2.0413  THET34=  43.29 PSI=   .00 OMT=   .00  MS= .1170  S3=-0.  S4=-0.

              X=   .9892   .9443   .8679   .7665   .6493   .5266   .4095   .3080   .2316   .1867
          THETA=  36.09   36.89   38.99   42.59   47.69   53.59   59.59   65.59   70.79   74.29
          ALPHA=   -.59    -.97   -1.08   -1.00    -.69    -.46    -.32    -.29     .05     .16
            PHI=  36.68   37.86   40.08   43.59   48.38   54.06   59.91   65.89   70.74   74.14
           BETA=   3.39    3.33    3.26    3.30    3.36    3.08    2.13    1.25     .36     .17
          PHI 0=  33.30   34.53   36.82   40.29   45.02   50.98   57.78   64.64   70.38   73.97
            CL3=   .138    .220    .317    .408    .478    .486    .377    .260    .110    .059
          CD/CL=  .0297   .0227   .0178   .0148   .0128   .0131   .0242   .0480   .2554   .4758
         DCP/DX=  .5132   .7587   .9341   .9572   .8204   .5590   .2619   .0974   .0193   .0068
         DCT/DX=  .2085   .3139   .3928   .4054   .3482   .2383   .1115   .0394   .0023  -.0020
       SECT.EFF.=  .8292   .8447   .8583   .8645   .8664   .8702   .8687   .8252   .2419  -.5877
       SECT.LOSS=  .0876   .1178   .1324   .1297   .1096   .0726   .0344   .0170   .0146   .0108
        SECT.MN=  .2128   .2061   .1950   .1807   .1652   .1504   .1382   .1295   .1242   .1218
        M/MCRIT=  .2130   .2066   .1957   .1815   .1675   .1529   .1388   .1298   .1242   .1218
        AIRFOIL=    1.      1.      1.      1.      1.      1.      2.      3.      3.      3.
              G= 13.8243 12.9675 11.6010  9.9653  8.3277  6.9036  5.8218  5.1030  4.6961  4.5107

COMPUTERIZED PROPELLER DESIGN TECHNIQUE PROGRAM WRITTEN BY HAMILTON STANDARD UNDER CONTRACT NO.F33615-70-C-1583 FOR AERO PROP. LAB

              K=   .74    .74    .74    .74    .74    .74    .74    .66    .66    .66
         GNOISE=  2.00   3.00   1.00    .00  -1.00  80.00  90.00   8.00    .06  -1.00
                   .00  -6.00    .00    .21   1.43   -.00   -.00   -.00   -.00   -.00
```

Figure 36. --- Continued

2- PROPELLER(S) , VORTEX NOISE OPTION= 3. , DETECTABILITY OPTION= 1 NIGHTTIME JUNGLE
NOISE IN DB RE .0002 MICROBAR

VALUES OF ATMOSPHERIC ABSORPTION (DB/1000FT) COMPUTED FOR 80.0 PCT REL. HUMIDITY , 90.0 DEG F

.003	.004	.005	.006	.008	.010	.013	.016	.020	.03	.03	.04	.05	.06	.08	.10	.13	.16	.20
.25	.32	.40	.50	.63	.81	1.01	1.28	1.63	2.04	2.56	3.31	4.17	5.26	6.72	8.69	9.82	12.60	16.43	21.47

FLIGHT VELOCITY= 77. KNOTS TAS = 75. KNOTS CAS , MACH NUMBER= .12 , BHP= 62.1 , THRUST= 226. LB , RPM= 340.
ROTATIONAL TIP VELOCITY= 200.3 FPS , ROTATIONAL TIP MACH NUMBER= .18 , HELICAL TIP MACH NUMBER= .21

X= 300.0 , Y= 1500. , DISTANCE= 1530. FT , ANGLE= 78.7 DEG WHEN HEARD , X= 484.4 , DISTANCE= 1576. FT WHEN NOISE PRODUCED

HARMONIC NUMBER	AZI	FREQ. HZ	ATMOS. ABSORP	LOADING NOISE	THICKNESS NOISE	HARMONIC NOISE	DETECTABLE TONE NOISE	MINIMUM UNDETECTABLE Y
1	0.	24.	-.1	38.9	9.4	38.9	69.3	44.
2	-1.	47.	-.2	32.8	3.3	32.8	43.8	421.
3	-1.	71.	-.2	26.7	-2.7	26.7	32.3	789.
4	-1.	94.	-.3	20.6	-8.8	20.6	25.2	895.
5	-1.	118.	-.4	14.5	-14.9	14.5	20.8	737.

HARMONIC NOISE SUMMATION - LOADING= 40.1 DB , THICKNESS= 10.6 DB , OVERALL HARMONIC NOISE= 40.1 DB
OVERALL VORTEX NOISE= 30.0 DB WITH MAX SPL AT 136. HZ , TOTAL OVERALL NOISE= 40.5 DB
1/3-OCTAVE BAND DATA IS

BAND CENTER FREQ. HZ	NUMBER OF HARMONICS	BAND SPL DB	VORTEX BROADBAND SPL - DB	MAXIMUM UNDETECTABLE BROADBAND DB	MINIMUM UNDETECTABLE VERTICAL DISTANCE - FT VORTEX	TOTAL NOISE
1.6	0	-18.8	-18.8	121.5	1.	1.
2.0	0	-16.6	-16.6	120.0	1.	1.
2.5	0	-14.5	-14.5	117.0	1.	1.
3.1	0	-12.3	-12.3	113.5	1.	1.
4.0	0	-10.0	-10.0	109.0	1.	1.
5.0	0	-7.9	-7.9	104.0	1.	1.
6.3	0	-5.7	-5.7	99.5	1.	1.
8.0	0	-3.4	-3.4	95.0	1.	1.
10.0	0	-1.2	-1.3	91.5	1.	1.
12.5	0	1.3	.8	87.5	0.	0.
16.0	0	7.6	3.2	82.0	0.	0.
20.0	0	28.5	5.3	74.5	1.	1.
25.0	1	38.9	7.4	65.0	2.	44.
31.5	0	14.8	9.6	56.0	7.	7.
40.0	0	22.8	11.9	48.0	23.	23.
50.0	1	32.8	14.0	41.5	63.	421.
63.0	1	25.0	16.1	35.5	161.	789.
80.0	0	23.9	18.4	32.0	313.	313.
100.0	1	23.5	20.3	30.0	496.	895.
125.0	1	22.1	21.3	29.0	623.	737.
160.0	0	21.2	21.2	29.5	591.	591.
200.0	0	20.1	20.1	29.5	524.	524.
250.0	0	18.5	18.5	30.5	395.	395.
315.0	0	16.8	16.8	31.5	296.	296.
400.0	0	14.9	14.9	32.5	220.	220.
500.0	0	13.2	13.2	33.0	176.	176.
630.0	0	11.7	11.7	32.5	164.	164.
800.0	0	10.2	10.2	32.5	146.	146.
1000.0	0	8.6	8.6	33.5	118.	118.
1250.0	0	6.9	6.9	37.0	72.	72.
1600.0	0	4.8	4.8	42.0	36.	36.
2000.0	0	2.5	2.5	47.5	17.	17.
2500.0	0	-.1	-.1	53.5	8.	8.
3150.0	0	-3.3	-3.3	59.0	4.	4.
4000.0	0	-7.3	-7.3	63.0	2.	2.
5000.0	0	-10.0	-10.0	65.0	2.	2.

Figure 36. --- Continued

6300.0	0	-15.3	-15.3	66.5	1.	1.
8000.0	0	-22.3	-22.3	68.0	1.	1.
10000.0	0	-31.1	-31.1	69.0	1.	1.

MINIMUM UNDETECTABLE Y= 895. FT AT X= 300.0 FT

X= .0 , Y= 1500. , DISTANCE= 1500. FT , ANGLE= 90.0 DEG WHEN HEARD , X= 176.7 , DISTANCE= 1510. FT WHEN NOISE PRODUCED

HARMONIC NUMBER	AZI	FREQ. HZ	ATMOS. ABSORP	LOADING NOISE	THICKNESS NOISE	HARMONIC NOISE	DETECTABLE TONE NOISE	MINIMUM UNDETECTABLE Y
1	0.	23.	-.1	38.6	9.9	38.6	70.1	39.
2	-1.	46.	-.2	32.5	3.8	32.5	44.6	372.
3	-1.	69.	-.2	26.5	-2.3	26.5	33.0	708.
4	-1.	92.	-.3	20.3	-8.4	20.3	25.7	817.
5	-1.	115.	-.4	14.3	-14.4	14.3	21.2	681.

HARMONIC NOISE SUMMATION - LOADING= 39.8 DB , THICKNESS= 11.1 DB , OVERALL HARMONIC NOISE= 39.8 DB
OVERALL VORTEX NOISE= 30.3 DB WITH MAX SPL AT 133. HZ , TOTAL OVERALL NOISE= 40.3 DB
1/3-OCTAVE BAND DATA IS

BAND CENTER FREQ. HZ	NUMBER OF HARMONICS	BAND SPL DB	VORTEX BROADBAND SPL - DB	MAXIMUM UNDETECTABLE BROADBAND DB	MINIMUM UNDETECTABLE VERTICAL DISTANCE - FT VORTEX	TOTAL NOISE
1.6	0	-18.2	-18.2	121.5	1.	1.
2.0	0	-16.1	-16.1	120.0	1.	1.
2.5	0	-14.0	-14.0	117.0	1.	1.
3.1	0	-11.8	-11.8	113.5	1.	1.
4.0	0	-9.5	-9.5	109.0	1.	1.
5.0	0	-7.4	-7.4	104.0	1.	1.
6.3	0	-5.1	-5.1	99.5	1.	1.
8.0	0	-2.8	-2.9	95.0	0.	0.
10.0	0	-.6	-.7	91.5	0.	0.
12.5	0	1.9	1.4	87.5	0.	0.
16.0	0	8.7	3.7	82.0	0.	0.
20.0	0	31.9	5.8	74.5	1.	1.
25.0	1	38.6	8.0	65.0	2.	39.
31.5	0	13.6	10.2	56.0	8.	8.
40.0	0	26.0	12.4	48.0	25.	25.
50.0	1	32.6	14.5	41.5	67.	372.
63.0	1	26.9	16.7	35.5	172.	708.
80.0	0	22.2	18.9	32.0	336.	336.
100.0	1	23.7	20.8	30.0	524.	817.
125.0	1	22.4	21.7	29.0	651.	681.
160.0	0	21.5	21.5	29.5	610.	610.
200.0	0	20.3	20.3	29.5	535.	535.
250.0	0	18.7	18.7	30.5	404.	404.
315.0	0	17.0	17.0	31.5	302.	302.
400.0	0	15.2	15.2	32.5	225.	225.
500.0	0	13.4	13.4	33.0	180.	180.
630.0	0	12.0	12.0	32.5	168.	168.
800.0	0	10.5	10.5	32.5	151.	151.
1000.0	0	9.0	9.0	33.5	121.	121.
1250.0	0	7.3	7.3	37.0	74.	74.
1600.0	0	5.2	5.2	42.0	37.	37.
2000.0	0	3.0	3.0	47.5	18.	18.
2500.0	0	.5	.5	53.5	8.	8.
3150.0	0	-2.6	-2.6	59.0	4.	4.
4000.0	0	-6.5	-6.5	63.0	2.	2.
5000.0	0	-9.1	-9.1	65.0	2.	2.
6300.0	0	-14.2	-14.2	66.5	1.	1.
8000.0	0	-21.0	-21.0	68.0	1.	1.
10000.0	0	-29.4	-29.4	69.0	1.	1.

MINIMUM UNDETECTABLE Y= 817. FT AT X= .0 FT

Figure 36. --- Continued

X= -300.0 , Y= 1500. , DISTANCE= 1530. FT , ANGLE= 101.3 DEG WHEN HEARD , X= -123.9 , DISTANCE= 1505. FT WHEN NOISE PRODUCED

HARMONIC NUMBER	AZI	FREQ. HZ	ATMOS. ABSORP	LOADING NOISE	THICKNESS NOISE	HARMONIC NOISE	DETECTABLE TONE NOISE	MINIMUM UNDETECTABLE Y
1	0.	22.	-.1	38.2	8.6	38.2	70.9	34.
2	-1.	45.	-.2	32.1	2.5	32.1	45.4	325.
3	-1.	67.	-.2	26.1	-3.5	26.1	33.6	626.
4	-1.	90.	-.3	20.0	-9.6	20.0	26.2	736.
5	-1.	112.	-.4	13.9	-15.7	13.9	21.6	621.

HARMONIC NOISE SUMMATION - LOADING= 39.4 DB , THICKNESS= 9.8 DB , OVERALL HARMONIC NOISE= 39.4 DB
OVERALL VORTEX NOISE= 30.5 DB WITH MAX SPL AT 130. HZ , TOTAL OVERALL NOISE= 39.9 DB
1/3-OCTAVE BAND DATA IS

BAND CENTER FREQ. HZ	NUMBER OF HARMONICS	BAND SPL DB	VORTEX BROADBAND SPL - DB	MAXIMUM UNDETECTABLE BROADBAND DB	MINIMUM UNDETECTABLE VERTICAL DISTANCE - FT VORTEX	TOTAL NOISE
1.6	0	-17.8	-17.8	121.5	1.	1.
2.0	0	-15.6	-15.6	120.0	0.	0.
2.5	0	-13.5	-13.5	117.0	0.	0.
3.1	0	-11.3	-11.3	113.5	1.	1.
4.0	0	-9.0	-9.0	109.0	1.	1.
5.0	0	-6.9	-6.9	104.0	1.	1.
6.3	0	-4.7	-4.7	99.5	1.	1.
8.0	0	-2.4	-2.4	95.0	0.	0.
10.0	0	-.2	-.3	91.5	0.	0.
12.5	0	2.4	1.8	87.5	0.	0.
16.0	0	9.8	4.2	82.0	0.	0.
20.0	0	35.4	6.3	74.5	1.	1.
25.0	1	36.6	8.4	65.0	2.	34.
31.5	0	13.0	10.6	56.0	8.	8.
40.0	0	29.4	12.9	48.0	26.	26.
50.0	1	30.6	15.0	41.5	71.	325.
63.0	1	26.6	17.1	35.5	181.	626.
80.0	0	22.2	19.4	32.0	353.	353.
100.0	1	23.3	21.2	30.0	547.	736.
125.0	1	22.4	21.9	29.0	673.	673.
160.0	0	21.7	21.7	29.5	623.	623.
200.0	0	20.4	20.4	29.5	540.	540.
250.0	0	18.8	18.8	30.5	408.	408.
315.0	0	17.1	17.1	31.5	305.	305.
400.0	0	15.3	15.3	32.5	225.	225.
500.0	0	13.5	13.5	33.0	181.	181.
630.0	0	12.1	12.1	32.5	171.	171.
800.0	0	10.7	10.7	32.5	153.	153.
1000.0	0	9.2	9.2	33.5	123.	123.
1250.0	0	7.5	7.5	37.0	75.	75.
1600.0	0	5.4	5.4	42.0	38.	38.
2000.0	0	3.2	3.2	47.5	18.	18.
2500.0	0	.7	.7	53.5	8.	8.
3150.0	0	-2.4	-2.4	59.0	4.	4.
4000.0	0	-6.3	-6.3	63.0	2.	2.
5000.0	0	-8.9	-8.9	65.0	2.	2.
6300.0	0	-14.0	-14.0	66.5	1.	1.
8000.0	0	-20.7	-20.7	68.0	1.	1.
10000.0	0	-29.2	-29.2	69.0	1.	1.

MINIMUM UNDETECTABLE Y= 736. FT AT X= -300.0 FT

Figure 36. --- Continued

```
HAMILTON STANDARD COMPUTER PROGRAM DECK NO. 6196 1A


1 SAMPLE CASE 3 , DETECTABILITY FLYBY , THRUST INPUT
2
                          BLADES   AF   CLI  DIA.  S.CO.P.REC.SHROUD
3 SAMPLE PROPELLER CONFIG, B   4.0 213.8  .538 11.25  .176 -.000  -.00

          X=   .9892   .9443   .8679   .7665   .6493   .5266   .4095   .3080   .2316   .1867
        H/B=   .032    .035    .041    .050    .062    .081    .120    .213    .540   1.000
        B/D=   .1400   .1422   .1420   .1400   .1341   .1235   .1060   .0815   .0560   .0400
     DES CL=   .240    .390    .525    .627    .676    .672    .589    .467    .335    .160
   DELTA Θ=  -7.20   -6.40   -4.30   -.70    4.40   10.30   16.30   22.30   27.50   31.00
    AIRFOIL=   1.      1.      1.      1.      1.      1.      2.      3.      3.      3.
      MCRIT=  1.000   1.000   1.000   1.000   1.000   1.000   1.000   1.000   1.000   1.000
  (CL A=0)=   .000    .000    .000    .000    .000    .000    .000    .000    .000    .000
       DOO=   .000    .000    .000    .000    .000    .000    .000    .000    .000    .000
             -.000   -.000   -.000   -.000   -.000   -.000   -.000   -.000   -.000   -.000
             1.000  10.000    .000    .000    .000-150.000    .000 1500.000    .000   1.000
              .000    .000    .000    .000    .000    .000    .000    .000    .000    .000
             -.000   -.000   -.000   -.000   -.000   -.000   -.000   -.000   -.000   -.000
             -.000   -.000   -.000   -.000   -.000   -.000   -.000   -.000   -.000   -.000
             -.000   -.000   -.000   -.000   -.000   -.000   -.000   -.000   -.000   -.000
             -.000   -.000   -.000   -.000   -.000   -.000   -.000   -.000   -.000   -.000
             -.000   -.000   -.000   -.000   -.000   -.000   -.000   -.000   -.000   -.000
             -.000   -.000   -.000   -.000   -.000   -.000   -.000   -.000   -.000   -.000

J LIMIT=99999.0010  1.0000  1.0000  1.0000  1.0000  1.0000  1.0000  1.0000  1.0000  1.0000  1.0000

 THRUST  PRPM    ALT.  V-KNOTS TEMP  REQ.CT     J      COMP.CT 03/4  AP.EFF.  M.N.     FT      EF.EFF. IND.EFF. HI/HG      F/M
 225.00   340.   1500.   77.0  513.   .1924   2.0413
                                                .0211  38.04   .453
                                                .0738  39.54   .785
                                                .1616  42.91   .861
                                                .1916  43.25   .859
                                                .1924  43.28   .859   .1170   1.000     .859     .893    .00000

                                                                PROPELLER BHP=  61.94

COMPUTERIZED PROPELLER DESIGN TECHNIQUE PROGRAM WRITTEN BY HAMILTON STANDARD UNDER CONTRACT NO.F33615-70-C-1583 FOR AERO PROP. LAB

          K=    .74    .74    .74    .74    .74    .74    .74    .66    .66    .66
     QNOISE=   1.00    .00   1.00    .00    .00    .00   -.00   8.00    .06  -1.00
               .00    .00    .00    .00   1.43   -.00   -.00   -.00   -.00   -.00

 1. PROPELLER(S) , VORTEX NOISE OPTION= 0. , DETECTABILITY OPTION=  1   NIGHTTIME JUNGLE
NOISE IN DB RE .0002 MICROBAR

STANDARD VALUES OF ATMOSPHERIC ABSORPTION (DB/1000FT) AT 70PCT HUMIDITY ,77DEG F ARE
          .003  .003  .004  .005  .007  .009  .010  .014  .020   .02   .03   .03   .04   .05   .07   .09   .11   .14   .17
   .22    .28   .35   .44   .55   .71   .87  1.11  1.41  1.78  2.22  2.87  3.65  4.70  5.90  7.60  8.60 11.10 14.90 20.40

FLIGHT VELOCITY=  77. KNOTS TAS =  75. KNOTS CAS , MACH NUMBER=  .12 , BHP=   62.0 , THRUST=  225. LB , RPM=  340.
ROTATIONAL TIP VELOCITY=  200.3 FPS , ROTATIONAL TIP MACH NUMBER=  .18 , HELICAL TIP MACH NUMBER=  .21

X=     .0 , Y= 1500. , DISTANCE=  1500. FT , ANGLE=  90.0 DEG WHEN HEARD , X=  176.7 , DISTANCE=  1510. FT WHEN NOISE PRODUCED
HARMONIC  AZI   FREQ.  ATMOS.  LOADING  THICKNESS  HARMONIC  DETECTABLE  MINIMUM
 NUMBER         HZ    ABSORP   NOISE     NOISE      NOISE    TONE NOISE  UNDETECTABLE Y
     1     0.    23.    -.1     17.9       6.9       18.1       70.1          4.
     2     0.    46.    -.1    -35.9     -39.0      -34.4       44.6          0.
     3     0.    69.    -.2    -89.3     -86.3      -84.7       33.0          0.
```

Figure 36. --- Continued

4	0.	92.	-.3	-143.2	-138.2	-133.9	25.7	0.
5	0.	115.	-.3	-192.7	-182.3	-184.1	21.2	0.
6	0.	138.	-.3	-192.7	-192.7	-189.7	18.3	0.
7	0.	161.	-.4	-192.8	-192.8	-186.8	16.4	0.
8	0.	184.	-.5	-192.9	-192.9	-186.9	15.1	0.

HARMONIC NOISE SUMMATION - LOADING= 17.6 DB , THICKNESS= 6.9 DB , OVERALL HARMONIC NOISE= 18.1 DB
OVERALL VORTEX NOISE= 53.7 DB WITH MAX SPL AT 125. HZ , TOTAL OVERALL NOISE= 53.7 DB
1/3-OCTAVE BAND DATA IS

BAND CENTER FREQ. HZ	NUMBER OF HARMONICS	BAND SPL DB	VORTEX BROADBAND SPL - DB	MAXIMUM UNDETECTABLE BROADBAND DB	MINIMUM UNDETECTABLE VERTICAL DISTANCE - FT VORTEX	TOTAL NOISE
1.6	0	4.7	4.7	121.5	1.	1.
2.0	0	10.4	10.4	120.0	1.	1.
2.5	0	17.3	17.8	117.0	1.	1.
3.1	0	20.4	20.4	113.5	1.	1.
4.0	0	25.0	25.0	109.0	0.	0.
5.0	0	27.4	27.4	104.0	0.	0.
6.3	0	30.2	30.2	99.5	1.	1.
8.0	0	32.3	32.3	95.0	1.	1.
10.0	0	34.2	34.2	91.5	2.	2.
12.5	0	35.6	35.6	87.5	4.	4.
16.0	0	37.0	37.0	82.0	8.	8.
20.0	0	38.1	38.1	74.5	22.	22.
25.0	1	39.1	39.1	65.0	75.	75.
31.5	0	40.0	40.0	56.0	232.	232.
40.0	0	40.8	40.8	48.0	647.	647.
50.0	1	41.4	41.4	41.5	1479.	1479.
63.0	1	41.9	41.9	35.5	3163.	3163.
80.0	0	42.4	42.4	32.0	4947.	4947.
100.0	1	42.6	42.6	30.0	6304.	6304.
125.0	2	42.7	42.7	29.0	6905.	6905.
160.0	1	42.7	42.7	29.5	6310.	6310.
200.0	1	42.4	42.4	29.5	5943.	5943.
250.0	0	41.9	41.9	30.5	4958.	4958.
315.0	0	41.2	41.2	31.5	4069.	4069.
400.0	0	40.2	40.2	32.5	3256.	3256.
500.0	0	39.1	39.1	33.0	2733.	2733.
630.0	0	37.6	37.6	32.5	2453.	2453.
800.0	0	35.8	35.8	32.5	2031.	2031.
1000.0	0	33.7	33.7	33.5	1533.	1533.
1250.0	0	31.4	31.4	37.0	902.	902.
1600.0	0	28.3	28.3	42.0	436.	436.
2000.0	0	25.1	25.1	47.5	193.	193.
2500.0	0	21.2	21.2	53.5	77.	77.
3150.0	0	16.7	16.7	59.0	31.	31.
4000.0	0	11.3	11.3	63.0	14.	14.
5000.0	0	6.9	6.9	65.0	8.	8.
6300.0	0	-.0	-.0	66.5	5.	5.
8000.0	0	-9.3	-9.3	68.0	3.	3.
10000.0	0	-20.8	-20.8	69.0	2.	2.

MINIMUM UNDETECTABLE Y= 6905. FT AT X= .0 FT

X= -150.0 , Y= 1500. , DISTANCE= 1507. FT , ANGLE= 95.7 DEG WHEN HEARD , X= 25.5 , DISTANCE= 1500. FT WHEN NOISE PRODUCED

HARMONIC NUMBER	AZI	FREQ. HZ	ATMOS. ABSORP	LOADING NOISE	THICKNESS NOISE	HARMONIC NOISE	DETECTABLE TONE NOISE	MINIMUM UNDETECTABLE Y
1	0.	23.	-.1	17.8	6.4	18.0	70.5	0.
2	0.	45.	-.1	-33.1	-39.6	-34.7	45.0	0.
3	0.	68.	-.2	-89.7	-87.1	-85.4	33.3	0.
4	0.	91.	-.3	-143.7	-135.1	-134.7	25.9	0.
5	0.	114.	-.3	-192.7	-183.4	-185.4	21.4	0.

Figure 36. --- Continued

6	0.	136.	-.3	-192.7	-192.7	-189.7	18.5	0.
7	0.	159.	-.4	-192.8	-192.8	-186.8	16.6	0.
8	0.	182.	-.5	-192.9	-192.9	-186.9	15.2	0.

HARMONIC NOISE SUMMATION - LOADING= 17.8 DB , THICKNESS= 6.4 DB , OVERALL HARMONIC NOISE= 18.0 DB
OVERALL VORTEX NOISE= 53.7 DB WITH MAX SPL AT 125. HZ , TOTAL OVERALL NOISE= 53.7 DB
1/3-OCTAVE BAND DATA IS

BAND CENTER FREQ. HZ	NUMBER OF HARMONICS	BAND SPL DB	VORTEX BROADBAND SPL - DB	MAXIMUM UNDETECTABLE BROADBAND DB	MINIMUM UNDETECTABLE VERTICAL DISTANCE - FT VORTEX	TOTAL NOISE
1.6	0	4.9	4.9	121.5	1.	1.
2.0	0	10.6	10.6	120.0	1.	1.
2.5	0	17.9	17.9	117.0	0.	0.
3.1	0	20.6	20.6	113.5	0.	0.
4.0	0	25.0	25.0	109.0	0.	0.
5.0	0	27.5	27.5	104.0	0.	0.
6.3	0	30.3	30.3	99.5	1.	1.
8.0	0	32.4	32.4	95.0	1.	1.
10.0	0	34.2	34.2	91.5	2.	2.
12.5	0	35.7	35.7	87.5	4.	4.
16.0	0	37.0	37.0	82.0	8.	8.
20.0	0	38.1	38.1	74.5	22.	22.
25.0	1	39.1	39.1	65.0	75.	75.
31.5	0	40.0	40.0	56.0	232.	232.
40.0	0	40.7	40.7	48.0	646.	646.
50.0	1	41.4	41.4	41.5	1477.	1477.
63.0	1	41.9	41.9	35.5	3162.	3162.
80.0	0	42.4	42.4	32.0	4947.	4947.
100.0	1	42.6	42.6	30.0	6309.	6309.
125.0	2	42.7	42.7	29.0	6912.	6912.
160.0	1	42.7	42.7	29.5	6318.	6318.
200.0	1	42.4	42.4	29.5	5951.	5951.
250.0	0	41.9	41.9	30.5	4965.	4965.
315.0	0	41.2	41.2	31.5	4073.	4073.
400.0	0	40.2	40.2	32.5	3259.	3259.
500.0	0	39.1	39.1	33.0	2735.	2735.
630.0	0	37.6	37.6	32.5	2453.	2453.
800.0	0	35.8	35.8	32.5	2031.	2031.
1000.0	0	33.7	33.7	33.5	1533.	1533.
1250.0	0	31.4	31.4	37.0	900.	900.
1600.0	0	28.3	28.3	42.0	435.	435.
2000.0	0	25.1	25.1	47.5	192.	192.
2500.0	0	21.2	21.2	53.5	77.	77.
3150.0	0	16.7	16.7	59.0	31.	31.
4000.0	0	11.3	11.3	63.0	14.	14.
5000.0	0	6.9	6.9	65.0	8.	8.
6300.0	0	-.0	-.0	66.5	5.	5.
8000.0	0	-9.2	-9.2	68.0	3.	3.
10000.0	0	-20.7	-20.7	69.0	2.	2.

MINIMUM UNDETECTABLE Y= 6912. FT AT X= -150.0 FT

X= -300.0 , Y= 1500. , DISTANCE= 1530. FT , ANGLE= 101.3 DEG WHEN HEARD , X= -123.9 , DISTANCE= 1505. FT WHEN NOISE PRODUCED

HARMONIC NUMBER	AZI	FREQ. HZ	ATMOS. ABSORP	LOADING NOISE	THICKNESS NOISE	HARMONIC NOISE	DETECTABLE TONE NOISE	MINIMUM UNDETECTABLE Y
1	0.	22.	-.1	17.3	5.6	17.5	70.9	3.
2	0.	45.	-.1	-37.1	-41.0	-35.8	45.4	0.
3	0.	67.	-.2	-91.2	-89.0	-87.1	33.6	0.
4	0.	90.	-.3	-145.7	-137.5	-137.0	26.2	0.
5	0.	112.	-.3	-192.7	-186.3	-188.9	21.6	0.
6	0.	135.	-.3	-192.7	-192.7	-189.7	18.7	0.
7	0.	157.	-.4	-192.8	-192.8	-186.8	16.7	0.

Figure 36. --- Continued

8	0.	180.	-.5	-192.9	-192.9	-186.9	15.3	0.
9	0.	202.	-.5	-192.9	-192.9	-186.9	14.4	0.

HARMONIC NOISE SUMMATION - LOADING= 17.3 DB , THICKNESS= 5.6 DB , OVERALL HARMONIC NOISE= 17.5 DB
OVERALL VORTEX NOISE= 53.5 DB WITH MAX SPL AT 125. HZ , TOTAL OVERALL NOISE= 53.5 DB
1/3-OCTAVE BAND DATA IS

BAND CENTER FREQ. HZ	NUMBER OF HARMONICS	BAND SPL DB	VORTEX BROADBAND SPL - DB	MAXIMUM UNDETECTABLE BROADBAND DB	MINIMUM UNDETECTABLE VERTICAL DISTANCE - FT VORTEX	TOTAL NOISE
1.6	0	5.0	5.0	121.5	1.	1.
2.0	0	10.6	10.6	120.0	1.	1.
2.5	0	17.9	17.9	117.0	1.	1.
3.1	0	20.5	20.5	113.5	0.	0.
4.0	0	24.9	24.9	109.0	0.	0.
5.0	0	27.4	27.4	104.0	0.	0.
6.3	0	30.1	30.1	99.5	0.	0.
8.0	0	32.2	32.2	95.0	1.	1.
10.0	0	34.0	34.0	91.5	2.	2.
12.5	0	35.5	35.5	87.5	4.	4.
16.0	0	36.9	36.9	82.0	8.	8.
20.0	0	38.0	37.9	74.5	22.	22.
25.0	1	38.9	38.9	65.0	73.	73.
31.5	0	39.8	39.8	56.0	229.	229.
40.0	0	40.6	40.6	48.0	633.	633.
50.0	1	41.2	41.2	41.5	1447.	1447.
65.0	1	41.8	41.8	35.5	3099.	3099.
80.0	0	42.2	42.2	32.0	4849.	4849.
100.0	1	42.5	42.5	30.0	6191.	6191.
125.0	2	42.6	42.6	29.0	6786.	6786.
160.0	1	42.5	42.5	29.5	6202.	6202.
200.0	2	42.2	42.2	29.5	5844.	5844.
250.0	0	41.7	41.7	30.5	4875.	4875.
315.0	0	41.0	41.0	31.5	3998.	3998.
400.0	0	40.0	40.0	32.5	3199.	3199.
500.0	0	38.9	38.9	33.0	2683.	2683.
630.0	0	37.4	37.4	32.5	2405.	2405.
800.0	0	35.6	35.6	32.5	1991.	1991.
1000.0	0	33.5	33.5	33.5	1502.	1502.
1250.0	0	31.2	31.2	37.0	889.	889.
1600.0	0	28.1	28.1	42.0	424.	424.
2000.0	0	24.8	24.8	47.5	187.	187.
2500.0	0	20.9	20.9	53.5	75.	75.
3150.0	0	16.5	16.5	59.0	30.	30.
4000.0	0	11.0	11.0	63.0	14.	14.
5000.0	0	6.6	6.6	65.0	8.	8.
6300.0	0	-.4	-.4	66.5	5.	5.
8000.0	0	-9.6	-9.6	68.0	3.	3.
10000.0	0	-21.1	-21.1	69.0	2.	2.

MINIMUM UNDETECTABLE Y= 6786. FT AT X= -300.0 FT

MINIMUM UNDETECTABLE Y = 6925. FT AT ANGLE= 93.2 DEG

X= 150.0 , Y= 1500. , DISTANCE= 1507. FT , ANGLE= 84.3 DEG WHEN HEARD , X= 329.7 , DISTANCE= 536. FT WHEN NOISE PRODUCED

HARMONIC NUMBER	AZI	FREQ. HZ	ATMOS. ABSORP	LOADING NOISE	THICKNESS NOISE	HARMONIC NOISE	DETECTABLE TONE NOISE	MINIMUM UNDETECTABLE Y
1	0.	23.	-.1	17.6	6.8	17.8	69.7	4.
2	0.	47.	-.1	-36.5	-39.2	-34.8	44.2	0.
3	0.	70.	-.2	-90.1	-86.7	-85.2	32.6	0.
4	0.	93.	-.3	-144.1	-134.7	-134.4	25.4	0.

Figure 36. --- Continued

5	0.	116.	-.3	-192.8	-183.0	-185.0	21.0	0.
6	0.	140.	-.3	-192.8	-192.8	-189.8	18.2	0.
7	0.	163.	-.4	-192.8	-192.8	-186.8	16.3	0.
8	0.	186.	-.5	-193.0	-193.0	-186.9	15.0	0.

HARMONIC NOISE SUMMATION - LOADING= 17.6 DB , THICKNESS= 6.8 DB , OVERALL HARMONIC NOISE= 17.8 DB
OVERALL VORTEX NOISE= 53.5 DB WITH MAX SPL AT 125. HZ , TOTAL OVERALL NOISE= 53.5 DB
1/3-OCTAVE BAND DATA IS

BAND CENTER FREQ. HZ	NUMBER OF HARMONICS	BAND SPL DB	VORTEX BROADBAND SPL - DB	MAXIMUM UNDETECTABLE BROADBAND DB	MINIMUM UNDETECTABLE VERTICAL DISTANCE - FT VORTEX	TOTAL NOISE
1.6	0	4.3	4.3	121.5	1.	1.
2.0	0	10.0	10.0	120.0	1.	1.
2.5	0	17.5	17.5	117.0	0.	0.
3.1	0	20.2	20.2	113.5	1.	1.
4.0	0	24.8	24.8	109.0	0.	0.
5.0	0	27.2	27.2	104.0	0.	0.
6.3	0	30.0	30.0	99.5	0.	0.
8.0	0	32.1	32.1	95.0	1.	1.
10.0	0	34.0	34.0	91.5	2.	2.
12.5	0	35.5	35.5	87.5	4.	4.
16.0	0	36.9	36.9	82.0	8.	8.
20.0	0	38.0	38.0	74.5	22.	22.
25.0	1	39.0	39.0	65.0	74.	74.
31.5	0	39.8	39.8	56.0	230.	230.
40.0	0	40.6	40.6	48.0	635.	635.
50.0	1	41.2	41.2	41.5	1452.	1452.
63.0	1	41.8	41.8	35.5	3102.	3102.
80.0	0	42.2	42.2	32.0	4849.	4849.
100.0	1	42.5	42.5	30.0	6176.	6176.
125.0	2	42.6	42.6	29.0	6765.	6765.
160.0	1	42.5	42.5	29.5	6178.	6178.
200.0	1	42.2	42.2	29.5	5818.	5818.
250.0	0	41.7	41.7	30.5	4855.	4855.
315.0	0	41.0	41.0	31.5	3984.	3984.
400.0	0	40.0	40.0	32.5	3190.	3190.
500.0	0	38.9	38.9	33.0	2678.	2678.
630.0	0	37.4	37.4	32.5	2402.	2402.
800.0	0	35.6	35.6	32.5	1990.	1990.
1000.0	0	33.5	33.5	33.5	1504.	1504.
1250.0	0	31.2	31.2	37.0	892.	892.
1600.0	0	28.1	28.1	42.0	428.	428.
2000.0	0	24.8	24.8	47.5	190.	190.
2500.0	0	20.9	20.9	53.5	76.	76.
3150.0	0	16.4	16.4	59.0	30.	30.
4000.0	0	11.0	11.0	63.0	14.	14.
5000.0	0	6.5	6.5	65.0	8.	8.
6300.0	0	-.5	-.5	66.5	5.	5.
8000.0	0	-9.8	-9.8	68.0	3.	3.
10000.0	0	-21.5	-21.5	69.0	2.	2.

MINIMUM UNDETECTABLE Y= 6765. FT AT X= 150.0 FT

X= 300.0 , Y= 1500. , DISTANCE= 1530. FT , ANGLE= 78.7 DEG WHEN HEARD , X= 484.4 , DISTANCE= 1576. FT WHEN NOISE PRODUCED

HARMONIC NUMBER	AZI	FREQ. HZ	ATMOS. ABSORP	LOADING NOISE	THICKNESS NOISE	HARMONIC NOISE	DETECTABLE TONE NOISE	MINIMUM UNDETECTABLE Y
1	0.	24.	-.1	16.8	6.4	17.1	69.3	4.
2	0.	47.	-.1	-37.8	-40.2	-36.0	43.8	0.
3	0.	71.	-.2	-91.9	-88.2	-86.8	32.3	0.
4	0.	94.	-.3	-146.5	-136.7	-136.4	25.2	0.
5	0.	118.	-.3	-192.8	-185.5	-188.0	20.8	0.
6	0.	141.	-.3	-192.8	-192.8	-189.8	18.0	0.

Figure 36. --- Continued

7	0.	165.	-.4	-192.9	-192.9	-186.8	16.2	0.
8	0.	188.	-.6	-193.0	-193.0	-186.9	14.9	0.

HARMONIC NOISE SUMMATION - LOADING= 16.6 DB , THICKNESS= 6.4 DB , OVERALL HARMONIC NOISE= 17.1 DB
OVERALL VORTEX NOISE= 53.2 DB WITH MAX SPL AT 125. HZ , TOTAL OVERALL NOISE= 53.2 DB
1/3-OCTAVE BAND DATA IS

BAND CENTER FREQ. HZ	NUMBER OF HARMONICS	BAND SPL DB	VORTEX BROADBAND SPL - DB	MAXIMUM UNDETECTABLE BROADBAND DB	MINIMUM UNDETECTABLE VERTICAL DISTANCE - FT VORTEX	TOTAL NOISE
1.6	0	3.8	3.8	121.5	1.	1.
2.0	0	9.6	9.6	120.0	1.	1.
2.5	0	16.9	16.9	117.0	0.	0.
3.1	0	19.7	19.7	113.5	1.	1.
4.0	0	24.4	24.4	109.0	0.	0.
5.0	0	26.8	26.8	104.0	0.	0.
6.3	0	29.7	29.7	99.5	0.	0.
8.0	0	31.8	31.8	95.0	1.	1.
10.0	0	33.7	33.7	91.5	2.	2.
12.5	0	35.2	35.2	87.5	4.	4.
16.0	0	36.6	36.6	82.0	8.	8.
20.0	0	37.7	37.7	74.5	21.	21.
25.0	1	38.7	38.7	65.0	71.	71.
31.5	0	39.5	39.5	56.0	221.	221.
40.0	0	40.3	40.3	48.0	613.	613.
50.0	1	40.9	40.9	41.5	1400.	1400.
63.0	1	41.4	41.4	35.5	2986.	2986.
80.0	0	41.9	41.9	32.0	4663.	4663.
100.0	1	42.1	42.1	30.0	5938.	5938.
125.0	2	42.2	42.2	29.0	6506.	6506.
160.0	1	42.1	42.1	29.5	5937.	5937.
200.0	1	41.9	41.9	29.5	5591.	5591.
250.0	0	41.4	41.4	30.5	4665.	4665.
315.0	0	40.7	40.7	31.5	3830.	3830.
400.0	0	39.7	39.7	32.5	3067.	3067.
500.0	0	38.5	38.5	33.0	2574.	2574.
630.0	0	37.0	37.0	32.5	2307.	2307.
800.0	0	35.2	35.2	32.5	1914.	1914.
1000.0	0	33.1	33.1	33.5	1447.	1447.
1250.0	0	30.7	30.7	37.0	858.	858.
1600.0	0	27.6	27.6	42.0	411.	411.
2000.0	0	24.3	24.3	47.5	182.	182.
2500.0	0	20.4	20.4	53.5	73.	73.
3150.0	0	15.8	15.8	59.0	29.	29.
4000.0	0	10.3	10.3	63.0	13.	13.
5000.0	0	5.8	5.8	65.0	8.	8.
6300.0	0	-1.3	-1.3	66.5	4.	4.
8000.0	0	-10.7	-10.7	68.0	3.	3.
10000.0	0	-22.6	-22.6	69.0	2.	2.

MINIMUM UNDETECTABLE Y= 6506. FT AT X= 300.0 FT

MINIMUM UNDETECTABLE Y = 6905. FT AT ANGLE= 90.0 DEG
PROPELLER UNDETECTABLE ABOVE Y= 6925. FT

Figure 36. --- Continued

```
HAMILTON STANDARD COMPUTER PROGRAM DECK NO. 6196 1A


1 SAMPLE CASE 4 , SAME AS CASE 3 EXCEPT UNNECESSARY PUNCHING OF INPUT
2 CARDS OMITTED , LAST CASE , MINIMUM PRINTING
                          BLADES   AF   CLI  DIA.  S.CO.P.REC.SHROUD
3 SAMPLE PROPELLER CONFIG. B   4.0 213.8  .538 11.25  .176 -.000  -.00

              X=   .9892   .9443   .8679   .7665   .6493   .5266   .4095   .3080   .2316   .1867
            H/B=   .032    .035    .041    .050    .062    .081    .120    .213    .540   1.000
            B/D=   .1400   .1422   .1420   .1400   .1341   .1235   .1060   .0815   .0500   .0400
         DES CL=   .240    .390    .525    .627    .676    .672    .589    .467    .335    .160
       DELTA Θ=  -7.20   -6.40   -4.30   -.70    4.40   10.30   16.30   22.30   27.50   31.00
        AIRFOIL=   1.      1.      1.      1.      1.      1.      2.      3.      3.      3.
          MCRIT=  1.000   1.000   1.000   1.000   1.000   1.000   1.000   1.000   1.000   1.000
     (CL A=0)=    .000    .000    .000    .000    .000    .000    .000    .000    .000    .000
          000=    .000    .000    .000    .000    .000    .000    .000    .000    .000    .000
                  -.000   -.000   -.000   -.000   -.000   -.000   -.000   -.000   -.000   -.000
                  -.000  10.000   -.000   1.000   -.000   -.000   -.0001500.000   -.000   -.000
                   .000    .000    .000    .000    .000    .000    .000    .000    .000    .000
                  -.000   -.000   -.000   -.000   -.000   -.000   -.000   -.000   -.000   -.000
                  -.000   -.000   -.000   -.000   -.000   -.000   -.000   -.000   -.000   -.000
                  -.000   -.000   -.000   -.000   -.000   -.000   -.000   -.000   -.000   -.000
                  -.000   -.000   -.000   -.000   -.000   -.000   -.000   -.000   -.000   -.000
                  -.000   -.000   -.000   -.000   -.000   -.000   -.000   -.000   -.000   -.000
                  -.000   -.000   -.000   -.000   -.000   -.000   -.000   -.000   -.000   -.000

J LIMIT=99999.0010  1.0000  1.0000  1.0000  1.0000  1.0000  1.0000  1.0000  1.0000  1.0000  1.0000

 THRUST  PRPM    ALT.  V-KNOTS TEMP  REQ.CT     J       COMP.CT 03/4  AP.EFF.  M.N.     FT      EF.EFF. IND.EFF. HI/HO       F/M
  225.00   340.   1500.   77.0  513.   .1924    2.0413
                                                 .0211  38.04   .453
                                                 .0738  39.54   .785
                                                 .1816  42.91   .861
                                                 .1916  43.25   .859
                                                 .1924  43.28   .859  .1170    1.000     .859     .893     .00000

                                                                PROPELLER BHP=   61.94

COMPUTERIZED PROPELLER DESIGN TECHNIQUE PROGRAM WRITTEN BY HAMILTON STANDARD UNDER CONTRACT NO.F33615-70-C-1583 FOR AERO PROP. LAB

              K=    .74     .74     .74     .74     .74     .74     .74     .66     .66     .66
         QNOISE=   1.00    -.00    1.00    -.00    -.00    -.00    -.00    8.00     .06   -1.00
                   -.00    -.00    -.00     .00    1.43    -.00    -.00    -.00    -.00    -.00

 1. PROPELLER(S) , VORTEX NOISE OPTION=-0. , DETECTABILITY OPTION=  1   NIGHTTIME JUNGLE
NOISE IN DB RE .0002 MICROBAR

STANDARD VALUES OF ATMOSPHERIC ABSORPTION (DB/1000FT) AT 70PCT HUMIDITY ,77DEG F ARE
          .003  .003  .004  .005  .007  .009  .010  .014  .020    .02   .03   .03   .04   .05   .07   .09   .11   .14   .17
      .22  .28   .35   .44   .55   .71   .87  1.11  1.41  1.78   2.22  2.87  3.65  4.70  5.90  7.60  8.60 11.10 14.90 20.40

FLIGHT VELOCITY=  77. KNOTS TAS =  75. KNOTS CAS , MACH NUMBER=  .12 , BHP=   62.0 , THRUST=  225. LB , RPM=  340.
ROTATIONAL TIP VELOCITY=  200.3 FPS , ROTATIONAL TIP MACH NUMBER=  .18 , HELICAL TIP MACH NUMBER=  .21


MINIMUM UNDETECTABLE Y =   6925. FT AT ANGLE=  93.2 DEG

MINIMUM UNDETECTABLE Y =   6905. FT AT ANGLE=  90.0 DEG
PROPELLER UNDETECTABLE ABOVE Y=   6925. FT
```

Figure 36. --- Continued

HAMILTON STANDARD COMPUTER PROGRAM DECK NO. 6196 1A

Figure 36. --- Concluded

The propeller performance should be computed for a pressure altitude which is the sum of the observer altitude and the expected minimum undetectable altitude above the observer.

The computer outputs shown in Figure 36 were obtained from a UNIVAC 1108 computer. The output on another computer, such as the CDC 6600, will not be identical to that in Figure 36 because of differences in word length. However, these differences are not expected to be significant to the user.

SECTION IX

PROPELLER NOISE DETECTABILITY TREND STUDY

1. INTRODUCTION

The major purpose of this contract is to develop a computer program which would predict propeller noise and compare the predicted noise spectrum with an aural detectability criteria. The program then provides an estimate of the minimum flight altitude which would avoid aural detection.

With this propeller noise detectability program available, one can investigate various propeller configurations and operating conditions to determine combinations which will permit lower flight altitudes without detection. A study was made of the effects of several propeller configuration parameters and of tip velocity on minimum undetectable altitude over a jungle at night. An acceptable propeller configuration was required to be able to meet the following 4 operating conditions:

Condition	Thrust	Indicated Airspeed	Altitude
1	1600 lb	0 knots	0 ft
2	1300	50	0
3	250	120	10000
4	225	75	1500

Aural detectability was evaluated only at the last condition.

The results of this study are summarized in Table XVII and Figure 37. The propeller rpm and blade angle are permitted to vary to achieve optimum performance at each condition. Recommended harmonic loads derived from data required in this program are included in the calculations.

It should be pointed out here that the harmonic load noise and the broadband noise predictions used by the propeller noise detectability program involve empirical coefficients derived from the data obtained for static conditions in this program. The accuracy of these coefficients has not been established for flight conditions such as number 4 in the table above. Indeed, the two spectra in Figure 29 suggest that the use of static data for predicting propeller noise characteristics in flight may lead to significant errors in predicted minimum undetectable altitude.

TABLE XVII

RESULTS OF PROPELLER NOISE DETECTABILITY TREND STUDY

Diameter, ft	Activity Factor	Number of Blades	Blade Planform	Operating Condition 1		2		3		4 with Tip Speed V_t of					
										150		200		300	
				Minimum HP	at V_t of, fps	Minimum HP	at V_t of, fps	Minimum HP	at V_t of, fps	HP	Detectability Altitude†	HP	Detectability Altitude†	HP	Detectability Altitude†
8.	240	4	Square	345	650	377	570	116	350	76*	6056*	70	6376	66	7778
10.	240	4	Square	275	525	330	475	113	330	72	5388	65	6086	66	7605
11.25	240	4	Square	247	460	312	425	115	290	68	5215	64	5961	67	7497
11.25	100	4	Square	228	625	299	545	106	340	71	8495	61	8897	60	9970
11.25	200	4	Square	240	475	310	450	117	300	67	5860	63	6572	65	8146
11.25	300	4	Square	253	450	317	410	119	270	69	4455	65	5208	71	6801
11.25	240	3	Square	238	525	314	465	112	330	70	5327	64	7264	65	9977
11.25	240	6	Square	245	400	315	375	121	275	68	6159**	66	7029	74	9009
11.25	160	6	Square	237	440	306	410	114	290	66	7851	63	8682	67	10445
11.25	240	4	V	242	490	310	440	113	270	66	6277	63	7024	66	8819
11.25	240	4	A	253	460	318	420	120	300	71	4705	65	5331	69	6676
11.25	113	4	47X-451							67	7397	62	7957		
11.25	214	4	47X-464							65	6373	62	6925		

†Minimum undetectable altitude, ft
*175 fps Tip Speed
**Also 110 HP, 5423 ft altitude at 100 fps

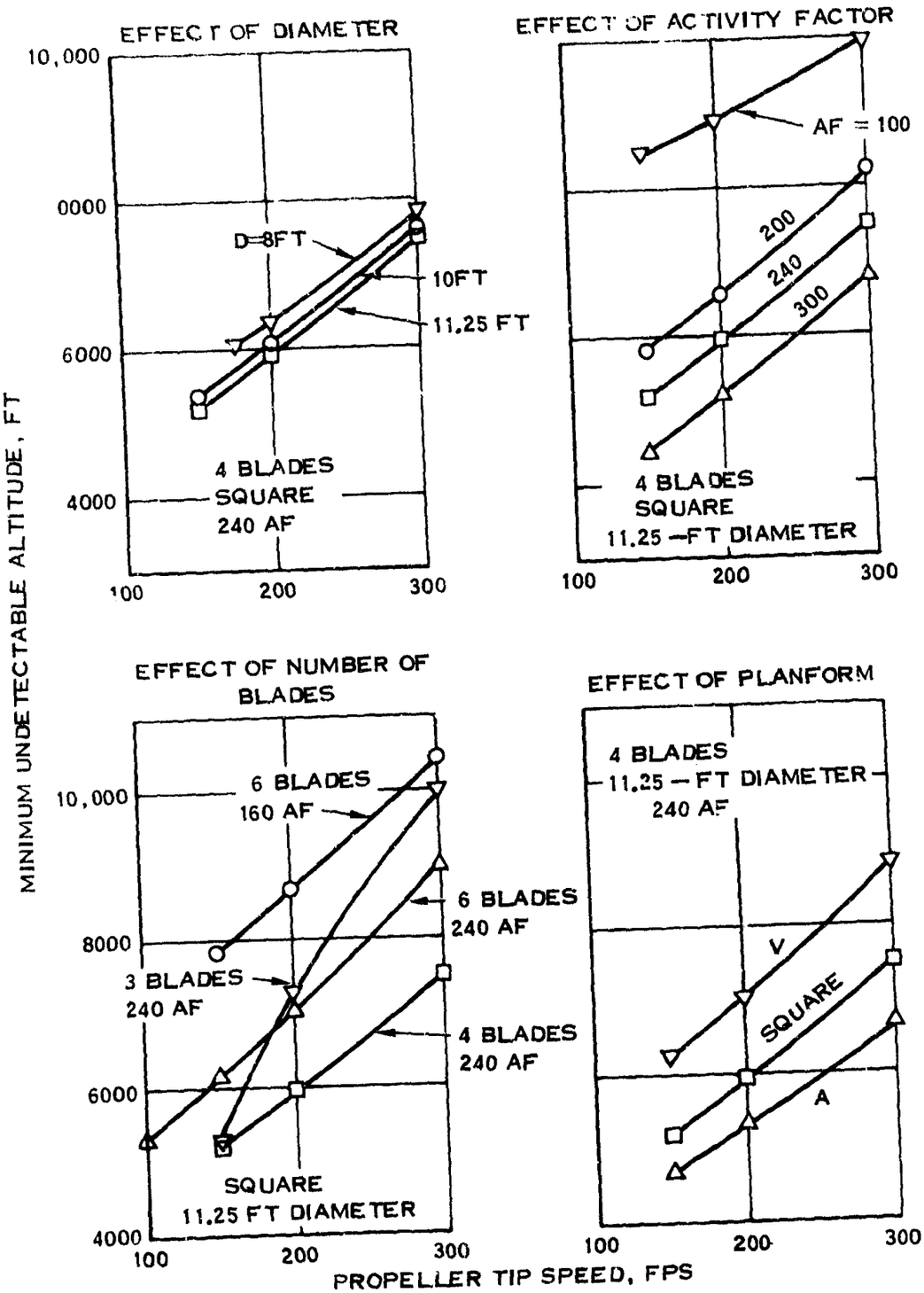

Figure 37. Propeller Noise Detectability Trends

2. EFFECT OF TIP SPEED

As would be expected, the minimum undetectable altitude decreases with decreasing tip speed. Figure 37 shows that the minimum undetectable altitude decreases about 1600 feet for a decrease of 100 fps in tip speed. The minimum tip speed is determined by the ability of the propeller to produce the thrust of 225 pounds required for condition 4. The horsepower is generally a minimum at a tip speed over 200 fps. Therefore, depending on the tradeoff between range (horsepower) and flight altitude, the tip speed should be near 200 fps.

3. EFFECT OF PROPELLER GEOMETRY

The effects of four geometry parameters on minimum undetectable altitude are shown in Figure 37. The top left sketch in the figure shows that increasing propeller diameter from 8 feet to 11.25 feet reduces the minimum undetectable altitude slightly and permits a lower tip speed. The top right sketch shows that increasing activity factor by increasing the blade chord reduces the altitude. Sketches of the blades are shown on the left of Figure 38. The bottom left sketch shows that increasing the number of blades from 4 to 6 increases altitude. This change is due to increased broad-band noise. A further increase in altitude is shown if the blade chord is reduced to maintain total activity factor. On the other hand, if the number of blades is reduced from 4 to 3 the harmonic loading noise increases considerably and increases the minimum undetectable altitude. Therefore, 4 blades appears to be the optimum.

The effect of radial distribution of blade chord is shown in the bottom right of Figure 37. Sketches of the 3 blades are presented on the right of Figure 38. The A-shaped blade configuration is quieter than the square- or V-shaped blade configurations but requires slightly more horsepower.

The last two lines of Table XVII are for two of the propeller configurations tested during the experimental phase of this contract. A study of the test data shows that the broad-band noise in the 250-1000 Hz range is 3.4 dB less from the new wide 47X-464 blades than from the narrower 47X-451 blades. The predicted reduction in minimum undetectable altitude shown in Table XVII is 14%. It is not known how much of the measured reduction in broad-band noise is due to the change in airfoil family from NACA 64A to 66A and how much is due to the change in planform. The computer program evaluates only the latter change. However, it is encouraging that the 47X-464 blades, which were designed to be quieter, are measured to be quieter.

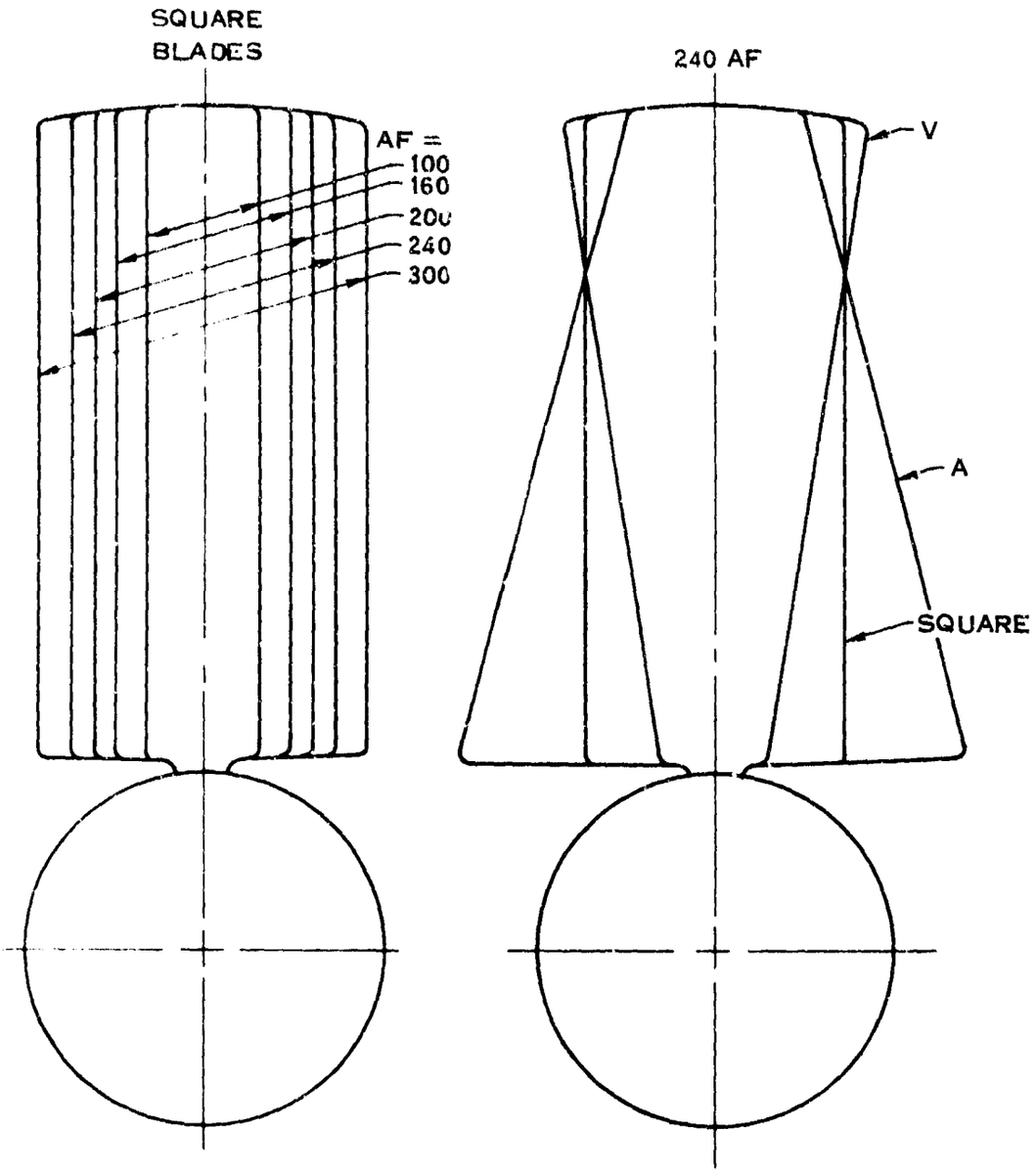

Figure 38. Blade Planforms

4. OPTIMUM PROPELLER DESIGN

The trends discussed in the two preceding sections may serve as a guide to designing a quiet propeller:

a. The propeller must be large enough (diameter, blade activity factor, number of blades) to achieve all required operating conditions.

b. The largest diameter evaluated is least detectable.

c. Detectability is reduced by increased blade activity factor (or chord). However the weight increases with diameter and activity factor and, therefore, a complete mission trade-off study is required to select an optimum propeller configuration. Of course advanced technology composite blades allow larger diameter designs to be used without undue weight penalty.

d. The tip speed in the quiet mode, condition 4, should be a minimum consistent with achieving the required thrust. A trade-off study to consider the increased horsepower required at low tip speeds may be required to select an optimum tip speed. Also, a thrust margin is required for flight safety reasons.

e. Four blades seems to be optimum. More blades increase detectability of broad-band noise and fewer blades increase detectability of harmonic noise.

f. The blade chord should decrease towards the tip. Probably a rounded tip is better than the "A" shape shown in Figure 38.

SECTION X

CONCLUSIONS

The following conclusions were derived from the analytical and experimental study described in this report.

1. The propeller noise levels measured during static tests conducted in this study are predicted within acceptable accuracy by the propeller noise detectability computer program using an experimentally-derived correlation of unsteady blade loads and the vortex noise strip-integration procedure developed in this study.

2. The presence of a narrow-band random noise source has been revealed by a detailed evaluation of the static test noise data. This noise appears as broad peaks at harmonics of the blade-passing frequency and is not explained by current propeller noise theories.

3. Although no suitable low-tip-speed propeller data was available during this study to show the effect of forward speed on propeller noise, data from a moderately-low-tip-speed propeller show a significant reduction in mid-frequency harmonic noise and in high-frequency broad-band noise in forward flight compared to static operation. Therefore, the ability of the propeller noise detectability program to predict noise spectra of a flying quiet aircraft with a low-tip-speed propeller requires further investigation.

4. A trend study using the propeller noise detectability program developed in this study shows that for minimum detectability, a propeller must a) operate at the lowest practicable tip speed, b) have a wide blade chord, c) have a larger diameter than required for performance, and d) have three to five blades. A reduction in broad-band noise due to an increase in blade chord predicted by the new vortex noise procedure was confirmed experimentally. A theoretical study of the effect of airfoil shape indicates that little change in vortex noise should be expected for different airfoils with good aerodynamic performance.

SECTION XI

RECOMMENDATIONS

As a result of the study reported here, the following recommendations are made:

1. The effect of forward flight on low-tip-speed propeller noise and on the correlations between measurements and predictions by the propeller noise detectability program should be investigated.

2. Further analytical and experimental studies should be undertaken to define the sources of the propeller noise observed in this study and to develop the computer program to establish correlation with measured flight data.

APPENDIX I

DERIVATIONS OF EQUATIONS FOR HARMONIC ROTATIONAL NOISE

Kemp and Arnoldi[18] derive and present equations for the near-field propeller harmonic loading sound pressure. In these equations (numbers 10 to 13 in Ref. 18) all distances are nondimensionalized by dividing by the propeller tip radius D/2. Equation (3) in this report is obtained by substituting Equations (12) and (13) into Equation (10) and by adding Equations (10a) and (10b) together. Also, the following replacements are made because of changes in nomenclature:

1. Replace R_t by D/2, s by 2S/D, x by 2X/D, θ by ϕ, $mBM_t\,(Mx+s)/\beta^2$ by $k\sigma$, and mBM_t/β^2 by $kD/2(1-M^2)$.

2. The local blade chord (A in Ref. 18) is replaced by the projection of the chord onto the propeller plane, b cos θ in the nomenclature of this report. Therefore, replace a by b cos $\theta/2r$.

3. The derivatives of the two force coefficients, C_T' and C_F', in Ref. 18 are replaced by $(D/2)dC_T/dr$ and by $(D/2\pi\, r)dC_P/dr$, respectively. The thrust coefficient C_T in Ref. 18 (see Equation (5)) and in this report have the same definition and the power coefficient $C_P = 2\pi rC_F/D$.

Alternatively, Equation (3) may be derived from Equations (21) and (23) of Ref. 17 by replacing β^2 by $1-M^2$, θ by ϕ, T and Q by corresponding terms involving the coefficients C_T and C_P, respectively and by noting that because of symmetry $S(-\phi) = S(\phi)$ and, therefore,

$$\int_0^{2\pi} f(S)e^{-imB\phi}\,d\phi = 2\int_0^{\pi} f(S)\cos mB\phi\,d\phi$$

Equation (4) for thickness noise in this report is derived from Arnoldi's[23] Equations (1) and (2). The parameters defined by his Equation (2) are substituted into Equation (1). These two equations are added together and multiplied by the factor $e^{-imB\Omega t}$. The resulting equation for P_m is rearranged, θ is replaced by ϕ, β^2 is replaced by $(1-M^2)$, $(Mx+S)/\beta^2$ is replaced by σ, and mBM_T/R is replaced by k to derive Equation (4) in this report.

Equation (5) for the far-field loading noise may be derived from Equation (3) by a similar process to that used by Kemp and Arnoldi[18] to derive their Equation (16) from their Equation (6). In doing this, a phase term i^{mB+1} is ignored because absolute phase is not important. Terms of order $1/s^2$ are neglected relative to terms of order 1/s, the substitutions listed above in connection with

the derivation of Equation (3) are made, and s_0 is replaced by $2S_0/D$. Also the Bessel function J_{mB} is replaced by the terms inside the [ ] brackets of Equation (7) of this report, which is a corrected version of the equation derived by Arnoldi[28].

Equation (6) for the far-field thickness noise is derived from Equation (15) in Ref. (38) by adding a factor $e^{-imB\Omega t}$, replacing ω by $m\Omega B$ and β^4 by $(1-M^2)^2$. As for Equation (5), the J_{mB} term is replaced by the terms in the [ ] brackets. Numerical calculations show that the relative phase between the loading and thickness noise sound pressures is the same for the far-field and near-field equations.

Equation (8) is obtained from Equation (36) of Ref. 20, Equation (2) of Ref. 21 or Equation (10) of Ref. 22 by eliminating the radial load terms $a_{\lambda C}$ and $b_{\lambda C}$ which are small for propellers, replacing n by mB, replacing a_0 by a, replacing r_1 and r by d, replacing $a_{\lambda D}$ by $a_{\lambda Q}/r$, and by replacing $b_{\lambda D}$ by $b_{\lambda Q}/r$.

Equation (9) is derived from Equation (8) by ignoring all terms with $J_{mB+\lambda}$, which is small relative to $J_{mB-\lambda}$, as a factor, replacing $ia_{\lambda T} - b_{\lambda T}$ by T_λ and replacing $ia_{\lambda Q} - b_{\lambda Q}$ by Q_λ because of the assumption of random phasing, and substituting S_0 for d.

APPENDIX II

ALTERNATE METHOD FOR CALCULATING UNCORRECTED DETECTION RANGE*

INTRODUCTION

The received noise from an aircraft during flyover is from multiple sources and is non-stationary and random in character. The magnitude and apparent frequency associated with each source continually changes as the aircraft approaches and passes a microphone making the separation of pure tone and broadband noise very difficult if not impossible.

An approach for determining the detection range from sailplane flyover measurements has been applied in Ref. 29. These results are discussed below and are followed by step by step procedures for obtaining the uncorrected detection range using only a pure tone detection spectrum for the case where flyover data are used and for the case where predicted noise spectra are used.

AURAL DETECTION OF SAILPLANES

Reference 29 reports the results of measurements of the noise radiated from three sailplanes. The reported results are in the form of overall sound pressure levels and one-third octave band spectra obtained from a microphone located five feet above the ground and directly under the sailplanes as they passed overhead. Measurements are reported from each of the sailplanes flying at various altitudes and speeds.

Also included in the report are the results from a subjective determination of the altitude at which two of the sailplanes could just be heard. One of the sailplanes, the Schweizer 2-33 was aurally detected by four observers at approximately 2000 feet altitude and 80 degrees elevation while flying at 50 miles per hour. The other sailplane, the Libelle, was aurally detected by three observers at approximately 2600 feet altitude and 80 degrees elevation while flying at 69 miles per hour. The aural detection range was also predicted from noise measurements of the sailplanes flying overhead. The predicted aural detection range, corrected for atmospheric absorption, was 1300 feet for the Schweizer 2-33 and 2100 feet for the Libelle.

These predicted ranges were obtained by comparing the spectrum level of the received noise to an aural detection spectrum for pure tones. The values for the spectrum levels were determined using a Hewlett-Packard 5450 Fourier Analyzer with an equivalent 50 millisecond averaging time. This averaging time is within the range of 20 to 250 milliseconds given for the integration time constant of the ear as reported in Ref. 39. The spectrum levels were arrived at by decreasing the bandwidth

---

* Does not include the effect of atmospheric absorption

of the analysis until the level remained constant. This procedure resulted in levels which were 9 to 12 dB greater than the constant energy spectrum level obtained from

$$SPL_{SL} = SPL_{1/3} - 10 \log \Delta f \quad \text{(dB)} \tag{51}$$

where, SPL_{SL} = Constant energy spectrum level, (dB)

$SPL_{1/3}$ = 1/3 octave band level, (dB)

Δf = Bandwidth of 1/3 octave band, (Hz)

From the results of the sailplane measurements it appears that the ear responds to rapid changes in amplitude and frequency and a detailed spectral analysis of the received noise is required in order to determine the aural detection range of an aircraft. This analysis should be conducted with an averaging time in the range of the ear's integration time constant. When equipment is not available to conduct narrow band analysis, the sailplane results indicate that the spectrum level from those portions of the spectrum where pure tones do not dominate may be obtained from

$$SPL_{SL} = SPL_{1/3} - 10 \log \Delta f + 10 \quad \text{(dB)} \tag{52}$$

These results have led to the following procedures for obtaining the uncorrected detection range from measured flyover data and from predicted noise spectra.

UNCORRECTED DETECTION RANGE FROM MEASURED FLYOVER NOISE

The following procedures are given for determining the uncorrected detection range of an aircraft flying directly over a microphone whose output is tape recorded. Also included in Figure 39 is an example taken from Ref. 29 where these procedures were followed.

1. From the hearing threshold and ambient noise measurements made at the test site, determine the pure tone detection spectrum as shown in Section II. An example is plotted in Figure 39.

2. Determine the maximum sound pressure level which occurs in each one-third octave band during the flyover. An alternate approach is to determine the one-third octave spectra when the signal has reached its maximum overall value. The time constant (averaging time) used in the data reduction should not exceed 0.3 seconds. An example one-third octave band spectrum is shown in Figure 39.

3. Determine the maximum difference between the one-third octave band spectrum and the detection level spectrum and note the frequency band at which this occurs. In the example in Figure 39 this difference is 30.5 dB and occurs in the one-third octave band centered at 315 Hz.

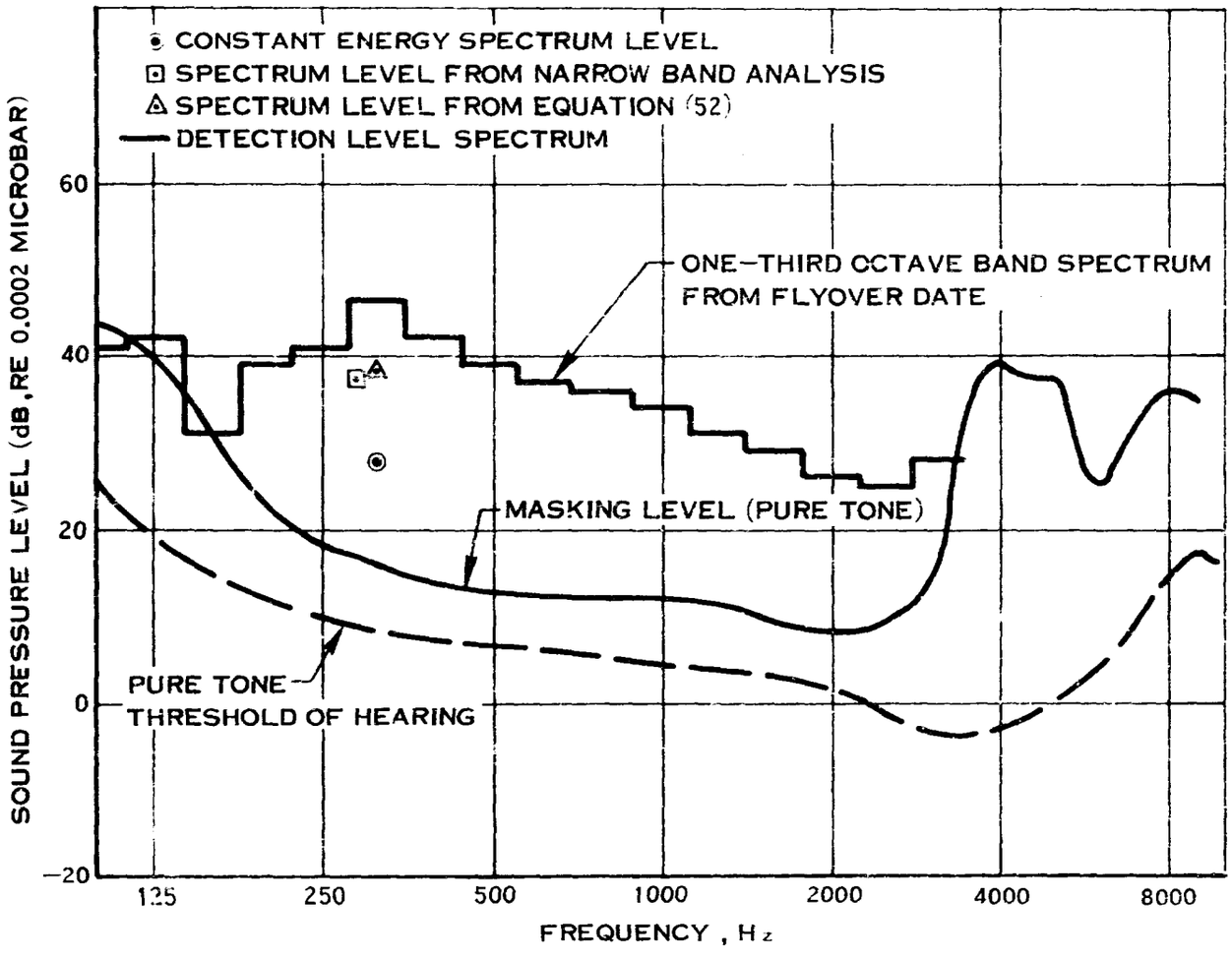

Figure 39. Aural Detection Evaluation (From Ref. 29)

4. Conduct a narrow band analysis over a frequency range including this one-third octave band. The averging time for this analysis should not exceed 0.1 seconds. This analysis should be repeated with narrower bandwidths until the peak spectrum level remains essentially constant. Note this spectrum level and the frequency at which it occurs. Determine the difference between this level and the detection level spectrum. In Figure 39 this spectrum level is 37 dB at 285 Hz resulting in a difference of 20.5 dB.

5. In the event that the received signal is not dominated by pure tones (which should appear in step 2) the spectrum level may be determined by substituting the level of the one-third octave band noted in step 3 in Equation (52).

$$SPL_{SL} = SPL_{1/3} - 10 \log \Delta f + 10$$

This level is applied at the center frequency of the one-third octave band and the difference between this level and the detection level spectrum is noted. In Figure 39 this level is 38 dB at 315 Hz resulting in a difference of 22 dB.

6. The uncorrected detection range is then determined from

$$20 \log \frac{R_u}{R_o} \approx SPL_{SL}(f) - L_d(f) \quad \text{(dB)} \qquad (53)$$

where, R_u = Uncorrected detection range, (ft)

R_o = Aircraft altitude above microphone, (ft)

$SPL_{SL}(f)$ = Spectrum level of received signal from step 4 or step 5, (dB)

$L_d(f)$ = Pure tone detection level from step 1, (dB)

The differences in Figure 39 found from step 4 and step 5 resulted in uncorrected detected ranges of 1340 and 1585 feet respectively.

Note that this detection range does not include corrections for atmospheric and terrain attenuation effects.

UNCORRECTED DETECTION RANGE FROM PREDICTED AIRCRAFT NOISE

The following procedures are given for determining the uncorrected detection range from predictions of aircraft noise.

1. For a given ambient noise environment, determine the pure tone detection level curve as shown in Section II.

2. Determine the power level and frequency of the fundamental and several of its harmonics for each pure tone noise source, using appropriate prediction methods.

3. Determine the power level and 1/3 - octave band spectrum of all broad-band noise sources associated with the aircraft configuration using appropriate prediction methods.

4. Obtain the combined 1/3 - octave band power level spectrum for all broad-band noise sources.

5. Determine the approximate power spectrum level of the combined broad-band noise sources by use of the following expression;

$$PWL_{SL} = PWL_{1/3Oct} - 10\Delta f + 10 \quad (dB) \tag{54}$$

where, PWL_{SL} = Power spectrum level, (dB)

$PWL_{1/3Oct}$ = 1/3 - Octave band PWL, (dB)

Δf = Bandwidth of the 1/3 - Octave band, (Hz)

6. Compare the power level of all pure tones and the power spectrum level of all broad-band noise sources with the pure tone detection level spectrum. Determine the maximum difference between the power level or power spectrum level and the detection level spectrum, and note the frequency at which this occurs.

7. The uncorrected detection range is then determined from

$$20 \log R_u \approx PWL\ (f) - L_d\ (f) \quad (dB) \tag{55}$$

where, R_u = Uncorrected detection ranges, (ft)

PWL (f) = Power level or power spectrum level at point of maximum difference from step 6, (dB)

L_d (f) = Pure tone detection level at point of maximum difference from step 6, (dB).

REFERENCES

1. Smith, D.L. and R.P. Paxson, The Aural Detection of Aircraft, Air Force Flight Dynamics Laboratory Paper TM-69-1-FDDA, AD859892, Sept. 1969

2. Robinson, D.W. and R.S. Dadson, "Threshold of Hearing and Equal-Loudness Relations for Pure Tones and the Loudness Function," J. of the Acoustical Society of America, Vol. 29, No. 12, Dec. 1957.

3. Shaw, W.A., E.B. Newman, and I.J Hirsh, "The Difference Between Monaural and Binaural Thresholds," J. of Experimental Psychology, Vol. 37, 1947.

4. Normal Equal-Loudness Contours for Pure Tones and Normal Threshold of Hearing Under Free Field Listening Conditions, ISO Recommendation R226, Dec. 1961.

5. Yeowart, N.S., M.E. Bryant, and W. Tempest, "The Monaural M.A.P. Threshold of Hearing at Frequencies from 1.5 to 100 c/s," J. of Sound and Vibration, Vol. 6, No. 3, pp. 335-342, 1967.

6. Corso, J.F., "Absolute Thresholds for Tones of Low Frequency," American J. of Psychology, Vol. 71, 1958.

7. Bryant, M.E. and W. Tempest, "Low-Frequency Noise Thresholds," J. of Sound and Vibration, Vol. 9, No. 3, 1969.

8. Robinson, D.W. and L.S. Whittle, "The Loudness of Octave-Bands of Noise," Acustica, Vol. 14, 1964.

9. Hawkins, J.E. and S.S. Stevens, "The Masking of Pure Tones and of Speech by White Noise," J. of the Acoustical Society of America, Vol. 22, No. 1, Jan. 1950.

10. Hand, R.F. and R.H. McLaughlin, Analysis of Background Sound from Data Recorded in Thailand - Final Report, ARPA order No. 236, amendment no. 21, contract no. DAHC-15-67-C-0119, AD817276, June 1967

11. Eyring, C.F., "Jungle Acoustics," J. of the Acoustical Society of America, Vol. 18, No. 2, Oct. 1946.

12. Gutin, L.J., On the Sound Field of a Rotating Propeller, TM1195, NACA, Oct. 1948.

13. Yudin, E.Y., On the Vortex Sound From Rotating Rods, TM-1136, NACA, 1947.

14. Morfey, C.L., "Sound Generation in Subsonic Turbomachinery," J. Basic Engineering, A.S.M.E., Vol. 92, Series D, No. 3, pp. 450-458, Sept. 1970.

15. Douglas Aircraft Co., Proposed Revision to Aerospace Recommended Practice ARP 866, SAE Committee A-21, April 1970.

16. U.S. Standard Atmosphere, U.S. Govt. Printing Office, Dec. 1962.

17. Garrick, I.E. and C.E. Watkins, A Theoretical Study of the Effect of Forward Speed on the Free-Space Sound-Pressure Field Around Propellers, Rept. 1198, NACA, 1954.

18. Kemp, N. and R.A. Arnoldi, Machine Calculation of Free-Space Sound-Pressure Field Around Propellers in Forward Motion, Rept. R-22673-1, UAC Research Dept., Feb 1954.

19. Schlegel, R., R. King and H. Mull, Helicopter Rotor Noise Generation and Propagation, Tech. Rept. 66-4, AD645884, USAAVLABS, Oct. 1966.

20. Lowson, M.V. and J.B. Ollerhead, Studies of Helicopter Rotor Noise, Technical Report 68-60, AD684394, USAAVLABS, Jan. 1969.

21. Ollerhead, J.B. and M.V. Lowson, Problems of Helicopter Noise Estimation and Reduction, Paper No. 69-195, AIAA, Feb. 17-19, 1969.

22. Lowson, M.V. and J.B. Ollerhead, "A Theoretical Study of Helicopter Rotor Noise," J. Sound and Vibration, Vol. 9, No. 2, pp. 197-222, March 1969.

23. Arnoldi, R.A., Near-field Computations of Propeller Blade Thickness Noise, Rept. R-0896-2, UAC Research Dept., Aug. 1956.

24. Hubbard, H.H., Propeller-Noise Charts for Transport Airplanes, TN-2968, NACA, June 1953.

25. Davidson, I.M. and T.J. Hargest, "Helicopter Noise," J. Royal Aeronautical Soc., Vol. 69, pp. 325-336, May 1965.

26. Stuckey, T.J. and J.O. Goddard, "Investigation and Prediction of Helicopter Rotor Noise. Part 1. Wessex Whirl Tower Results," J. Sound and Vibration, Vol. 5, No. 1, pp. 50-80, Jan. 1967.

27. Widnall, S.E., "A Correlation of Vortex Noise Data From Helicopter Main Rotors," J. Aircraft, Vol. 6, No. 3, pp. 279-281, May-June 1969.

28. Sharland, I.J., "Sources of Noise in Axial Flow Fans," J. of Sound and Vibration, Vol. 1, No. 3, pp. 302-322, May 1964.

29. Smith, D.L., R.P. Paxson, R.D. Talmadge and E.R. Hotz, Measurements of the Radiated Noise From Sailplanes, TM-70-3-FDDA, AD709689, AFFDL, May 1970.

30. Bodner, M., J.B. Gibbs and G.J. Healy, Far Field Aerodynamic Noise Measurement Program, LR23640, Lockheed-California Co., June 1970.

31. Lowson, M.V., "The Sound Field for Singularities in Motion," Proc. Roy. Soc. of London, Series A, Vol. 286, pp. 559-572, Aug. 1965.

32. Chuan, R.L. and R.J. Magnus, Study of Vortex Shedding as Related to Self-Excited Torsional Oscillations of an Airfoil, TN2429, NACA, Sept. 1951.

33. Ffowes Williams, J.E. and D.L. Hawkings, "Theory Relating to the Noise of Rotating Machinery," J. of Sound and Vibration, Vol. 10, No. 1, pp. 10-21, July 1969.

34. Tanna, H.K. and C.L. Morfey, "Sound Radiation From a Point Force in Circular Motion," Symposium on Aerodynamic Noise, Paper E5, Sept. 14-17, 1970.

35. Allen, H.J., General Theory of Airfoil Sections Having Arbitrary Shape or Pressure Distribution, Report 833, NACA, 1945.

36. Griffiths, J.W.R., "The Spectrum of Compressor Noise of a Jet Engine", J. Sound and Vibration, Vol. 1, No. 2, pp. 127-140, 1964.

37. Barry, F.W., User's Manual for Propeller Noise Detectability Computer Program, AFAPL-TR-71-38, June 1971.

38. Arnoldi, R.A., Propeller Noise Caused by Blade Thickness, Rept. R-0896-1, UAC Research Dept., Jan. 1956.

39. Zwislocki, J., "Theory of Temporal Auditory Summation," J. of the Acoustical Society of America, Vol. 32, No. 2, pp. 1046-1060, Aug. 1960.

BIBLIOGRAPHY ON AURAL DETECTABILITY

Beranek, L.L., Noise Reduction, McGraw-Hill Co., 1960.

Bryant, M. E. and W. Tempest, "Low-Frequency Noise Thresholds," J. of Sound and Vibration, Vol. 9, No. 3, 1969.

Campbell, R.A., "Detection of a Noise Signal of Varying Duration," J. of the Acoustical Society of America, Vol. 35, No. 11, Nov. 1963.

Corso, J.F., "Absolute Thresholds for Tones of Low Frequencies," American J. of Psychology, Vol. 71, 1958.

Duifhuis, H., "Audibility of High Harmonics in a Periodic Pulse," J. of the Acoustical Society of America, Vol. 48, No. 4 (part 2), 1970.

Egan, J.P., G.Z. Greenberg and A.I. Schulman, "Interval of Time Uncertainty in Auditory Detection," J. of the Acoustical Society of America, Vol. 33, No. 6, 1961.

Eyring, C.F., "Jungle Acoustics," J. of the Acoustical Society of America, Vol. 18, No. 2, Oct. 1946.

Finck, A., "Low-Frequency Pure Tone Masking," Letter to Editor, J. of the Acoustical Society of America, Vol. 33, No. 8, Aug. 1961.

Fletcher, H. and W.A. Munson, "Loudness, Its Definition, Measurement and Calculation," J. of the Acoustical Society of America, Vol. 5, Oct., 1933.

Gayne, W.J., Aural Detection of an Aerial Vehicle Operating of Low Altitudes, AIAA paper No. 65-329, 1965.

Green, D., "Auditory Detection of a Noise Signal," J. of the Acoustical Society of America, Vol. 32, No. 1, Jan. 1960.

Hand, R.F. and R.H. McLaughlin, Analysis of Background Sound from Data Recorded in Thailand-Final Report, ARPA Contract DAHC-15-67-C-0119, AD817276, June 1967.

Hawkins, J.E. and S.S. Stevens, "The Masking of Pure Tones and of Speech by White Noise," J. of the Acoustical Society of America, Vol. 22, No. 1, Jan. 1950.

Hubbard, H.H. and D.J. Maglieri, An Investigation of Some Phenomena Relating to Aural Detection of Airplanes, NACA TN 4337, Sept. 1958.

Loewy, R.G., "Aural Detection of Helicopters in Tactical Situations," J. of the American Helicopter Society, Vol. 8, No. 4, 1963.

Mulligan, B.E., J.C. Adams, M.J. Mulligan and R.E. Burwinkle, "Prediction of Monaural Detection," J. of the Acoustical Society of America, Vol. 43, No. 3, 1968.

Mulligan, B.E., M.J. Mulligan and J.F. Stonecypher, "Critical Band in Binaural Detection," J. of the Acoustical Society of America, Vol. 41, No. 1, 1967.

Normal Equal-loudness Contours for Pure Tones and Normal Threshold of Hearing Under Free Field Listening Conditions, ISO Recommendation R226, Dec. 1961.

Plomp, R. and A.M. Mimpen, "The Ear as a Frequency Analyzer II," J. of the Acoustical Society of America, Vol. 43, No. 4, 1968.

Richards, A.M., Monaural Loudness Functions Under Masking, U.S. Naval Submarine Medical Center, Report No. 509, Feb. 1968.

Robinson, D.W., and R.S. Dadson, "Threshold of Hearing and Equal-Loudness Relations for Pure Tones and the Loudness Function," J. of the Acoustical Society of America, Vol. 29, No. 12, Dec. 1957.

Robinson, D.W., and L.S. Whittle, "The Loudness of Octave-Bands of Noise," Acustica, Vol. 14, 1964.

Schafer, T.H., R.S. Gales, C.A. Shewmaker, and P.O. Thompson, "The Frequency Selectivity of the Ear as Determined by Masking Experiments," J. of the Acoustical Society of America, Vol. 22, No. 4, 1950.

Shaw, W.A., E.B. Newman and I.J. Hirsh, "The Difference Between Monaural and Binaural Thresholds," J. of Experimental Psychology, Vol. 37, 1947.

Shipley, E.F., "Dependence of Successive Judgements in Detection Tasks: Correctness of the Response," Letter to Editor, J. of the Acoustical Society of America, Vol. 33, 1961.

Smith, D.L. and R.P. Paxson, The Aural Detection of Aircraft, Air Force Flight Dynamics Lab. Paper TM-69-1-FDDA, AD859592, Sept. 1969.

Swets, J.A. and D.A. Green, "On the Width of Critical Bands," J. of the Acoustical Society of America, Vol. 34, No. 1, 1962.

Taylor, M.M. and C.D. Creelman, "PEST: Efficient Estimates on Probability Functions," J. of the Acoustical Society of America, Vol. 41, No. 4, 1967.

van den Brink, G., "Detection of Tone Pulses of Various Durations in Noise of Various Bandwidths," J. of the Acoustical Society of America, Vol. 36, No. 6, 1964.

Wandsdronk, C., "Threshold Mechanism and Masking by Noise," Letter to Editor, J. of the Acoustical Society of America, Vol. 35, No. 5, May 1963.

Yeowart, N.S., "Low-Frequency Noise Thresholds," J. of Sound and Vibration, Vol. 9, No. 3, pp. 447-453, 1969.

Yeowart, N.S., M.E. Bryant, and W. Tempest, "The Monaural M.A.P. Threshold of Hearing at Frequencies from 1.5 to 100 c/s," J. of Sound and Vibration, Vol. 6, No. 3, pp. 335-342, 1967.

Zwicher, E., G. Flottorp, and S.S. Stevens, "Critical Bandwidth in Loudness Summation," J. of the Acoustical Society of America, Vol. 29, No. 5, May 1957.